Advances in Chemical Engineering

OPEN ACCESS
eBooks

INDEX

Published in: Mar 2019

Online Edition available at: http://openaccessebooks.com/

Reprints request: info@openaccessebooks.com

Advances in Chemical Engineering

Chapter 1

POM-based Chiral Hybrids Synthesis via Organoimidization Covalent Modification of Achiral Precursors

Yifei Zhang [1,4]†, Yichao Huang [2+], Huan Wang [1+], Jiangwei Zhang [1,2,3]*, Gao Li[1]*, and Yongge Wei[2]*

[1]State Key Laboratory of Catalysis & Gold Catalysis Research Center, Dalian Institute of Chemical Physics, Chinese Academy of Sciences (CAS), Dalian 116023, PR China.

[2]Key Lab of Organic Optoelectronics & Molecular Engineering of Ministry of Education, Department of Chemistry, Tsinghua University, Beijing 100084, PR China.

[3]State Key Laboratory of Physical Chemistry of Solid Surfaces, Xiamen University, Xiamen 361005, PR China.

[4]College of Chemistry and Chemical Engineering, Shenyang Normal University, Shenyang, 110034, PR China.

† Equal Contribution

***Correspondence to: Jiangwei Zhang,** State Key Laboratory of Physical Chemistry of Solid Surfaces, Xiamen University, Xiamen 361005, PR China.*

Email: jwzhang@dicp.ac.cn

***Gao Li,** State Key Laboratory of Catalysis & Gold Catalysis Research Center, Dalian Institute of Chemical Physics, Chinese Academy of Sciences (CAS), Dalian 116023, PR China.*

Email: gaoli@dicp.ac.cn

***Yongge Wei,** Key Lab of Organic Optoelectronics & Molecular Engineering of Ministry of Education, Department of Chemistry, Tsinghua University, Beijing 100084, PR China*

Email: yonggewei@mail.tsinghua.edu.cn

Citation: *Jiangwei Zhang, Saravanathamizhan R, Radhakrishnan S, C M Narayanan, Taha Mahdi, Antonela Ninčević Grassino (2019) Advances in Chemical Engineering, Vol. 1, pp. 1-181.*

Abstract In this chapter, covalent modification of POMs (polyoxometalates) clusters especially by organo imidization via the well-developed DCC(N,N′-dicyclohexylcarbodiimide)-dehydrating protocol by our group is briefly reviewed. The functionalization of POMs with covalently organic moiety is one of the effective ways to increase the diverse POMs family and incorporate exceptional properties that these organic molecules attach to POM clusters in a reliable and predefined manner, which is expected to be applied to the design of molecular functionalized materials. The combination chirality with POMs is a crucial but challenging issue since POMs usually possess high symmetry. Organo imidization covalent modification of achiral precursors Lindquist $[Mo6O19]^{2-}$ has been proved to be a flexible strategy for applying in the generation of POM-based chiral hybrids. The organic ligands offer great opportunities to install stereogenic elements to POMs structure as structure directing-agents to remove symmetric elements in POM clusters, and some special POM clusters bearing amino group on its surface serves as special imido ligands. This takes full advantage of the intrinsic hindrance of the bulky and heavy POMs,Which will greatly extend chirality in polyoxometalate chemistry since the primary chiral POM anions are rare. In consideration of the fact that there exist plenty of chiral natural products L- amino acids and many POM clusters anchor amino group as remote group on the surface. It can foresee that more and more POM-based chiral hybrids will be generated by organo imidization covalent modification of achiral precursors Lindquist $[Mo6O19]^{2-}$ in the future.

Graphical abstract

1. Introduction

Polyoxometalates (POMs) are an exceptional family of inorganic oxide anions consisting of early transition metal ions such as Mo, W, V, etc. at their highest oxidization states bridging by oxide anions with structural versatility and a wide range of properties including catalysis, medicine and materials science [1-3]. Since the first salt of POM, ammonium 12-molybdophosphate, $(NH_4)_3[PMo_{12}O_{40}]$ was reported by Berzelius in 1826, the chemistry of POMs has gained dramatic development, with the development of structure characterization technology, especially single X-ray diffraction, the structure of POMs cluster can be precisely

confirmed. Since Keggin reported the famous Keggin structure in 1934. The topology structure of Keggin [4], Anderson [5], Dawson [6], Waugh [7], Silverton [8], Lindqvist [9] were discovered sequentially and formed into the six basic structure of POMs. In 1970s-1980s, several novel structures including Weakley [10], Standberg [11], Finke [12], and Preyssler [13] were reported (**Figure 1**). POMs, as inorganic multidentate ligands, are prime candidates for the design and construction of different dimensional architectures with judicious selection of appropriate cations and organic molecules and POMs can serve as electron containers due to the property of multi-electron reduction without loss of the architecture. These aspects make POMs more valuable with charming electrical and optical properties such as electrochromism, photochromism, conductivity, and redox activities that suitable in a wide range of potential application [14-21] such as reversible redox activity that can be utilized as efficient solid-acid catalysts and electron-transfer catalysts for diverse organic reactions.

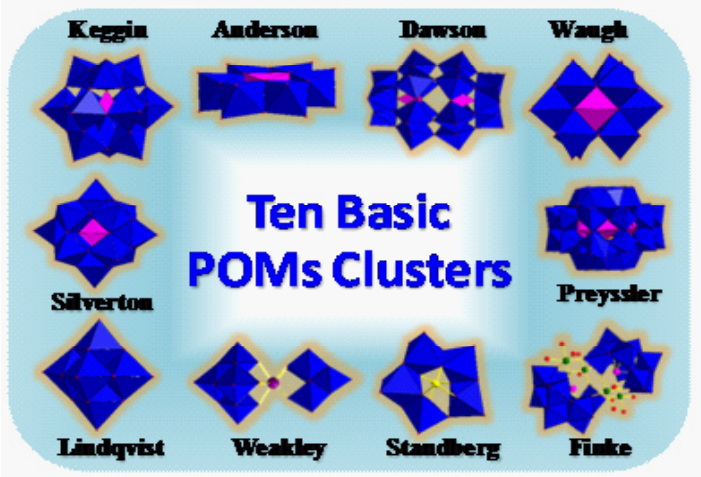

Figure 1: Ten basic structural topology of POM clusters.

Chirality has become an increasingly crucial issue in many fields, ranging from pharmaceuticals to asymmetric catalysis and clinical analysis [22-23]. The synthesis and resolution of chiral polyoxometalates (POMs) is an interesting but challenging area since POMs usually possess high symmetry. Chemists are urgent to break this symmetry so as to get chiral POMs. Preparation of POMs' chiral structures would provide ultimate control of the synthesis of those nanosized objects. Generally speaking, chirality of POMs-based inorganic-organic hybrids

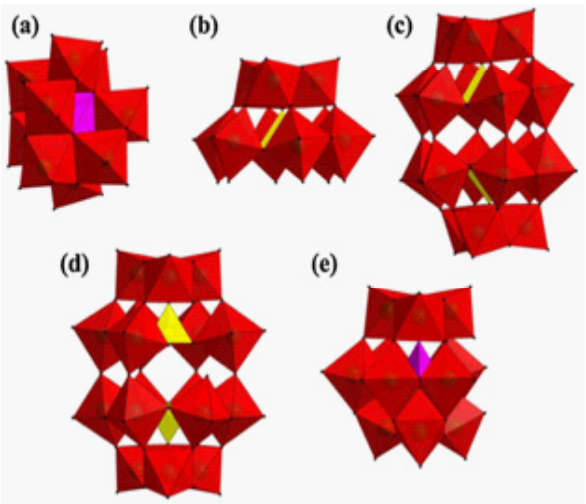

Figure 2: Classical intrinsic chiral POM frameworks.

can manifest itself in two distinct ways [24-26] : (1) They can be intrinsically chiral in the framework of POMs by bond length alteration, geometrical distortion, the formation of structural lacunae and replacement with other metals. Classical intrinsic chiral POM frameworks are $[MnMo_9O_{32}]^{6-}$ (**Figure 2a**), $[PMo_9O_{31}(OH)_3]^{3-}$ (**Figure 2b**), α-$[P_2Mo_{18}O_{62}]^{6-}$ (**Figure 2c**), α1-$[P_2W_{17}O_{61}]^{10-}$ (**Figure 2d**) and β2-$[SiW_{11}O_{39}]^{8-}$ (**Figure 2e**). However, such enantiomers are very easily racemized and difficult to beseparated and isolated. Such a problem has seriously hindered the application of chiral POM-based materials. (2) POMs are chemically modified through coordination bonding, electrostatic interaction and covalent modification. Since metal ions, organic cation especially chiral organic cation and surfactants, organic ligands can dramatically affect the final architectures. Such strategy may lead to the rational design and synthesis of chiral POM-based materials in enantiopure forms.

Organic–inorganic POMs hybrids can be categorized into two classifications [20,27], classification I and classification II (**Figure 3**), which are well-defined according to the interactions between the organic and inorganic moieties, to be exact, non-covalent and covalent interactions, respectively. Classification I organic–inorganic hybrids can be assembled by electrostatic interactions, hydrogen bonding, as well as/or van der Waals interactions.

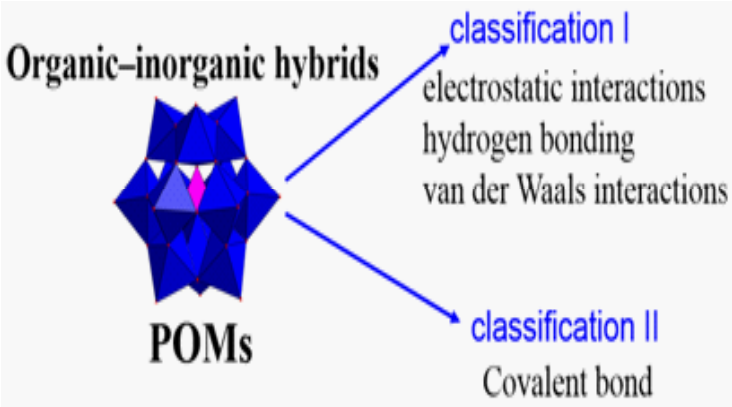

Figure 3: Definition of the two classifications (I and II) of organic/inorganic hybrid POMs

Covalent modification, by grafting organic moieties onto POMs framework, namely, the organic ligand can substitute an oxo group of the POM and be directly linked to the metallic center, resulting in the formation of classification II hybrids. The later has gained much attentional though they are vastly different in molecular structures, POMs and conjugated organic molecule are both electrically active materials with similar electrical and optical properties such as photochromism, electrochromism, and conductivity. The fundamental mechanisms of these properties are, however, different for these two types of materials, with dπ electrons responsible for the inorganic POM clusters, and delocalized pπ electrons responsible for the organic counter part. While both areas have been enjoying considerable success, there has been only a few success in bringing these two types of materials together through covalent bonds to make novel POM-based organic-inorganic hybrids owing to the lacks of reliable strategy to functionalize POMs and prepare their organic derivatives in high yield. As could be expected,

however, such organic-inorganic hybrid materials will not only combine the advantages of organic materials: such as good process ability and fine-regular structure and electronic properties, with those of inorganic POM clusters, such as good chemical stability and strong electron acceptability, to produce so-called ‘‘value-adding properties’’, but also may bring exciting synergistic effects due to the close interaction of delocalized organic pπ orbits with the inorganic POM cluster’s dπ orbits.

Compared with such organic-inorganic hybrids, POMs are conventionally prepared by coordination bonding or electrostatic interaction approaches, which lack predictability and controllability. However, the ability of covalently modify the POM clusters in a reliable and predefined manner holds promise for the development of molecular materials that bridge the gap between molecular organic and bulk semiconducting POMs cluster. Furthermore, giving exceptional physical and structural properties intrinsic to POM superstructures can be achieved by post-functionalized through common organic reactions and apply organically functionalized POM clusters as building blocks [28-29].

Grafting organic moieties onto a POMs cluster requires an anchorage point ensuring the link between the two components. This link is closely dependent on the chemical structure nature and electronic properties of the POMs cluster. The nucleophilic character of the oxygen atoms localized on the surface of the POMs can lead to covalent interactions with electrophilic groups bearing organic groups. The presence of the negative charge borne by the POMs cluster is an important point that needs to be considered for the grafting of the organic moieties. Neutral or negatively charged organic moieties will be chosen in order to favor covalent grafting over electrostatic interactions. The functionalization of POMs through oxygen atoms located at the periphery of the POM structure is the most conventional route. Organic ligand which is the isoelectronic of O^{2-} can substitute an oxo group of the POM and be directly linked to the metallic center [30].

Based on the coordination modes to covalently link organic moieties onto the POM cluster surface. The commonly synthetic strategies can be categorized into the following main classifications: Organoimidization [28,31-34], Organoalkoxylation [35-48], Organotin [49-54], Organosilylation [55-63], Organophosphonylation and organoarsonylation [64-72] (**Figure 4**). Organically functionalized POMs applying specific organic ligands as linkers make POMs-based inorganic-organic chiral hybrids more accessible and flexible. In this review, we specially focus on the issue that such POMs-based inorganic-organic chiral hybrids were obtained by the covalent modification of achiral POM cluster precursors applying organic ligands as structure-directing agents by symmetry reduction or breaking the achiral POM cluster.

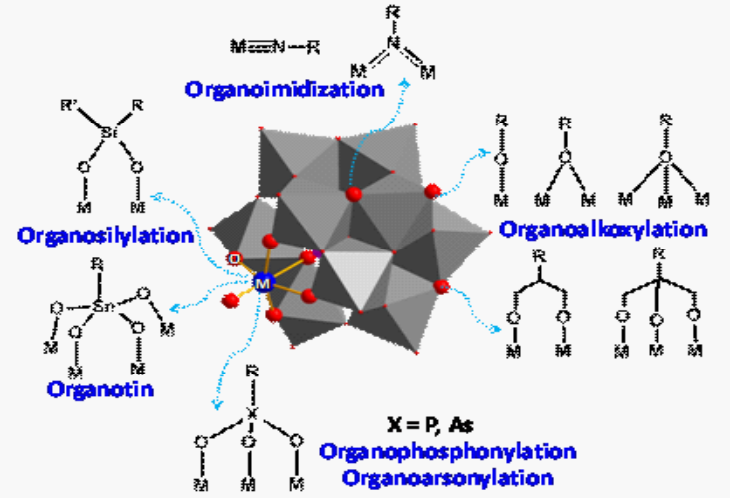

Figure 4: Current existed synthetic strategies and main coordination modes to covalently link organic moieties onto surface of the POM clusters.

2. Organoimidization by the DCC-dehydrating protocol

Among the above mentioned synthetic strategies concerning covalent modification of POM clusters, organoimidization has attracted particular interest. Strictly speaking, the direct covalent modification of the POM cluster without the bridging through the transition metal the organoimidization of $[Mo_6O_{19}]^{2-}$ is the only system. Various synthetic approaches to prepare organoimido derivatives of $[Mo_6O_{19}]^{2-}$ using different organoimido-releasing reagents have-been summarized in a previous book chapter by us [31]. Recently, a lot of arylimido derivatives including polymers of the Lindqvist hexamolybdate cluster, $[Mo_6O_{19}]^{2-}$, have been synthesized continuously [28]. Since the π electrons in the organic component of such derivatives may extend their conjugation to the inorganic POM framework via the N atoms of the imido groups, thus result in strong d–pπ interactions and dramatically modify the electronic structure and redox properties of the corresponding parent POMs.

In addition, organoimido derivatives of POMs with a remote active functional group can be exploited as building blocks to conveniently and controllably fabricate the complicated covalently-linked POM-based organic-inorganic hybrids, including the nano-dumbbells, polymeric chains and even networks of POMs [28]. This modular building block approach brings rational design and structure regulation into the synthesis of organic-inorganic hybrid molecular materials.

In this review, we will just focus on organoimidization of $[Mo_6O_{19}]^{2-}$ by the DCC-dehydrating protocol in brief which has also been well reviewed by our group [28,34] and demonstrated how this protocol can be applied in chiral POMs hybrids synthesis through covalent modification. As it can be expected, the reaction chemistry of organoimido derivatives of POMs stands for the fascinating future of the chemistry of organoimido derivatives of POMs since it opens not only a new road to the chemical modification of POMs, but also an exciting research arena where a variety of hybrid materials containing covalently bonded POM clusters

and organic conjugated segments can be prepared in more controllable and rational manner.

The hexamolybdate ion, $[Mo_6O_{19}]^{2-}$, is amongst the most well-known POM clusters for its thermal and chemical robust and easy to be prepared, which has the so-called Lindqvist structure. As it is depicted in **Figure 5**, the Lindqvist structure consists of a central oxyanion surrounded in an octahedral cage formed by six metal atoms. All the six metal atoms also have an octahedral environment.

Besides the central oxygen atom, they each coordinate triply to one terminal oxygen atom, forming a terminal metal-oxo group (M≡O), and share an additional four double-bridging oxygen atoms (μ_2-O atoms) with neighboring metal atoms. Generally speaking, a Lindqvist ion has a super-octahedral structure approach to O_h point group and features its six terminal metal-oxo groups aligned along the Cartesian axes. For the hexamolybdate, these molybdyl groups (Mo≡O) are reactive enough for the terminal oxygen atoms to be directly replaced by various nitrogenous species. The organoimido derivatives of $[Mo_6O_{19}]^{2-}$ is generated by the substitution of one or more $Mo{=}O_{term}$ bond(s) by one or more Mo≡NR bond(s). Monosubstituted derivatives can be obtained with a variety of organoimido ligands using the hexamolybdate anion $[Mo_6O_{19}]^{2-}$ directly or starting from the octamolybdate anion $[Mo_8O_{26}]^{4-}$ involving the POM reconstruction both in the presence of the N,N′-dicyclohexylcarbodiimide (DCC) dehydrating agent.

2.1. Monosubstituted Derivatives

In the presence of one equivalent of DCC, one equivalent of primary amines reacts smoothly with stoichiometric $(n\text{-}Bu_4N)_2[Mo_6O_{19}]$ under dry N_2 gas and refluxing acetonitrile, to give the corresponding mono-substituted imido derivatives usually in excellent yield of more than 90%. Not only a variety of primary amines occur this reaction, but also it is usually completed in less than 12 hours, and pure *crystalline* products can be readily obtained with convenient bench manipulations. Moreover, this reaction can be carried out in the open air without nitrogen protection if slightly over one equivalent of DCC (1.2 equivalent) is added. (**Scheme 1**)

$$[Mo_6O_{19}]^{2-} + RNH_2 + DCC \longrightarrow [Mo_6O_{18}(NR)]^{2-} + DCU$$

Scheme 1. The Monosubstituted organoimido derivatives $[Mo_6O_{18}(NR)]^{2-}$ synthesis by $[Mo_6O_{19}]^{2-}$ directly functionalization.

Moreover, in our recent attempts to functionalize the octamolybdtates with organoimido groups, we discovered that in the presence of DCC, a proton could dramatically speed up the reaction of α-$[Mo_8O_{26}]^{4-}$ with primary amines under much milder condition. Mean while, monofunctionalized organoimido derivatives of $[Mo_6O_{19}]^{2-}$ were selectively synthesized in high purity and moderate yield with easy workup. This acid-assisting route has allowed the facile

synthesis of a large number of mono-imido hexamolybdates. It is worth pointing out that, the proton was crucial to the above route for the formation of monofunctionalized derivatives. It was observed that in the absence of hydrochloride salt–which offer the protons, amines reacted with α-$[Mo_8O_{26}]^{4-}$ to yield only the bifunctionalized arylimido derivatives of hexamolybdate. (**see Scheme 2**)

$$3(\text{N-Bu}_4)_4[Mo_8O_{26}]+4RNH_2.HC1+6DCC \xrightarrow{CH_3CN\ \text{refluxing}} 4(Bu_4N)_2[Mo_6O_{18}(NR)]+6DCU+4Bu_4NC1$$

Scheme 2. The Monosubstituted organoimido derivatives $[Mo_6O_{18}(NR)]^{2-}$ synthesis by $[Mo_8O_{26}]^{4-}$ reconstruction.

2.2. Disubstituted Derivatives

A characteristic feature of the derivatization of $[Mo_6O_{19}]^{2-}$ with organoimido ligands is the capacity for polyfunctionalization. Among organoimido derivatives of $[Mo_6O_{19}]^{2-}$, the bifunctionalized ones are the easiest and most common potential building blocks for constructing POM-based hybrids.

$$2RNH_2+(\text{N-Bu}_4)_4[Mo_8O_{26}]+2DCC \xrightarrow{CH_3CN\ \text{refluxing}} (Bu_4N)_2[Mo_6O_{17}(NR)_2]+2DCU+(Bu_4N)_2[Mo_2O_7]$$

Scheme 3: The disubstituted organoimido derivatives $[Mo_6O_{17}(NR)_2]^{2-}$ synthesis by $[Mo_8O_{26}]^{4-}$ reconstruction.

In the past years, we also checked the possibility of our DCC-dehydrating protocol in the preparation of di-organoimido derivatives of the hexamolybdate. In most cases, attempts to use the same route as for the mono-substituted derivatives but with astoichiometric ratio of two equivalent aromatic primary amines failed to obtain the disubstituted derivatives in high yields. Instead, mixture of various polysubstituted hexamolybdates were generated since there are six equally reactive sites on a hexamolybdate ion, and thus repeated recrystallization is needed for purification of the anticipant product.

However, an attempt to functionalize the α-isomer of octamolybdate ion α-$[Mo_8O_{26}]^{4-}$, with this reaction routine resulted in the selective synthesis of difunctionalized arylimido derivatives of hexamolybdate with good yield and high purity. The reaction of $(n\text{-}Bu_4N)_2$ [α-Mo_8O_{26}] with DCC and organoimido ligands at the ratio of 1 : 2 : 2 in refluxing dry acetonitrile for 6 to 12 hours afforded the corresponding disubstituted organoimido derivatives $[Mo_6O_{17}(NR)_2]^{2-}$. This novel route allowed the efficient and selective synthesis of a number of di-organoimido hexamolybdates with more convenient and simple bench operations in good yield and high purity [73] (**Scheme 3**).

Considering exclusively steric hindrance, the trans structure of the disubstituted hexamolybdate is expected to be the principal product compared with the cis isomer. However, the trans-disubstituted hexamolybdates have hardly been detected in the above reaction route. Such a result is amazing, which suggests that the steric effect is less important here and the

presence of an excessive imido substituent induces an activating effect on the adjacent molybdyl groups. A DFT study on hexamolybdate derivatives reveals that the cis-disubstituted derivatives are more stable in energy than the corresponding trans-isomers [74].

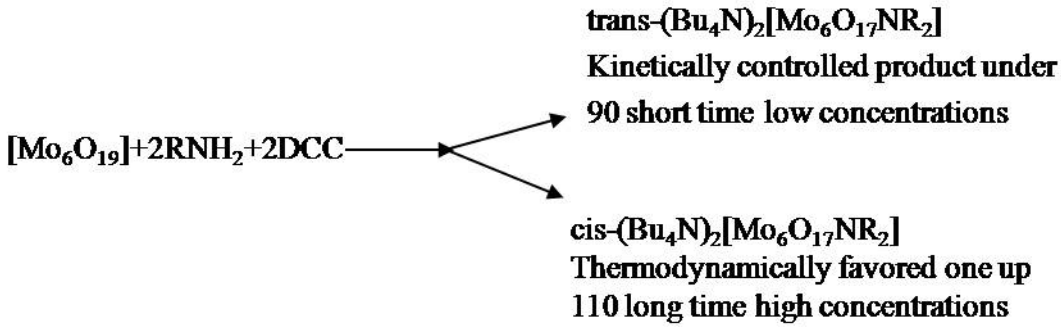

Scheme 4: The disubstituted organoimido derivatives $[Mo_6O_{17}(NR)_2]^{2-}$ synthesis by $[Mo_6O_{19}]^{2-}$ directly functionalization.

We conducted our DCC-dehydrating protocol for the direct functionalization of $[Mo_6O_{19}]^{2-}$ with stoichiometric ratios of $(n\text{-}Bu_4N)_2[Mo_6O_{19}]$ and the corresponding organoimido ligands [75-76]. Both the cis- and trans-disubstituted imido derivatives could be obtained in reasonable yields, respectively, by careful control of the refluxing time, reaction temperature and concentration. It should be noted that the cis-isomer is by far the most common structure among the disubstituted species even if the kinetically controlled trans isomer has been recently isolated [75-77]. In general, prolonged refluxing time at high concentration and high temperature promotes the formation of the cis-isomer, while the trans-isomer can be isolated from a relative short-time at low concentration and low temperature reaction system (see **Scheme 4 and Figure 5**).

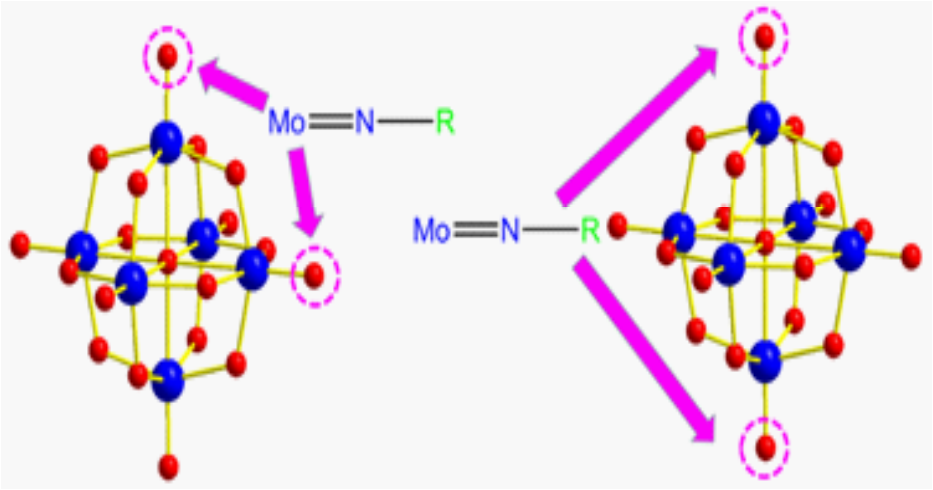

Figure 5: The cis- and trans-disubstituted mode imido derivatives of $[Mo_6O_{19}]^{2-}$.

2.3. Polysubstituted Derivatives

We are also interested in the preparation of the polysubstituted hexamolybdates in the context of our DCC-dehydrating protocol using primary amines as the imido-releasing agents. In a recent attempt to synthesize the fac-tri-2,6-dimethylanilido hexamolybdate, contrary to our expectation, the as-resulted tri-imido derivative, $(Bu_4N)_2[cis\text{-}Mo_6O_{16}\mu_2\text{-}(NAr)(NAr)_2]$, was not exclusively terminal-oxo replaced complex, and instead, one of bridging-oxo groups was substituted. This indicated a very important fact that not only the terminal oxo group can be substituted, but also the bridging oxo groups can be replaced by amine groups [78] (**Figure 6**).

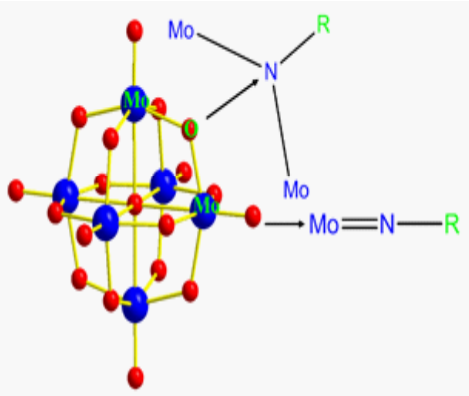

Figure 6: Two substitution modes of terminal or bridging oxygen by organoimido ligands.

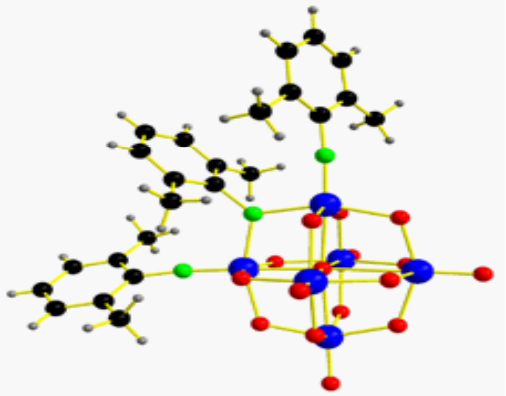

Figure 7: Ball-and-stick model of the trisubstituted hexamolybdate.

This compound has a feature that the μ_2-bridging oxygen atom sharing by the two imido-bearing Mo atoms in a cis-diimido hexamolybdate is substituted with a μ_2-bridging organoimido ligand. It suggests that such oxygen atoms in the cis-diimido hexamolybdates have been doubly activated by the neighboring imido groups and become more negative (nucleophilic) than other oxygen atoms, resulting in the easy electrophilic attack by DCC. It stands for the first example of a bridging oxygen atom in POMs replaced by the bridging imido groups. It breaks the myth that only the terminal oxo groups can be directly replaced with imido ligands before and brings us a wonderful prospect in the chemistry of organoimido derivatives of POMs (**Figure 7**).

2.4. Organoimido Derivatives of other POMs

While there are fruitful developments in the synthetic chemistry of hexamolybdate, related studies on other POMs keep scarcely well developed. So far, there only has been obtained quite limited success in extending the above approaches to the other Lindqvist POMs.

Attempts to directly functionalize the hexatungstate anion, $[W_6O_{19}]^{2-}$, another important Lidquvist homopolyoxometalate besides the hexamolybdate, have failed to utilize all the existing approaches, since $[W_6O_{19}]^{2-}$ does not react at all with phosphinimines, isocyanates or aromatic primary amines under the present developed conditions. It seems that compared to

the molybdyl groups in the hexamolybdate, the tungstyl groups in the hexatungstate is rather unreactive. The only one example of imidosubstituted hexatungstates, $(Bu_4N)_2[W_6O_{18}(NAr)]$, Ar = 2,6-diisopropyl-$C_6H_3$, was obtained about twenty years ago by Maatta [79].

Although the hexatungstate cluster is less labile, replacement of tungstyl groups with reactive molybdyl groups will exert an activate effect on the cluster. Surely, we discovered that the pentatungstenmolybdate ion, $[MoW_5O_{19}]^{2-}$, a Lidquvist heteropolyoxometalate, could be directly functionalized with primary amines using the DCC-dehydrating protocol [80].

$$[MoW_5O_{19}]^{2-} + RNH_2 + DCC \longrightarrow [W_5O_{18}(MoNR)]^{2-} + DCU$$

Scheme 5. The Monosubstituted organoimido derivatives $[W_5O_{18}(MoNR)]^{2-}$ synthesis by $[MoW_5O_{19}]^{2-}$ directly functionalization.

In addition of one and a half equivalents of DCC, the reaction of one equivalent of 2,6-dimethylaniline with one equivalent of $(Bu_4N)_2[MoW_5O_{19}]$ does occur in hot acetonitrile under nitrogen, affording the mono-imido derivatives $(Bu_4N)_2$ $[W_5O_{18}(MoNR)]^{2-}$. Indeed as expected, the terminal oxygen atom bonded to the molybdenum atom was selectively replaced by an imido substituent. This result opens a general road for the synthesis of organo imido derivatives of less reactive POM clusters, namely, by replacement one of the inert terminal metal-oxo groups with a functionalizable Mo-O group.

3. POM-Based Chiral Hybrids Synthesis via Organo imidization

The organo imidization strategy is applying in POM-based chiral hybrids synthesis through covalent modification of achiral precursors POM cluster $[Mo_6O_{19}]^{2-}$ mainly focuses on the construction of chiral axle species. The determination criterion of whether organic-inorganic POM hybrids have chirality or not depends on the overlapping with their mirror structure. Even there does not exist a chiral carbon in organic-inorganic POM hybrids structure, they can still be chiral if there is a chiral axle in the structure. Chirality that results from chiral axle can be catalogued into three types: propadiene-type, biphenyl-type and handle-type.

For the biphenyl-type chiral axle containing POM-based chiral hybrids design. Peng designed two pairs of enantiopure C_2-symmetric 1,1'-binaphthyl units based organic ligand. Through the post-functionalization, achiral precursors monosubstituted organo imido derivatives $[Mo_6O_{18}(NR)]^{2-}$covalently linked to such chiral organic ligand and the chirality transfer from organic ligand to the whole POM-based hybrids [81]. Such hybrids showed moderate chiroptical behaviour in solution, and Cotton effects are observed up to 450 nm, indicating chiral extension from the binaphthyl core of the cluster-containing π-conjugated arms (**Figure 8**).

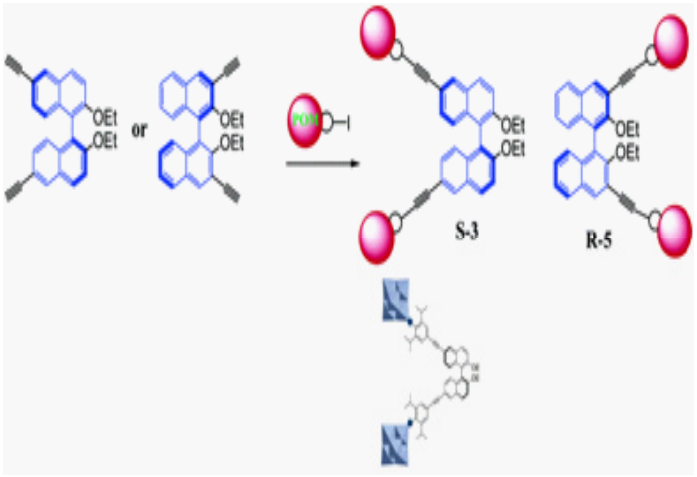

Figure 8 : The 1,1'-binaphthyl units based chiral organic ligand covalent modification of achiral precursors monosubstituted organoimido derivatives $[Mo_6O_{18}(NR)]^{2-}$.

In the view of applying chiral organic ligands as structure-directing agents to transfer chirality to the whole POM-based hybrids strategy, chiral species are still consumed. This organoimidization covalent modification would be more valuable if applying intrinsic hindrance of the bulky and heavy POMs. Then we further promoted this strategy. POM–organic hybrid chiral molecular nanorods were obtained through organo imidization of achiral precursors Lindquist $[Mo_6O_{19}]^{2-}$ applying achiral precursors Anderson type POMs as special imido ligands. They also displayed biphenyl-type chiral axle and C_2-symmetry due to the hindrance of the bulky and heavy POMs to the rotation around the N–C single bond, which stabilized a chiral conformation [82] (**Figure 9**).

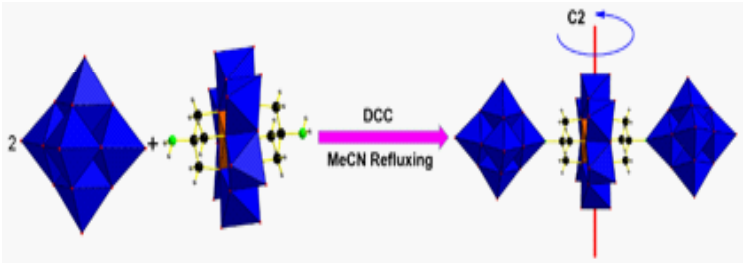

Figure 9: The chiral nanorods synthesis through organoimidization of $[Mo_6O_{19}]^{2-}$ applying Anderson type POMs as special imido ligands.

Such chiral nanorods were obtained in enantioenriched forms by spontaneous resolution. Their chirality was confirmed by the single crystal X-ray diffraction analyses and solid CD spectroscopy measurements. Although such C_2-symmetric frameworks do not possess stereogenic metal ions, the synthetic strategy provides an original route for the development of novel chiral POM architectures. We also extended this strategy to design another type of chiral axle POM-based chiral hybrids such as handle-type POM-based chiral hybrids.

We applied anthranilic alkyl ether as imidization reagent, which is moderately flexible and non-plane organic molecule. By removing symmetric plane and symmetric centers in POM clusters and the formation of ring, we couldobtain chiral metal macro-cyclic compo unds$[Mo_6O_{17}(C_{18}H_{20}N_2O_2)]_2(\pm)$ through organoimidizationcovalent modification by reacting

$[Bu_4N]_4[\alpha\text{-}Mo_8O_{26}]$, binary aromatic amines (1,4 - bis (o- amino- phenoxy)-butane, 1,6 - bis (o - amino- phenoxy) hexane, 1,8 - bis (o - amino- phenoxy)-octane), their hydrochloride and DCC in anhydrous acetonitrile [83].

The flexible alkyl chains which connect two benzene rings in organic ligand can result in the creation of chirality. Since the two ends of organic ligand are fixed on the $Mo_6O_{18}^{2-}$ by Mo-N triple bond, the flexible chain cannot be wiggle freely, so that an asymmetric chain is formed and the symmetry of the original $Mo_6O_{19}^{2-}$ can be broken. In this way, the whole metal macro-cycle turns to be chiral. This isan important breakthrough in POM metal macro-cyclic compounds synthesis (**Figure 10**).

Taking the advantage of disubstituted organoimidization strategy, we also attempt to design multifunctional hybrid materials by introducing aromatic and aliphatic organic amine moieties simultaneously, indeed in such *cis*-disubstituted imido derivatives the symmetry was reduced to C_i point group from reactants $Mo_6O_{19}^{2-}$ cluster which has high symmetry O_h point group. Unfortunately spontaneous resolution and chiral separation of such disubstituted imido derivatives have not yet achieved, however this indicated the important issue that disubstituted/polysubstituted organoimidization strategy should also be an effective strategy in chiral POM-based multifunctional hybrid materials design [84] (**Figure 11**).

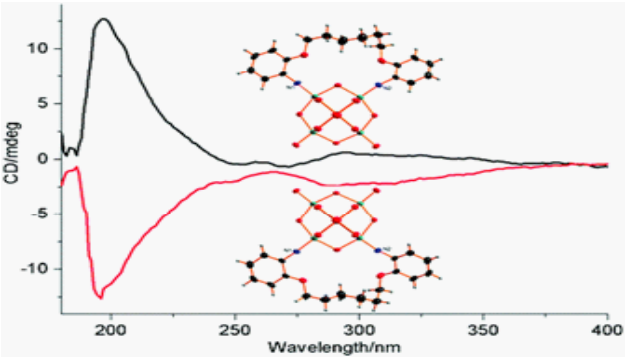

Figure 10: Chiral metal macro-cyclic compounds $[Mo_6O_{17}(C_{18}H_{20}N_2O_2)]_2(\pm)$ through organoimidization covalent modification and their solid CD spectroscopy.

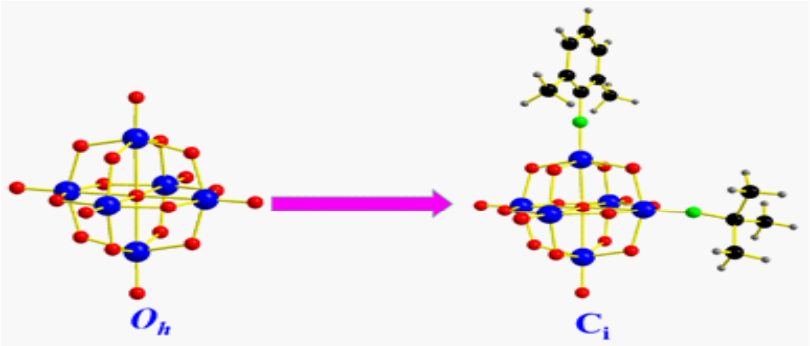

Figure 11: The symmetry reduction by mix disubstituted organoimidization.

Recently, we also attempted to synthesize trisubstituted imido derivatives by introducing the bioactive amine molecule- amantadine, and this is the first reported trisubstituted derivatives using aliphatic organoimido ligands. Similarly, such fac-trisubstituted imido derivatives the symmetry was reduced to D3d point group which couldserve as a potential chiral synthon [85] (**Figure 12**).

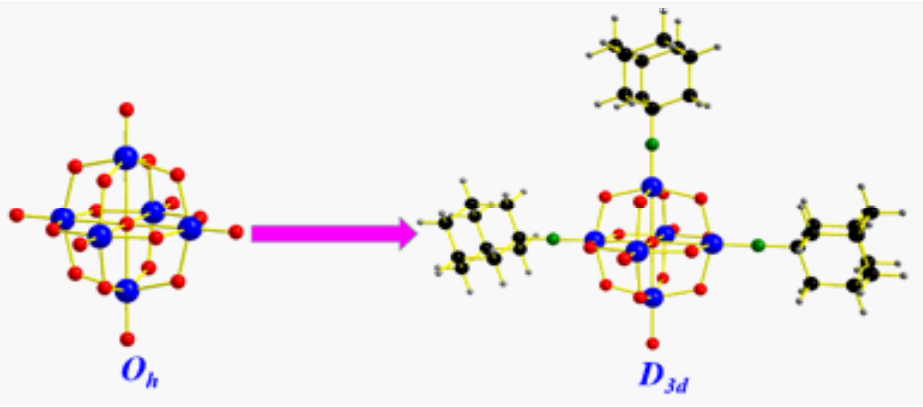

Figure 12: The symmetry reduction by trisubstituted organoimidization

Considering the polyfunctionalization capacity character of the derivatizational $[Mo_6O_{19}]^{2-}$, this strategy designing through the post-functionalization monosubstituted organoimido derivatives as building block becomes more accessible and flexible. We have proved that the remaining terminal reactive oxygen atoms in such organoimido derivatives can be further functionalized by other imido ligands [86]. Since the fact that there exist plenty of chiral natural products L- amino acids and remote amino groups on the surface in POM clusters including $\{[NH_2C(CH_2O)_3]_2V_6O_{13}\}^{2-}$ [87], δ-$\{[NH_2CC(CH_2O)_3]Cr(OH)_3Mo_6O_{18}\}^{3-}$ [88], $\{[C_2H_5C(CH_2O)_3]MMo_6O_{18}[(OCH_2)_3CNH_2]\}^{3-}$ [89], χ-$\{[NH_2CC(CH_2O)_3]Cr(OH)_3Mo_6O_{18}\}^{3-}$ [90], $\{[NH_2C(CH_2O)_3]_2P_2V_3W_{15}O_{59}\}^{6-}$ [43], $\{Ni_6O_{12}[NH_2C(CH_2O)_3](a\text{-}PW_9O_{34})\}$ [91]. (**Figure 13**)

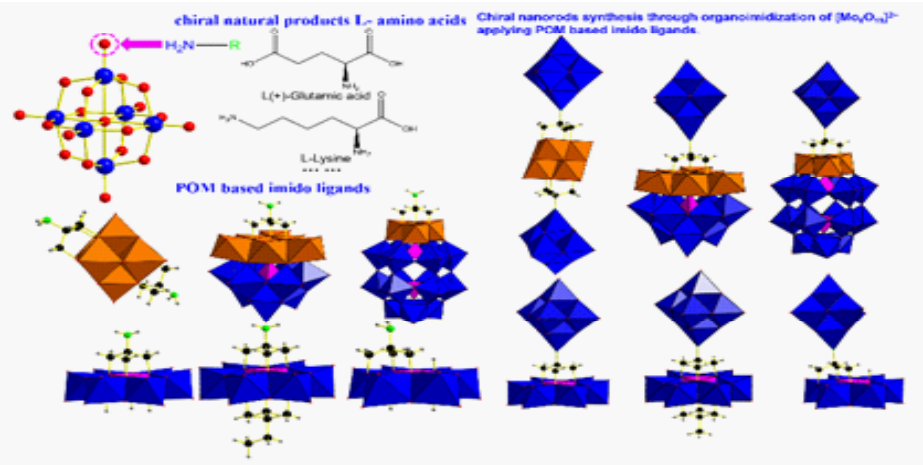

Figure 13: The perspective of POM-based chiral hybrids synthesis by organoimidizationcovalent modification of achiral precursors Lindquist $[Mo_6O_{19}]^{2-}$ strategy.

4. Conclusion and Outlook

Organoimidization covalent modification of achiral precursors Lindquist $[Mo_6O_{19}]^{2-}$ is a flexible strategy applying in the generation of POM-based chiral hybrids. It possesses steric hindrance to remove symmetric elements in POM clusters, by introducing specific customized organic ligands, which includes chiral organic ligands as structure-directing agents or POM clusters that bear amino group on the POM surface and serve as special imido ligands takingfull advantage of intrinsic hindrance of the bulky and heavy POMs. It can fore see that more and more POM-based chiral hybrids will be generated by organoimidization covalentmodifi-

cation in the future and some related investigation is being conducted in our lab now

5. Acknowledgement

We thank the financial support by the National Natural Science Foundation of China (NSFC No. 21471087, 21631007, 21606220and 21701168), the fund of the "Thousand Youth Talents Plan", Liaoning Natural Science Foundation (No. 20170540897) and open project Foundation of State Key Laboratory of Physical Chemistry of Solid Surfaces, Xiamen University (No.201709).

6. References

1. M. T. Pope and A. Muller, Angew. Chem. Int. Ed., 1991, 30, 34.

2. A. Muller and P. Gouzerh, Chem. Soc. Rev., 2012, 41, 7431.

3. J. T. Rhule, C. L. Hill and D. A. Judd, Chem. Rev., 1998, 98, 327.

4. J. F. Keggin, Proceedings Of the Royal Society Of London Series a-Containing Papers Of a Mathematical And Physical Character, 1934, 144, 0075.

5. J. S. Anderson, Nature, 1937, 140, 850.

6. B. Dawson, Acta Crystallographica, 1953, 6, 113.

7. G. Bergman and J. L. T. Waugh, Acta Crystallographica, 1953, 6, 93.

8. D. D. Dexter and Silverto.Jv, J. Am. Chem. Soc., 1968, 90, 3589.

9. M. Che, M. Fournier and J. P. Launay, J. Chem. Phys., 1979, 71, 1954.

10. R. D. Peacock and T. J. R. Weakley, Journal Of the Chemical Society a -Inorganic Physical Theoretical, 1971, 1836.

11. K. Y. Matsumoto, M. Kato and Y. Sasaki, B. Chem. Soc. Jpn., 1976, 49, 106.

12. R. G. Finke, M. Droege, J. R. Hutchinson and O. Gansow, J. Am. Chem. Soc., 1981, 103, 1587.

13. Preyssle.C, Bulletin De La Societe Chimique De France, 1970, 30.

14. J. M. Clemente-Juan, E. Coronado and A. Gaita-Arino, Chem. Soc. Rev., 2012, 41, 7464.

15. H. J. Lv, Y. V. Geletii, C. C. Zhao, J. W. Vickers, G. B. Zhu, Z. Luo, J. Song, T. Q. Lian, D. G. Musaev and C. L. Hill, Chem. Soc. Rev., 2012, 41, 7572.

16. M. Nyman and P. C. Burns, Chem. Soc. Rev., 2012, 41, 7354.

17. X. Lopez, J. J. Carbo, C. Bo and J. M. Poblet, Chem. Soc. Rev., 2012, 41, 7537.

18. H. N. Miras, J. Yan, D. L. Long and L. Cronin, Chem. Soc. Rev., 2012, 41, 7403.

19. A. Proust, B. Matt, R. Villanneau, G. Guillemot, P. Gouzerh and G. Izzet, Chem. Soc. Rev., 2012, 41, 7605.

20. Y. F. Song and R. Tsunashima, Chem. Soc. Rev., 2012, 41, 7384.

21. P. C. Yin, D. Li and T. B. Liu, Chem. Soc. Rev., 2012, 41, 7368.

22. J. He, S. H. Li, Y. Q. Deng, H. Y. Fu, B. N. Laforteza, J. E. Spangler, A. Homs and J. Q. Yu, Science, 2014, 343, 1216.

23. S. N. Mlynarski, C. H. Schuster and J. P. Morken, Nature, 2014, 505, 386.

24. B. Hasenknopf, K. Micoine, E. Lacote, S. Thorimbert, M. Malacria and R. Thouvenot, Eur. J. Inorg. Chem., 2008, 5001.

25. W.-L. Chen, H.-Q. Tan and E.-B. Wang, J. Coord. Chem., 2012, 65, 1.

26. D. Y. Du, L. K. Yan, Z. M. Su, S. L. Li, Y. Q. Lan and E. B. Wang, Coord. Chem. Rev., 2013, 257, 702.

27. A. Dolbecq, E. Dumas, C. R. Mayer and P. Mialane, Chem. Rev., 2010, 110, 6009.

28. Z. H. Peng, Angew. Chem. Int. Ed., 2004, 43, 930.

29. D. L. Long, R. Tsunashima and L. Cronin, Angew. Chem. Int. Ed., 2010, 49, 1736.

30. A. Proust, R. Thouvenot and P. Gouzerh, Chem. Commun., 2008, 1837.

31. Y. Wei, P. Wu, Y. Wang and M. Shao, Nova Science Publishers, Inc., 2007, pp. 97.

32. Y. G. Wei, B. B. Xu, C. L. Barnes and Z. H. Peng, J. Am. Chem. Soc., 2001, 123, 4083.

33. Q. Li, Y. G. Wei, J. Hao, Y. L. Zhu and L. S. Wang, J. Am. Chem. Soc., 2007, 129, 5810.

34. J. Zhang, F. P. Xiao, J. Hao and Y. G. Wei, Dalton. Trans., 2012, 41, 3599.

35. S. C. Liu, S. N. Shaikh and J. Zubieta, Inorg. Chem., 1987, 26, 4303.

36. H. K. Kang, S. C. Liu, S. N. Shaikh, T. Nicholson and J. Zubieta, Inorg. Chem., 1989, 28, 920.

37. D. Hou, G. S. Kim, K. S. Hagen and C. L. Hill, Inorg. Chim. Acta, 1993, 211, 127.

38. M. I. Khan, Q. Chen and J. Zubieta, Chem. Commun., 1992, 305.

39. P. C. Yin, P. F. Wu, Z. C. Xiao, D. Li, E. Bitterlich, J. Zhang, P. Cheng, D. V. Vezenov, T. B. Liu and Y. G. Wei, Angew. Chem. Int. Ed., 2011, 50, 2521.

40. D. Li, J. Song, P. C. Yin, S. Simotwo, A. J. Bassler, Y. Y. Aung, J. E. Roberts, K. I. Hardcastle, C. L. Hill and T. B. Liu, J. Am. Chem. Soc., 2011, 133, 14010.

41. H. D. Zeng, G. R. Newkome and C. L. Hill, Angew. Chem. Int. Ed., 2000, 39, 1772.

42. C. P. Pradeep, M. F. Misdrahi, F. Y. Li, J. Zhang, L. Xu, D. L. Long, T. B. Liu and L. Cronin, Angew. Chem. Int. Ed., 2009, 48, 8309.

43. C. P. Pradeep, D. L. Long, G. N. Newton, Y. F. Song and L. Cronin, Angew. Chem. Int. Ed., 2008, 47, 4388.

44. C. Allain, S. Favette, L. M. Chamoreau, J. Vaissermann, L. Ruhlmann and B. Hasenknopf, Eur. J. Inorg. Chem., 2008, 3433.

45. B. Hasenknopf, R. Delmont, P. Herson and P. Gouzerh, Eur. J. Inorg. Chem., 2002, 1081.

46. P. F. Wu, P. C. Yin, J. Zhang, J. Hao, Z. C. Xiao and Y. G. Wei, Chem.-Eur. J., 2011, 17, 12002.

47. J. W. Zhang, Y. C. Huang, J. Zhang, S. She, J. Hao and Y. G. Wei, Dalton. Trans., 2014, 43, 2722.

48. C. Aronica, G. Chastanet, E. Zueva, S. A. Borshch, J. M. Clemente-Juan and D. Luneau, J. Am. Chem. Soc., 2008, 130, 2365.

49. S. Bareyt, S. Piligkos, B. Hasenknopf, P. Gouzerh, E. Lacote, S. Thorimbert and M. Malacria, J. Am. Chem. Soc., 2005, 127, 6788.

50. S. Bareyt, S. Piligkos, B. Hasenknopf, P. Gouzerh, E. Lacote, S. Thorimbert and M. Malacria, Angew. Chem. Int. Ed., 2003, 42, 3404.

51. I. Bar-Nahum, J. Ettedgui, L. Konstantinovski, V. Kogan and R. Neumann, Inorg. Chem., 2007, 46, 5798.

52. K. Micoine, B. Hasenknopf, S. Thorimbert, E. Lacote and M. Malacria, Org. Lett., 2007, 9, 3981.

53. C. Boglio, K. Micoine, E. Derat, R. Thouvenot, B. Hasenknopf, S. Thorimbert, E. Lacote and M. Malacria, J. Am. Chem. Soc., 2008, 130, 4553.

54. K. Micoine, M. Malacria, E. Lacote, S. Thorimbert and B. Hasenknopf, Eur. J. Inorg. Chem., 2013, 1737.

55. W. H. Knoth, J. Am. Chem. Soc., 1979, 101, 759.

56. P. Judeinstein, C. Deprun and L. Nadjo, J. Chem. Soc. Dalton. Trans., 1991, 1991.

57. E. V. Radkov and R. H. Beer, Inorg. Chim. Acta, 2000, 297, 191.

58. D. Agustin, C. Coelho, A. Mazeaud, P. Herson, A. Proust and R. Thouvenot, Z. Anorg. Allg. Chem., 2004, 630, 2049.

59. C. N. Kato, Y. Kasahara, K. Hayashi, A. Yamaguchi, T. Hasegawa and K. Nomiya, Eur. J. Inorg. Chem., 2006, 4834.

60. F. Bannani, R. Thouvenot and M. Debbabi, Eur. J. Inorg. Chem., 2007, 4357.

61. T. Hasegawa, K. Shimizu, H. Seki, H. Murakami, S. Yoshida, K. Yoza and K. Nomiya, Inorg. Chem. Commun., 2007, 10, 1140.

62. C. Cannizzo, C. R. Mayer, F. Secheresse and C. Larpent, Adv. Mater., 2005, 17, 2888.

63. D. Agustin, J. Dallery, C. Coelho, A. Proust and R. Thouvenot, J. Organomet. Chem., 2007, 692, 746.

64. W. Kwak, M. T. Pope and T. F. Scully, J. Am. Chem. Soc., 1975, 97, 5735.

65. J. K. Stalick and C. O. Quicksall, Inorg. Chem., 1976, 15, 1577.

66. M. P. Lowe, J. C. Lockhart, G. A. Forsyth, W. Clegg and K. A. Fraser, J. Chem. Soc. Dalton. Trans., 1995, 145.

67. M. P. Lowe, J. C. Lockhart, W. Clegg and K. A. Fraser, Angew. Chem. Int. Ed., 1994, 33, 451.

68. B. J. S. Johnson, R. C. Schroden, C. C. Zhu and A. Stein, Inorg. Chem., 2001, 40, 5972.

69. U. Kortz, M. G. Savelieff, F. Y. A. Ghali, L. M. Khalil, S. A. Maalouf and D. I. Sinno, Angew. Chem. Int. Ed., 2002, 41, 4070.

70. B. J. S. Johnson, R. C. Schroden, C. C. Zhu, V. G. Young and A. Stein, Inorg. Chem., 2002, 41, 2213.

71. U. Kortz, J. Vaissermann, R. Thouvenot and P. Gouzerh, Inorg. Chem., 2003, 42, 1135.

72. U. Kortz, C. Marquer, R. Thouvenot and M. Nierlich, Inorg.Chem., 2003, 42, 1158.

73. L. Xu, M. Lu, B. B. Xu, Y. G. Wei, Z. H. Peng and D. R.Powell,Angew. Chem. Int. Ed., 2002, 41, 4129.

74. L. K. Yan, G. C. Yang, W. Guan, Z. M. Su and R. S. Wang, J. Phys. Chem. B, 2005, 109, 22332.

75. Y. Xia, Y. G. Wei, Y. Wang and H. Y. Guo, Inorg. Chem., 2005, 44, 9823.

76. Y. Xia, P. F. Wu, Y. G. Wei, Y. Wang and H. Y. Guo, Crystal Growth & Design, 2006, 6, 253.

77. J. W. Zhang, J. Hao, R. N. N. Khan, J. Zhang and Y. G. Wei, Eur. J. Inorg. Chem., 2013, 1664.

78. J. Hao, Y. Xia, L. S. Wang, L. Ruhlmann, Y. L. Zhu, Q. Li, P. C. Yin, Y. G. Wei and H. Y. Guo, Angew. Chem. Int. Ed., 2008, 47, 2626.

79. T. R. Mohs, G. P. A. Yap, A. L. Rheingold and E. A. Maatta, Inorg. Chem., 1995, 34, 9.

80. Y. G. Wei, M. Lu, C. F. C. Cheung, C. L. Barnes and Z. H. Peng, Inorg. Chem., 2001, 40, 5489.

81. M. Lu, J. H. Kang, D. G. Wang and Z. H. Peng, Inorg. Chem., 2005, 44, 7711.

82. J. Zhang, J. Hao, Y. Wei, F. Xiao, P. Yin and L. Wang, J. Am. Chem. Soc., 2010, 132, 14.

83. F. P. Xiao, J. Hao, J. Zhang, C. L. Lv, P. C. Yin, L. S. Wang and Y. G. Wei, J. Am. Chem. Soc., 2010, 132, 5956.

84. C. L. Lv, R. N. N. Khan, J. Zhang, J. J. Hu, J. Hao and Y. G. Wei, Chem.-Eur. J., 2013, 19, 1174.

85. S. She, S. Bian, J. Hao, J. Zhang, J. Zhang and Y. Wei, Chem.-Eur. J., 2014, 20, 16987.

86. J. Zhang, P. C. Yin, J. Hao, F. P. Xiao, L. Y. Chen and Y. G. Wei, Chem.-Eur. J., 2012, 18, 13596.

87. A. Bayaguud, J. Zhang, R. N. N. Khan, J. Hao and Y. Wei, Chem. Commun., 2014, 50, 13150.

88. J. W. Zhang, Z. L. Zhao, J. Zhang, S. She, Y. C. Huang and Y. G. Wei, Dalton. Trans., 2014, 43, 17296.

89. J. Zhang, J. Luo, P. Wang, B. Ding, Y. Huang, Z. Zhao, J. Zhang and Y. Wei, Inorg. Chem., 2015, 54, 2551.

90. J. W. Zhang, Z. H. Liu, Y. C. Huang, J. Zhang, J. Hao and Y. G. Wei, Chem. Commun., 2015, 51, 9097.

91. S. T. Zheng, J. Zhang, X. X. Li, W. H. Fang and G. Y. Yang, J. Am. Chem. Soc., 2010, 132, 15102.

Advances in Chemical Engineering

Chapter 2

Ultrasonic Assisted Heat Transfer and its Application in Chemical Engineering

Saravanathamizhan R[1]*; Perarasu V T[1]

[1]Department of Chemical Engineering, A.C.Tech., Anna University, Chennai-600025, India.

*[*]**Correspondence to: Saravanathamizhan R,** Department of Chemical Engineering, A.C.Tech., Anna University, Chennai-600025, India.*

Email: rsthamizhan@gmail.com

1. Introduction

Sonochemistry is considered to be a general technique like thermo chemistry (heat) and piezochemistry (pressure). The sound frequency which is higher than 16 kHz is called as ultrasound. Some animals utilize ultrasound for navigation (dolphins) or hunting (bats) using the information carried by back-scattering sound waves. Ultrasound is one of the emerging technologies that were developed to minimize processing, maximize quality and ensure the safety of food products. The ultrasound and cavitational effects were found 100 years before. The cavitation was first reported by Thornycroft and Barnaby in 1895 [1]. They noticed that the propeller of the submarine was pitted and eroded. They observed the consequence of collapsing bubbles due to hydrodynamic cavitation that generated intense pressure and temperature gradients in the local vicinity. In 1917, Lord Rayleigh [2] published the first mathematical model describing a cavitation event in an incompressible fluid. After 1927, when Richards and Loomis [3] reported the first chemical and biological effects of ultrasound, the workers recognised that cavitation could be an useful tool in chemical reaction processes. One of the first applications reported in the literature was the use of ultrasound induced cavitation to degrade a biological polymer [4]. Since then, applications of ultrasound induced cavitation have increased in popularity, particularly as novel alternatives to processes such as the production of polymer [5], for the enhancement of chemical reactions [6], emulsification of oils [7] and degradation of chemical or biological pollutants [8]. The advantage of using acoustic cavitation for these applications is that much more mild operating conditions are utilized in comparison to conventional techniques and many reactions which may require toxic reagents or solvents are not necessary [9].

Ultrasound induced cavitation is an extremely useful and versatile tool to carry out chemical reactions. Sonochemistry refers to the area of chemistry where chemical reactions are induced by sound. Sonication is also useful in Nanomaterial synthesis, shear and mechanical mixing, medical applications, food industry and Sonochemical degradation of pollutants. Ultrasound is also helpful to improve and enhance the efficiency of the process. Enhance the chemical reaction, mass transfer and heat transfer process such as drying, mixing etc [10-12]. Some of the potential application of ultrasound where it finds vital role are listed below [13].

Table 1: Application of ultrasound

S. No	Application	Examples
1	Machining of materials	Welding; cutting; drilling; soldering
2	Cleaning	General surface cleaning; washing of soil and ores
3	Homogenization / Spraying	Emulsification and atomization of liquids
4	Separation	Crystallization; sieving; filtration
5	Degassing	Treatment of HPLC eluents
6	Water treatment	Removal of chemical and biological pollution
7	Biological uses	Cell disruption
8	Medical uses	Dental descaling; scalpels; lithotripsy; HIFU; preparation of protein microspheres; nebulizers

Heat transfer enhancement is an important area of thermal engineering. Although it is understood that ultrasound can enhance the heat transfer in the thermal system. The heat transfer can be increased by the passive or active methods. Passive method consists of roughing the tube inner surface, inserting the swirl-flow devices into the tube, and adding the solid-particles into the fluid. Traditional active method is the application of mechanical aids, vibration, and electrostatic fields on the tube. Imposing acoustic vibration onto a liquid pool has been proven to enhance natural convection and boiling heat transfer for several decades. In acoustic vibration the frequency is ranging from 20Hz to 20kHz, but in the ultrasound, the frequency is above 20kHz.

F and [14] and Li and Parker [15] reported enhancement of natural convection heat transfer by virtue of ultrasonic waves. Wong and Chon [16] and Iida and Tsutsui [17] investigated the effects of ultrasonic vibration on pool boiling heat transfer as well as natural convection heat transfer. They found that the natural convection heat transfer is enhanced more than pool boiling by ultrasonic vibration. Park and Bergles [18] and Bonekamp and Bier [19] studied the influence of ultrasound on nucleate boiling heat transfer, to find that the stronger enhancement is achieved at lower heat fluxes. Yamashiro et al. [20] showed enhanced quenching behavior for a hot wire in water when ultrasonic vibration is imposed.

The article focused overview of ultrasound and particularly attempted to influence of heat transfer processes and its application in chemical engineering field. The recent adaptation of ultrasonic technologies to heat exchanger devices is discussed thoroughly, with examples

drawn from new patents and current laboratory work.

2. Cavitation

Generally, cavitation is classified into four types based on the mode of its generation: Acoustic cavitation; Hydrodynamic cavitation; Optic cavitation; Particle cavitation [21,22].

2.1. Acoustic cavitation

The main effects of ultrasonication in liquids are acoustic cavitation and acoustic streaming. In the acoustic cavitation, the sound energy creates the bubble and sudden collapse of this bubble under ultrasonic irradiations which can release high amount of energy in a small location. Ultrasound occurs at a frequency above 16 kHz, higher than the audible frequency of the human ear and is typically associated with the frequency range of 20 kHz to 500 MHz. Cavitation can be generated within fluid using transducers, which convert one form of energy to another. In addition to this phenomenon, propagation of ultrasonic waves in the liquid medium generates local turbulence and micro-circulation in liquid which is known as acoustic streaming. Acoustic streaming can mainly cause physical effects and also influence chemical processing limited by mass transfer.

2.2. Hydrodynamic cavitation

Cavitation can also be generated by forcing the fluid through an orifice, resulting in a pressure drop in the fluid. When the pressure falls below that of the vapor pressure of the fluid stream, cavitation sites are created. The magnitude of the pressure drop is dependent upon the flow rate of the fluid and the size of the orifice. Usually it occurs in ship propellers, pumps, turbines, hydrofoils and nozzles. For most cases, cavitation can cause severe damage to the materials and should be avoided in hydraulic machinery. If the cavitation phenomenon occurs in the centrifugal pump, it can damage the pump.

2.3. Optic cavitation

When the medium is radiated by high-intensity of laser pulses optic cavitation is occurred. Under this condition break down of liquid medium and bubbles are formed. High speed camera is used to record the single and multiple bubbles formed during the behavior.

2.4. Particle cavitation

In addition to photons in optic cavitation, other elementary particles such as protons, neutrons can also be generating the cavitation bubbles. A small fraction of medium will be ionized and rapidly heated when the high energy particle pass through the medium results in the formation of tiny bubbles.

3. Types of Sonoreactors

3.1. Ultrasonic bath

In bath type sonicator is shown in the figure1, the transducers are located at the bottom of the reactor and the ultrasound irradiations transmit into the system indirectly. Bath systems are widely used in sonochemical research because they are readily available and relatively inexpensive. Generally, bath type sonicator should be used where a specific power number or ultrasonic intensity is not required, because ultrasonic power does not change in this type of reactors. It is not easy to obtain a uniform distribution of ultrasonic energy with ultrasonic bath and use of more than one transducer is mandatory for large scale applications [23,24].

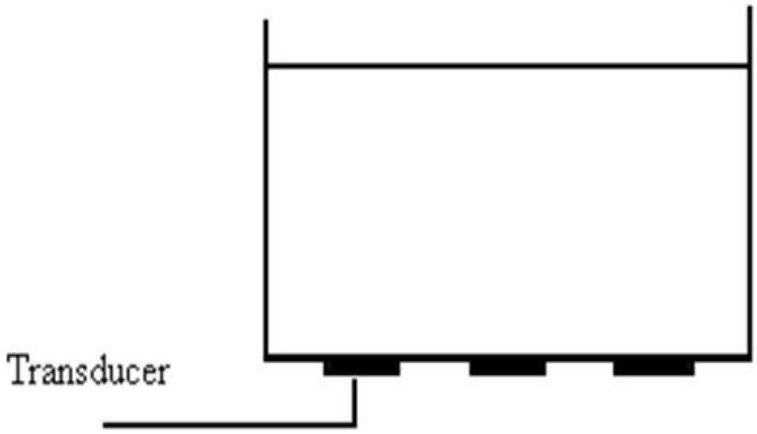

Figure 1: Bath type sonicator

3.2. Ultrasonic horn

In ultrasonic horn or probe type (**figure 2a**) consist of cylindrical probe which submerges in the liquid and transmits the wave in to the medium directly. The horn is usually made of transition metals such as titanium which has the diameter range between 5mm and 1.5cm. In the probe type, erosion and pitting of the probe tip may contaminate the solution medium. Ultrasonic horn is applied in many experimental studies such as micromixing, transesterification of biodiesel, saccharification, microfiltration, etc. Ultrasonic horn can also be used longitudinally in the vessel for different applications. The longitudinal horns usually have higher surface area of irradiation in the medium and the magnitude of energy efficiency in this type of ultrasonic is higher than the convention alone . Furthermore, the large irradiation area of longitudinal ultrasonic horn (**figure 2b**)leads to uniform distribution of cavitational activity in the whole reactor volume which can be more beneficial in pilot scale in comparison with simple ultrasonic horn [23,25].

3.3. Low power and high power ultrasound

The power is inversely proportional to frequency of the sonication. There are two category, “low frequency ultrasound” or “power ultrasound” and “high frequency ultrasound” or “low power ultrasound”. Ultrsound waves between 20 kHz to 100 kHz, are defined as “low frequency ultrsound”; between 100 kHz–1MHz, waves are defined as “high frequency

ultrasound". Low-frequency ultrasound does alter the state of the medium and is the type of ultrasound typically used for sonochemical applications. High frequency ultrasound (in the megahertz range) does not alter the state of the medium through which it travels and is commonly used for nondestructive evaluation and medical diagnosis. **Figure 3** shows some typical uses of ultrasound according to frequency and power [26].

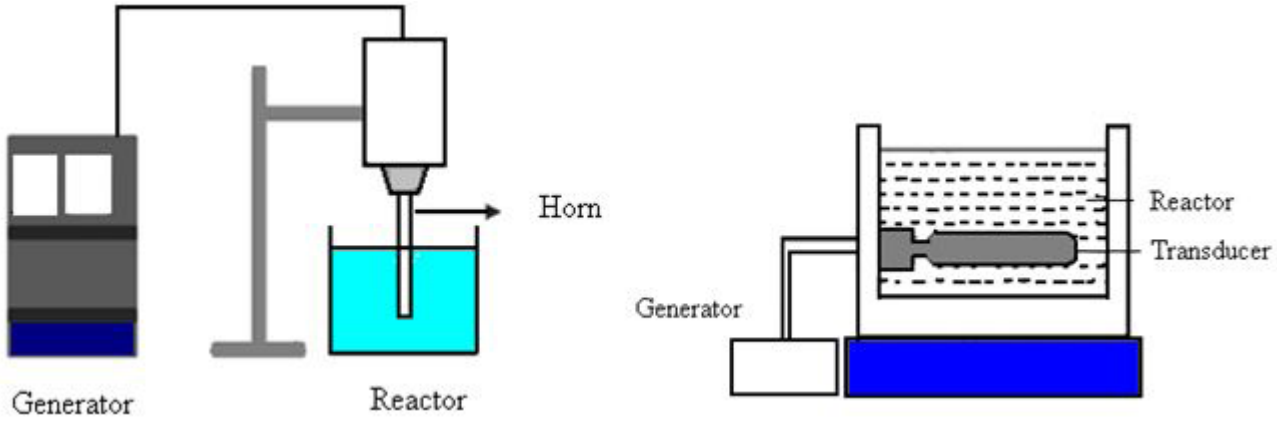

Figure 2: (a) Probe type sonicator (b) longitudinal horns

3.3. Low power and high power ultrasound

The power is inversely proportional to frequency of the sonication. There are two category, "low frequency ultrasound" or "power ultrasound" and "high frequency ultrasound" or "low power ultrasound". Ultrsound waves between 20 kHz to 100 kHz, are defined as "low frequency ultrsound"; between 100 kHz–1MHz, waves are defined as "high frequency ultrasound". Low-frequency ultrasound does alter the state of the medium and is the type of ultrasound typically used for sonochemical applications. High frequency ultrasound (in the megahertz range) does not alter the state of the medium through which it travels and is commonly used for nondestructive evaluation and medical diagnosis. Figure 3 shows some typical uses of ultrasound according to frequency and power [26].

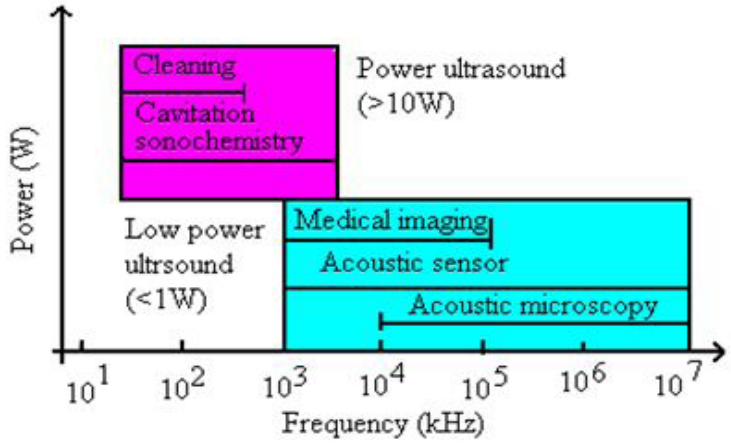

Figure 3: Power versus frequency

3.4. Acoustic power measurement

Several methods are available to determine the acoustic power dissipated to the system by sonication. The most commonly used approach to determine the ultrasonic power is calorimetry, which assumes that all of the energy delivered to the system is dissipated as heat, as

shown by equation (1) [27].

$$P_{diss} = \left(\frac{dT}{dt}\right)_{t=0} m_{solvent} C_{P,solvent} \quad (1)$$

$m_{solvent}$ $Cp_{solvent}$ are the mass and heat capacity of the solvent, respectively, and $\left(\frac{dT}{dt}\right)_{t=0}$ is the initial slope of the temperature rise of the solution versus time of exposure to ultrasonic irradiation. The initial temperature rise of the system is independent of the initial bulk liquid temperature. Equation (1) is used to estimate the power dissipated in the reaction system and it is found it to be inadequate. It predicted that only 33% of the power delivered by the transducer was dissipated as heat, which would indicate that the other 67% of the power was lost in the transfer process, or by other means. Hence that the Equation (1) needed to be modified to account for the heat absorbed by the vessel as well as the solvent, as shown by equation (2)

$$P_{diss} = \left(\frac{dT}{dt}\right)_{t=0} (m_{solvent} C_{P,solvent}) + \left(\frac{dT_v}{dt}\right)_{t=0} (A_{WS} X_W) \rho_{Vessel} C_{P,Vessel} \quad (2)$$

where T_v is the temperature of the inner vessel wall, A_{ws} is the area of the wetted surface of the vessel, and X_w is the thickness of the inner wall. This provides a much more reasonable result. It was found that 51.5% of the power delivered by the probe was dissipated as heat, more closely agreeing with the manufacturer's information. The other methods to determine the power dissipated in a reaction system are by using chemical dosimeters (such as the generation of HNO_3 from NO_3 in water) and the Weissler reaction (which measures the liberation of iodine from potassium iodide). The comparison of calorimetry and the Weissler reaction as measures of ultrasonic power showed that the two methods provided similar predictions.

4. Enhancement of Heat Transfer Rate

Heat transfer processes has broad application in processing industries like chemical, gas, oil and food industries and also in the functioning of various devices and systems. In a wide variety of situations, heat transfer principles are used to increase, decrease or preserve temperature to achieve desired process at a controlled rate. The enhancement of heating or cooling in an industrial process may save energy, reduce process time, raise the thermal rating and lengthen the working life of equipment. Thus, the advent of high heat flow processes has created significant demand for new technologies to enhance heat transfer [28,29].

There are three methods widely used to increase the rate of heat transfer. The methods are (1) active method (2) Passive method (3) combined method. Following three methods are discussed in detail [30-32].

4.1. Active method

In the active method, some external power input enhances the heat transfer rate. The active method including mechanicals aids, surface vibration, fluid vibration, electrostatic fields, suction or injection and jet impingement requires an external activator/power supply to bring about the enhancement.

Mechanical aids: Stirring or agitating of the fluid by means of mechanical force to increase the heat transfer rate. Generally used for viscous liquids in the chemical process industry.

Surface vibration: High or low frequency surface vibration has been used to increase the single-phase heat transfer. In this case a piezoelectric device is used to vibrate a surface to enhance the heat transfer rate.

Fluid vibration: It is more practical type of vibration enhancement because of the mass of most heat exchangers. The vibrations range from pulsations of about 1 Hz to ultrasound. Single phase fluids are of primary concern. They are applied in many different ways to dielectric fluids. Electrostatic fields : Can be directed to cause greater bulk mixing of fluid in the vicinity of the heat transfer surface.

Injection: It is utilized by supplying gas through a porous heat transfer surface to a flow of liquid or by injecting the same liquid upstream of the heat transfer section. The injected gas augments single-phase flow. Surface degassing of liquids may produce similar effects.

Suction: It involves vapor removal, in nucleate or film boiling, or fluid withdrawal in single phase flow through a porous heated surface.

Jet impingement: It forces a single-phase fluid normally or obliquely toward the surface. Single or multiple jets may be used and boiling is possible with liquids.

4.2. Passive method

This method generally uses surface or geometrical modifications to the flow channel by incorporating inserts or additional devices. For example, inserts extra component, swirl flow devices, treated surface, rough surfaces, extended surfaces, displaced enhancement devices, coiled tubes, surface tension devices and additives for fluids.

Coated surfaces: They involve metallic or nonmetallic coating of the surface. Examples include a nonwetting coating, such as Teflon, to promote drop wise condensation, or a hydrophilic coating that promotes condensate drainage on evaporator fins, which reduces the wet air pressure drop. A fine-scale porous coating may be used to enhance nucleate boiling.

Swirl flow devices: They produce and super impose swirl flow or secondary recirculation on the axial flow in a channel. These devices include helical strip or cored screw type tube inserts, twisted tapes .They can be used for single phase or two-phase flow heat exchanger.

Treated Surfaces: They are heat transfer surfaces that have a fine-scale alteration to their finish or coating. The alteration could be continuous or discontinuous, where the roughness is much smaller than what affects single-phase heat transfer, and they are used primarily for boiling and condensing duties.

Rough surfaces: They are generally surface modifications that promote turbulence in the flow field, primarily in single-phase flows, and do not increase the heat transfer surface area. Their geometric features range from randoms and-grain roughness to discrete three-dimensional surface protuberances

Extended surfaces: They provide effective heat transfer enlargement. The newer developments have led to modified fin surfaces that also tend to improve the heat transfer coefficients by disturbing the flow field in addition to increasing the surface area.

Displaced enhancement devices: These are the insert techniques that are used primarily in confined force convection. These devices improve the energy transfer indirectly at the heat exchange surface by displacing the fluid from the heated or cooled surface of the duct/pipe with bulk fluid to the core flow.

Coiled tubes: These techniques are suitable for relatively more compact heat exchangers. Coiled tubes produce secondary flows and vortices which promote higher heat transfer coefficient in single phase flow as well as in most boiling regions. Surface tension devices: These consist of wicking or grooved surfaces, which directly improve the boiling and condensing surface. These devices are mostly used for heat exchanger occurring phase transformation.

Additives for liquids: These include the addition of solid particles, soluble trace additives and gas bubbles into single phase flows and trace additives which usually depress the surface tension of the liquid for boiling systems. Additives for gases: These include liquid droplet or solid particles, which are in traduced in single-phase gas flows either as dilute phase (gas–solid suspensions) or as dense phase (fluidized beds).

4.3. Compound method

Combination of the above two methods, such as rough surface with a twisted tape swirl flow device, or rough surface with fluid vibration, rough surface with twisted tapes .

Among the new possible technologies as discussed above, that could be developed and optimized in order to improve heat transfer processes, the use of ultrasonic waves appears to be one of the most recent and new sustainable technical solutions in the recent years [33].

5. Enhancement of Heat Transfer by Ultrasound

In recent years, ultrasound technology has been used as an alternative processing option

to conventional thermal approaches.

Ultrasound has several applications in engineering industries such as improving systems efficiencies, intensifying chemical reactions, drying, welding, and cleaning etc. An analogous observation can be made for heat transfer processes, which are omnipresent in the industry: cooling applications, heat exchangers, temperature control etc. [26]. This chapter details the use of ultrasonication with special attention on enhancement of heat transfer applications in Chemical Engineering.

5.1. Factors affecting the ultrasonic assisted heat transfer

The various factors that affect the ultrasonic assisted heat transfer [34] are given below.

5.1.1. Influence of ultrasound power

The ultrasonic transducer can produce different power levels of ultrasound with 21 kHz in frequency. Experimental Study on Heat Transfer Enhancement of Water-water Shell-and-Tube Heat Exchanger three power levels, i.e. 40W, 60W and 100W, were used. High-intensity ultrasound can induce cavitation bubbles and acoustic streaming in liquid, which makes it possible for power ultrasonic to be applied to the improvement of heat transfer process. In the present work, the experimental study was made on the heat transfer enhancement of water-water heat exchanger in shell-and-tube type assisted by power ultrasonic. An experimental study shows that the power level of 40W brings about 3% enhancement whereas the power level increases to 60 and 100 W, the enhanced ratio increases to 13% and 17% respectively [34]. It is supposed that the enhanced ratio would further increase if the higher ultrasound power level was applied.

5.1.2. Influence of velocity of liquid

The heat transfer rate is influenced by flow rate of fluid passing through the heat exchanger. It is clear that the heat transfer has an obvious increase after 100W ultrasound is emitted into the heat exchanger. Different flow behavior leads to different degree of heat transfer enhancement. The heat transfer rate increases with increase in liquid flow rate. This is due to that the cavitation bubbles and acoustic streaming induced by the ultrasound in liquid will increase the turbulence degree of movement of fluid, which is equivalent to increasing the fluid velocity. Therefore, it is reasonable to suppose that the effect of ultrasound on the heat transfer would increase with the decreasing flow rate.

5.1.3. Influence of inlet temperature of the fluid

Although the water temperature produces little effect on the heat transfer coefficient,

it may influence the efficiency of heat transfer. The phenomenon may be explained by the relationship between the acoustic cavitation and the liquid temperature. As mentioned above, cavitation induced by the ultrasound is the main force that intensifies the turbulence of fluid. Therefore, maximizing cavitation of the liquid is obviously very important for ultrasound to enhance the heat transfer process. Temperature may be the most important parameter to be considered in maximizing cavitation intensity. This is because many liquid properties affecting cavitation intensity are related to temperature, such as the viscosity, the solubility of gas in the liquid, and the vapor pressure. Increasing liquid temperature, on one hand, will decrease viscosity of liquid and make it easier to form cavitation bubbles, on the other hand, will be adverse to the formation of acoustic cavitation because of the reduction of dissolved gas in the liquid and the rising of vapor pressure required.

5.2. Application of ultrasonication in heat transfer studies

5.2.1. Preparation of nanofluids

Nanofluids have been considered in various applications as advanced heat transfer fluids for almost two decades. Nanofluids are a new class of fluids engineered by dispersing nanometer-sized materials (nanoparticles, nanofibers, nanotubes, nanowires, nanorods, nanosheet, or droplets) in base fluids. Base fluids mostly used in the preparation of nanofluids are the common working fluids of heat transfer applications; such as, water, ethylene glycol and engine oil. In order to improve the stability of nanoparticles inside the base fluid, some additives are added to the mixture in small amounts. Nanofluids have been found to possess enhanced thermo physical properties such as thermal conductivity, thermal diffusivity, viscosity, and convective heat transfer coefficients compared to those of base fluids like oil or water.

Generally, a preparation of nanofluids is an important step in experiments on nanofluids. To achieve a stable nanofluid that exhibits true nano behavior, the particles should be dispersed with no or very little agglomeration. There are mainly two methods of nanofluid production, namely, two-step technique and one-step technique. In the one-step technique, production and dispersion of nanoparticles is carried out simultaneously. In the two-step technique, the first step is the production of nanoparticles and the second step is the dispersion of the nanoparticles in a base fluid. Two-step technique has advantageous when mass production of nanofluids is considered.

The dispersion of the nanoparticles is achieved with the help of any one of the following technologies, intensive magnetic force agitation, ultrasonic agitation, high-shear mixing and homogenizing. Due to the high surface area and surface activity, nanoparticles have the tendency to aggregate. Out of various methods of dispersion described above, the most commonly used technique is ultrasonication.

The heat transfer intensification studies with the use of nanofluids have captured significant attention of researchers across the globe in recent years. Though it is still completely unexplored, there are several works published and continuing in exponential way. In almost all the reported works, the mechanism used for dispersing the nanopowders into base fluids is by ultrasonication.

5.2.2. Heat transfer with phase change

Boiling heat transfer in the presence of an ultrasonic field is described apart for being a very active research field. ultrasound allows improvement of boiling heat transfer almost systematically. The first bubbles appearing in the nucleation sites are swept away by the vibrations, and the apparition of film boiling is therefore delayed so that higher heat fluxes are reached. According to several authors, this is still due to acoustic cavitation, which helps the creation and growth of the bubbles, whereas their oscillations enable to create micro streaming and local agitation near the surfaces to sweep them away [3538].

Power ultrasound is a method to reduce the size of ice crystals on the frozen products and gain in quality [39]. This leads to finest ice crystals and shortens the time between the onset of crystallization and the complete formation of ice, mainly due to acoustic cavitation. Birth of nucleation sites, micro streaming, and some cleaning action of heat exchangers are among the subsequent advantages. Besides, ultrasound is a nonintrusive technique. Comprehensive reviews of the uses of ultrasound in food technology exist [40,41], with many examples of processing, crystallization, and freezing. The freezing temperature of supercooled water can also be controlled by ultrasonic vibrations to make ice slurry, a solid-liquid mixture very interesting to store and transport cold thermal energy. The probability of phase change is increased with the total number of cavitation bubbles, acting as nuclei for solidification inception [42,43].

Ultrasonic technologies have also gaining significant attention in food industry. Food drying is one of the best examples. If there is a good acoustic match between the transducer and the food material, ultrasonic vibrations can be directly applied to the material to be dried [44,45]. This can produce a sponge effect, contraction and expansion cycles, leading to a better drying result. The effect is much more pronounced for very porous products [46], which is why the porosity of the product to be dried is an important parameter to take into account before applying ultrasonic waves. Power ultrasound mainly affects the external thermal resistance. If the transducer is not in contact with the material and ultrasound is air-borne, it is reported that high air flow rate may introduce modifications in the acoustic field, decreasing also the acoustic energy transmitted to the medium.

5.2.3. Enrichment of convection

Convection is also one of the most studied modes of heat transfer like boiling under the

influence of ultrasonic vibrations. Increases in heat transfer coefficients up to 25 times are reported [47]. When dealing with convection, it is crucial to observe that ultrasound can be considered as an “external help” to heat transfer. Therefore, it is interesting to wonder if it is not more appropriate to speak of forced convection rather than free convection when ultrasound is turned on.

Bergles [48] made a survey on the techniques to enhance heat transfer with ultrasonic vibrations. He reported that authors generally found significant increases in nonboiling heat transfer at moderate flow velocity. Improvements were clearly related to cavitation, reported not to be as effective as established boiling. The main restriction came from the attenuation of the ultrasonic energy by the vapour and the difficulties to locate the transducer so as to obtain good coupling with the fluid and suffer minimum attenuation, also reported in [49].

Kiani et al [50] have experimentally observed that, ultrasound irradiation was able to enhance the cooling process of a stationary sphere immersed in the cooling medium significantly and resulted in increased heat transfer rates. They have identified that, increasing the intensity of ultrasound led to the increase in the cooling rate. Enhancement factors from 1.02 to 4 were detected for different intensities and sphere locations. According to them, the position of the sphere played an important role during the ultrasound assisted cooling due to the position-related cavitation bubble population and acoustic streaming patterns. Closer distances to the transducer surface showed higher cooling rates. Concentrated cavitation bubbles at the interfaces were the main reason for the heating effect of ultrasound. They have developed an analytical solution for the ultrasound assisted heat transfer with regards to the heat generation at the surface.

5.2.4. Use in Heat Exchangers

One of the first studies was carried out by Kurbanov and Melkumov in 2003 [51]. They explained comprehensively why ultrasonic vibrations are very well suited to increase performances of liquid to liquid heat exchangers. According to them, acoustic waves homogenize the velocity vectors of the sub flows in pipes and decrease the surface tension of the fluid near the boundaries. The latter phenomenon is even more interesting if a thin film of lubricant is stuck to the pipes surfaces, which usually happens in refrigeration systems. This thin film induces a thermal resistance and its removal is very interesting for performance improvement.

Microstructured heat exchangers show significant advantages in comparison with conventional heat exchangers. But, they are prone to fouling very easily. Benzinger et al [52] studied and exemplified that the use of ultrasound is a useful supplement of micro heat exchangers. Micro heat exchangers could be used for the heating of substances which show a higher tendency of fouling. The combination of micro heat exchanger and ultrasound presents a development, which should improve the performance characteristic. Their investigations indicated

that the use of ultrasonic power influences the fouling and opens up possibilities todiminish the fouling in microchannels significantly.

Monnot et al [53] experimentally and analytically analysed the cooling of sonochemical reactors by cold water flowing into a coil, The cooling time of a certain amount of water, stored in the chemical reactor, was compared with and without high-frequency ultrasonic vibrations. The convection coefficient was enhanced between 135 and 204% in the presence of acoustic waves, reducing effectively the cooling time. Their observation in improvement was explained in terms of overall agitation due to the combined effects of local mixing (acoustic cavitation) and global fluid motion within the reactor (acoustic streaming).

A shell-and-tube configuration for a fluid-to-fluid vibrating heat exchanger was built and studied by Gondrexon et al [54]. The ratio between the overall heat transfer coefficient with ultrasound and the one without ultrasound for this shell-and-tube heat exchanger was calculated and found ranging from 1.2 up to 2.6 depending on the liquid flow rate at the shell side. The ultrasonic power had negligible influence on the heat exchange rate and the overall heat transfer coefficient was always higher with ultrasound than without, whatever the liquid flow rates or range of temperatures tested. Further investigations on the same system showed that higher improvements could be expected, especially for slow laminar flows in the shell.

Legay et al [55] designed, built and studied a new kind of ultrasonically-assisted vibrating heat exchanger. They demonstrated that ultrasound can be used efficiently as a heat transfer enhancement technique, even in such complex systems as heat exchangers. Overall heat transfer coefficients were determined with and without ultrasound. Their results showed that, whatever the heat exchanger flow configurations, the overall heat transfer coefficients in the presence of ultrasound are higher than under silent conditions. It was assumed that the conduction thermal resistance through the thickness of the internal pipe and that the convection thermal resistance inside the internal pipe are not affected by ultrasonic waves. Hence, they have concluded that only the convection thermal resistance in the annular space was decreased, leading to an enhanced exchanged heat flow rate. It is considered that physical effects induced by cavitation as well as vibrations of the walls result in a disturbance of the dynamic boundary layer. They strongly concluded that, ultrasound is an interesting way to improve heat exchanger performances.

Legay et al [56] investigated the potential use of ultrasonic waves directly applied to a heat exchanger structure in order to clean some fouling layers. The heat exchanger was a double pipe configuration in which the central pipe is removable. Glass and stainless steel central pipes were tested after being painted with spraying paint to simulate some fouling layers. After ultrasound exposure at minimal available power, almost all paint can be removed from the zone subjected to structure vibrations. The cleaning process starts at the antinodes

of the ultrasonic wave and expands to all the vibrating length. They claimed that the results were very encouraging since the fouling layers can be removed both from the external side of the pipe and, with more difficulties, from the internal side. Therefore, the overall heat transfer coefficient, previously decreased by the thermal resistance of the paint thickness, was found again up to its initial value, corresponding to that of a clean tube.

5.2.5. Some other advantages of sonication

Sonication in a process offers several subsequent advantages and few of its significant advantages are listed below

- Another important phenomenon resulting from ultrasonic vibrations application is surface cleaning (due to acoustic cavitation). This is very important because it could be part of a solution to reduce the natural fouling process in heat exchangers. Indeed, the environmental conditions in such devices make them prone to corrosion or microorganisms deposition. They induce additional thermal resistances which prevent the system from operating in optimal conditions, adding environmental and economical costs.

- Ultrasound is efficient to reduce hysteresis effect, which is the tendency of a system to remain in its initial state in spite of the cause supposed to produce a change.

- Ultrasonic vibrations could be interesting to achieve a complete activation of nucleation sites in large evaporators with extended surfaces, normally reached with a sufficiently high heat flux.

- Biofouling control is a possible application of ultrasound, that is, the prevention of microorganism growth (algae, fungi, bacteria) on surfaces by application of ultrasonic vibrations.

6. Conclusion

Earlier during 20th century, although researches shows ultrasound can play an important role in process industries, lack of knowledge keeps industry from implementing ultrasound in their processes. A recent survey and market study of the possible future applications of new process technologies (like microwave, ultrasound) in the process industries has revealed that many companies are reluctant to apply these new technologies due to poor understanding of these new techniques by professionals. Recently, that is during the last decade, ultrasound has gained a growing interest from industry, resulting in the development of several specific applications. Ultrasonic waves appear as an interesting way to improve processes productivity especially to overcome transfer limitations.

For heat transfer applications, ultrasound can also be regarded as a possible technical

solution for heat exchange enhancement. Hence, a lot of publications dealing with fundamental studies can be found in the literature. But most of these works are performed at the laboratory scale involving academic setups and usually using classical low frequency ultrasound. Several well-known factors responsible for heat transfer improvement such as acoustic cavitation, acoustic streaming, and fluid particles oscillations were observed by researchers. But, it is also very important to note here that it is very difficult to distinguish the influence of these effects since they often occur simultaneously. Literatures demonstrate that the local heat transfer coefficient was shown to be multiplied between 2 and 5 times in the presence of an ultrasonic field. Phase change heat transfer also covers a great number of studies that shows the beneficial effect of ultrasound on boiling as well as melting or solidification. A more recent research field that focuses on heat exchangers has shown that the use of ultrasonic waves can improve overall performances regarding heat transfer and/or fouling [26].

Overall, it can be concluded that ultrasonication have significant potential for chemical process intensification [57]. But, the scale up of the ultrasonic technology to pilot or industrial scale heat exchangers has not been yet deeply investigated. The combined efforts of the involved stake holders including chemists, material scientists, chemical engineers and instrumentation/electrical engineers would be required to translate the small scale marvel into commercial scale realization

7. References

1. J. Thorneycroft and S.W. Barnaby, “Torpedo-boat destroyers”, Inst. Civil Eng., 1895; 122: 51-69.

2. L. Rayleigh, “On the pressure developed in a liquid during the collapse of a spherical cavity”, PMag, 1917; 34: 94-98

3. W.T. Richards and A.L. Loomis, “The chemical effects of high frequency sound waves I. A preliminary survey”, J. Am. Chem.Soc., 1927; 49: 3086-3100

4. S. Brohult, “Splitting of the haemocyanin molecule by ultrasonic waves”, Nature, 1937; 140: 805

5. B.M. Teo, M. Ashokkumar and F. Grieser, “Microemulsion polymerizations via high-frequency ultrasound irradiation”, J.Phys. Chem. B., 2008; 112: 5265-5267.

6. K.S. Suslick, J.W. Goodale, P.F. Schubert and H.H. Wang, “Sonochemistry and sonocatalysis of metal-carbonyls”, J. Am. Chem. Soc., 1983; 105: 5781-5785.

7. T.S.H. Leong, T.J. Wooster, S.E. Kentish and M. Ashok kumar, “Minimising oil droplet size using ultrasonic emulsification”, Ultrason. Sonochem., 2009; 16: 721-727.

8. R. Singla, M. Ashokkumar and F. Grieser, “The mechanism of the sonochemical degradation of benzoic acid in aqueous solutions”, Res. Chem. Intermed., 2004; 30:723-733.

9. Thomas Leong, Muthupandian, Ashokkumar and Sandra Kentish, “The Fundamentals Of Power Ultrasound – A Review”, Acoustics Australia, 2011; 39: 54-63.

10. M. Ashokkumar, “Applications of ultrasound in food and bioprocessing”, UltrasonicsSonochemistry, 2015; 25: 17.

11. K.P. Gopinath, K. Muthukumar, M. Velan, “Sonochemical degradation of Congo red: optimization through response surface methodology ”, Chemical engineering journal, 2009; 157: 427-433.

12. A. Monnot, P. Boldo, N. Gondrexon, A. Bontemps, “Enhancement of Cooling Rate by Means of High Frequency Ultrasound”, Heat Transfer Engineering, 2007; 28: 3–8.

13. J.Timothy , Mason and Dietmar Peters, “Practical Sonochemistry, Power Ultrasound Uses and Applications”, 2nd Edition, Horwood Publishing Series in Chemical Sciences, (2004).

14. R.M. Fand, “The influence of acoustic vibrations on heat transfer by natural convection from a horizontal cylinder to water”, J. Heat Transfer, 1965; 87: 309–310.

15. K.W. Li, J.D. Parker, “Acoustical effects on free convective heat transfer from a horizontal wire”, J. Heat Transfer, 1967; 89: 277–278.

16. S.W. Wong, W.Y. Chon, “Effects of ultrasonic vibration on heat transfer to liquids by natural convection and by boiling”, AlChE J., 1969; 15: 281–288.

17. Y. Iida, K. Tsutsui, “Effects of ultrasonic waves on natural convection, nucleate boiling and film boiling heat transfer from a wire to a saturated liquid”, Exp. Thermal Fluid Sci., 1992; 5: 108–115.

18. K.A. Park, A.E. Bergles, “Ultrasonic enhancement of saturated and subcooled pool boiling”, Int. J. Heat Mass Transfer, 1988; 31: 664–667.

19. S. Bonekamp, K. Bier, “Influence of ultrasound on pool boiling heat transfer to mixtures of the refrigerants R23 and R134A”, Int. J. Refrig., 1997; 20: 606–615.

20. H. Yamashiro, H. Kakamatsu, H. Honda, “Effect of ultrasonic vibration on transient boiling heat transfer during rapid quenching of a thin wire in water”, J. Heat Transfer, 1998; 120: 282–286.

21. P. R. Gogate, “Cavitation: an auxiliary technique in wastewater, treatment schemes” Advances in Environmental Research, 2002; 6: 335-358.

22. P. R. Gogate, “Cavitational reactors for process intensification of chemical processing applications: A critical review”, Chemical Engineering and Processing, 2008; 47: 515–527.

23. S. Ali, Asgharzadehahmadi, A.Aziz, A.Raman, R. Parthasarathy , BaharakSajjadi, “Sonochemical reactors: Review on Features, advantages and limitations”, Renewable and Sustainable Energy Reviews. 2016; 63: 302–314.

24. P.R Gogate,M. Sivakumar ,A.B. Pandit, “Destruction of RhodamineB using novel sonochemical reactor with capacity of 7.5l”, SeparationPurif Technol. 2004; 34: 13–24.

25. L. Csoka , S.N. Katekhaye, P.R. Gogat, “Comparison of cavitational activity in different configurations of sonochemical reactors using model reaction supported with theoretical simulations”,Chemical Eng Journal. 2011; 178: 384–90.

26. M. Legay, N. Gondrexon, S L Person, P. Boldo, A. “Bontemps, Enhancement of Heat Transfer by Ultrasound: Review and Recent Advances, International Journal of Chemical Engineering,(2011), Article ID 670108, 17 pages.

27. L. H. Thompson, L. K. Doraiswamy, “Sonochemistry: Science and Engineering”, Ind. Eng. Chem. Res. 1999; 38: 1215-1249.

28. V. T. Perarasu, M. Arivazhagan, P. Sivashanmugam, "Heat Transfer of TiO2/Water Nanofluid in a Coiled Agitated Vessel with Propeller", Journal of Hydrodynamics, 2012; 24: 942-950.

29. V. T. Perarasu, M. Arivazhagan, P. Sivashanmugam, "Heat Transfer Characteristics of TiO2/Water Nanofluid in a Coiled Agitated Vessel Provided with Disk Turbine Agitator", Chemical Engineering Communication, 2013; 200: 783-797.

30. S. Liu, M.Sakr , “A comprehensive review on passive heat transfer enhancements in pipe exchangers”, Renewable and Sustainable Energy Reviews. 2013; 19: 64–81.

31. Zaid S. Kareem, M.N. Mohd Jaafar, Tholudin M. Lazim, Shahrir Abdullah, Ammar F. Abdulwahid , “ Passive heat transfer enhancement review in corrugation” , Experimental Thermal and Fluid Science. 2015; 68: 22–38.

32. M. Siddique, A.-R. A. Khaled, N. I. Abdulhafiz, and A. Y. Boukhary, “Recent Advances in Heat Transfer Enhancements: A Review Report International Journal of Chemical Engineering 2010(2010) 1-28 .

33. L. Leal, M. Miscevic, P. Lavieille, M. Amokrane, F. Pigache, F. Topin, B. Nogarède,L. Tadrist, Int. J. Heat Mass Transf. 2013; 61: 505–524.

34. Yao, Ye; Zhang, Xingyu; and Guo, Yiying, "Experimental Study on Heat Transfer Enhancement of Water-water Shell-and-Tube Heat Exchanger Assisted by Power Ultrasonic" (2010). International Refrigeration and Air Conditioning Conference. Paper 1110.

35. B. Schneider, A. Kos¸ar, C. J. Kuo et al., “Cavitation enhanced heat transfer in microchannels,” Journal of Heat Transfer, 2006; 128: 1293–1301.

36. H. Y. Kim, Y. G. Kim, and B. H. Kang, “Enhancement of natural convection and pool boiling heat transfer via ultrasonic vibration,” International Journal of Heat and MassTransfer, 2004; 47: 2831–2840.

37. D. W. Zhou, D. Y. Liu, X. G. Hu, and C. F. Ma, “Effect of acoustic cavitation on boiling heat transfer,” Experimental Thermal and Fluid Science, 2002; 26: 931–938.

38. D. Zhou and D. Liu, “Boiling heat transfer in an acoustic cavitation field,” Chinese Journal of Chemical Engineering, 2002; 10: 625–629.

39. B. Li and D. W. Sun, “Effect of power ultrasound on freezing rate during immersion freezing of potatoes,” Journal of Food Engineering, 2002; 55: 277–282.

40. L. Zheng and D. W. Sun, “Innovative applications of power ultrasound during food freezing processes—a review,” Trends in Food Science and Technology, 2006; 17: 16–23.

41. T. J. Mason, L. Paniwnyk, and J. P. Lorimer, “The uses of ultrasound in food technology,” Ultrasonics Sonochemistry, 1996; 3: S253–S260.

42. T. Inada, X. Zhang, A. Yabe, and Y. Kozawa, “Active control of phase change from supercooled water to ice by ultrasonic vibration 1. Control of freezing temperature,” International Journal of Heat and Mass Transfer, 2001; 44: 4523–4531.

43. X. Zhang, T. Inada, A. Yabe, S. Lu, and Y. Kozawa, “Active control of phase change from supercooled water to ice by ultrasonic vibration 2. Generation of ice slurries and effect of bubble nuclei,” International Journal of Heat and Mass Transfer, 2001; 44: 4533–4539.

44. J. A. Gallego-Ju´arez, G. Rodriguez-Corral, J. C. Galvez-Moraleda, and T. S. Yang, “A new high-intensity ultrasonic technology for food dehydration,” Drying Technology, 1999; 17: 597–608.

45. J. V. Garcıa-P´erez, J. A. Carcel, E. Riera, and A. Mulet, “Influence of the applied acoustic energy on the drying of carrots and lemon peel,” Drying Technology, 2009; 27: 281– 287.

46. J. V. Garcıa-Perez, J. A. Carcel, J. Benedito, and A. Mulet, “Power ultrasound mass transfer enhancement on food drying,” Food and Bioproducts Processing, 2007; 85: 247– 254.

47. V. Uhlenwinkel, R. Meng, and K. Bauckhage, “Investigation of heat transfer from circular cylinders in high power 10 kHz and 20 kHz acoustic resonant fields,” International Journal of Thermal Sciences, 2000; 39: 771–779.

48. A. E. Bergles, “Survey and evaluation of techniques to augment convective heat and mass transfer,” Progress in Heat

and Mass Transfer, 1969; 1: 331–424.

49. A. E. Bergles and P. H. Newell, “The influence of ultrasonic vibrations on heat transfer to water flowing in annuli”, International Journal of Heat and Mass Transfer, 1965; 8: 1273–1280.

50. H. Kiani, Da-W. Sun, Z. Zhang, “The effect of ultrasound irradiation on the convective heat transfer rate duringimmersion cooling of a stationary sphere”, Ultrasonics Sonochemistry. 2012; 19: 1238–1245.

51. U. Kurbanov and K. Melkumov, “Use of ultrasound for intensification of heat transfer process in heat exchangers,” in Proceedings of the International Congress of Refrigeration, 4(2003)1–5, Washington, DC, USA.

52. W. Benzinger, U. Schygulla, M. Jäger and K. Schubert, “Anti Fouling Investigations with Ultrasound in a Microstructured Heat Exchanger”, Proceedings of 6th International Conference on Heat Exchanger Fouling and Cleaning - Challenges and Opportunities, Engineering Conferences International, Kloster Irsee, Germany, 5 - 10, 2005.

53. A. Monnot, P. Boldo, N. Gondrexon, and A. Bontemps,“Enhancement of cooling rate by means of high frequency ultrasound,” Heat Transfer Engineering, 28(2007) no. 1, 3–8.

54. N. Gondrexon, Y. Rousselet, M. Legay, P. Boldo, S. Le Person, and A. Bontemps, “Intensification of heat transfer process: improvement of shell-and-tube heat exchanger performances by means of ultrasound,” Chemical Engineering and Processing, 2010; 49: 936–942.

55. M. Legay, B. Simony, P. Boldo, N. Gondrexon, S. Le Person, A. Bontemps, “Improvement of heat transfer by means of ultrasound: Application to a double-tube heat exchanger”, Ultrasonics Sonochemistry, 2012; 19: 1194–1200.

56. M. Legay, Y. Allibert, N. Gondrexon, P. Boldo, S. Le Person, “Experimental investigations of fouling reduction in an ultrasonically-assisted heat exchanger”, Experimental Thermal and Fluid Science, 2013; 46: 111–119.

57. Parag R Gogate, “Intensification of chemical processing applications using ultrasonic and microwave irradiations”, Current Opinion in Chemical Engineering, 2017; 17: 9–14.

Advances in Chemical Engineering

Chapter 3

Label-free Electrochemical Detection of Oligonucleotide Hybridization Based on Composites of Intrinsically Conducting Polymers

Radhakrishnan S[1]*; Navaneethan Duraisamy[2]; Gopi Dhanaraj[2]; Kavitha Kandiah[3#]

[1]Electrodics and Electrocatalysis Division, CSIR-Central Electrochemical Research Institute, Karaikudi-630 003, Tamil Nadu, India

[2]Department of Chemistry, Periyar University, Salem, Tamil Nadu, India

[3]Department of Microbiology, Periyar University, Salem, Tamil Nadu, India

Corresponding author (s)

*[*]**Radhakrishnan S,** Electrodics and Electrocatalysis Division, CSIR-Central Electrochemical Research Institute, Karaikudi-630 003, Tamil Nadu, India*

Email: s.rkn168@gmail.com

*[#]**Kavitha Kandiah,** Department of Microbiology, Periyar University, Salem, Tamil Nadu, India*

Email: kkavitha07@gmail.com

Abstract

We are focusing on the application of biosensor technology for the successful detection of selected DNA and mutated DNA sequences based on conduting polymer nanostructures. There are several tasks in the current research which need great concerns over the sensitivity, selectivity and throughput. Therefore, developing simple, efficient and cost effective methods for routine analysis of DNA hybridization is of great importance. Compared with other techniques electrochemical technique is an attractive and many advantages including high sensitivity, inherent simplicity and miniaturization and low-cost. It is well-known that electroactive conducting polymer (such as polyaniline, polypyrrole, poly (3, 4-ethylenedioxythiophene) is widely used in biosensors due to their unique physical and chemical properties and also low cost, easy preparation, and environment stability. In this book chapter, we have discussed a new sensing platform using nanostructure conduting polymers to detect target ssDNA and mutated ssDNA

sequences. A motivation behind this book chapter is an understand the basic concept of DNA hybridization and electrode fabrication, important parameter to improve the DNA hybridization efficiency including selectivity, sensitivity and low concentration detection and role of the nanostructured conducting polymer matrix in DNA sensing.

Keywords: DNA detection; electrochemical; biosensor; conducting polymers

1. Introduction

In the nucleic acids, deoxyribonucleic acid (DNA) and ribonucleic acid (RNA) are polymers of nucleotides. Both DNA and RNA has two major purine bases, adenine (A), and guanine (G), and three major pyrimidines bases such as cytosine (C), thymine (T) and uracil (U). The chemical structures of the five major bases were given below in **Figure1**.

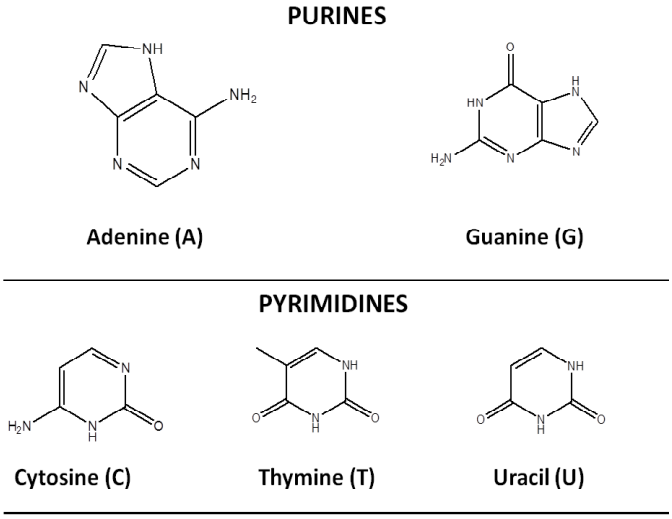

Figure 1: Chemical structures of major purine and pyrimidine bases.

Initially, James Watson and Francis Crick claimed double strand DNA helical structure in the year 1953 and create the new route in biological research for understanding the genome in living organisms [1].

DNA is the important basic biomolecules, which is used as chemical building block to store the gentic information in the cells and also it gives the blue print for entire characteristics of most living organisms. Researchers found that the DNA is the the most important molecular structure of the hereditary molecule in the cells. Based on the Watson - Crick Model, the DNA molecules present as helical structure with two polynucleotiede strands coiled around each other. Further, the sugar-phosphate backbone was present at the outside of the double helix structure and purine/pyrimidine bases were present in the inside of the helical structure.

The two single strand of the DNA double helix strcutre present in the opposite to each other. For example, one is the 5’ to 3’ direction, the other in the 3’ to 5’ direction. The 5’end having a phosphate group, which is linked with the 5’ carbon of its terminal DNA, whereas the 3’ end will usually having a hydroxyl on the 3’ carbon of its terminal deoxyribonucleotide.

The each signle strand DNA will bind to form as double helix structure through by the

hydrogen bond between Adenine - Thymine, and Cytosine – Guanine. In addition, here three hydrogen bonds are involving between Cytosine – Guanine pairs. Similarly, two hydrogen bonds are involving between Adenine - Thymine pairs. The phosphate group of the DNA molecules have negative charge, which provides in electrostatic repulstion of the two strands. In order to join the two singe strands together, positive ions were much essential in solution for keep the negative charges neutralized.

The joining of two complementary single strands of DNA through hydrogen bonding to form a double-stranded DNA is called hybridization [2]. Further, the double stranded DNA was splite into two sing strands (dehybridize) when applying the particular temperature. This particular temperature of this transition is called the melting temperature (Tm), which is a more sensitive function of environmental conditions including ionic strength, pH and solvent conditions. Interestingly, when the temperature is reduced, the two strands will eventually come together by diffusion and rehybridize to form the double stranded structure [2].

2. Method of DNA Hybridization Detection

2.1. Conventional methods for the detection of DNA hybridization

It is well-known that the Southern blot method is conventionally used for the DNA sequences detection through gel-transfer hybridization process (**Figure 2**).

It is specifically fabricated to locate a particular sequence of DNA within a complex mixture by permanently attaching single-stranded DNA (ssDNA), which means denatured DNA to a solid support. Traditionally, a nitrocellulose membrane is widely used as the solid support, although a positively charged nylon membrane may also be used.

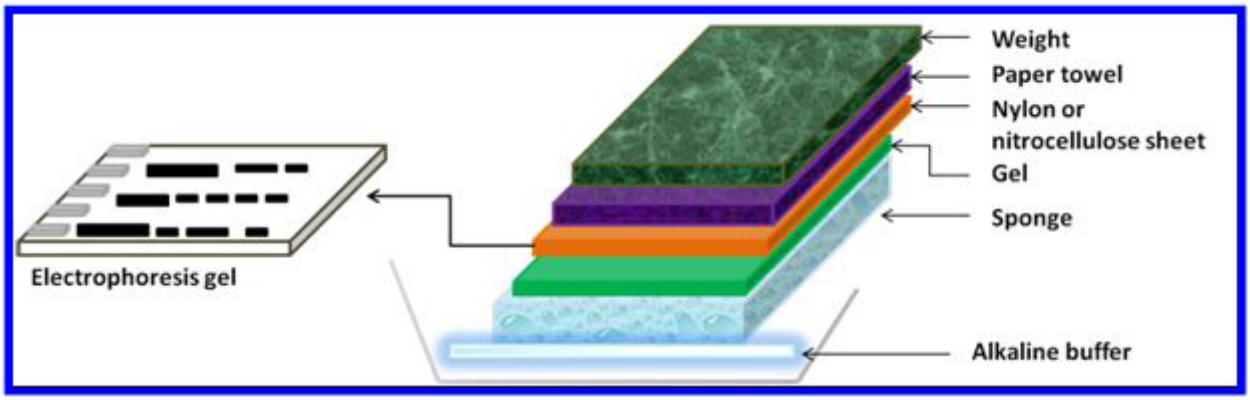

Figure 2: The schematic illustration of Southern blotting apparatus.

The denatured ssDNA fragments are kept on an agarose gel and split through electrophoresis. A thin sheet of nitrocellulose membrane is laid onto the gel and the separated DNA fragments are transferred to the sheet in a blotting set-up. The gel is sustained by a layer of sponge in a alkaline bath of buffer solution and this is further transferred via the gel and the nitrocellulose membrane through paper towels and weight stacked on top of the nitrocellulose thin sheet. The separated DNA fragments are transferred from the gel into the surface of the ni-

trocellulose sheet, where they adhere firmly and become permanently fixed after cross-linking with UV irradiation. The attached ssDNA over the nitrocellulose membrane has been further exposed into the labeled target DNA probes for a particular period time under good environment to enhance hybridization process. In general, different labled probe DNA was used including 32P, biotin/streptavidin or a bioluminescent molecule. For example,

If 32_p probe DNA is taken, an auto radiograph has been applied to evaluate hybridization where the DNA that has been hybridized to the labled probe will show up as bands on the autoradiograph. In the case of biotin/streptavidin detection is evaluated by colorimetric methods while bioluminescent visualization needs luminescence detection technique.

2.2. DNA hybridization biosensor

Biosensors are analytical instruments, ideally small and portable instruments that usually join the bio-recognition elements with the physical transducers (**Figure 3**), most generally electrochemical, optical, microgravimetry which utilize current, light or frequency to transduce the bio-recognition events, respectively.

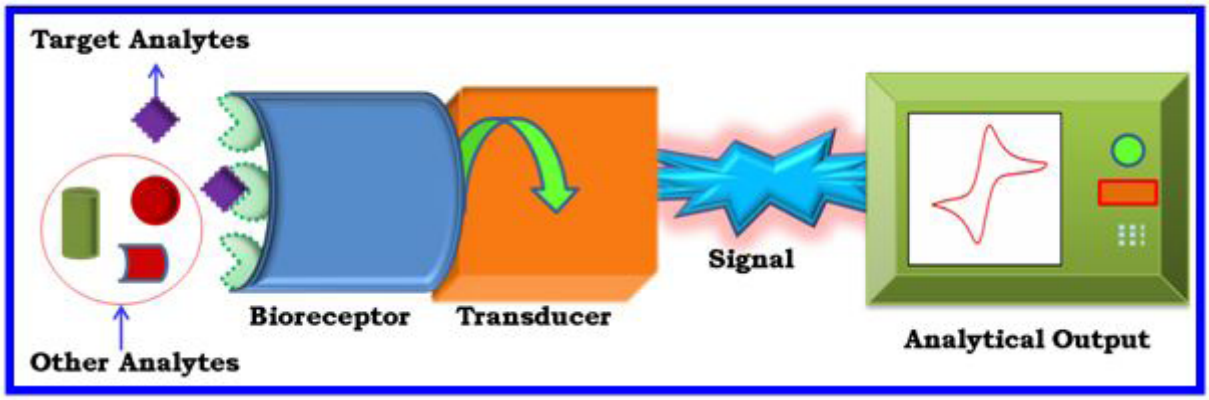

Figure 3: Schematic illustration of a biosensor which consists of a bioreceptor on a transducer attached to an analytical output

The sensing elements and/or receptors (antibodies, cell receptors, nucleic acids, imprinted polymers, porous nanostructure or catalytic reactions) were usually employed for enhance the specificity of the sensor [3].

As Southern blotting hybridization is labor intensive, time-consuming, requires expensive and hazardous probe labeling and normally needs to couple with expensive PCR instrument. Hence, this method is limited within hospital and research laboratories. This has been induced among research communites to develop an alternate detection technique with attractive features including simple, poratable, rapid, and high sensitivity and cost-effective. A DNA hybridization biosensor through electrical detection is able to fulfill these requirements. The electrical detection using most recent technological advances and nanostructure materials has provided great platform for the fabrication of portable DNA hybridization devices for rapid genetic screening and detection.

It is well known that the DNA hybridization biosensors represent a very important class

of affinity biosensor. A typical construction for a DNA biosensor consists of a probe ssDNA, which is fixed with the physical transducer. The probe ssDNA coupled transderuce will interact (hybridize with) corresponding complementary target DNA in the solution, i.e. the sample to be investigated.

2.3. Probe ssDNA immobilization

One of the most critical steps in the development of a DNA biosensor is the method used to attach the probe ssDNA on the physical transducer surface. A typical DNA biosensor is constructed by the immobilization of a probe ssDNA on a transducer surface to recognize its corresponding complementary (target) DNA sequence through hybridization event. DNA has to be attached on transducer in a way that the bases remain available for further bio-recognition event of the complementary target ssDNA strand. In this sense, the immobilized probe ssDNA should be vertical from the transducer (electrode) surface. Whereas, if it is attach the probe ssDNA horizontal onto the electrode surface, the bases of the DNA may restrict the interaction with corresponding complimentary target ssDNA. Hence, it is difficult to form a DNA double helix formation. So the probe ssDNA attachment on the transducer surface is an important role in the development of DNA biosensor. The following methods were commonly applied for the probe ssDNA attachment onto the transducer surface.

2.3.1. Entrapment in a polymeric matrix

In this method, the probe ssDNA can be retained in a matrix including agar gel, polyacrylamide, or conducting polypyrrole, which have been immobilized in advance on a solid support. The matrix has a mesh and porous size effective investigated by their large area of adsorption, which increases the amount of probe DNA strand attached, improving the sensitivity of the resulting system. However, the main problem in this method is the lack of probe DNA orientation, which decreases the accessibility to the target ssDNA. For example, Pividori et al. studied the nylon membrane has been used for the immobilize the probe ssDNA through adsorption [4]. Further, Li et al. used a polyacetic acid nanofiber membrane as a transducer substrate for probe DNA immobilization [5]. Similarly, Vivek et al. explored sol-gel matrix for the immobilization of the biomolecules [6].

2.3.2. Covalent binding

Another one of the most important method for DNA immobilization on transducer surface is covalent attachment. In this method, the probe ssDNA is attached via covalent chemical bonding between the transducer surface and a specifc functional group of the DNA, onto derivatized surfaces (e.x. glassy carbon or carbon paste modified electrode), functional groups (-COOH, -NH_2 etc.) substituted electro-active conduting polymers. In most commonly, coupling or cross-link reagents such as gluteraldehyde (GA), 1-ethyl-3-(3-dimethylaminopropyl)

carbodiimide (EDC) or a self-assembled monolayer were applied for creation of covalent bond between the probe ssDNA and modified transducer surface.

For example, Malhotra et al. gluteraldehyde (GA) used as a cross-linker for cross-link between the NH_2 modified probe ssDNA and electro-dposited thin film of polyaniline [7]. Similarly, Jadranka et al. investigated the electropolymerization of poly(pyrrole-co-4-(3-pyrrolyl) butanoic acid) onto which NH_2 modified probe DNA was anchored by the use of 1-ethyl-3-(3-dimethylaminopropyl) carbodiimide coupling reagent [8].

2.3.3. Adsorption

This adsorption method is very simplest method. This technique involve based on the direct adsorption of probe ssDNA on the particular substrate including nitrocellulose, nylon membranes, polystyrene, metal surface and carbon. Adsorption mechanisms are most commonly classified as either physical adsorption and electrochemical. The physical adsorption is carried out by soaking the surface with the desired solution that needs to be immobilized and leaving the surface to dry at room temperature. In the case of electrochemical adsorption, DNA backbone has negatively charged groups, so that a positive potential applied to a substracte (electrode) attracts these ssDNA probe. It has the advantages of its ease of operation and it does not need any other chemicals or any other special nucleic acid modifications but its major limitation is the variability of the nucleic acid layer due to distortion of the molecule by adsorption and consequently the poor hybridization efficiency.

For example, Arora et al. investigated the application of physically adsorbed double stranded calf thymus DNA onto polypyrrole-polyvinyl sulfonate (PPy-PVS) film coated onto ITO glass substrate for sensing o-chlorophenol and 2-aminoanthracene [9].

2.3.4. Self-assembled monolayer

Self-assembled monolayer (SAM) of thiolated probe ssDNA or regular DNA is formed by spontaneous adsorption or chemical binding of molecules from a homogeneous solution onto a substrate. Most literature studies have used this method for the immobilization of DNA in the form of a SAM onto a gold surface through well-known thiol chemistry.

SAM of terminally thiol labled probe ssDNA onto gold surface offers a direct simple method of chemisorption of DNA probes onto transducer surface based on the formation of gold-thiol (Au-S) bonds [10]. The most widely used SAM in DNA immobilization is made by the adsorption of sulphur based compounds such as thiols, disulphides or sulphide on glass or a metal surface such as gold, silver, palladium, copper and platinum.

A mixed SAM has recent trend to fabricate the DNA biosensor, it shows the better hybridization discrimination efficiency when compared to conventional SAM. In this mixed

SAM method, the probe DNA with different thiol compounds used as diluent molecules such as 6-mercapto-1-hexanol (MCH), 3-mercaptopropionic acid (MPA) and so on [11,12]. The main advantage of this method, we can control the immobilized probe ssDNA orientation as well as probe ssDNA density onto the transducer surface.

2.3.5. Affinity interactions

It is well-known that streptavidin and avidin are the most stable proteins in nature. It has peculiar properties along with the ability of biotin to be incorporated easily into various biological molecules, allow streptavidin to serve as a versatile, powerful affinity tag in a variety of biological applications. Due to the reason behind that the strong binding between streptavidin/avidin and biotin, the both have been the most widely used affinity interaction in ssDNA immobilization [13,14]. Tetramer binding is created between streptavidin and biotin, yield in a very high affinity bond, with stability as high as a covalent bond. This strong binding does not affect by other external factors including pH or temperature, organic solvents and denaturing agent. But, the presence of the large protein molecules may possible to create a non-specific binding sites and compromise the sensitivity and selectivity of particular types of sensors [15]. For example, Singh et al. prepared chitosan-iron oxide film and used for immobilization of biotinylated probe ssDNA over chitosan-iron oxide film [16]. Similarly, nanostructured electroactive conduting polyaniline film on ITO glass plate has been fabricated using avidin-biotin as cross link for the sexually transmitted disease (STD) DNA detection [17].

2.4. Hybridization detection and amplification in DNA sensors

The conventional methods for identification of specific DNA sequences are based on hybridization with corresponding complimentary targe DNA, polymerase chain reaction (PCR), Southern blotting and various chemical methods. These are expensive, time-consuming techniques require highly trained person and lengthy sample preparations.

To overcome these difficulties several research groups have reported DNA biosensors based on probe ssDNA has been immobilized onto a suitable matrix coupled to a physical transducer. The transducers are generalized into three main categories: optical, microgravimetric and electrochemical techniques.

2.4.1. Optical DNA hybridization biosensor

Different types of optical DNA hybridization biosensors have been explored till now. These techniques commonly involve the use of fluorescent or surface plasmon resonance (SPR) spectroscopy depending on weather a fluorescent label is used in the probe ssDNA. Typical fluorescent DNA biosensor works on the emission signal from a fluorescent-label which is generally attached into either the DNA duplex or target DNA to transduce the hybridization via

the use of fluorometry. In most commonly, fiber optics have been used as the medium to transduce this signal produced from DNA hybridization process as they allow light transmission by series of internal reflection. A wide range of different optical transducers for DNA sensors has been extensively studied [18-20].

2.4.2. Microgravimetric DNA hybridization biosensor

As with using SPR for DNA sensing, the microgravimetric DNA biosensor is also able to offer label-free in situ detection of DNA hybridization through acoustic waves, surface acoustic waves or love waves. Acoustic wave identification using the quartz crystal microbalance (QCM) has been demonstrated by several research groups [21-25]. The QCM is well-known and popular as an extremely sensitive mass-measuring instrument as its resonance frequency decreases with an increase in mass on the QCM [26]. This QCM method can also applied to detect the single mismatch targe DNA sequences. For example, it is observed that 26-31 % decrease in resonant frequency when using single mismatch target DNA in the DNA hybridization study by QCM [23].

2.4.3. Electrochemical DNA hybridization biosensor

Electrochemical sensors have distinctive and very attractive advantages over the other detection methods (such as optical and microgravimetric sensing systems), including simple, rapid, low cost, point-of-care detection for selected target DNA and suitable for microfabrication technology [27-31].

Electrochemical biosensors combine the analytical power of electrochemical techniques (cyclic voltammetry, amperometry, electrochemical impedance spectroscopy, coulometry and so on) with the specificity of biological recognition processes (DNA hybridization). In general, the bioreaction produces an electrical signal that relates to the concentration of an analyte. For this purpose, a biospecific reagent is either immobilized or retained at a suitable electrode surface, which converts the bio-recognition event into a quantitative amperometric or potentiometric response. The combination of the electrode surface with a biomolecule provides new and attractive platform that are useful to solve the many challenging problem [32]

An impressive number of new designs for electrochemical DNA hybridization sensing have been emerged. Owing to their unique advantages, currently several publication and review articles can see in the literature. For example, good review articles were published by Kerman et al. [33], Drummond et al. [34], Wang [35] and Gooding [36] summarized the state-of-the-art and recent trend in electrochemical DNA hybridization biosensor technology. The most general strategy for electrochemical DNA hybridization detection is through the use of a redox-active labeled probe. The siginificant changes were observed from the affinity of the redox molecule after the interaction probe ssDNA when interaction with sample target DNA.

The labels range from redox-active DNA specific molecules, e.g. DNA groove binders [37] and intercalators [38-40], biological molecules such as enzymes [41-43] or metal nanoparticles [44-46]. In addition to that the label-free DNA detection is also possible through monitoring by the either the intrinsic redox-active properties (e.g. direct oxidation) of DNA bases (guanine or adenine) [47-50] or a changes in electrical properties on the transducer surface [51].

2.4.4. Amplification of DNA Biosensor

The novel elecroactive materials with special structure and modified substrates such as nano gold [52-55] quantum dots [56-58], carbon nanotubes [59-63], graphene [64-66], and CPs [67,68] have been used in a DNA hybridization biosensors as a signal amplifiers. Among them, conducing polymers (CP) are well-known as functional materials for biosensing applications due to their unique electrical, electronic, magnetic and optical properties, which are found only in inorganic system.

3. Brief Overview of Conducting Polymers (CPs)

Conducting Polymers (CPs) are polymers that inherently transmit the electricity and have attracted a great deal of attention over the past few decades. The first study about CPs was demonstrated by Letheby in the year of 1863 [69]. He has reported the chemical oxidation products of aniline in acidic media such as the human stomach. In the early 1900s, German chemists found and named different compounds as “aniline black” or “pyrrole black” and applied them on an industrial scale. However, detailed research about synthesis of polyaniline through chemical method was investiaged in 1962 by Moliner et al. [70]. Followed by, Bolto and co-workers were reported the iodine-doped polypyrroles in 1963 [71]. However, the electrical conducing properties of polyaniline and polypyrrole, as well as the relationship of their chemical structure remained unknown [72]. Interestingly, these issues were solved by Alan MacDiarmid, Hideki Shirakawa in 1977 by the discovery of highly conductive polyacetylene doped with iodine, which is the first study to demonstrate the conductivity of the polymers [73,74]. Following this great discovery, other different types of conducing polymers including polyaniline (PANi) [75], polypyrrole (PPy) [76], polythiophene (PT) [77], polyphenylene (PP) [78] and poly(phenylene vinylene) (PPV) [79] were found and studied in details.

3.1. Synthesis of conducting polymers (CPs)

Conducting Polymers can be widely synthesized through two methods including chemicallly and/or electrochemically oxidative polymerization of the appropriate monomers [80, 81]. Typically, chemical polymerization usually carried out by using some chemical oxidizing reagent ($FeCl_3$ or $(NH_4)_2S_2O_8$)), which is play a two role one is oxidize the monomer and secone role is provide a dopant anions. The chemical polymerization has the following advantages and disadvantages.

Advantages

Large-scale production possible

Post-covalent modification of bulk CP possible

More options to modify CP backbone covalently

Disadvantages

Can not make thin films

Complicated synthesis and purification process

Electrochemical polymerization commonly involves the formation of low molecular weight oligomers that are further oxidized by applying through lower potential than the initial monomer to form a polymer film on the conduting electrode surface (platinum, gold, glassy carbon and so on). It has the following merits and demerits.

Advantages

Thin film synthesis possible

Easy of synthesis

Entrapment of molecules in CP

Doping is simultaneously possible

Disadvantages

Difficult to remove film from electrode surface

Post-covalent modification of bulk CP is difficult

The different electrochemical techniques can be used including potentiostatic (constant potential) [82], galvanostatic (constant current) [83] and potentiodynamic (cyclic voltammetry) [84].

A counter ion is added during electro-polymerization to balance the positive charge created within the polymer chain. This process is usually called as doping and the counter ion is called dopant. The dopant can be provided by the oxidant employed during chemical polymerization or can involve electrolyte ions used during the electrochemical polymerization. The dopant incorporated into the CP during synthesis has a main responself for the effect of the conductivity, chemical and physical properties of asprepared CPs.

In addition to chemical and electrochemical oxidation polymerization, CPs have also been synthesized by methods including photochemical polymerization [85], plasma polymerization [86], enzyme-catalyzed polymerization [87], organometallic cross-coupling reaction [88] etc. However, most of these techniques for the preparation CPs involve the use of expensive chemicals and time-consuming.

3.1.1. Polyaniline

Polyaniline (PANi) known for approximately more than 150 years, PANi is the oldest and potentially one of the most useful electro-active CPs because of its much simple synthesis, environmental stability, and simple acid/base doping/de-doping chemistry. The polymeric structure of PANi is shown in **Figure 4**. It has three oxidation states, the fully reduced leucoemeraldine form (y = 1), the fully oxidized pernigraniline form (y = 0), and the half oxidized emeraldine form (y = 0.5) [75].

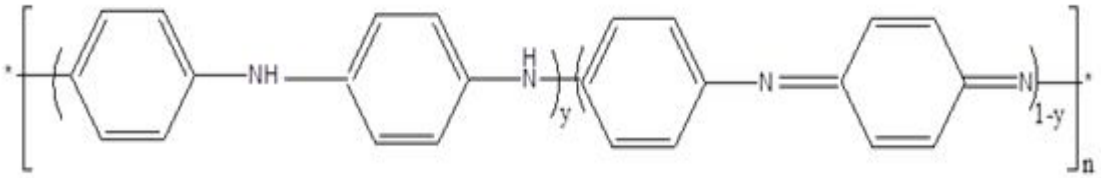

Figure 4: Polymeric structure of polyaniline

3.1.2. Polypyrrole

Polypyrrole (PPy) comprising of five-membered hetrocyclic rings is one of the most promising CPs (Figure 5). PPy was first chemically polymerized in 1916 by oxidation with H_2O_2 to give an amorphous black powder known as pyrrole black [89,90]. Later, Bolto et al. reported highly electrically conductive iodine doped polypyrrole in 1963 [71]. Since then numerous extensive reports with attractive properties have been developed on all aspects of this type of CP because of their easy synthesis, tunable conductivity, reversible redox property, high mechanical stability and good environmental stability.

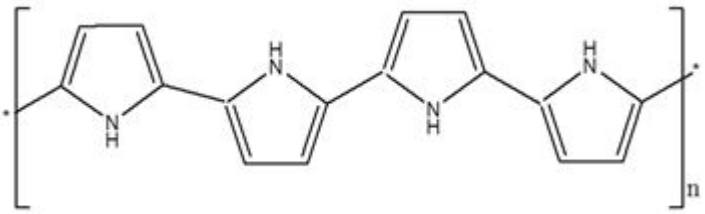

Figure 5: Polymeric structure of polypyrrole

3.1.3. Poly (3,4-ethylenedioxythiophene)

Poly (3,4-ethylenedioxythiophene) (PEDOT) is a conducting polymer based on the 3,4-ethylenedioxythiophene (EDOT) monomer, having the chemical structrue shown in **Figure 6.** This derivative of polythiophene was fabricated in the second half of the 1980s by the scientists at the Bayer AG research laboratories in Germany [91]. Since then the PEDOT polymer has been attracted considerable attention in many potential areas due to it is high electrical conductivity and stability in the oxidized state.

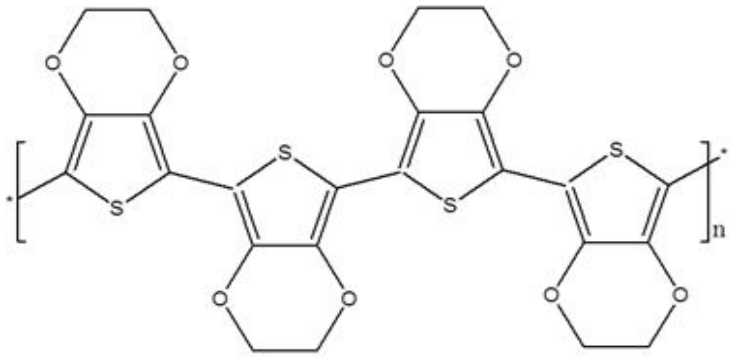

Figure 6: Structure of PEDOT

3.1.4 Preparation of PEDOT

PEDOT is most commonly prepared by chemical or electrochemical oxidative polymerization methods. Chemical oxidative polymerization of EDOT monomer has been carried out using several ways and oxidizing reagents. For example S. Armes and R. Corradi [92] have synthesized PEDOT by using $FeCl_3$, $Ce(SO_4)_2$ and $(NH_4)_2Ce(NO_3)_6$ as oxidizing reagents. They have stated that oxidizing reagent concentration should be higher than the monomer concentration to get good yields and conduting of the product. Followed by, ferric toyslate used as oxidant at an elevated temperature (110˚C) in combination with imidazole as a base and formed a black, insoluble and infusible PEDOT film that demonstrated conductivity up to 550 S/cm was reported [93]. Jonas and Krafft has been developed soluble PEDOT based on $Na_2S_2O_8$ as the oxidizing agent in an aqueous solution of poly (styrenesulfonic acid) (PSS) [94].

In electrochemical polymerization results in the formation of a highly transmissive sky-blue in colour, doped PEDOT film at the anode was obtained [95]. The electrochemical polymerization of EDOT is normally carried out in organic solution and/or aqueous micellar media. For example, PEDOT films have been synthesized from alkyl ammonium or lithium salts as supporting electrolyte in acetonitrile or propylene carbonate as elecrolyte [96]. The generally accepted mechanism of electro-polymerization of PEDOT is similar with that of polypyrrole formation mechanism. However unlike pyrrrole, only the α-α’ coupling of the 3,4-ethylene-dioxythiophene is expected due to the blocked structure of the monomer. Hence, PEDOT is expected to have few defects than PPy.

4. Fabrication of Nano-Structured Conducting Polymers

In recent developments in nanoscience and nanotechnology, micro/nano-strctured electro-active conduting polymers have played an important role because of their unique physical and chemical properties. The nanostructure has several advantages when compared to that of bulk polymeric materials including high surface area, low density, along with special chemical and physical properties. The nanostructure CPs fabricated through template based method either hard or soft-template method.

4.1. Hard-template methods

The first prpration of conducting polymer nanofiber and nanotube nanostructure has been reported by Martin [97]. Following this great method, a different nanostructure CPs including polyaniline [98,99], polypyrrole [99,100] and poly (3,4-ethylenedioxythiophene) [99,101] has been reported. The commonly used hard-templates are aluminium oxdie membrane and track-etched polycarbonate membrane to fabricate the nanostructure CPs.

The hard-template methods are the most commonly used and the most efficient approach for the fabrication of highly controlled and uniform nanostructures. However, the used hard-template commonly has to be eliminated with help of strong acids/bases or organic solvents or with high temperature after the preparation. These kinds of removal steps may increase the cost and restrict for large scale synthesis. Further, these processes have severely affected the nanostructure of the resulting products.

4.2. Soft-template methods

The soft-template method is also commonly known as self-assembly techniques. Surfactant self-assembly in a solution has been studied in details including both theoretically and experimentally because of their importance in synthesis of micro/nano-structures with controlled dimension [102]. The self-assembly ability of surfactants in a bulk solution therefore creates the possibility of surfactant micells serving as soft-templates to form CP nanostructures. The main advantages of this method are that the soft templates promote the CP to grow in a tubular form and need not be removed after the polymerization. However, the soft templates are often not quite stable, the versatility for different systems is poor and the multiformity of final products is obvious [103,104].

5. Electorchemical Detection of DNA Hybridization Based Nanostructured Conduting Polymers

5.1. Role of nano-structured CPs in biosensor applications

It is well-known that electro-active CPs acts as versatile platform for sensing applications because they not only posses unique properties but also can be applied as immobilization matrix, receptors and transducers in biosensors fabrication process. In recent years, studies of CP-based sensors have shown a trend towards the development of nano-structured CP based sensors, owing the ability to tailor the sizes and structures. Because of their very high aspect ratio, high electronic conductivity and small size, nanowires and nanotubes offer the potential of high sensitivity, low power operation, and massive redundancy in nanosensor array. CP nano-structures not only retain these unique properties, but also have the characteristics of nanomaterials (e.g. large surface area, size and quantum effect), which further increases the

merit of CP in designing and making novel sensors.

5.2. Nano-structued materials in DNA hybridization biosensor

Over the past few years, nano-structured materials and technologies have played an important role for the design of new types of DNA sensing methods and devices, which have led to excellent improvements in terms of high sensitivity, selectivity, multiplexing capacity, and simplicity. Moreover, multifunctional nanostructured materials can be composited together to desing the versatile sensing platform, to meet the demands of fast, simple, and inexpensive methods for DNA biosensing. For example, Fang et al. [105] has been reviewed the applications of carbon nanotubes (CNTs) in electrochemical DNA hybridization biosensors specifically. He stated that in this review CNT plays a two significant role: (i) using CNTs as sensing platform for immobilizing DNA molecules as well as powerful signal enhancement to amplify signal where produced from the DNA hybridization process; (ii) CNTs help as effective carrier and/or indicator to concentrate proteins and/or electroactive analytes for electrochemical sensing of DNA hybridization. Followed by, Wang's group designed a CNT-based dual amplification route by using a chronopotentiometry for ultrasensitive electrical bioassay of DNA. The application of CNT amplifiers was combined with the preconcentration feature of CNT transducers to provide a dramatic improvement of the sensitivity of the sensor [106]. Zhang et al. [107] fabricated a high sensitive DNA hybridization biosensor using MWCNT-AuNP nanohybrid synthesized through layer-by-layer covalent attachment. Further, they have achieved a limit of detection to be 6.2 pM. Similarly, Sun et al. described the dendritic nanogold-reduced graphene oxide nano-composite for the electrochemical DNA hybridization detection by differential pulse voltammetry technique [108].

5.3. Nano-structured CPs in DNA hybridization biosensor

Different nano-structured conducing PANi nanotube have been fabricated by Zhang et al. [109] and successfully applied for the electrochemical detection of DNA hybridization. Feng et al. demonstrated gold nanoparticles and polyaniline nanotubes membrane and used for the DNA hybridization with high sensitivity [110]. Similarly, Zhou et al. fabricated sulfonated polyaniline nanofiber and AuNP for label-free potentiometric DNA hybridization biosensor [111]. Zhou et al. [112] reported DNA hybridization detection by electrochemical impedance spectroscopy using AuNP/CNT/PANi nanofiber.

It is well-known that the fabrication of nanostructured CPs is another issue currently limiting their application in DNA hybridization biosensor. In most commonly, hard and soft-template approaches were broadly used in the synthesis of CP nanostructures. However, simple, efficient, controlled and large-scale method for the preparation of nanostructured CPs are still lacking.

Recently, PPy nanotubes with excellent electrical conductivity have been prepared by using the fibrillar complex of $FeCl_3$ and methyl orange (MO), acting as a reactive self-degraded template. This novel template is stable in acidic aqueous solution of MO and can be dissolved under mild neutral aqueous conditions after the polymerization of monomers on its surface. In other words, it formally acts as a "hard-template", but effectively as a "soft-template". This can be considered an alternative to conventional soft and hard-template methods. This method was introduced by Yang et al. to prepare the PPy nanotubes with diameter as small as 50 nm [113]. $FeCl_3$/MO is a key template material for the fabrication of nanotubes because it can provide large effective surface area, nanometer size structures with high aspect ratio and can be fabricated in large scale with inexpensively and reproducibly.

The PPy nanotubes have been used as a core for the fabrication of PPy-PANi & PPy-PEDOT core-shell nanotubes. These core-shell nanotubes were synthesized by in-situ chemical oxidative polymerization of monomers on the surface of PPy nanotubes to form core-shell nanotubes [114 -116]. The as-prepared core-shell PPy-PANi nanotube has been used for the DNA hybridization detection. The detailed electrode fabrication process for the DNA sensor was shown in **Figure 7**. In the first step, the asprepared core-shell PPy-PANi nanotube has been modified over the gold transducer surface (electrode B) and then the polymer nanocomposite modified surface was soaked into gluteraldehyde (GA) solution to activate the surface (electrode C). It is well-known that gluteraldehyde has been widely used as crosslinker in biosensors that can covalently attach the capture probe ssDNA onto the modified electrode surface. Followed by, NH_2 modified probe ssDNA was immobilized (electrode D) over the gluteraldehyde activated polymer nanocomposite surface through cross-link between aldehyde and NH_2 functional groups. Finally, the probe ssDNA modified surface further utilized for the detection of DNA hybridization with target DNA. The hybridization event has been monitored through differential pulse voltammetry in the presence of methylene blue as intercalator. Methylene blue (MB) is a phenothiazine dye that is broadly used in electrochemical DNA biosensors. In general there are three different binding modes between MB and DNA. MB can interact with the negatively charged anionic phosphate backbone of DNA by electrostatic binding, intercalation with the major or minor grooves of the dsDNA helix and preferential binding between MB and guanine bases.

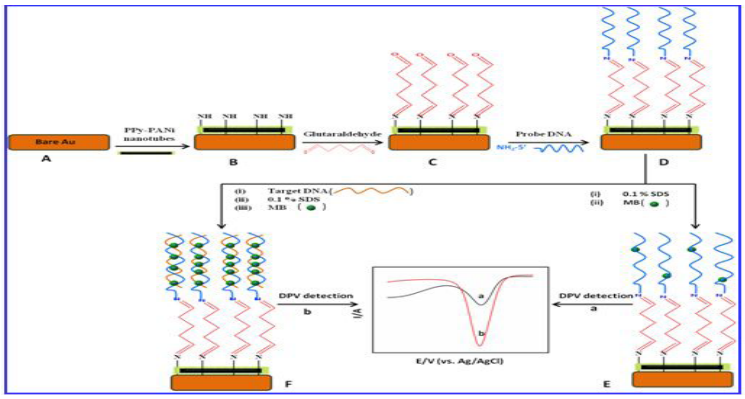

Figure 7: Fabrication procedure of this electrochemical DNA biosensor. (A) Bare Au, (B) A + PPy-PANi nanotubes, (C) B + GA, (D) C + ssDNA, (E) D + non-complementary and (F) D + complementary target [114]. Reproduced from Ref [114] with permission from the Royal Society of Chemistry.

Here, intercalation binding of MB with the major/minor grooves of the dsDNA helix structure have key role to get the greater DPV signal (electrode F) when compared to that of un-hybridized surface (probs ssDNA; electrode E). Further, the fabricated DNA sensor can detect mismatched target DNA with greater changes (**Figure 8**). In **Figure 8** shows the DPV response of the probe ssDNA (curve a) modified surface after interact with complemetarnty (curve b), non-complementary (curve c), single mismatched and double mismatched targe DNAs. Each target DNA has exhibited clear different peak current. It is suggested that PPy-PANi nanocomposite modified electrode has effectively distinguish the complementary, non-complementary and mismatched target DNAs. The fabricated sensor surface showed good linear range (1.0×10^{-9} to 1.0×10^{-13} M) and detection limit (50 fM)

Similarly, poly (3,4-ethylene dioxy thiophene) coated polypyrrole nanotubes (PPy-PEDOT) has prepared by chemical oxidative polymerization method and then silver nanoparticles self-assembled over the PPy-PEDOT nanocomposite to form PPy-PEDOT-AgNP nancomposite. The formed silver nanoparticles over the PPy-PEDOT was well dispersed, which is much benefits to attached the probe ssDNA with enough spacing between each HS-ssDNA for efficient coiling of target DNA.

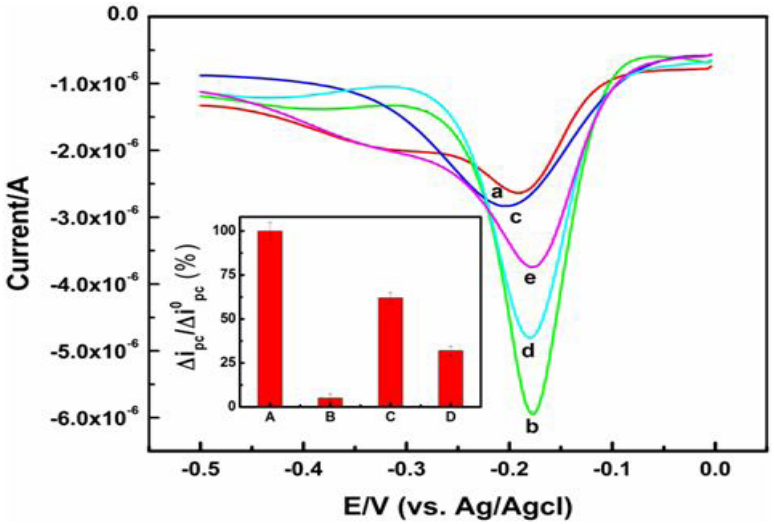

Figure 8: DPV of intercalated MB reduction peak current at (a) PPy-PANi-GA-ssDNA, (b) PPy-PANi-GA-dsDNA (com), (c) PPy-PANi-GA-dsDNA (non-com), (d) PPy-PANi-GA-dsDNA (SMM) and (e) PPy-PANi-GA-dsDNA (DMM). Inset: Corresponding bar diagram of normalized change in Ipc. Reproduced from Ref [114] with permission from the Royal Society of Chemistry.

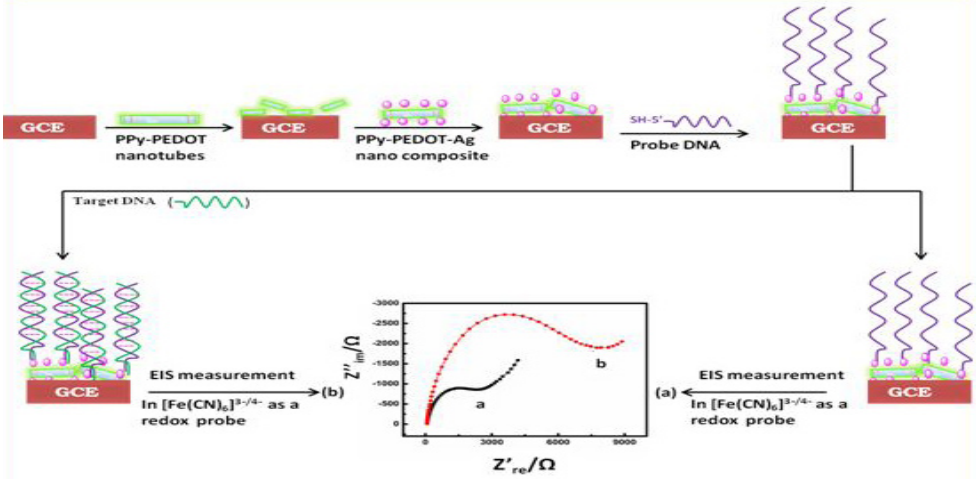

Figure 9: Schematic illustration of HS-ssDNA covalently immobilized onto the PPy PEDOT-AgNP nanocomposite by the Ag-thiol interaction at room temperature. Reproduced from Ref [116] with permission from the Elsevier.

The detailed electrode fabrication process has been explained in **Figure 9**. In this process, initially PPy-PEDOT-AgNP nanocomposite modified over the glassy carbon electrode by simple drop-casting method and then SH-ssDNA was immobilized through self-assembled monolayer. The ssDNA modified surface finally used to detect the different target DNA by electrochemical impedance spectroscopy in presence of $[Fe(CN)_6]^{3-/4-}$ as redox probe. **Figure 10** showed the electrochemical impedance spectroscoapy of different modified surfaces and inset figure 10 showed change in the charge transfer resistance for different modified electrode surface.

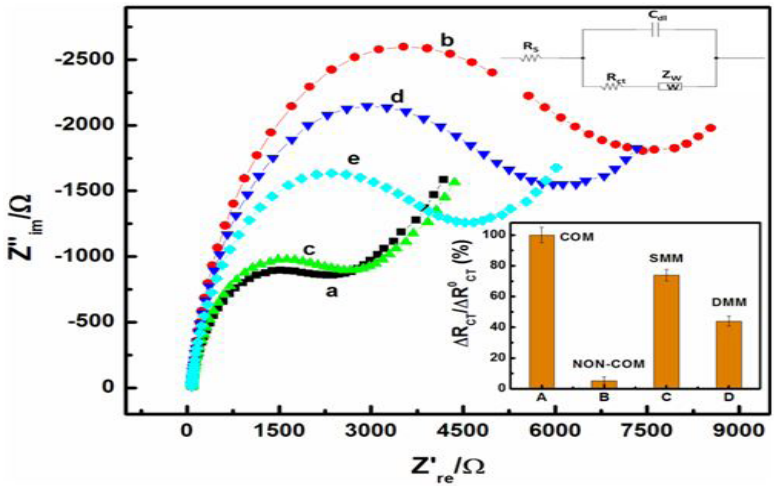

Figure 10: EIS behaviour of (a) PPy-PEDOT-AgNP-S-ssDNA, (b) PPy-PEDOT-AgNP-dsDNA (com), (c) PPy-PEDOT-AgNP-dsDNA (non-com), (d) PPy-PEDOT-AgNP-dsDNA (SMM) and (e) PPy-PEDOT-AgNP-dsDNA (DMM) in presence of 1mM $[Fe(CN)_6]^{3-/4-}$ in PB (p^H 7.0) solution. Inset: Corresponding bar diagram of normalized change in RCT. Reproduced from Ref [116] with permission from the Elsevier.

From the bar diagram clearly observed that the R_{CT} value much higher for complementary target DNA than other modified surfaces. It is due to the fact that complementary target DNA form perfect helical structure with probe ssDNA and the electrode surface has become more negatively charge created. Hence, the negatively charge electrode surface has strongly repel the negatively charged redox probe. Hence, the R_{CT} values were much higher than other modified electrode surface. The PPy-PEDOT-AgNP modified electrode surface exhibited good linear range from 1.0×10^{-11} M to 1.0×10^{-14} M with detection limit of 5.4×10^{-15} M. The

derived values is superior than that for MWCNT-Ag, PANi-Au, MWCNT-PPy-Au and PPy-PANi-Au nancomposite reported in literature [117-119].

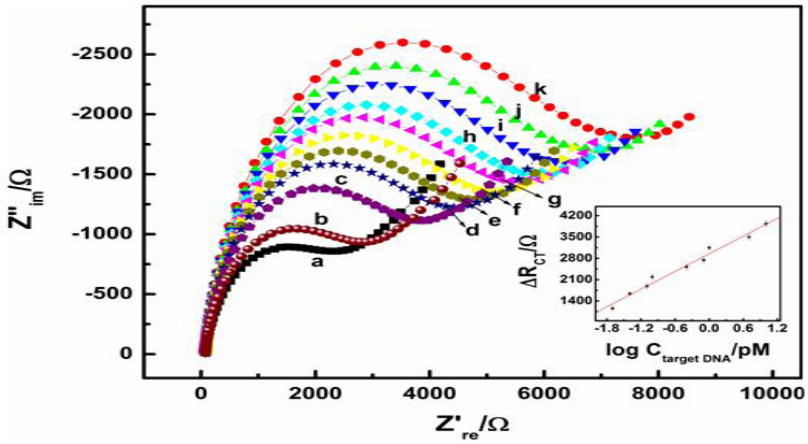

Figure 11: EIS detection of different target concentration using the PPy-PEDOT-AgNP-S-ssDNA. (a) 0, (b) 1.0 × 10-14, (c) 2.0 × 10-14, (d) 4.0 × 10-14, (e) 8.0 × 10-14, (f) 1.0 × 10-13, (g) 4.0 × 10-13, (h) 8.0 × 10-13, (i) 1.0 × 10-12, (j) 5.0 × 10-12 and (k) 1.0 × 10-11 M. Inset: Variation of ΔRCT with log (Ctarget DNA). Reproduced from Ref [116] with permission from the Elsevier.

6. Conclusion and Perspectives

Based on the unique properties of electroactive conducting polymers have been ultilized for DNA hybridization biosensor application. The conducting polmers were modified with nanoparticles (gold or silver) and/or using cross-link for probe ssDNA immobilization. The conducting polymers nanostructures can produce a synergic effect with enhance catalytic activity, conductivity and stability. Therefore, the preparation of conducting polymers with 1-D nanotubes has been utilized as platform for prbe ssDNA immobilization and hybridization with target ssDNA. In addition, the electrochemical method, which promising advantages of label-free detection of DNA hybridization event, should be a promising direction for the fabrication of portable DNA sensor tool. The role of conduting polymers in DNA hybridization biosensor not only provide an high sensitivity but also provide stable immobilization of probe ssDNA for ultra-low detection of target ssDNA. We hope these kinds of DNA hybridization biosensor based conducting polymer nanostructure have siginificant impact and hold a potential for future application in medical diagnosis.

7. Acknowledgements

Dr. S. Radhakrishnan acknowledges the DST, New Delhi, India for the DSTInspire Faculty Award (DST/INSPIRE/04/2015/002259). Dr. Navaneethan Duraisamy and Kavitha Kandiah acknowledged UGC-Dr. D.S. Kothari Postdoctoral Fellowship (Ref no: No.F.4-2/2006 (BSR)/EN/15-16/0031) and (Ref. no: No.F.4-2/2006 (BSR)/BL/15-16/0225), UGC, New Delhi.

8. References

1. J.D. Waston, F.H.C. Crick, Molecular structure of deoxypentose nucelic acids. Nature. 1953, 171: 737-738.

2. Y. Sun, C-H. Kiang, DNA-based artificial nanostructures: Fabrication, properties, and applications. Chapter V in "Handbook of nanostructured biomaterials and their applications in nanobiotechnology" Ed. By Nalwa, Americal Scientific Publishers. 2005.

3. A.P.F. Turner, Biosensors-sense and sensitivity. Science. 2000, 290: 1315-1317.

4. M.I. Pividor, A. Mcrkoci, S. Alegret, Classical dot-blot format implemented as an amperometric hybridization genosensor. Biosensors and Bioelectronics. 2001, 16: 1133-1142.

5. D. Li, M.W. Frey, A.J. Bacumner. Electrospun polyacetic acid nanofiber membranes as substrate for biosensor assemblies. Journal of Membrane Science. 2006, 179: 254-263.

6. K. Vivek, T. Vijay, J. Huangxian, Immobilization of biomolecules in sol-gels: Biological and analytical applications. Critical Reviews in Analytical Chemistry. 2006, 36: 73-106.

7. N. Prabhakaran, K. Arora, H. Sing, B.D. Malhotra, Polyaniline based nucelic acid sensors. Journal of Physical Chemistry B. 2008, 112: 4808-4816.

8. T-S. Jadranka, H. Peng, P.A. Kilmartin, M.B. Cannell, G.A. Bowmaker, R.P. Coonery, C. Soller, DNA sensor based on functionalized polypyrrole. Synthetic Metals. 2005, 152: 37-40.

9. K. Arora, A. Chaubey, R. Singhal, R.P. Singh, M.K. Pandey, S.B. Samanta, B.D. Malhotra, S. Chand, Application of electrochemically prepared polypyrrole-polyvinyl sulfonate films to DNA biosensor. Biosensors and Bioelectronics. 2006, 21: 1777-1783.

10. A.B. Steel, R.L. Levicky, T.M. Herne, M.J. Tarlov, Immobilization of Nucelic Acids at Solid Surfaces: Effect of Oligonucleotide Length on Layer Assembly. Biophysical Journal. 2000, 79: 975-981.

11. V. Dharuman, J.H. Hahn, Effect of short chain alkane diluents on the label free electrochemical DNA hybridization discrimination at the HS-ssDNA/diluent binary mixed monolayer in presence of cationic intercalators. Sensors and Actuators B. 2007, 127: 536-544.

12. V. Dharuman, J.H. Hahn, Label free electrochemical DNA hybridization discrimination effects at the binary and ternary mixed monolayers of single stranded DNA/diluents in presence of cationic intercalators. Biosensors and Bioelectronics. 2008, 23: 1250-1258.

13. N.M. Green, Avidin and streptavidin. Methods Enzymol. 1990, 184: 51-67.

14. D. Hernandez-Santos, M.B. Gonzales-Garcia, A. Costa-Garcia, Geneosensor based on platinum (II) complex as electrocatalytic label. Analytical Chemistry. 2005, 77: 2868-2874.

15. M.L. Jones, G.P. Kurzban, Non-cooperatives of biotin binding to tetrameric streptavidin. Biochemistry. 1995, 34: 11750-11756.

16. R. Singh, R. Verma. A. Kaushik, G. Sumana, S. Sood, R.K. Gupta, B.D. Malhodra, Chitosan-iron oxide nano-composite platform for mismatch discriminating DNA hybridization for Neisseria gonorhoeae detection

causing sexually transmitted disease. Biosensors and Bioelectronics. 2011, 26: 2967-2974.

17. R. Singh, R. Prasad, G. Sumana K. Arora, S. Sood, R.K. Gupta, B.D. Malhotra, STD sensor based on nucleic acid functionalized nanostructrued polyaniline. Biosensors and Bioelectronics. 2009, 24: 2232-2238.

18. B.S. Gaylord, A.J. Heeger, G.C. Bazan, DNA detection using water-soluble conjugated polymers and peptide nucleic acid probes. Proceedings of the National Academy of Science of the United States of America. 2002, 99: 10954-

10957.

19. A.W. Peterson, L.K. Wolf. R.M.J. Georgiadis, Hybridization of mismatched on partially matched DNA at surfaces. Journal of American Chemical Society. 2002, 124: 14601-14607.

20. T.A. Taton, Two-color Labeling of oligonucleotide arrays via size-selective scattering of nanoparticle probes. Journal of American Chemical Society. 2001, 123: 5164-5165.

21. X.D. Su, R. Robelek, Y.J. Wu, G.Y. Wang, W. Knoll, Detection of point mutation and insertion mutations in DNA using a quartz crystal microbalance and MutS, a mismatch binding protein. Analytical chemistry. 2004, 76: 489-494.

22. S. Yamaguchi, T. Shimomura, T. Tatsuma, N. Oyama, Adsorption, immobilization, and hybridization of DNA studies by use of quartz crystal oscillators. Analytical Chemistry. 1993, 65: 1925-1927.

23. Y. Okahata, Y. Matsunobu, K. Ijiro, M. Mukae, A. Murakami, K. Makino, Hybridization of nucleic acids immobilized on a quartz crystal microbalance. Journal of American Chemical Society. 1992, 114: 8299-8300.

24. K. Ito, K. Hashimoto, Y. Ishimori, Quantitative analysis for solid-phase hybridization reaction and binding reaction of DNA binder to hybrids using a quartz crystal microbalance. Analytica Chimica Acta. 1996, 327: 29-35.

25. N.C. Fawcett, J.A. Evans, L.C. Chien, N. Flowers, Nucleic acid hybridization detected by piezoelectric resonance. Analytical Letters. 1988, 21: 1099-1114.

26. G.Z. Sauerbrey,Use of quartz crystal vibrator for weighting thin films on a microbalance. Physics. 1959, 155: 206-222.

27. H. Cai, C. Shang, I.M. Hsing, Sequence-specific electrochemical recognition of multiple species using nanoparticles labels. Analytical Chimica Acta. 2004, 523: 61-68.

28. E. Palecek, Past, present and future of nucleic acids electrochemistry. Talanta. 2002, 6: 809-819.

29. J. Wang, D. Xu, A. Erdem, R. Polsky, A.M. Salazar, Genomagnetic electrochemical assay of DNA hybridization. Talanta. 2002, 56: 931-938.

30. Y.W.C. Cao, R.C. Jin, C.A. Mirkin, Nanoparticles with Raman Spectroscopic Finger prints for DNA and RNA Detection. Science. 2002, 297: 1536-1540.

31. S.J. Park, T.A. Taton, C.A. Mirkin, Array-based electrical detection of DNA with nanoparticle probes. Science. 2002, 295: 1503-1506.

32. J. Wang, Analytical Electrochemistry, 3rd Edition, New York, A John Wiley & Sons. 2006.

33. K. Kerman, M. Kobayashi, E. Tamiya, Recent trends in electrochemical DNA biosensor technology. Measurement Science and Technology. 2004, 15, R1.

34. T.G. Drummond, M.G. Hill, J.K. Barton, Electrochemical DNA sensors. Nature Biotechnology. 2003, 21: 1192-1199.

35. J. Wang, Electrochemical nuceleic acid biosensors. Analytica Chimica Acta. 2002, 469: 63-71.

36. J.J. Gooding, Electrochemical DNA hybridization biosensors. Electroanalysis. 2002, 14: 1149-1156.

37. S.O. Kelley, E.M. Boon, J.K. Barton, N.M. Jackson, M.G. Hill, Single-base mismatch detection based on charge transduction through DNA. Nucleic Acids Research. 1999, 27: 4830-4837.

38. E.L.S. Wong, J.J. Gooding, Electronic detection of target nucelic acids by a 2,6-disulfonic acid anthraquinone intercalator. Analytical Chemistry. 2003, 75: 3845-3852.

39. S.O. Kelley, J.K. Barton, N.M. Jackson, M.G. Hill, Electrochemistry of methylene blue bound to a DNA-modified electrode. Bioconjugate Chemistry. 1997, 8: 31-37.

40. S. Takenaka, K. Yamashita, M. Takagi, Y. Uto, H. Kondo, DNA sensing on a DNA probe-modified electrode using ferrocenylnapthalene diimide as electrochemically active. Analytical Chemistry. 2000, 72: 1334-1341.

41. T. deLumley Woodyear, C.N. Campbell, A. Heller, Direct enzyme-amplified electrical recognition of a 30-base model oligonucleotide. Journal of American Chemical Society. 1996, 118: 5504-5505.

42. D.J. Caruana, A. Heller, Enzyme-amplified amperometric detection of hybridization and of a single base pair mutation in an 18-base oligonucleotide on a 7-μm- diameter microelectrode. Journal of American Chemical Society. 1999, 121: 769-774.

43. C.N. Campbell, D. Gal, N. Cristler, C. Banditrat, A. Heller, Enzyme-amplified amperometric sandwich test for RNA and DNA. Analytical Chemistry. 2002, 74: 158-162.

44. J. Wang, R. Polsky, D.K. Xu, Silver-enhanced colloidal gold electrochemical stripping detection of DNA hybridization. Langmuir. 2001, 17: 5739-5741.

45. J. Wang, D.K. Xu, R. Polsky, Magnetically-induced solid-state electrochemical detection of DNA hybridization. Journal of the American Chemical Society. 2002, 124: 4208-4209.

46. M. Ozsoz, A. Erdem, K. Kerman, D. Ozkan, B. Tugrul, N. Topcuoglu, H. Ekren, M. Taylan, Electrochemical genosensor based on colloidal gold nanoparticles for the detection of factor V leiden mutation using disposable pencil graphite electrode. Analytical Chemistry. 2003, 75: 2181-2187.

47. F. Lucarelli, G. Marrazza, I. Palchetti, S. Cesaretti, M. Mascini, Coupling of an indicator-free electrochemical DNA biosensor with polymerase chain reaction for the detection of DNA sequences related to tha apolipoprotein E. Analytica Chimica Acta. 2002, 469: 93-99.

48. D. Ozkan, A. Erdem, P. Kara, K. Kerman, B. Meric, J. Hassmann, M. Ozsoz, Allele-specific genotype detection of factor V leiden mutation from polymerase chain reaction amplicons based on label-free electrochemical genosensor. Analytical Chemistry 2002, 74: 5931-5936.

49. E. Palecek, S. Billova, L. Havran, R. Kizek, A. Miculkova, F. Jelen, DNA hybridization at microbeads with cathodic stripping voltammetric detection. Talanta. 2002, 56: 919-930.

50. J. Wang, G. Rivas, J.R. Fernandes, J.L.L. Paz, M. Jiang, R. Waymire, Indicator-free electrochemical DNA hybridization biosensor. Analytica Chimica Acta. 1998, 375: 197-203.

51. J.J. Gooding, A. Chou, F.J. Mearns, E. Wong, K.L. Jericho, The ion gating effect: Using a change in flexibility to allow label free electrochemical detection of DNA hybridization. Chemical Communication. 2003, 1938-1939.

52. J. Zhang, S. Song, L. Wang, D. Pan, C. Fan, A gold nanoparticle-based chronocoulometric DNA sensor for amplified detection of DNA, Nature Protocols. 2007, 2: 2888-2895.

53. M.T. Castaneda, S. Alegret, A. Merkoci, Electrochemical sensing of DNA using gold nanoparticles. Electroanalysis. 2007, 19: 743-753.

54. A.A. Ensafi, M. Taei, H.R. Rahmani, T. Khayamian, Sensitive DNA impedance biosensor for detection of cancer, chronic lymphocytic leukemia, based on gold nanoparticles/gold modified electrode. Electrochemica Acta. 2011, 56: 8176-8183.

55. X. Liu, X. Qu, J. Dong, S. Ai, R. Han, Electrochemical detection of DNA hybridization using a change in flexibility. Biosensors and Bioelectronics. 2011, 26: 3679-3682.

56. C-Y. Zhang, H-C. Yeh, M.T. Kuroki, T-H. Wang, Single-quantum-dot-based DNA nanosensor. Nature Materials.

2005, 4: 826-831.

57. H. Peng, L. Zhang, T.H.M. Kjallman, C. Soller, T-S. Jadranka, DNA hybridization detection with blue luminescent quantum dots and dye-labeled single-stranded DNA. Journal of American Chemical Society. 2007, 129: 3048-3049.

58. E. Sharon, R. Freeman, I. Willner, CdSe/ZnS quantum dots-G-quadruplex/hemin hybrids as optical DNA sensors and aptasensors, Analytical Chemistry. 2010, 82: 7073-7077.

59. M.T. Martinez, Y.C. Tseng, N. Ormategui, I. Loinaz, R. Eritja, J. Bokor, Label-free DNA biosensors based on functionalized carbon nanotube field effect transistors. Nano Letters. 2009, 9: 53-536.

60. Bansaruntip, N. Nakayama, E. Yenilmez, Y-L. Chang, Q. Wang, Carbon nanotube DNA sensors and sensing mechanism. Nano Letters. 2006, 6: 1632-1636.

61. J. Li, Q. Liu, Y. Liu, S. Liu, S. Yao, DNA biosensor based on chitosan film doped with carbon nanotubes, Analytical Biochemistry. 2005, 346: 107-114.

62. R. Singh, D. Pantarotto, D. Mccarthy, O. Chaloin, J. Hoebeke, C.D. Partidos, J-P. Briand, M. Prato, A. Bianco, K. Kostarelos, Binding and condensation of plasmid DNA onto functionalized carbon nanotubes: Toward the construction of nanotube-based gene delivery vectors. Journal of American Chemical Society. 2005, 127: 4388-4396.

63. J. Wang, G. Liu, M. Rasul Jan, Ultrasensitive electrical biosensing of proteins and DNA: Carbon-nanotube derived amplification of the recognition and transduction events. Journal of American Chemical Society. 2004, 126: 3010-3011.

64. N. Mohanty, V. Berry, Graphene-based single-bacterium resolution biodevice and DNA transistor: Interfacing graphene derivatives with nanoscale and microscale biocomponents. Nano Letters. 2008, 8: 4469-447.

65. T. Kuila, S. Bose, P. Khanra, A.K. Mishra, N.H. Kim, J.H. Lee, Recent advances in graphene-based biosensors. Biosensors and Bioelectronics. 2011, 26: 4637-4648.

66. Y. Shi, W.T. Huang, H.Q. Luo, N.B. Li, A label-free DNA reduced graphene oxide- based fluorescent sensor for highly sensitive and selective detection of hemin. Chemical Communications. 2011, 47: 4676-4678.

67. H. Peng, L. Zhang, C. Soeller, J-S. Jadranka, Conducting polymers for electrochemical DNA sensing. Biomaterials. 2009, 30: 2132-2148.

68. B. Kannan, D.E. Williams, M.A. Booth, T-S. Jadranka, High-sensitivity, label-free DNA sensors using electrochemically active conducting polymers. Analytical Chemistry. 2011, 83: 3415-3421.

69. H. Letheby, On the production of a blue substance by the electrolysis of sulphate of aniline. Journal of the Chemical Society, Transactions. 1862, 15: 161-163.

70. D.M. Mohilner, R.N. Adams, W.J. Argersinger, Investigation of the kinetics and mechanism of the anodic oxidation of aniline in aqueous sulphuric acid solution at a platinum electrode. Journal of American chemical Society. 1962, 84: 3618-3622.

71. B.A. Bolto, R.McNeill, D.E. Weiss, Electronic conduction in polymers the chemical structure of polypyrrole. Australian Journal of Chemistry. 1963, 16: 1056-1075.

72. P. Chandrasekhar, Conducting polymers, fundamentals and applications: A practical approach, Kluwer Academic: Boston. 1999.

73. H. Shirakawa, E.J. Louis, A.G. MacDiarmid, C.K. Chiang, A.J. Heeger, Synthesis of electrically conducting organic polymers: Halogen derivatives of polyacetylene. Journal of Chemical Society, Chemical Communications. 1977, 578-580.

74. A.J. Heeger, Semiconducting and metallic polymers: the fourth generation of polymeric materials. Angewandte.

Chemie. International Edition. 2001, 40: 2591-2611.

75. S. Radhakrishnan, Chepuri R.K. Rao, M. Vijayan, Performance of conduting polyaniline-DBSA and polyaniline-DBSA/Fe3O4 composites as electrode materials for aqueous redox supercapacitors. Journal of Applied Polymer Sciecne. 2011,122:1510-1518

76. A.F. Diaz, K.K. Kanazawa, G.P. Gardini, Electrochemical polymerization of pyrrole. Journal of the Chemical Society, Chemical Communications. 1979, 635-636.

77. F. Garnier, New conducting polymers, polythiophene. Actual Chimique. 1984, 59-60.

78. L.W. Shacklette, R.L. Elsenbaumer, R.R. Chance, H. Eckhardt, J.E. Frommer, R.H. Baughman, Conducting complexes of polyphenylene sulphides. Journal of Chemical Physics. 1981, 75: 1919-1927.

79. I. Murase, T. Ohnishi, T. Noguchi, M. Hirooka, Highly conducting poly(phenylenevinylene) prepared from a sulfonium salt. Polymer Communication. 1984, 25: 327-329.

80. S. Radhakrishnan, S. Prakash, Chepuri R.K. Rao, M. Vijayan, Organically soluble bifunctional polyaniline-magnetite composites for sensing and supercapacitor applicaitons. Electrochemical and Solid-State Letters. 2009, 12: A84-A87.

81. S. Radhakrishnan, Chepuri R.K. Rao, M. Vijayan, Electrochemical synthesis and studies of polypyrroles doped by renewable dopant cardanol azophenylsulfonic acid derived from cashew nutshells. Journal of Applied Polymer Science. 2009, 114: 3125-3131.

82. N. Balci, L. Toppare, U. Akbulut, D. Stanke, M.L. Halbensleben, Polypyrrole grafts synthesized via electrochemical polymerization. Journal of Macromolecular Science, Part A Pure and Applied Chemistry. 1998, A35: 1727-1739.

83. M. Fujii, K. Aril, K. Yoshino, Branching patterns of a conducting polymer polymerized electrochemically with a constant-current source. Journal of Electrochemical Society. 1993, 140: 1838-1842.

84. S. Radhakrishnan, R. Muthukannan, U. Kamatchi, Chepuri R. K. Rao, M. Vijayan, Performance of phosphoric acid doped polyaniline as electrode material for aqueous redox supercapacitor. Indian Journal of Chemistry. 2011, 50A: 970-978.

85. S. Uemura, T. Nakahir, N. Kobayashi, Photopolymerization of aniline derivatives by photoinduced electron transfer for application to image formation. Journal of Materials Chemistry. 2001, 11: 1585-1589.

86. X. Gong, L. Dai, A. W.H. Mau, H.J. Griesser, Plasma-polymerized polyaniline films; synthesis and characterization. Journal of Polymer Science Part A: Polymer Chemistry. 1998, 36: 633-643.

87. Y. Shen, J. Sun, J. Wu, Q. Zhou, Synthesis and characterization of water-soluble conducting polyaniline by enzyme catalysis. Journal of Applied Polymer Science. 2005, 96: 814-817.

88. C. Weder. Organometallic conjugated polymer network. Journal of Inorganic and Organomatallic Polymers and Materials. 2006, 16: 101-113.

89. A. Angeli, Pyrrole black. Preliminary note. I. Gazzetta Chimica Italiana. 1916, 46: 279-283.

90. A. Angeli. L. Alessandri, Pyrrole black. Preliminary note.II. Gazzetta Chimica Italiana. 1916, 46: 283-300.

91. F. Jonas, G. Heywang, W. Schmidtberg, J. Heinze, M. Dietrich, Preparation and use of thiophene derivative polymers. European. Patent. 1986, 106236.

92. R. Corradi, S.P. Armes, Chemical synthesis of poly(3,4-ethylenedioxy- thiophene) Synthetic Metals. 1997, 84: 453-454.

93. D.M. De Leeuw, P.A. Kraakman, P.F.G. Bongaerts, C.M.J. Mutsaers, D.B.M. Klassen, Electroplating of conducting polymers for the metallization of insulators. Synthetic Metals. ..1994, 66: 263-273.

94. F. Joans, W. Krafft, New polythiophene dispersions, their preparation and their use. European Patent. 1991, 124841440957.

95. Q. Pei, G. Zuccarello, M. Ahlskog, O. Inganaes, Electrochromic and highly stable poly(3,4-ethylenedioxythiophene) switches between opaque blue-black and transparent sky blue. Polymer. 1994, 35: 1347-1351.

96. P. Elena, L. Mao, B. Arkady, B. Michael, Major effect of electropolymerization solvent on morphology and electrochromic properties of PEDOT films. Chemistry of Materials. 2010, 22: 4019-4025.

97. R. Parthasarathy, C.R. Martin, Synthesis of polymeric microcapsule arrays and their use for enzyme immobilization, Nature. 1994, 369: 298-301.

98. S. Radhakrishnan, K. Krishnamoorthy, C. Sekar, J. Wilson, S-J. Kim, A promising electrochemical sensing platform based on ternary composite of polyaniline-Fe2O3-reduced graphene oxide for sensitive hydroquinone determination. Chemical Engineering Journal. 2015, 259: 594-602.

99. B.H. Kim, D.H. Park, J. Joo, S.G. Yu, S.H. Lee, Synthesis characteristics, and field emission of doped and de-doped polypyrrole, polyaniline, poly(3,4- ethylenedioxythiophene) nanotubes and nanowires. Synthetic Metals. 2005, 150: 279-284.

100. M.H. Rose, R. Lee, S. Steve, S. Stephan, E.M. Thomas, Template fabrication of protein-functionalized gold-polypyrrole-gold segmented nanowires. Chemistry of Materials. 2004, 16: 3431-3438.

101. S. Radhakrishnan, C. Sumathi, V. Dharuman, J. Wilson, Gold nanoparticles functionalized poly(3,4-ethylenedioxythiophene) thin film for highly sensitive label free DNA detection. Analytical Methods. 2013, 5: 684-689.

102. R.E. Lamont, W.A. Ducker, Surface-induced transformations for surfactant aggregates. Journal of American Chemical Society. 1998, 120: 7602-7607.

103. Z.X. Wei, Z.M. Zhang, M.X. Wan, Formation mechanism of self-assembled polyaniline micro/nanotubes. Langmuir. 2002, 18: 917-921.

104. Z.M. Zhang, Z.X. Zhang, M.X. Wan, Nanostructures of polyaniline doped with inorganic acids. Macromolecules. 2002, 35: 5937-5942.

105. P.G. He, Y. Xu, Y.Z. Fang, Applications of carbon nanotubes in electrochemical DNA bio-sensors. Microchimica Acta. 2006, 152: 175-186.

106. J. Wang, G.D. Liu, M.R. Jan, Ultrasensitive electrical biosensing of proteins and DNA: Carbon-nanotubes derived amplification of the recognition and transduction events. Journal of American Chemical Society. 2004, 126: 3010-3011.

107. Y. Zhang, H. Ma, K. Zhang, S. Zhang, J. Wang, An improved DNA biosensor built by layer-by-layer covalent attachment of multi-walled carbon nanotubes and gold nanoparticles. Electrochimica Acta. 2009, 54: 2385-2391.

108. W. Sun, X. Qi, Y. Zhang, H. Yang, H. Gao, Y. Chen, Z. Sun, Electrochemical DNA biosensor for the detection of Listeria monocytogenes with dendritic nanogold and electrochemical reduced graphene modified carbon ionic liquid electrode. Electrochimica Acta. 2012, 85: 145-151.

109. L. Zhang, H. Peng, P.A. Kilmartin, C. Soeller, J. Travas-Sejdic. Polymeric acid doped polyaniline nanotubes for oligonucleotide sensors, Electroanalysis. 2007, 19: 870-875.

110. Y. Feng, T. Yang, W. Zhang, C. Jiang, K. Jiao, Enhanced sensitivity for deoxyribonucleic acid electrochemical impedance sensor: Gold nanoparticle/polyaniline nanotubes membranes. Analytica Chemica Acta. 2008, 616: 144-151.

111. M. Du, T. Yang, K. Jiao. Rapid DNA electrochemical biosensing platform for label-free potentiometric detection of DNA hybridization. Talanta. 2010, 81: 1022-1027.

112. N. Zhou, T. Yang, C. Jiang, M. Du, K. Jiao, Highly sensitive electrochemical impedance spectroscopic detection of DNA hybridization based on Aunano-CNT/PANinano films. Talanta. 2009, 77: 1021-1026.

113. X. Yang, Z. Zhu, T. Dai, Y. Lu, Facile fabrication of functional polypyrrole nanotubes via a reactive self-degraded template. Macromolecular Rapid Communications. 2005, 26: 1736-1740.

114. S. Radhakrishnan, C. Sumathi, V. Dharuman, J. Wilson, Polypyrrole nanotubes-polyaniline composite for DNA detection using methylene blue as intercalator. Analytical Methods. 2013, 5: 1010-1015.

115. J. Wilson, S. Radhakrishnan, C. Sumathi, V. Dharuman, Polypyrrole-polyaniline-Au (PPy-PANi-Au) nano composite films for label-free electrochemical DNA sensing. Sensors and Actuators B. 2012, 171-172: 216-222.

116. S. Radhakrishnan, C. Sumathi, A. Umar, S-J. Kim, J. Wilson, V. Dharuman, Polypyrrole-poly(3,4-ethylenedioxythiophene)-Ag (PPy-PEDOT-Ag) nanocomposite films for label-free electrochemical DNA sensing. Biosensors and Bioelectronics. 2013, 47: 133-140.

117. N. Shuyan, B. Han, W. Cao, Z. Shusheng, Sensitive DNA biosensor improved by Luteolin copper (II) indicator based on silver nanoparticles and carbon nanotubes modified electrode. Analytica Chimica Acta. 2009, 651: 42-47.

118. X. Liu, Z. Cheng, H. Fan, A. Shiyan, R. Han, Electrochemical detection of avian influenza virus H5N1 gene sequence using a DNA aptamer immobilized onto a hybrid nanomaterial-modified electrode. Electrochimica Acta. 2011, 56: 6266-6270.

119. Y. Feng, T. Yang, W. Zhang, C. Jiang, K. Jiao, Enhanced sensitivity for deoxyribonucleic acid electrochemical impedance sensor: gold nanoparticles/polyaniline nanotubes membranes. Analytica Chimica Acta. 2008, 616: 144-151.

Advances in Chemical Engineering

Chapter 4

Computer Aided Design of Shell and Tube Heat Exchangers (Incorporating Most Recent Developments)

C M Narayanan[1]*; Sneha Bhadra; Mukul Kanta Das[2]

[1]National Institute of Technology, Durgapur, India.

*[*]**Correspondence to: CM Narayanan,** National Institute of Technology, Durgapur, India.*

Email: cmn_recd@yahoo.co.in

1. Introduction

Heat exchangers are practically omnipresent in all process industries, power plants, heat recovery units and the like. The feedstock is to be preheated or the product solution (product gas mixture) is to be cooled down to a specific temperature and for these, heat exchangers become invariable. As a result, efficient and economical design and operation of heat exchangers becomes a fundamental parameter that is crucial to the overall economy of the industry.

Among the industrial heat exchangers, exchangers of shell and tube configuration are one of the most popular ones, particularly for large capacity installations. These exchangers are composed of a tube bundle (consisting of 50 – 1000 or more tubes) enclosed within a large diameter shell. The tubes are held at both ends by drilling them into two tubesheets (fixed tubesheet construction). The *effective length* of each tube (L_e) is the length of the tube between the two tubesheets (those portions of the tubes that are drilled into the tubesheets are excluded). Popular values of L_e used in industrial exchangers are 2.5 m, 3.0 m, 3.5 m, 5.0 m and 6.0 m. Of these, L_e = 5.0 m, 6.0 m are most popular. Tubes are usually either 19 mm OD or 25.4 mm OD and the tube pitch (p_T), which is the center to center distance between adjacent tubes, is commonly maintained at 1.25 to 1.5 times the tube OD (see tube count **Tables 3A** to **3F**).

Table 3A: Tube Count Tables (Database – 3)

19 mm OD tubes on 25.4 mm triangular pitch											
Shell ID mm	Fixed tubesheet construction (T.E.M.A. L or M) Number of passes				Floating head construction (T.E.M.A. P or S) Number of passes				U – tube construction (T.E.M.A. U) Number of passes		
	1	2	4	6	1	2	4	6	2	4	6
203.2	42	40	26	24	31	26	16	12	32	24	24
254.0	73	66	52	44	56	48	42	40	52	48	40
304.8	109	102	88	80	88	78	62	68	84	76	74
336.5	136	128	112	102	121	106	94	88	110	100	98
387.3	183	172	146	148	159	148	132	132	152	140	136
438.1	237	228	208	192	208	198	182	180	206	188	182
488.9	295	282	258	248	258	250	228	220	266	248	234
539.7	361	346	318	320	320	314	290	276	330	316	296
590.8	438	416	382	372	400	384	352	336	400	384	356
635.0	507	486	448	440	450	442	400	392	472	440	424
685.8	592	574	536	516	543	530	488	468	554	528	502
736.6	692	668	632	604	645	618	574	556	648	616	588
787.4	796	774	732	708	741	716	666	648	744	716	688
838.2	909	886	836	812	843	826	760	740	852	816	788
889.0	1023	1002	942	920	950	930	878	856	974	932	908
939.8	1155	1124	1058	1032	1070	1052	992	968	1092	1056	1008
990.6	1277	1254	1194	1164	1209	1184	1122	1096	1224	1180	1146
1066.8	1503	1466	1404	1372	1409	1378	1314	1296	1434	1388	1350
1143.0	1726	1690	1622	1588	1635	1608	1536	1504	1652	1604	1560
1219.2	1964	1936	1870	1828	1887	1842	1768	1740	1894	1844	1794
1371.6	2519	2466	2380	2352	2399	2366	2270	2244	2426	2368	2326
1524.0	3095	3058	2954	2928	2981	2940	2832	2800	3006	2944	2884

Table 3B: Tube count tables (Database – 3)

19 mm OD tubes on 25.4 mm square / rotated square pitch							
Shell ID mm	**Floating head construction (T.E.M.A. P or S) Number of passes**				**U – tube construction (T.E.M.A. U) Number of passes**		
	1	**2**	**4**	**6**	**2**	**4**	**6**
203.2	28	26	16	12	28	24	12
254.0	52	48	44	24	52	44	32
304.8	80	76	66	56	78	72	70
336.5	104	90	70	80	96	92	90
387.3	136	128	128	114	136	132	120
438.1	181	174	154	160	176	176	160
488.9	222	220	204	198	224	224	224
539.7	289	272	262	260	284	280	274
590.8	345	332	310	308	348	336	328
635.0	398	386	366	344	408	392	378
685.8	477	456	432	424	480	468	460
736.6	554	532	510	496	562	548	530
787.4	637	624	588	576	648	636	620
838.2	730	712	682	668	748	728	718
889.0	828	812	780	760	848	820	816
939.8	937	918	882	872	952	932	918
990.6	1048	1028	996	972	1056	1044	1020
1066.8	1224	1200	1170	1140	1224	1224	1212
1143.0	1421	1394	1350	1336	1436	1408	1398
1219.2	1628	1598	1548	1536	1640	1628	1602
1371.6	2096	2048	2010	1992	2108	2084	2068
1524.0	2585	2552	2512	2476	2614	2584	2558

Table –3C: Tube count tables (Database – 3)

25.4 mm OD tubes on 31.75 mm square / rotated square pitch							
Shell ID mm	Floating head construction (T.E.M.A. P or S) Number of passes				U – tube construction (T.E.M.A. U) Number of passes		
	1	2	4	6	2	4	6
203.2	17	12	8	12	14	8	6
254.0	30	30	16	18	30	24	12
304.8	52	48	42	24	44	40	32
336.5	61	56	52	50	60	48	44
387.3	85	78	62	64	80	72	74
438.1	108	108	104	96	104	100	100
488.9	144	136	130	114	132	132	120
539.7	173	166	154	156	172	168	148
590.8	217	208	194	192	212	204	198
635.0	252	240	230	212	244	240	230
685.8	296	280	270	260	290	284	274
736.6	345	336	310	314	340	336	328
787.4	402	390	366	368	400	384	372
838.2	461	452	432	420	456	444	440
889.0	520	514	494	484	518	504	502
939.8	588	572	562	548	584	576	566
990.6	661	640	624	620	664	644	640
1066.8	776	756	738	724	764	748	750
1143.0	900	882	862	844	902	880	862
1219.2	1029	1016	984	972	1028	1008	1004
1371.6	1310	1296	1268	1256	1320	1296	1284
1524.0	1641	1624	1598	1576	1634	1616	1614

Table –3D: Tube count tables (Database – 3)

25.4 mm OD tubes on 31.75 mm triangular pitch											
Shell ID mm	Fixed tubesheet construction (T.E.M.A. L or M) Number of passes				Floating head construction (T.E.M.A. P or S) Number of passes				U – tube construction (T.E.M.A. U) Number of passes		
	1	2	4	6	1	2	4	6	2	4	6
203.2	27	26	8	12	18	14	8	12	14	12	6
254.0	42	40	34	24	33	28	16	18	28	24	24
304.8	64	66	52	44	51	48	42	44	52	40	40
336.5	81	74	62	56	73	68	52	44	64	56	52
387.3	106	106	88	92	93	90	78	76	90	80	78
438.1	147	134	124	114	126	122	112	102	122	112	102
488.9	183	176	150	152	159	152	132	136	152	140	136
539.7	226	220	204	186	202	192	182	172	196	180	176
590.8	268	262	236	228	249	238	216	212	242	224	216
635.0	316	302	274	272	291	278	250	240	286	264	246
685.8	375	360	336	324	345	330	298	288	340	320	300
736.6	430	416	390	380	400	388	356	348	400	380	352
787.4	495	482	452	448	459	450	414	400	456	436	414
838.2	579	554	520	504	526	514	484	464	526	504	486
889.0	645	622	586	576	596	584	548	536	596	572	548
939.8	729	712	662	648	672	668	626	608	668	636	614
990.6	808	792	744	732	756	736	704	692	748	728	700
1066.8	947	918	874	868	890	878	834	808	890	856	830
1143.0	1095	1068	1022	1000	1035	1008	966	948	1028	992	972
1219.2	1241	1220	1176	1148	1181	1162	1118	1092	1180	1136	1100
1371.6	1577	1572	1510	1480	1520	1492	1436	1416	1508	1468	1442
1524.0	1964	1940	1882	1832	1884	1858	1800	1764	1886	1840	1794

Table 3E: Tube count tables (Database – 3)

15.875 mm OD tubes on 20.637 mm square / rotated square pitch							
Shell ID mm	Floating head construction (T.E.M.A. P or S) Number of passes				U – tube construction (T.E.M.A. U) Number of passes		
	1	2	4	6	2	4	6
203.2	55	48	34	24	52	40	32
254.0	88	78	62	56	90	80	74
304.8	140	138	112	100	140	128	108
336.5	178	172	146	136	180	164	148
387.3	245	232	208	192	246	232	216
438.1	320	308	274	260	330	312	292
488.9	405	392	352	336	420	388	368
539.7	502	484	442	424	510	488	460
590.8	610	584	536	508	626	596	562
635.0	700	676	618	600	728	692	644
685.8	843	812	742	716	856	816	780
736.6	970	942	868	840	998	956	920
787.4	1127	1096	1014	984	1148	1108	1060
838.2	1288	1250	1172	1148	1318	1268	1222
889.0	1479	1438	1330	1308	1492	1436	1388
939.8	1647	1604	1520	1480	1684	1620	1568
990.6	1840	1794	1700	1664	1882	1816	1754
1066.8	2157	2112	2004	1968	2196	2136	2068
1143.0	2511	2458	2326	2288	2530	2464	2402
1219.2	2856	2808	2686	2656	2908	2832	2764
1371.6	3656	3600	3462	3404	3712	3624	3556
1524.0	4538	4472	4310	4256	4608	4508	4426

Table 3F: Tube count tables (Database – 3)

19 mm OD tubes on 23.8 mm triangular pitch											
Shell ID mm	**Fixed tubesheet construction (T.E.M.A. L or M) Number of passes**				**Floating head construction (T.E.M.A. P or S) Number of passes**				**U – tube construction (T.E.M.A. U) Number of passes**		
	1	**2**	**4**	**6**	**1**	**2**	**4**	**6**	**2**	**4**	**6**
203.2	64	48	34	24	34	32	16	18	32	24	24
254.0	85	72	52	50	60	62	52	44	64	52	52
304.8	122	114	94	96	109	98	78	68	98	88	78
336.5	151	142	124	112	126	120	106	100	126	116	108
387.3	204	192	166	168	183	168	146	136	180	160	148
438.1	264	254	228	220	237	228	202	192	238	224	204
488.9	332	326	290	280	297	286	258	248	298	280	262
539.7	417	396	364	348	372	356	324	316	370	352	334
590.8	495	478	430	420	450	430	392	376	456	428	408
635.0	579	554	512	488	518	498	456	444	534	500	474
685.8	676	648	602	584	618	602	548	532	628	600	570
736.6	785	762	704	688	729	708	650	624	736	696	668
787.4	909	878	814	792	843	812	744	732	846	812	780
838.2	1035	1002	944	920	962	934	868	840	978	928	904
889.0	1164	1132	1062	1036	1090	1064	990	972	1100	1060	1008
939.8	1304	1270	1200	1168	1233	1196	1132	1100	1238	1200	1152
990.6	1460	1422	1338	1320	1365	1346	1266	1244	1390	1336	1290
1066.8	1703	1664	1578	1552	1611	1580	1498	1464	1632	1568	1524
1143.0	1960	1918	1830	1800	1875	1834	1736	1708	1882	1820	1770
1219.2	2242	2196	2106	2060	2132	2100	1998	1964	2152	2092	2044
1371.6	2861	2804	2682	2660	2730	2684	2574	2536	2748	2680	2628
1524.0	3527	3476	3360	3300	3395	3346	3228	3196	3420	3340	3286

1.1. Tube Sheet Layout

Tubes may be laid on the tubesheet using a square pitch arrangement, in which the tubes are aligned in line (**Figure 1**) or using a rotated square or triangular layout, in which cases a staggered tube arrangement is employed (Figures 2, 3). When the arrangement of tubes is staggered, the flow of shellside fluid (which flows over the tubes) becomes more tortuous, there shall be more intimate contacting between fluid elements and consequently, the shellside heat transfer coefficient gets enhanced. It has been observed that the magnitude of shellside heat transfer coefficient (h_0) attained with a triangular pitch layout is often 1.25 to 1.30 times that obtained with a square pitch layout. However, increased totuosity of flow path causes increased resistance to flow of shellside fluid and this would demand higher pumping power requirement and higher operating cost.

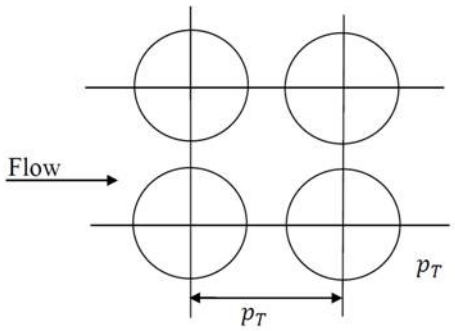

Figure 1: Square pitch layout

A *square pitch arrangement*, therefore, though provides the lowest shellside heat transfer coefficient among the three, causes the lowest pressure drop as well and thereby brings down the operating cost. In an arrangement like this, the tubes remain easily accessible for external cleaning. Thus, if large scale fouling is anticipated on the outer surface of tubes, a square pitch arrangement is to be preferred. The number of tubes that can be accommodated within a given shell diameter is, however, lower in this case as compared to a triangular pitch layout (see tube count tables 3A to 3F in the Appendix). From Figure [1], it can be seen that for a layout like this,

$$p_n = p_P = p_T \qquad (1)$$

Where

p_n = tube pitch normal to flow

p_P = tube pitch parallel to flow

In a *rotated square layout* **(Figure 2)**, the number of tubes within a shell diameter does not differ much from that in a square pitch layout, but since the tubes are staggered, the layout provides larger shellside heat transfer coefficient. The shellside pressure drop shall nevertheless be higher (demanding higher pumping cost) and the tubes shall be less accessible for external cleaning. For this type of layout, p_P and p_n shall be equal in magnitude, but not

equal to p_T. From **Figure (2),** based on simple geometry,

$$p_n = p_P = (p_T / \sqrt{2}) = (0.707\, p_T) \quad (2)$$

A *triangular pitch arrangement* **(Figure 3),** as stated earlier, contributes the largest shellside heat transfer coefficient. This layout also accommodates the largest number of tubes within a given shell diameter and thus provides large heat transfer surface to the exchanger. On the other hand, the shellside pressure drop shall be of larger magnitude and this leads to increased operating cost. The accessibility of tubes for external cleaning when fouled shall also be lower. From **figure (3)**, it can be easily deduced that for a triangular pitch layout like this, p_P and p_n are related to p_T as

$$p_P = 0.866\, p_T \quad (3)$$

$$p_n = 0.5\, p_T \quad (4)$$

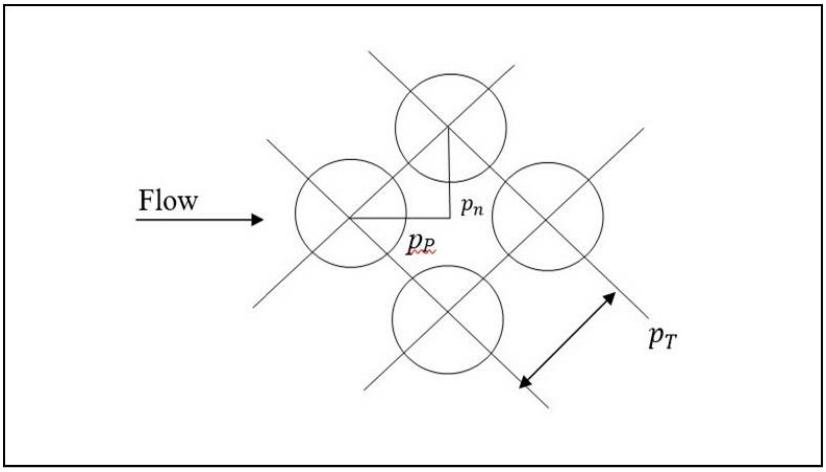

Figure 2: Rotated squre pitch layout

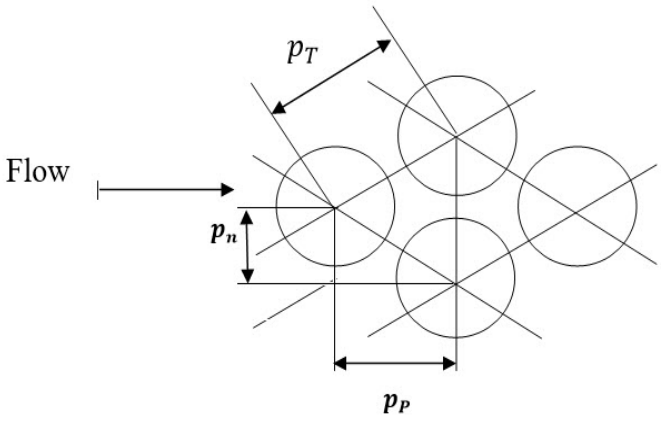

Figure 3: Triangular pitch layout

The tube sheet layout must be thus selected keeping all the above pros and cons in mind.

1.2. Tube sheet Construction

Fixed tubesheet construction **(Figure 4)** is the simplest and cheapest mode of construction for these heat exchangers. Obviously, it is the first choice of the manufacturers. However, this type of construction becomes unreliable when the temperature difference handled by the exchanger is too large. At high working temperatures, the tubes tend to expand and this could lead to fracture (or cracking) of tubes. In such cases, an exchanger with a floating head at one end and a fixed tubesheet at the other end could be used **(Figure 5)**. In such a *pull through floating head construction*, the tubes are free to expand and this differential expansion between the shell and the tube bundle shall not cause damage to the exchanger. The tube bundle is removable for inspection, repair and replacement. However, this type of construction is much more expensive than the conventional fixed tubesheet construction and is therefore recommended only when large scale differential expansion of tubes is anticipated or when frequent mechanical cleaning of tube surfaces due to fouling is imperative.

A still further alternative is to use the *U – tube construction*. In U – tube exchangers, each tube is bent in the shape of the English letter U (U – shaped tube) and these U – tubes are enclosed in the shell. The tubes are supported only at one end using a fixed tube sheet, the U – ends of the tubes remain free or floating. However, the total number of tubes that can be accommodated within a given shell diameter shall be less in this case since tubes cannot be bent to form a sharp U (they tend to crack).

1.3. Baffles and Baffle Pitch

Baffles are installed in the shells of practically all shell and tube heat exchangers. These are mostly circular plates with a number of holes punched (drilled) on them, through which the tubes pass. But, each baffle does not occupy the entire cross – section of the shell. 25% cut segmental baffles are most popular, which are circular discs with 25 per cent of surface being chopped off. The height of the baffle thus becomes three – fourth (75 %) of the shell diameter. The distance between the bottom tip of the baffle and the shell wall is called the *baffle cut* (B_C). For 25% cut segmental baffles, $B_C = (D_S)/4$.

Baffles are seldom welded to the shell wall. They are held in position by means of tie rods and spacers. The spacing between two adjacent baffles is called the *baffle spacing or baffle pitch* (B_S) and is an important design parameter. If L_e is the effective length of each tube, then the number of baffles (N_b) shall be

$$N_b = (L_e / B_S) - 1 \qquad (5)$$

This is based on the assumption that a uniform baffle spacing or baffle pitch has been used through the length of the exchanger. Often, a larger baffle spacing may have to be used at

the inlet and also at the outlet to accommodate inlet and outlet shellside nozzles. If B_{Si} is the baffle spacing employed at the inlet and B_{So} that at the outlet, then

$$N_b = [(L_e - B_{Si} - B_{So}) / B_S] + 1 \quad (6)$$

No doubt, it is most preferable to use a uniform baffle spacing throughout, as far as practicable. The shellside fluid flows over the tubes, between two baffles. This flow space between two adjacent baffles is called the *crossflow section*. The shellside fluid thus flows up or down each crossflow section and thereby moves from one end of the exchanger to the other see (**Figure 4**). The smaller the baffle pitch (B_S) used (and thereby the larger the number of baffles used), the smaller will be the flow area between baffles and the larger the flow velocity of shellside fluid. Consequently, the shellside Reynolds number (Re_S) shall be of higher magnitude and this enhances the shellside heat transfer coefficient (h_o).

It is due to the presence of baffles the shellside fluid tends to execute more and more crossflow (between baffles) and the heat transfer coefficient in crossflow is much higher than that in countercurrent flow or co-current flow (parallel flow).

Baffles also act as support plates for tubes and help in minimizing tube vibrations. Tubes tend to vibrate when shellside fluid flows over them. If these vibrations are of large amplitude, then the tubes tend to undergo fracture or fatigue failure. By supporting tubes between baffles, chances of such fatigue failure of tubes are minimized. To note that the maximum unsupported length of each tube is equal to the baffle pitch (B_S).

However, it is not all smiles with respect to the use of baffles. When the baffle pitch or baffle spacing chosen is small (or the number of baffles installed is large), the flow velocity of shellside fluid increases (as stated earlier) and this leads to increase in the shellside pressure drop as well. It is to be noted that the shellside pressure drop is proportional to the square of the shellside fluid velocity (see equations discussed subsequently in this Chapter) and consequently, a small increase in flow velocity could cause a substantial increase in the pressure drop penalty. A large increase in the shellside pressure drop means large pumping power requirement and increased operating cost.

The baffle spacing (B_S) and the number of baffles to be installed must be, therefore, judiciously chosen. The number of baffles must be sufficiently large (the baffle spacing sufficiently small) so as to maintain the shellside heat transfer coefficient sufficiently large and also to ensure adequate support to tubes, but it should also be not too large such that the shellside pressure drop penalty does not exceed the maximum permissible limit. TEMA (Tubular Exchangers Manufacturers Association) specifies the following criterion for the selection of baffle spacing / baffle pitch in a shell and tube heat exchanger:

$$(D_S/5) \leq B_S \leq (D_S) \quad (7)$$

In other words, the baffle spacing must be so chosen that it never falls below 20% (one – fifth) of the shell diameter (D_S) and should also never exceed the shell diameter itself. Thus

$$B_S \text{ (min)} = (D_S/5) \quad (8)$$

$$B_S \text{ (max)} = (D_S) \quad (9)$$

During the design of the exchanger, it is common practice to choose the minimum baffle spacing at the outset and subsequently increase it if the shellside pressure drop is found to exceed the maximum permissible limit.

There are occasions where tubes are avoided in the baffle window. This is called the *no – tubes – in – baffle window* construction. The *baffle window* is the space between two *alternate* baffles and adjacent to the shell wall see **(Figures 4 and 5)**. It is therefore obvious that the maximum unsupported length of each tube in the baffle window is ($2B_S$) and not one baffle pitch as is the case with other tubes in the crossflow section. Consequently, the tubes in the baffle window tend vibrate at larger amplitudes when the shellside fluid flows over them and the chances of fatigue failure of these tubes become larger. However, by avoiding tubes in the baffle window, the effective number of tubes in the exchanger gets reduced, thereby bringing down the heat transfer surface available. The *no – tubes – in – baffle window* construction must be therefore used only when the shellside mass velocity is too large and large scale tube vibrations are anticipated in the baffle window.

1.4. Multipass Construction

Most of the industrial shell and tube heat exchangers employ multipass construction. For example, a 1 – 2 exchanger (in which the number of shellside passes = n_S = 1 and the number of tubeside passes = n_t = 2) is what is sketched in **Figure (4).** This uses one pass partition at one end of the exchanger. The tubeside fluid enters at this end, flows through all the tubes above the pass partition (there could be 50 to 500 or more tubes in this section) and after reaching the other end of the exchanger, flows back through the remaining tubes below the pass partition and is discharged from the end – 1 itself. Since the fluid traverses the length of the exchanger twice, the number of tubeside passes becomes equal to 2 (n_t = 2). The shellside fluid, on the other hand, enters at one end of the exchanger, flows over tubes in each crossflow section and is discharged from the other end, thereby constituting only one pass (n_S = 1).

In a similar way, a 2 – 4 heat exchanger (n_S = 2, n_t = 4) is what is sketched in figure (5). There are three tubeside pass partitions in the exchanger, two at one end (where the tubeside fluid enters) and one at the other end. The tubeside fluid is thus made to traverse the length

of the exchanger four times (each time through one – fourth of the total number of tubes), thereby executing four tubeside passes ($n_t = 4$). On the shellside, there is one longitudinal pass partition (along the axis of the shell) which forces the shellside fluid to execute two shellside passes ($n_S = 2$).

Multipass constructions provide higher heat transfer coefficients and thereby help in attaining improved heat transfer effectiveness for the exchanger. However, such exchangers are more expensive to fabricate, install and maintain. Both the tubeside and shellside pressure drop penalties shall be higher. There shall be additional pressure drop due to flow reversal.

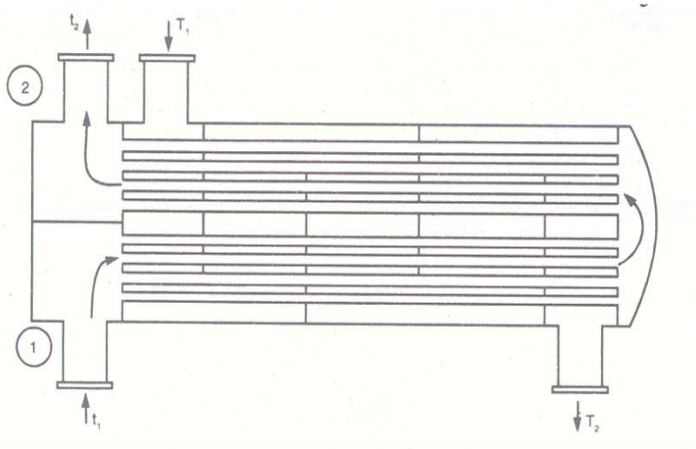

Figure 4: Schematic of a 1 – 2 shell and tube heat exchanger (with fixed tube sheets)

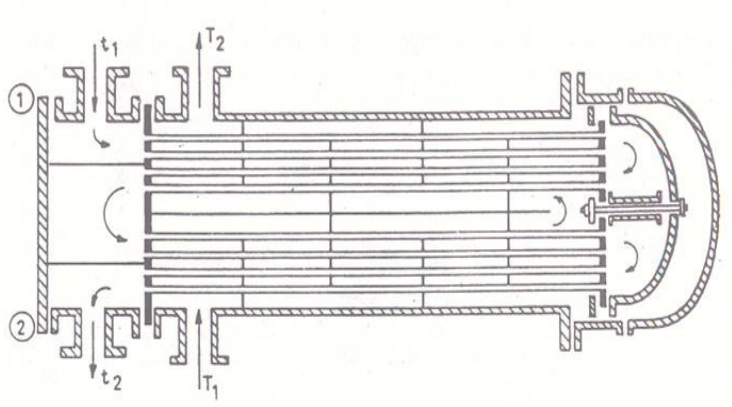

Figure 5: Schematic of a 2 – 4 shell and tube heat exchanger (with floating head construction)

A construction with larger number of passes must be therefore employed only at high capacities, when the amount of fluid to be handled (the amount of fluid being heated or cooled) is large. It is usual practice to start with an exchanger with one shellside pass ($n_S = 1$) and two or more tubeside passes ($n_t = 2, 4, 6$ etc) and if it is found unsuitable for the purpose, then go for a 2 – 4 construction or an exchanger with two shellside passes ($n_S = 2$) and four or more tubeside passes ($n_t = 4, 8, 12$ etc). During the estimation of the required heat transfer surface (discussed later under the CAD package in Section – 2), we do get signals regarding the suitability of the pass arrangement chosen. For example, during the computation of the heat transfer surface using F_T method, if the computed value of F_T factor happens to be negative or indeterminate (logarithm of a negative quantity appears in the expression), then it means

that the chosen pass arrangement is non-operable and an alternate pass arrangement is to be selected. In the same way, under ϵ - NTU Method, if the computed value of $NTU\ (max)$ is found to be negative or indeterminate, then again it means that the pass arrangement considered is unsuitable.

In high capacity installations, it is also common practice to use exchangers in series or in parallel.

1.5. Selection of Tube Side and Shell Side Fluids

Among the cold and hot fluids, the question of which one is to be placed on the tubeside and which one on the shellside is mostly dictated by economic considerations. A few thumb rules could be useful here. For example, the more corrosive or more fouling fluid is recommended to be used on the tubeside, since cleaning and replacement of the large diameter shell shall be more laborious and expensive. When the fluids are pumped at high pressure (mainly in the case of gases), the high pressure fluid be used on the tubeside to avoid an expensive, thick-walled, high pressure shell.

When there is large difference between the flow rates of the two fluids, the larger stream be placed on the tubeside and the smaller stream on the shellside. This is because fully developed turbulent flow can be achieved on the shellside at much lower Reynolds number (at $Re_S \geq 3000$), while Reynolds numbers exceeding 10000 are required on the tubeside for maintaining fully developed turbulent flow. However, in such cases, special care should be taken to ensure that the pressure drop penalty on the tubeside is well within the maximum permissible limit prescribed.

The CAD package discussed may very well be re-executed considering both alternatives and based on the results, the choice could be made.

2. CAD Preliminaries

Design of heat exchangers involves, broadly speaking, two steps:

(a) Estimation of the heat transfer surface requirement of the exchanger,

(b) Estimation of the pressure drop penalty in each fluid stream (in the cold fluid stream and in the hot fluid stream).

For a well – designed heat exchanger, the heat transfer surface requirement must be reasonably low. In other words, the exchanger must be able to perform the duty (must heat the cold fluid to the specified temperature at the specified rate or cool the hot fluid to the desired temperature at the desired rate) with a reasonably low heat transfer surface requirement.

By pressure drop penalty, we mean the pressure difference driving force required for pumping the cold fluid / hot fluid at the required flow rate through the exchanger. The operating cost (pumping cost of fluids) of the exchanger is thus decided by the pressure drop penalty and for an economic operation of the exchanger, this penalty must be reasonably low.

On occasions, the above two conditions could contradict against each other and we would have to make a compromise between the two. For example, to restrict the operating cost (to maintain the pressure drop penalty in both fluid streams below the maximum permissible limit), we may have to accommodate a larger heat transfer surface. Conversely, to retain the heat transfer surface requirement of the exchanger at a reasonably low value, a larger pressure drop penalty and thereby a larger operating cost may have to be tolerated.

Heat exchanger problems could be a sizing problem or a rating problem. In a *sizing problem*, we design a heat exchanger for a specific duty, while in a *rating problem*, the heat exchanger is available and we estimate whether the available heat exchanger is suitable for performing the given duty. The design procedures are similar, though the sizing problem demands an iterative (trial and error) procedure, while in a rating problem, the computations are relatively straightforward.

2.1. Cad Package for Sizing Problem

Let us first consider a sizing problem. As stated above, here we design a shell and tube heat exchanger for a specific purpose, such as for heating a cold fluid from temperature t_1 to temperature t_2 at the rate of $\dot{m}$ kg / hr using a hot fluid flowing at $\dot{m}_S$ kg/hr or vice versa. The step by step procedure is described below. This entire procedure has also been illustrated in all details in the CAD flow sheet of this section **(Figures 7A to 7p).**

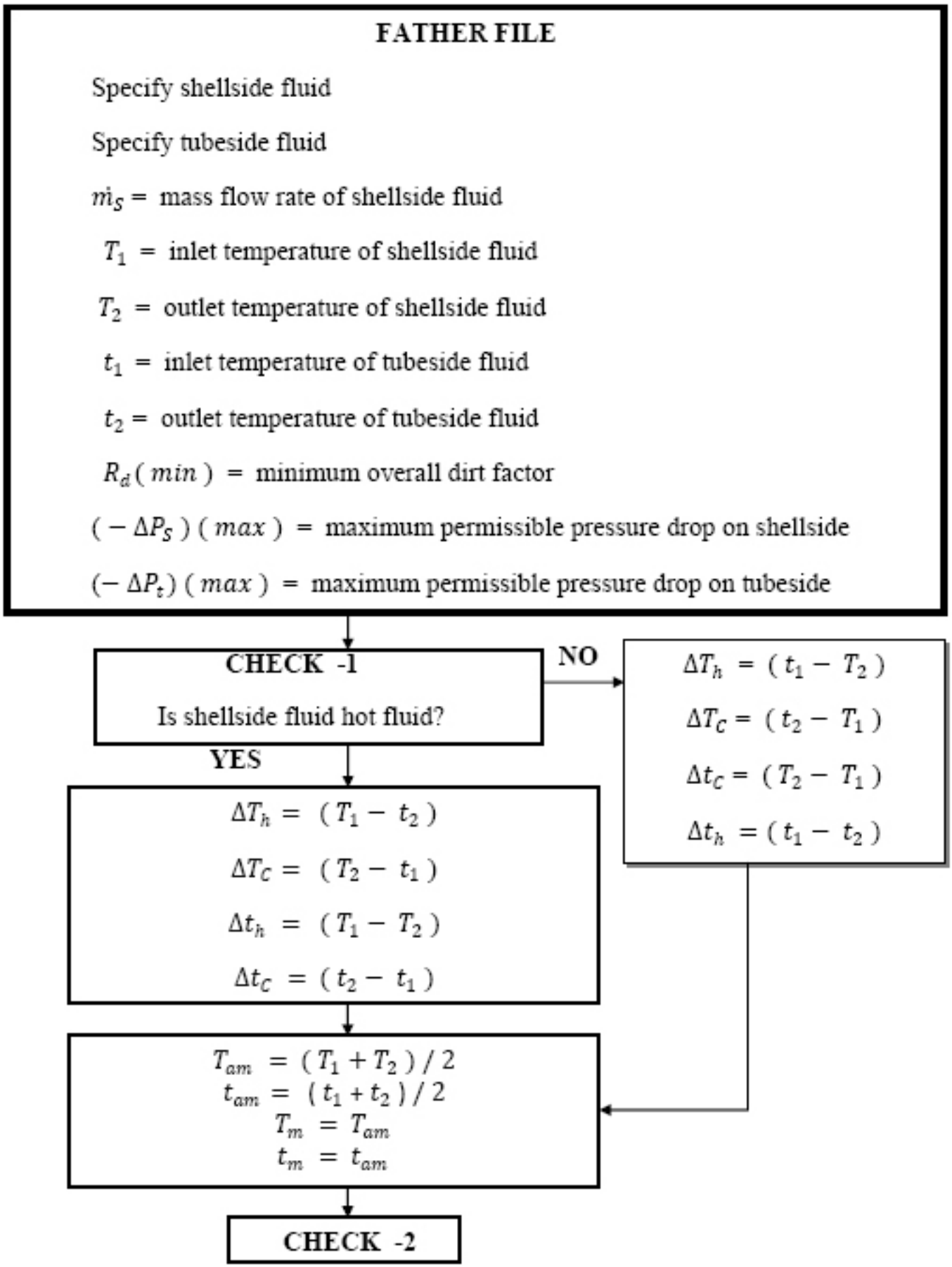

Figure 7A: Computer Aided Design of Shell and Tube Heat Exchangers (Sizing Problem)

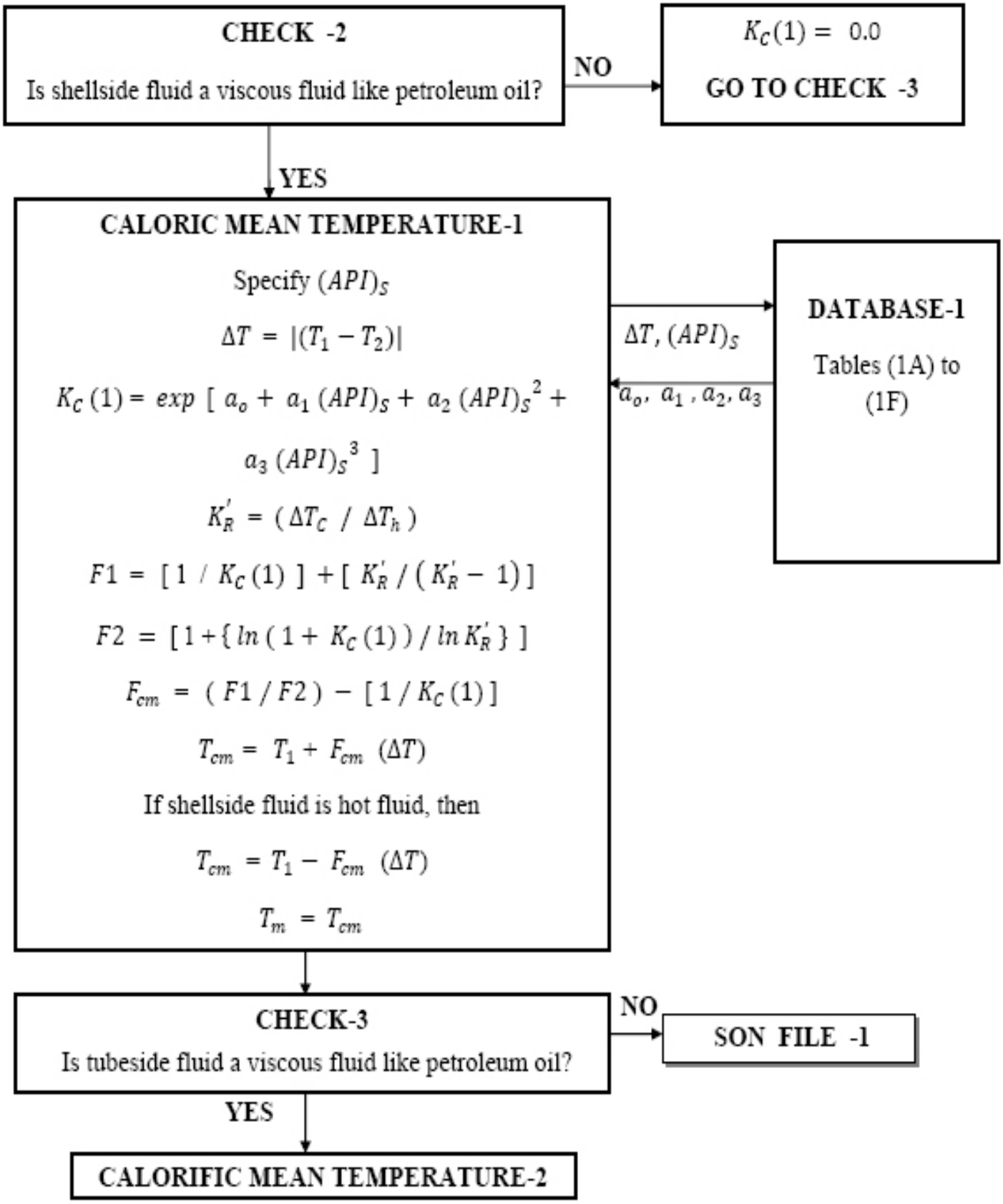

Figure 7B: CAD of Shell and Tube Heat Exchangers (Sizing Problem)-continued

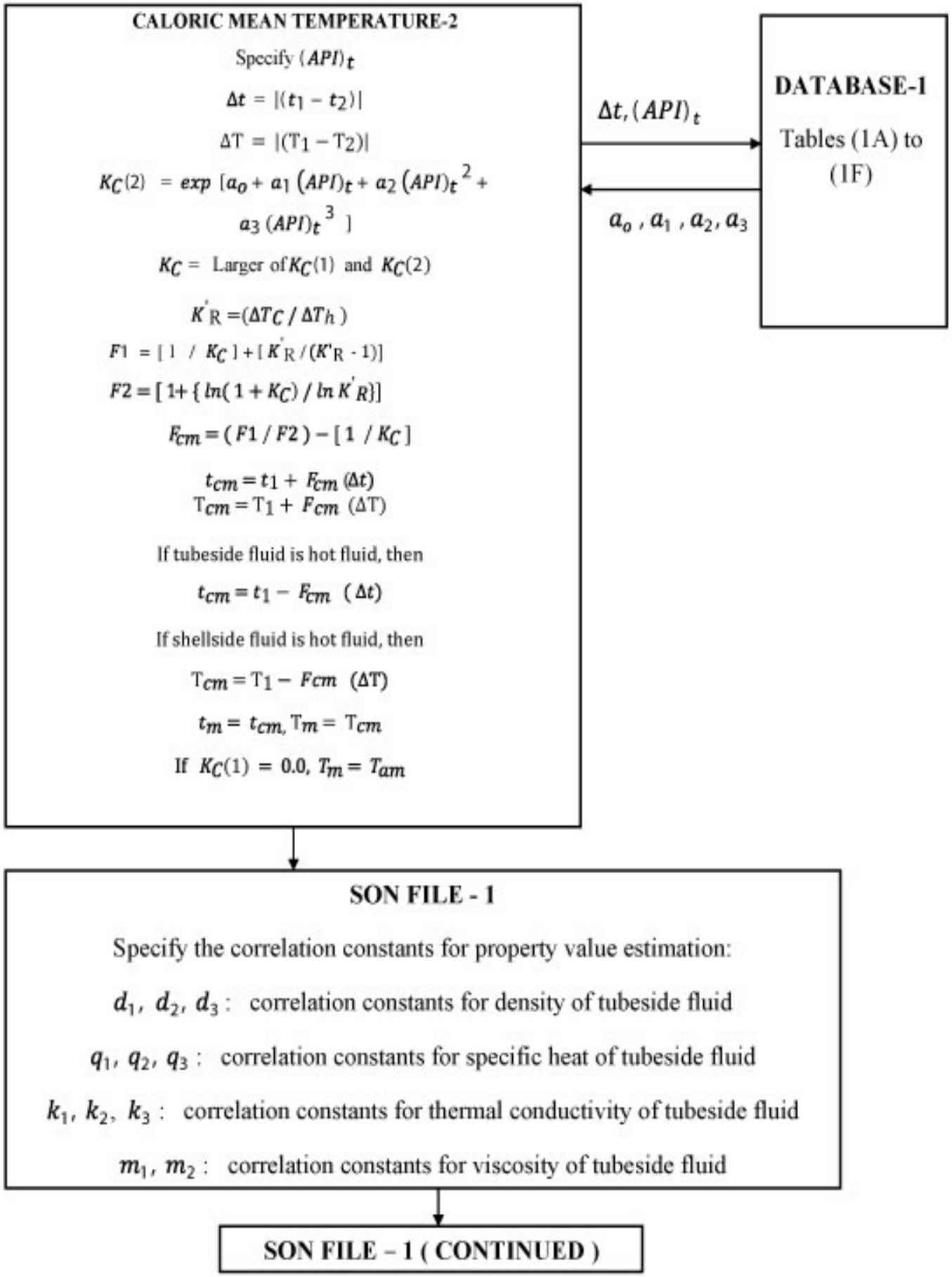

Figure 7C: CAD of shell and Tube Heat Exchangers (Sizing Problem)- countinued

SON FILE – 1 (CONTINUED)

d_4, d_5, d_6 : correlation constants for density of shellside fluid

q_4, q_5, q_6 : correlation constants for specific heat of shellside fluid

k_4, k_5, k_6 : correlation constants for thermal conductivity of shellside fluid

m_3, m_4 : correlation constants for viscosity of shellside fluid

PROPERTY VALUES

$$\rho_f = d_1 + d_2 (d_3 - t_m)$$

$$C_P = q_1 + q_2 (q_3 - t_m)$$

$$k_f = k_1 + k_2 (k_3 - t_m)$$

$$\mu_f = exp [- m_1 - (m_2 / t_m)]$$

$$\rho_{fS} = d_4 + d_5 (d_6 - T_m)$$

$$C_{PS} = q_4 + q_5 (q_6 - T_m)$$

$$k_{fS} = k_4 + k_5 (k_6 - T_m)$$

$$\mu_{fS} = exp [- m_3 - (m_4 / T_m)]$$

HEAT BALANCE

$$\Delta T = |(T_1 - T_2)|$$

$$\Delta t = |(t_1 - t_2)|$$

$$Q = \dot{m}_S C_{PS} \Delta T$$

$$\dot{m} = Q / (C_P \Delta t)$$

Select overall design heat transfer coefficient U_D from specified range given in Database – 2 .

Let $U_i = U_D$

HEAT TRANSFER AREA

Figure 7D: CAD of shell and Tube Heat Exchangers (Sizing Problem)- countinued

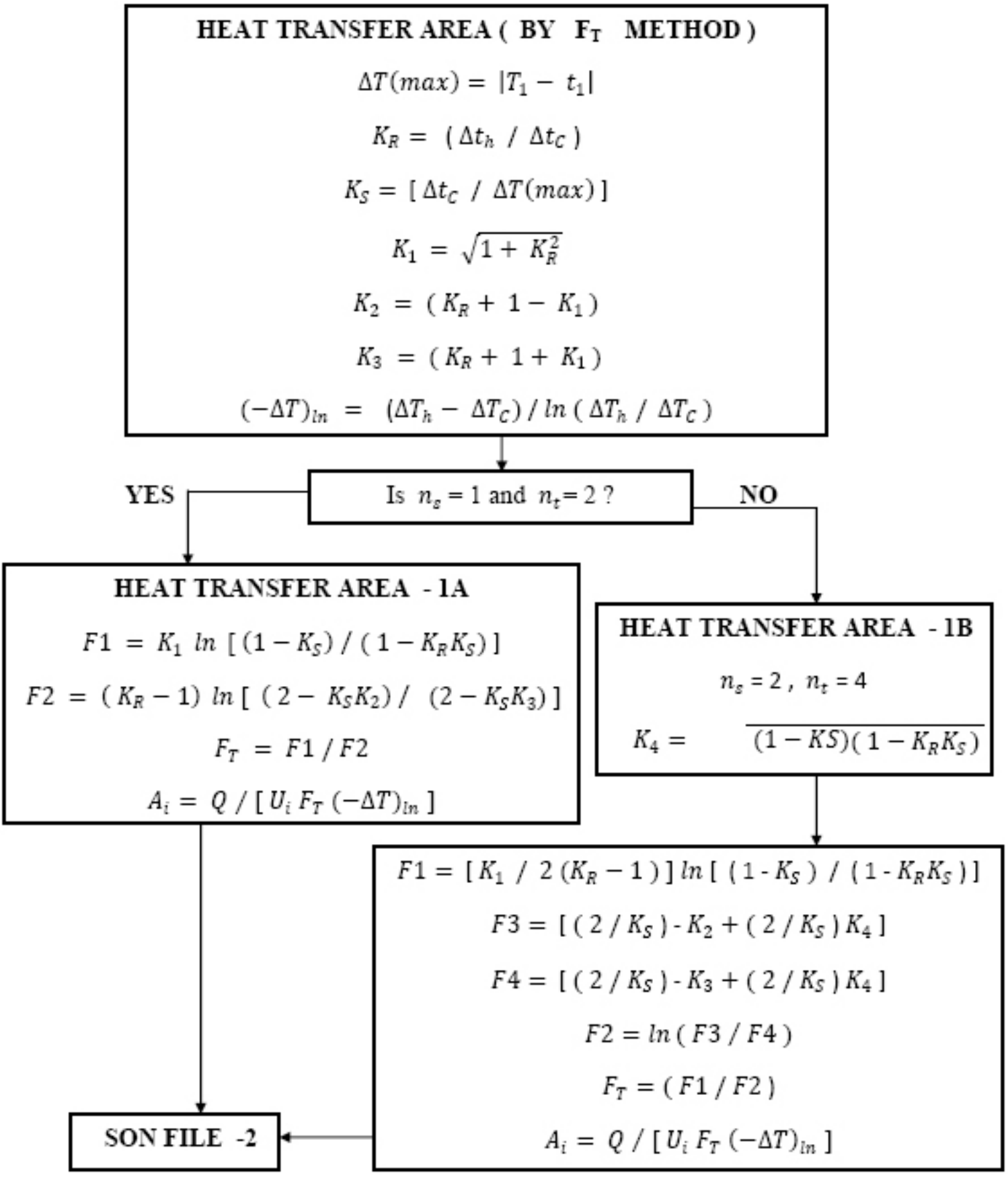

Figure 7E: CAD of shell and Tube Heat Exchangers (Sizing Problem)- countinued

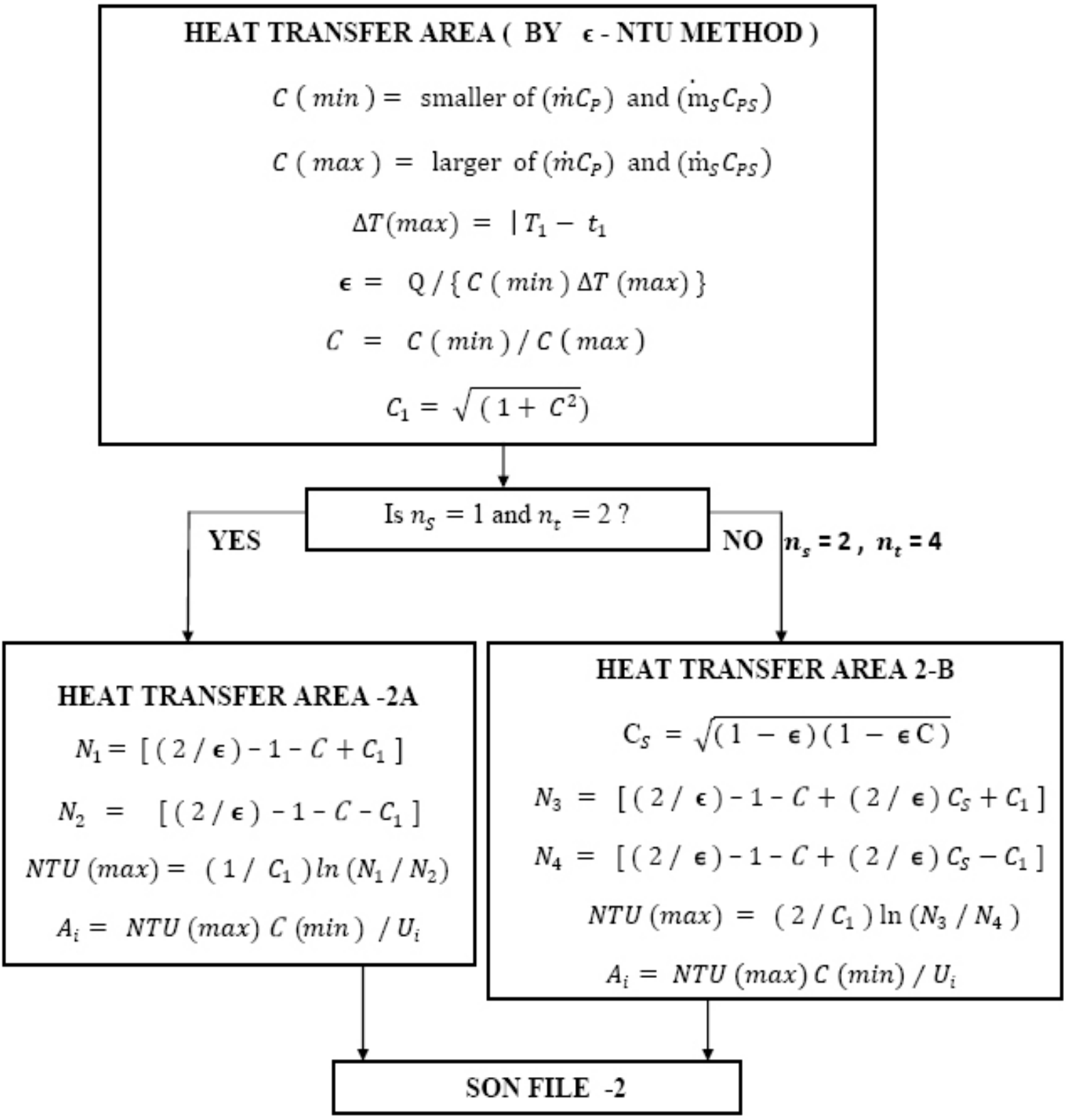

Figure 7F: CAD of shell and Tube Heat Exchangers (Sizing Problem)- countinued

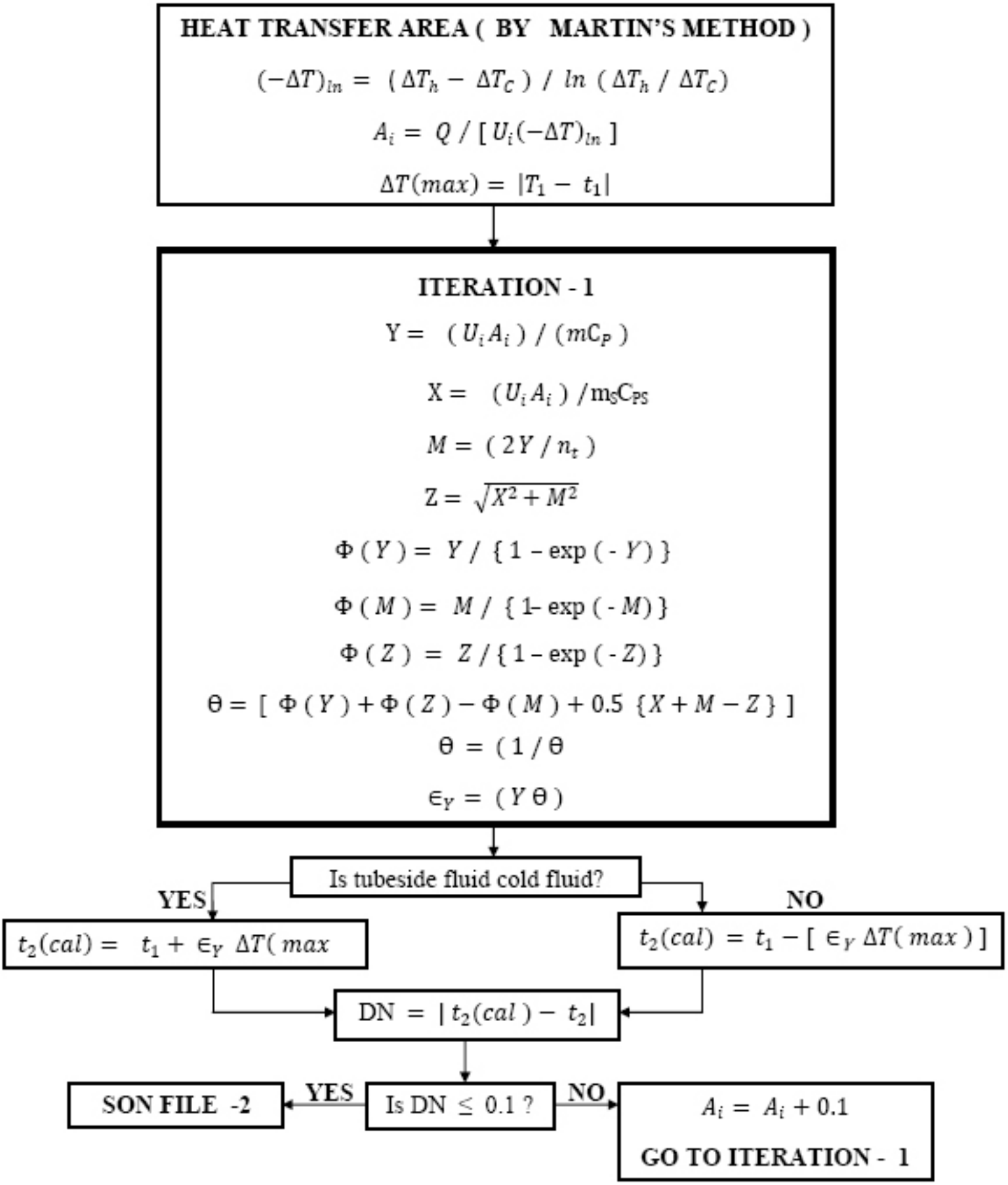

Figure 7G: CAD of shell and Tube Heat Exchangers (Sizing Problem)- countinued

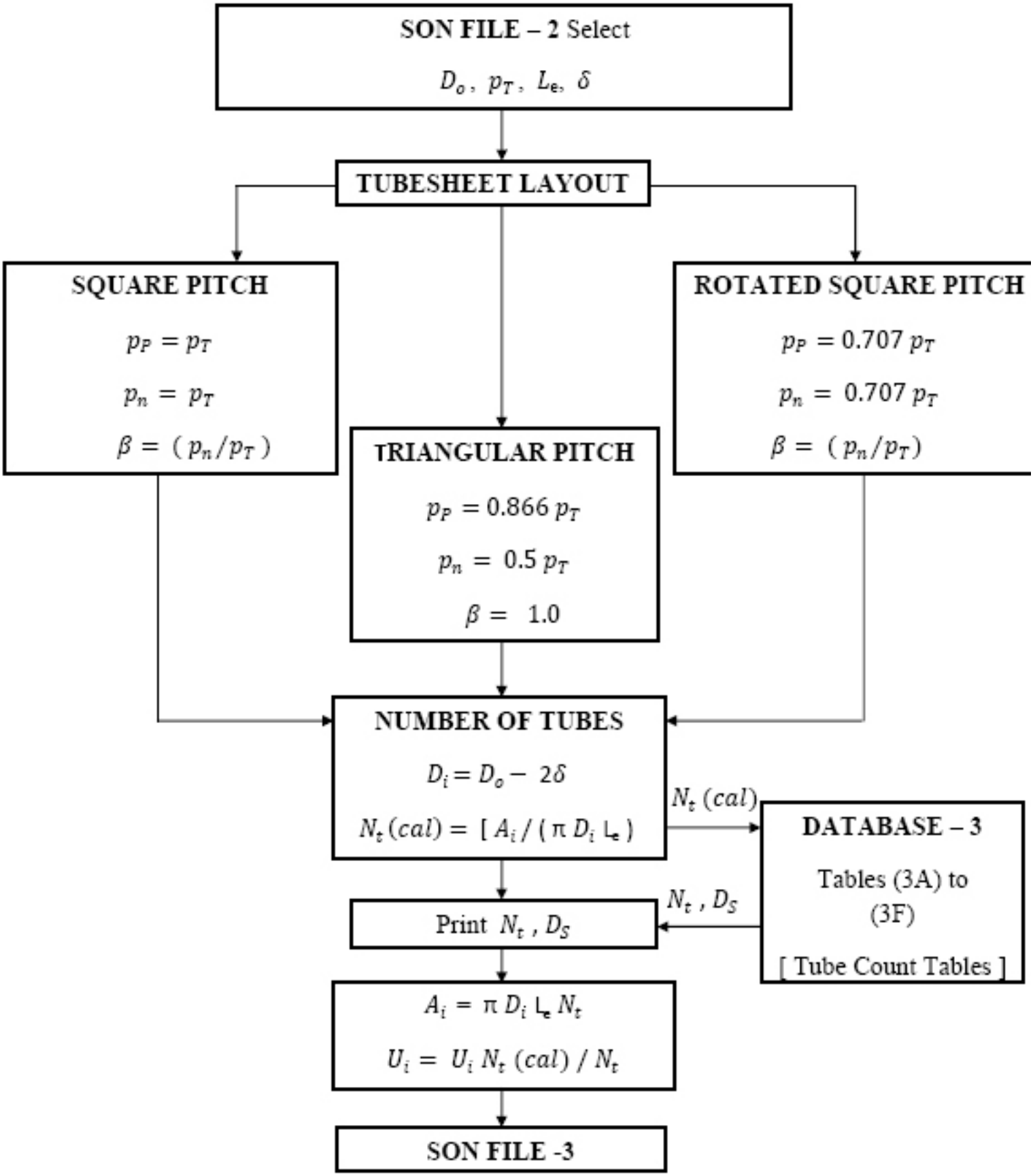

Figure 7H: CAD of shell and Tube Heat Exchangers (Sizing Problem)- countinued

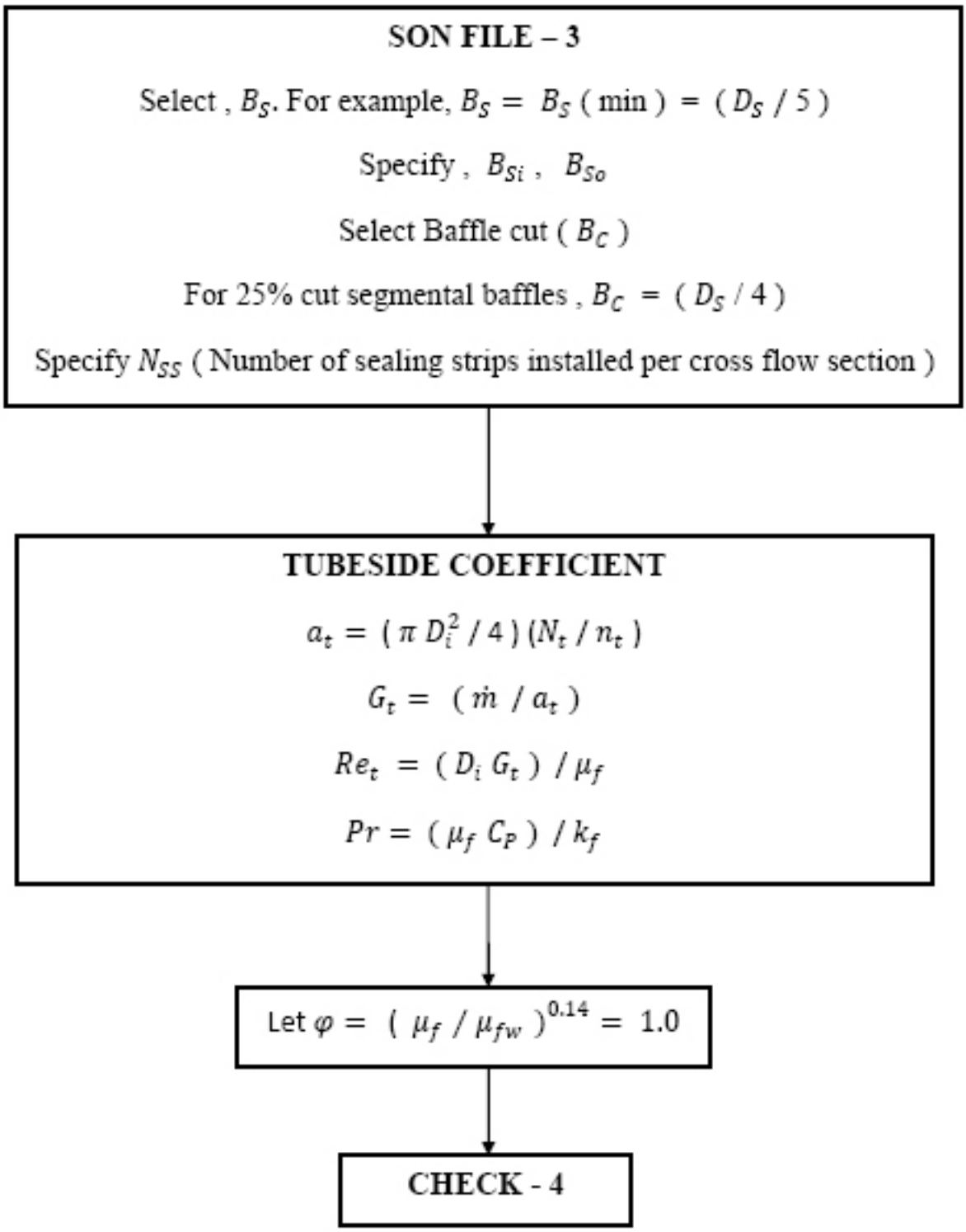

Figure 7I: CAD of shell and Tube Heat Exchangers (Sizing Problem)- countinued

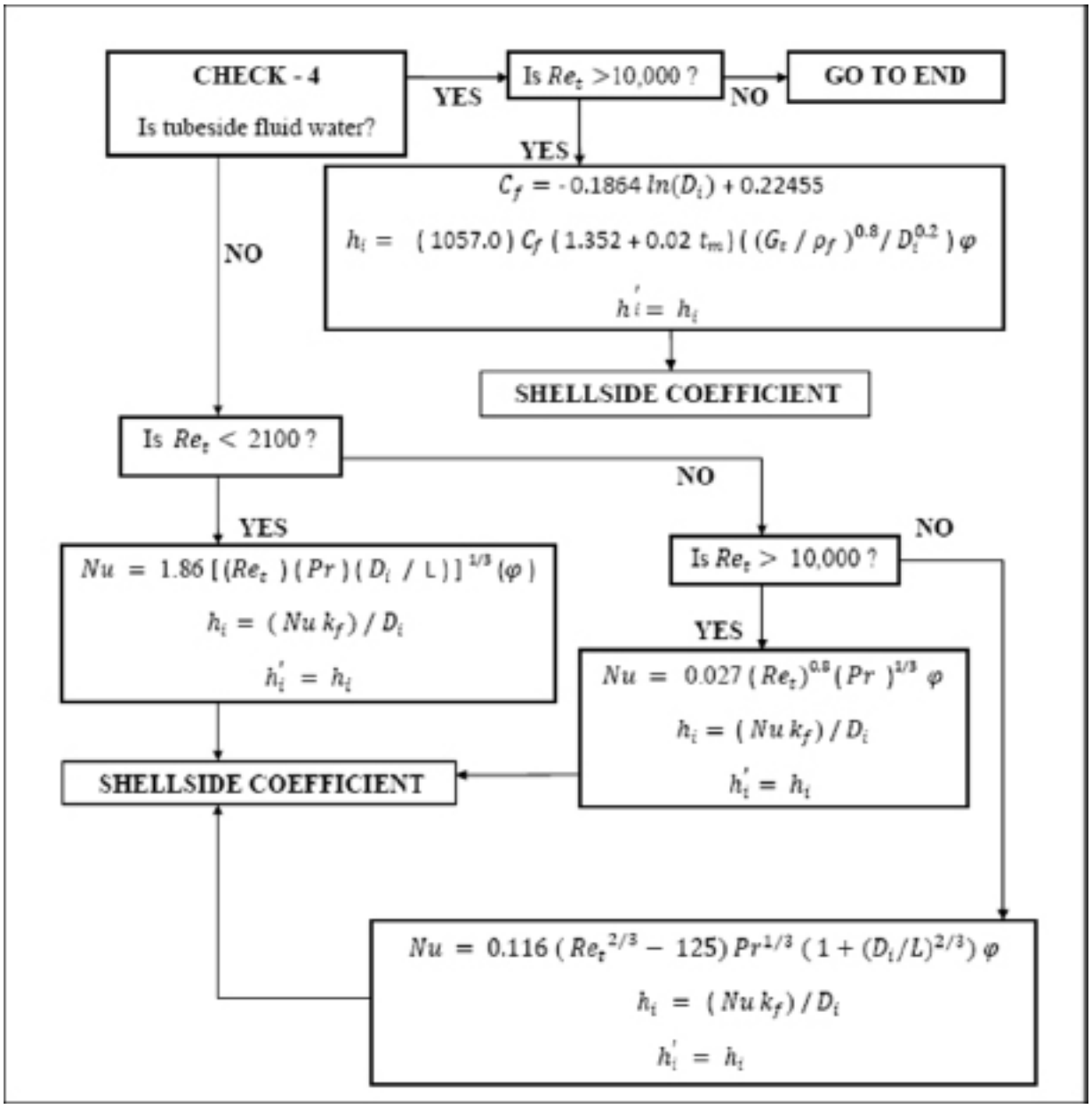

Figure 7J: CAD of shell and Tube Heat Exchangers (Sizing Problem)- countinued

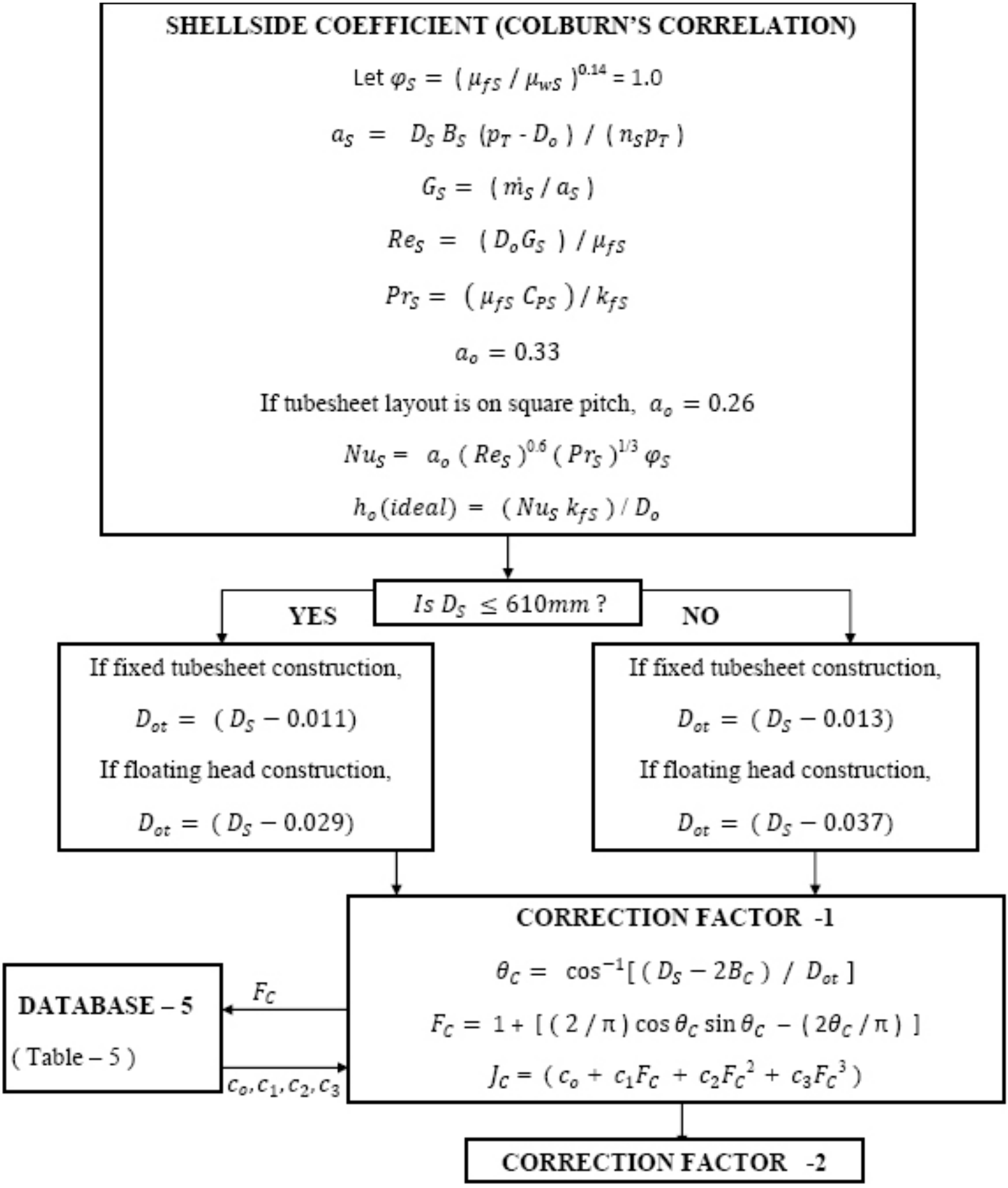

Figure 7K: CAD of shell and Tube Heat Exchangers (Sizing Problem)- countinued

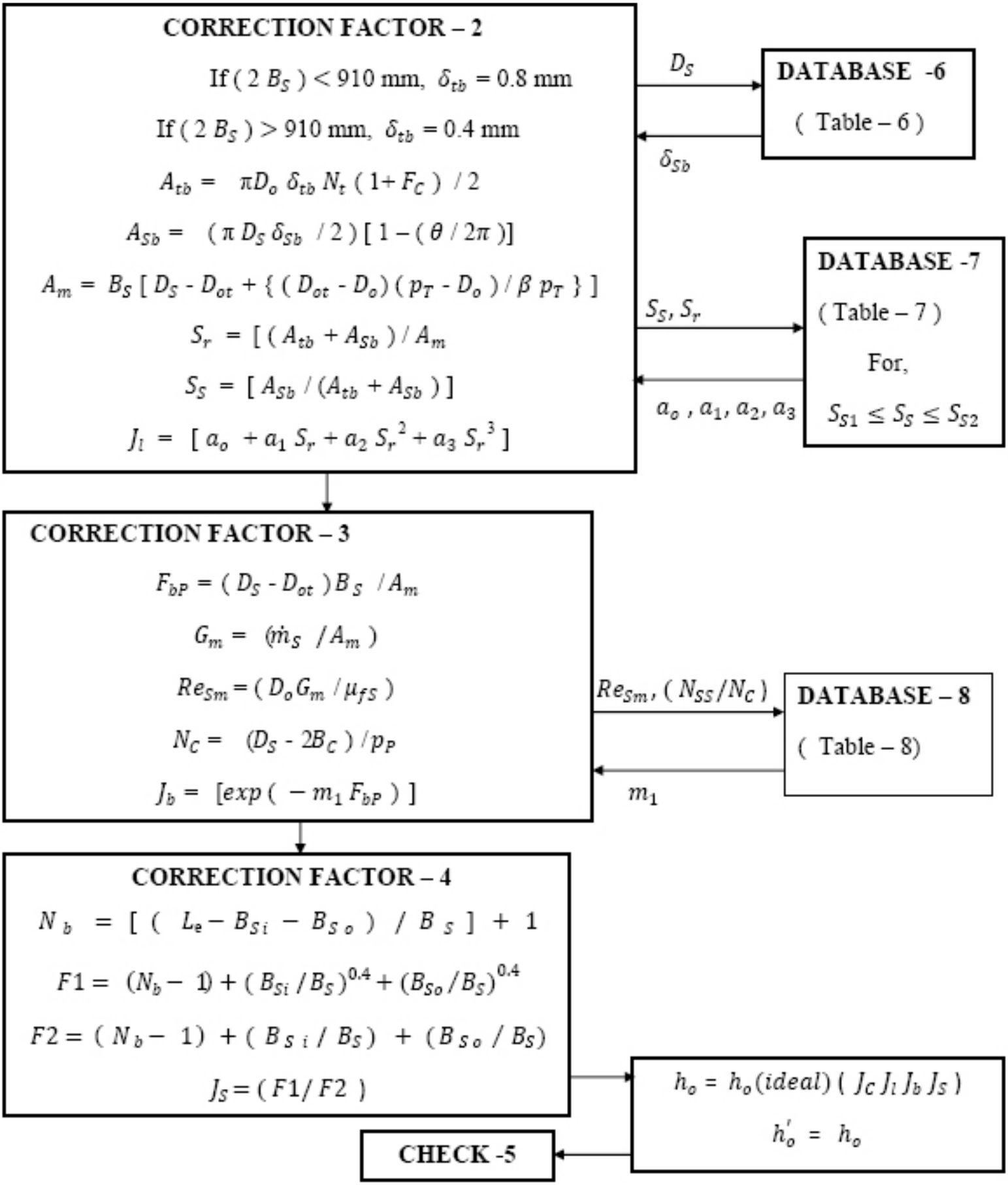

Figure 7L: CAD of shell and Tube Heat Exchangers (Sizing Problem)- countinued

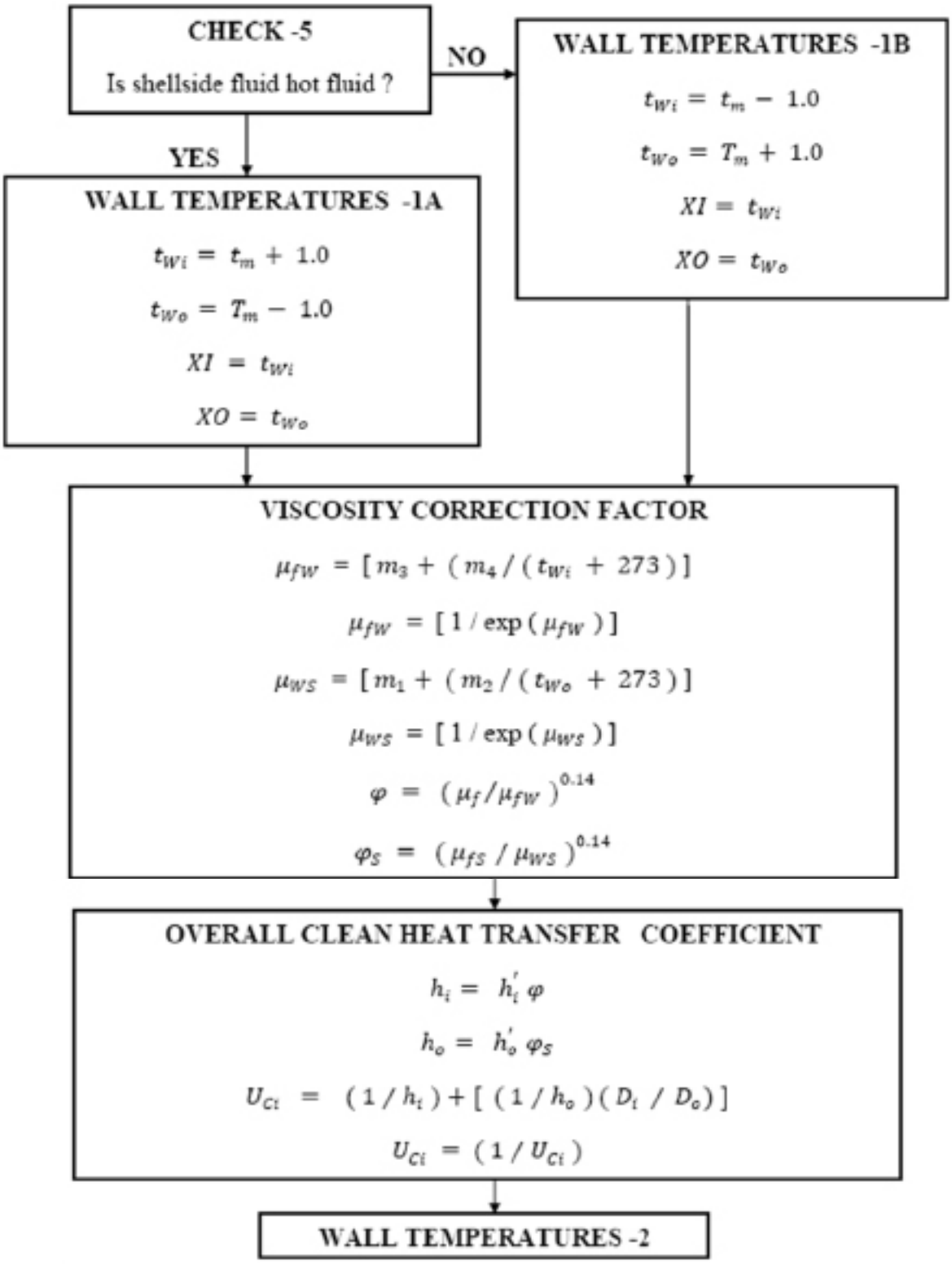

Figure 7M: CAD of shell and Tube Heat Exchangers (Sizing Problem)- countinued

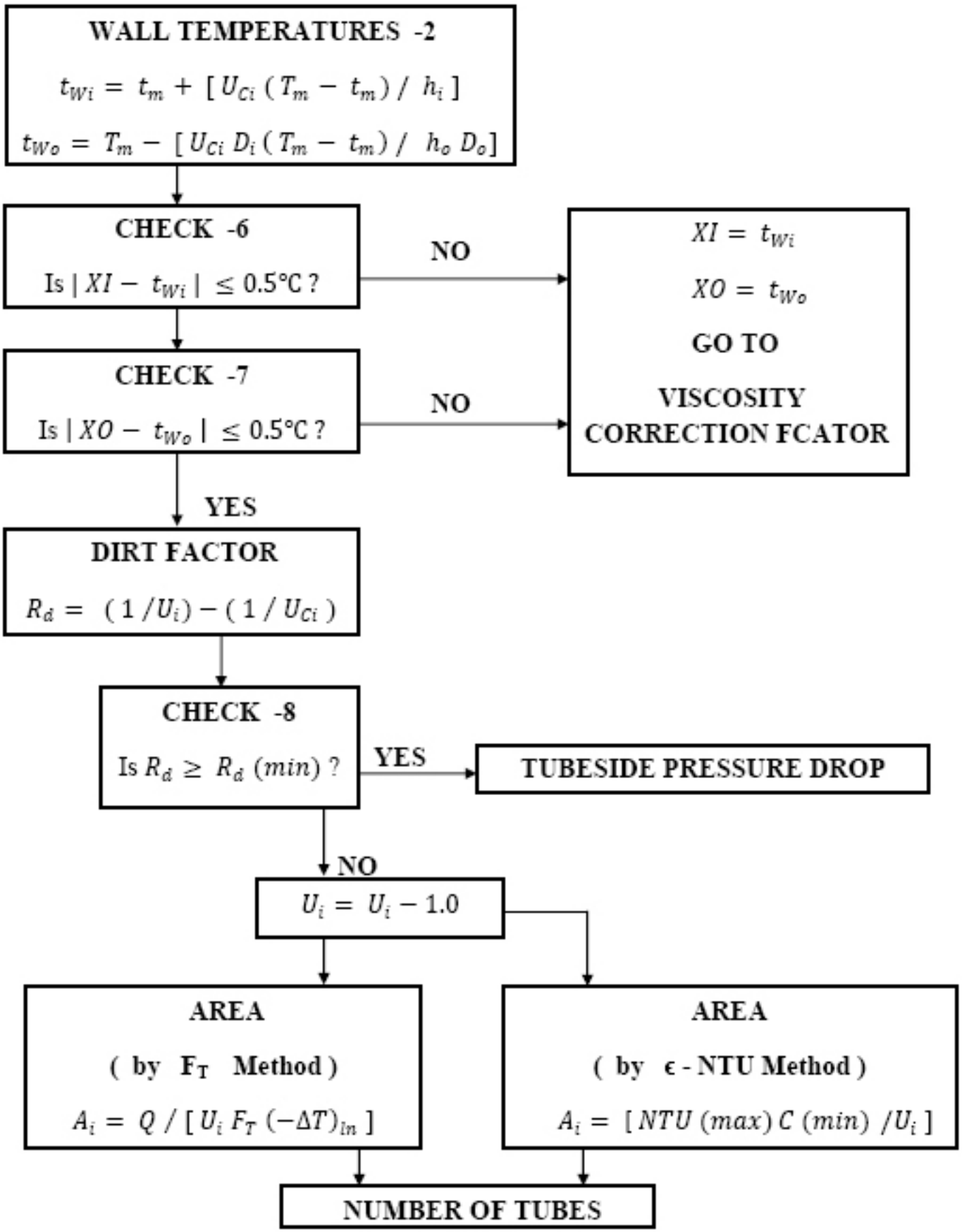

Figure 7N: CAD of shell and Tube Heat Exchangers (Sizing Problem)- countinued

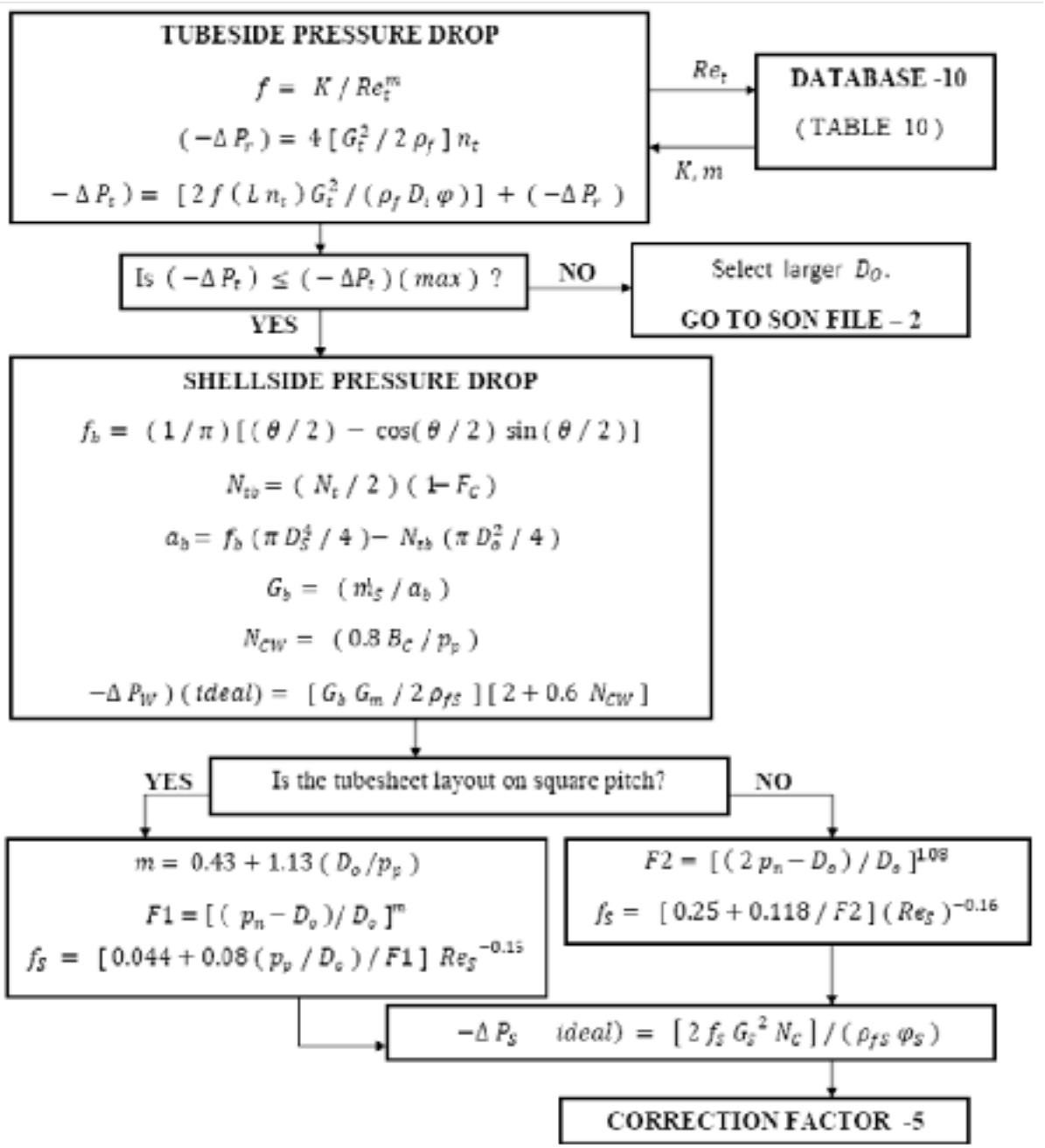

Figure 7O: CAD of shell and Tube Heat Exchangers (Sizing Problem)- countinued

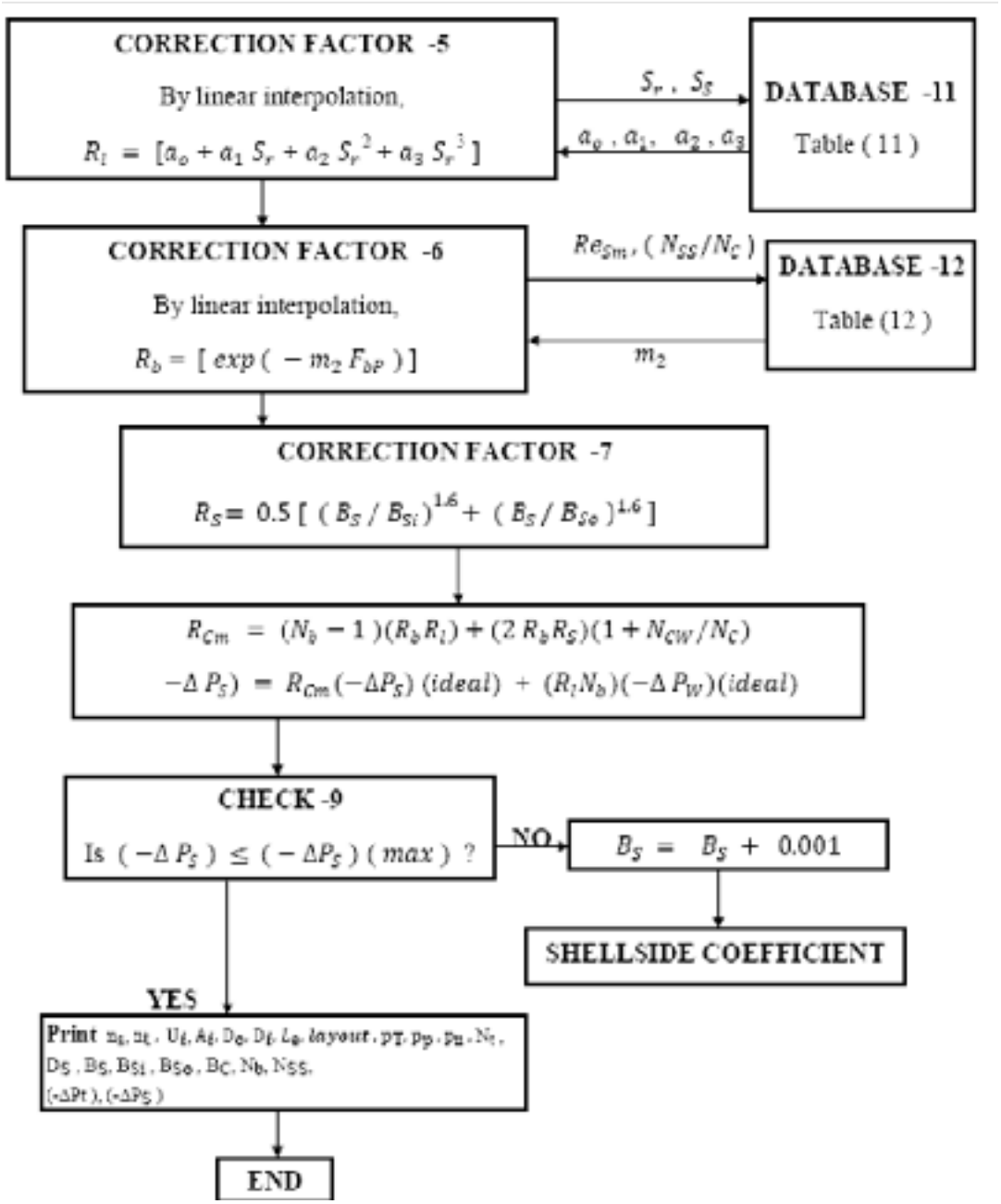

Figure 7P: CAD of shell and Tube Heat Exchangers (Sizing Problem)- countinued

Step 1: specification of father file parameters:

The *father file* is the memory file of the computer in which we enlist the initial problem specifications such as the mass flow rate of shellside fluid and that of tubeside fluid ($\dot{m}_S$, $\dot{m}$),the terminal temperatures of heat exchanger (t_1, t_2, T_1, T_2).

In most cases, one among these parameters could be unknown. For example, let the problem specify $\dot{m}_S$ (mass flow rate of shellside fluid), inlet and outlet temperatures of shellside fluid (T_1, T_2) and also inlet and outlet temperatures of tubeside fluid (t_1, t_2).The mass flow rate of the tubeside fluid ($\dot{m}$) is unknown. This is then evaluated from the overall heat balance shown in step – 3.

It is also required to specify the maximum permissible pressure drop on shellside, ($-\Delta P_S$) (max) and that on tubeside, ($-\Delta P_t$) (max) and also the minimum overall dirt factor prescribed, R_d(min).

Step 2: Estimation of property values of process fluids

Since the physical and transport properties of the fluids (density, viscosity, thermal conductivity) are functions of temperature, they are specified at the mean fluid temperatures (t_m or T_m). Here, t_m is the mean temperature of tubeside fluid and T_m is the mean temperature of the shellside fluid.

If the fluid is a low viscous liquid such as water or aqueous solution, then its property values may be specified at the arithmetic mean temperature (t_{am}, T_{am}). Thus,

$$t_{am} = (t_1 + t_2)/2 \quad (10)$$

$$T_{am} = (T_1 + T_2)/2 \quad (11)$$

In the case of viscous liquids such as petroleum oils, the property values are better specified at caloric mean temperature (t_{cm} or T_{cm}) rather than at the arithmetic mean temperature. The caloric mean temperature is to be computed as given below:

$$t_{cm} = t_1 \pm F_{cm}|t_1 - t_2| \quad (12)$$

$$T_{cm} = T_1 \pm F_{cm}|T_1 - T_2| \quad (13)$$

The plus sign is to be used for cold fluid and minus sign for hot fluid.

F_{cm} = caloric fraction = ($F1/F2$) – ($1/K_C$) (14)

Where,

$$F1 = [1/K_C] + [K_R'/(K_R' - 1)] \quad (15)$$

$$F2 = [1 + \{ln(1 + K_C)/ln K_R'\}] \quad (16)$$

$$K_R' = (\Delta T_C / \Delta T_h) \quad (17)$$

(ΔT_C) = temperature difference at the cold end of the heat transfer surface / heat exchanger.

(ΔT_h) = temperature difference at the hot end of the heat transfer surface / heat exchanger.

Let the tubeside fluid be the cold fluid and shellside fluid be the hot fluid. Then, from figures (6a) and (6b), **end -1** is the cold end (where the cold fluid enters and the hot fluid leaves) and the **end -2** is the hot end (where, hot fluid enters and the cold fluid leaves).

Accordingly,

$$\Delta T_c = (T_2 - t_1) \quad (18)$$

$$\Delta T_h = (T_1 - t_2) \quad (19)$$

This situation will be reversed if the tubeside fluid is the hot fluid. In such a case, **end-1** shall be the hot end and **end-2** will be the cold end. And,

$$\Delta T_h = (t_1 - T_2) \quad (20)$$

$$\Delta T_c = (t_2 - T_1) \quad (21)$$

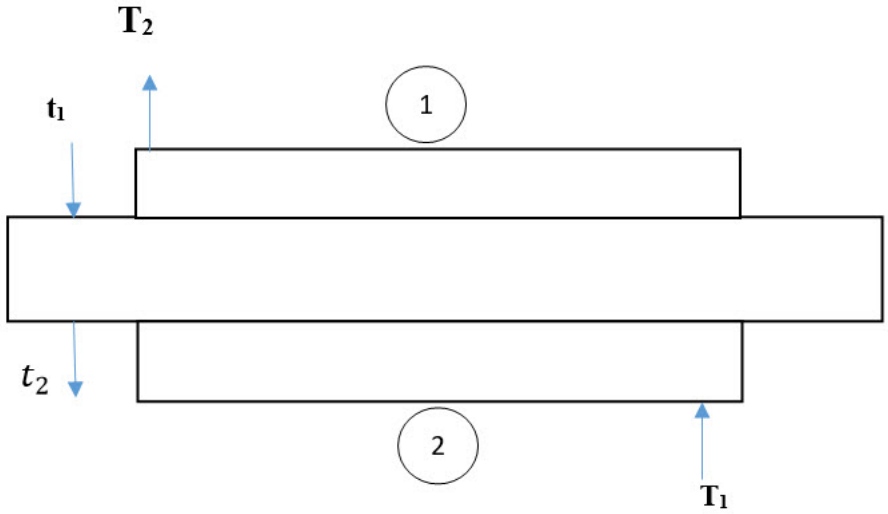

Figure 6 (a): 1-2 Exchanger, indicating the two ends of heat transfer surface.

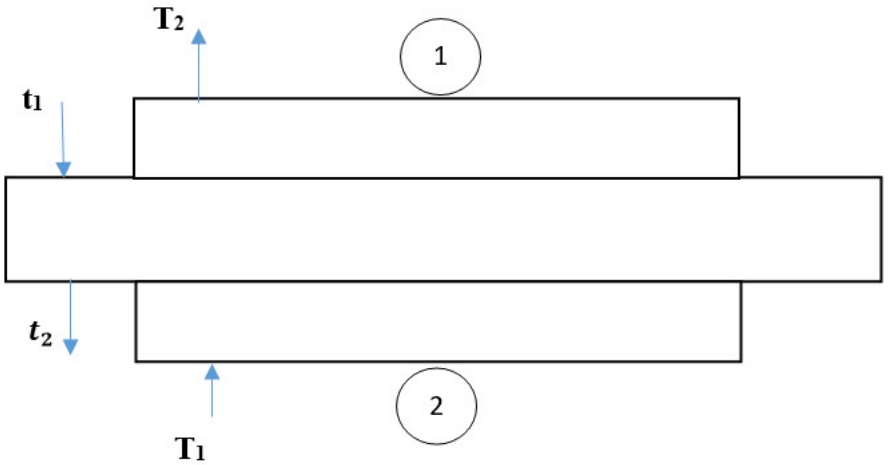

Figure 6 (b): 2-4 Exchanger, indicating the two ends of heat transfer surface.

The value of the parameter K_C depends on the API gravity of the petroleum oil and the temperature difference of the fluid. It may be computed from the correlation given below:

$$\ln K_C = a_0 + a_1(API) + a_2(API)^2 + a_3(API)^3 \quad (23)$$

The values of the correlation coefficients a_0, a_1, a_2, a_3 depend upon the API gravity of the oil and the temperature difference (Δt_C or Δt_h) and are listed in Tables (1A) to (1F). Here,

Δt_C = temperature difference of cold fluid

Δt_h = temperature difference of hot fluid

For example, if the tubeside fluid is the cold fluid, then

$$\Delta t_C = (t_2 - t_1) \quad (24)$$

$$\Delta t_h = (T_1 - T_2) \quad (25)$$

For intermediate values of Δt_C or Δt_h, the value of K_C could be estimated by linear interpolation. It is also important to keep in mind that if both the fluids are viscous fluids like petroleum oils, then the value of K_C is to be computed separately for each of them and the larger value is to be used for the computation of caloric fraction, F_{Cm} **(from equation 14)**. For example, let

K_C (1) = the value of K_C for tubeside fluid

K_C (2) = the value of K_C for shellside fluid

Then K_C = larger of K_C (1) and K_C (2)

This has been illustrated in the CAD flow sheet **(Figures 7B to 7C)** under ***Caloric Mean Temperature.***

Table 1A

Table 1A: Values of Correlation Constants for Computation of K_C – factor (Equation – 23) [Database -1]

Coefficients	Δt_C or Δt_h = 278^{0}C				**R² value**
	API = 20 – 29	API = 29 – 39	API = 39 – 50	API = 50 – 70	
a_o	6.3085	−0.47	2.09	0.606	0.996
a_1	−1.818	0.04	−0.036	a.12 x 10^{-3}	
a_2	−2.73 x 10^{-3}	−6.42 x 10^{-4}	7.36 x 10^{-6}	−3.2 x 10^{-5}	
a_3	9.445 X 10^{-5}	2 x 10^{-5}	9.8 x 10^{-7}	−1.92 x10^{-6}	

Table 1B

Coefficients	Δt_C or Δt_h = 222^{0}C				**R² value**
	API = 13 –28.5	API =28.5 - 41.8	API = 41.8 - 55.5	API = 55.5-70	
a_o	2.43	6.594	87.06	– 5.8768	0.991
a_1	– 0.025	5.743 x10^{-3}	– 45.672	0.0337	
a_2	– 3.858 x10^{-4}	7.482 x10^{-6}	0.879	1.486 x 10^{-4}	
a_3	– 1.552 x10^{-5}	– 1.0289 x10^{-5}	– 4.915 x 10^{-6}	1.2856 x 10^{-5}	

Table 1C

Coefficients	Δt_C or Δt_h = 167^{0}C				**R² value**
	API= 13 - 26	API = 26 - 38.5	API = 38.5 - 53	API = 53 - 68.2	
a_o	2.077	3.074856	4.0074	– 1.8865	0.991
a_1	– 0.0393	– 0.20098	– 0.0799	7.2938 x 10^{-3}	
a_2	2.674 x 10^{-3}	0.00377	– 9.643 x 10^{-6}	4.51 x 10^{-6}	
a_3	– 1.18 x 10^{-4}	– 0.00003	8.7598 x 10^{-8}	2.647 x 10^{-6}	

Table 1D

Coefficients	Δt_C or Δt_h = 111°C				R^2 value
	API = 10 –23	API = 23.7 –32	API = 33 – 42	API = 43 –55.5	
a_o	0.917844	28.1986	– 9.4515	– 294.69	0.991
a_1	– 0.0435737	– 3.14375	0.620646	17.6774	
a_2	0.00225156	0.116005	– 0.0142829	– 0.353604	
a_3	0.00023358	– 0.0014481	0.000093020	– 0.00234255	

Table 1E

Coefficients	Δt_C or Δt_h = 56°C			R^2 value
	API = 10 – 20	API = 21 – 30	API = 31 – 48	
a_o	– 1.48379	4.99609	13.1336	0.996
a_1	0.502394	– 0.5937	– 1.07437	
a_2	– 0.039699	0.0217476	0.0264278	
a_3	0.00086013	– 0.00030225	– 0.000223917	

Table 1F

Coefficients	Δt_C or Δt_h = 28°C				R^2 value
	API = 10 – 14	API = 15 – 20	API = 21 – 30	API = 31 – 35	
a_o	– 16.2581	– 9.60895	– 14.3198	1.43606	0.990
a_1	4.54308	1.55559	1.77582	– 0.194326	
a_2	– 0.40621	– 0.0829894	– 0.0761433	0.00416506	
a_3	0.0116306	0.00133767	0.00103175	– 0.0000396	

In many cases, correlations are available for the estimation of property values at any specified temperature. As for example, let the tubeside fluid be water and its property values are being specified at the arithmetic mean temperature t_{am}, while the shellside fluid is a viscous petroleum oil and its property values are being specified at the caloric mean temperature, T_{cm}. In other words, $t_m = t_{am}$ and $T_m = T_{cm}$. Now, for the tubeside fluid,

$$C_p = [\, q_1 + q_2 \,(\, q_3 - t_{am}\,)\,] \qquad (26)$$

$$\rho_f = [d_1 + d_2(d_3 - t_{am})] \quad (27)$$

$$k_f = [\, k_1 + k_2(k_3 - t_{am})] \quad (28)$$

$$ln\, \mu_f = [\, m_1 + (m_2 / t_{am})\,] \quad (29)$$

Similarly, for the shellside fluid,

$$C_{PS} = [q_4 + q_5(q_6 - T_{Cm})\,] \quad (30)$$

$$\rho_{fS} = [d_4 + d_5\,(d_6 - T_{Cm})] \quad (31)$$

$$k_{fS} = [\, k_4 + k_5(k_6 - T_{Cm})] \quad (32)$$

$$ln\, \mu_{fS} = [\, m_3 + (m_4 / T_{Cm})\,] \quad (33)$$

Where q_1 to q_6, d_1 to d_6, k_1 to k_6 and m_1 to m_4 are correlation constants.

Step 3: **Overall heat balance:**

As stated earlier, out of the six parameters such as the two flow rates ($\dot{m}, \dot{m}_S$) and the four terminal temperatures (t_1, t_2, T_1, T_2), one of them could be unknown. This is evaluated from the

following overall heat balance:

$$Q = \dot{m} C_P |t_2 - t_1| = \dot{m}_S C_{PS} |T_1 - T_2| \quad (34)$$

This step also computes the magnitude of all overall rate of heat transfer, Q.

Step 4: **Initial choice of overall design heat transfer coefficient (U_D)**

The recommended range of values of overall design heat transfer coefficient (U_D) for different process fluids are given by TEMA and these are listed in Table (2). The value of U_D is to be selected based on this table. The maximum value of U_D is first selected (since this would correspond to minimum heat transfer surface requirement for the exchanger) and the value of U_D is subsequently decreased if the computed value of overall dirt factor (R_d) is found to be below the minimum prescribed value, such as, $R_d(\,min\,)$.

For example, let the specified range of U_D for the process fluids at hand be 425 – 850 $W/(m^2.K)$. Then, the computations are started by assuming U_D = 850 $W/(m^2.K)$. This value of U_D is decreased subsequently and computations repeated if R_d(computed) is found to be less than $R_d(\,min\,)$.

The selected value of U_D may be specified as U_0 or U_i. In the CAD flowsheet, it has been

specified as U_i. It must be kept in mind that since ($U_i A_i$) = ($U_0 A_0$), the final results shall remain the same in spite of whether U_D has been selected as U_i or U_0.

Step 5: Computation of heat transfer surface (A_o, A_i)

For the computation of the required heat transfer surface of the exchanger, there are three alternate methods, such as

(a) F_T Method

(b) ϵ - NTU Method

(c) Martin's Method

All the above three methods are based on the heat balance equations written separately for each pass of the exchanger and then clubbed together. Accordingly, each of the above methods should predict the same value of the heat transfer surface (A_o or A_i). The choice of the method, therefore, lies on the convenience of the user. All of the above three methods are illustrated in the CAD flowsheet.

Table 2: Recommended Values of Overall Design Heat Transfer Coefficient (U_D) [Database – 2]

Hot fluid	Cold fluid	$U_D, W/(m^2K)$
Water, methanol, ammonia, aqueous solutions	Water	1420 – 2840
Water	Brine	570 – 1135
Aqueous solutions	Aqueous solutions	1420 – 2840
Light organics (liquids with viscosities less than 0.5 cp like benzene, toluene, acetone, ethanol, MEK, gasoline, naphtha)	Light organics	227 – 425
Light organics	Water	425 – 850
Medium organics (liquids with viscosities 0.5 to 1.0 cp like kerosene, light gas oil)	Medium organics	113 – 340
Medium organics	Water	284 – 710
Heavy organics (liquids with viscosities more than 1.0 cp like lube oils, fuel oils, reduced crude oils, tars, asphalts)	Heavy organics	57 – 227
Heavy organics	Light organics	170 – 340
Heavy organics	Water	30 – 425
Light organics	Heavy organics	56 – 227
Steam	Aqueous solutions (< 2 cp)	1135 – 3975

Steam	Aqueous solutions (> 2 cp)	570 – 2840
Steam	Light organics	570 – 1135
Steam	Medium organics	284 – 570
Steam	Heavy organics	34 – 340
Steam	Water, methanol, ammonia	1135 – 3975
Steam	Gases	30 – 284
Gases	Water	12 – 284

Source: TEMA standards

(a) F_T Method

This method utilises a correction factor F_T , such that,

$$Q = U_i A_i F_T(-\Delta T)_{ln} = U_0 A_0 F_T(-\Delta T)_{ln} \quad (35)$$

where, $(-\Delta T)_{ln}$ = logarithmic mean temperature difference

$$= (\Delta T_h - \Delta T_C) / ln (\Delta T_h / \Delta T_C) \quad (36)$$

ΔT_h = temperature difference at the hot end of the heat transfer surface / heat exchanger (defined earlier)

ΔT_C = temperature difference at cold end of the heat transfer surface / heat exchanger (defined earlier)

The correction factor F_T is to be computed as per the equations given below. For a 1-2 heat exchanger (or for an exchanger with n_S = 1 and n_t = 2, 4, 6 etc),

$$K_1 = \sqrt{(1 + K_R^2)} \quad (37)$$

$$K_2 = (K_R + 1 - K_1) \quad (38)$$

$$K_3 = (K_R + 1 + K_1) \quad (39)$$

$$F1 = K_1 ln [(1 - K_S)/(1 - K_R K_S)] \quad (40)$$

$$F2 = (K_R - 1) ln[(2 - K_S K_2)/(2 - K_S K_3)] \quad (41)$$

$$F_T = F1 / F2 \quad (42)$$

In the above equations,

$$K_S = \Delta t_{C/} \Delta T(max) \quad (43)$$

$$K_R = (\Delta t_{h/} \Delta t_C) \quad (44)$$

$$\Delta T(max) = \text{maximum temperature difference} = |T_1 - t_1| \quad (45)$$

It is obvious that the maximum temperature difference in the case of any exchanger shall be the difference between the inlet temperature of the hot fluid (highest temperature) and the inlet temperature of the cold fluid (lowest temperature). *It must be noted that the parameter* K_R *defined above is different from* K_R' *defined in equation (17) and used for the computation of caloric mean temperature.*

For a 2-4 heat exchanger (or for an exchanger with n_S = 2 and n_t = 4, 8, 12 etc),

$$K_1 = \sqrt{(1 + K_R^2)} \quad (46)$$

$$K_2 = (K_R + 1 - K_1) \quad (47)$$

$$(K_R + 1 + K_1) \quad (48)$$

$$K_4 = \sqrt{(1 - K_S)(1 - K_R K_S)} \quad (49)$$

$$F1 = [K_1 / \{2 (K_R - 1)\}] \ln [(1 - K_S) / (1 - K_R K_S)] \quad (50)$$

$$F3 = [(2 / K_S) - K_2 + (2 / K_S) K_4] \quad (51)$$

$$F4 = [(2 / K_S) - K_3 + (2 / K_S) K_4] \quad (52)$$

$$F2 = ln(F3 / F4) \quad (53)$$

$$F_T = (F1 / F2) \quad (54)$$

Once the value of F_T has been computed, then the heat transfer surface required (A_o or A_i) can be estimated from equation (35).

As stated earlier, it is better to choose a 1 – 2 exchanger (n_S = 1, n_t = 2) at the outset. If the computed value of F_T factor turns out to be negative or indeterminate, then it means that such an exchanger is unsuitable and we have to proceed to design an exchanger of larger number of passes (such as a 2 – 4 exchanger).

b) ϵ - NTU Method

Here, we define two parameters such as heat exchanger effectiveness (ϵ) and number of transfer units, $NTU\ (max)$. These are defined as given below:

$$\epsilon = Q / [C\ (min) \Delta T\ (max)] \quad (55)$$

$$NTU\ (max) = [\ U_o A_o\ /C\ (min)] \quad (56)$$

$$= [\ U_i A_i\ /C\ (min)] \quad (57)$$

where,

$$C\ (\text{min}) = \text{ smaller of } (\dot{m}C_P) \text{ and } (\dot{m}_S C_{PS}) \quad (58)$$

The number of transfer units, $NTU\ (max)$, can be computed as described below.

For a 1-2 heat exchanger (or for an exchanger with n_S = 1 and n_t = 2, 4, 6 etc),

$$N_1 = [\ (2/\epsilon) - 1 - C + C_1\ ] \quad (59)$$

$$N_2 = [\ (2/\epsilon) - 1 - C - C_1\ ] \quad (60)$$

$$NTU\ (max) = (1/\ C_1)\ ln\ (N_1/\ N_2) \quad (61)$$

where

$$C = C\ (min)\ /\ C\ (max) \quad (62)$$

$$C_1 = \sqrt{(1 + C^2)} \quad (63)$$

$$C\ (max) = \text{ larger of } (\dot{m}C_P) \text{ and } (\dot{m}_S C_{PS}) \quad (64)$$

For a 2-4 heat exchanger (or for an exchanger with n_S = 2 and n_t = 4, 8, 12 etc),

$$C_S = \sqrt{(1 - \epsilon)(1 - \epsilon C)} \quad (65)$$

$$C_S = \sqrt{(1 - \epsilon)(1 - \epsilon C)} \quad (65)$$

$$N_3 = [\ (2/\epsilon) - 1 - C + (2/\epsilon)\ C_S + C_1\ ] \quad (66)$$

$$N_4 = [\ (2/\epsilon) - 1 - C + (2/\epsilon)\ C_S - C_1\ ] \quad (67)$$

$$NTU\ (max) = (2/C_1)\ \ln\ (N_3\ /\ N_4) \quad (68)$$

Once the value of $NTU\ (max)$ has been computed, then the heat transfer surface required (A_o or A_i) can be estimated from equation (56) or (57). As stated under F_T – method, in this case also, if by considering a 1 – 2 exchanger, the computed value of $NTU\ (max)$ is seen to be negative or indeterminate, then it indicates that the selected exchanger is inadequate and we have to go for a 2 – 4 exchanger.

C) Martin's Method

The method proposed by Martin involves a trial and error procedure. A value of A_o or A_i

is to be assumed at the outset and subsequently verified. The procedure is outlined below:

1. Assume a value of A_o or A_i.

For example, let

$$A_o = Q / [\, U_o(-\Delta T)_{ln} \,] \tag{69}$$

or,

$$A_i = Q / [\, U_i(-\Delta T)_{ln} \,] \tag{70}$$

2. Compute parameters X, Y, Z as

$$X = (\, U_i A_i) / (\dot{m}_S C_{Ps}) \tag{71}$$

$$Y = (\, U_i A_i) / (\dot{m}\, C_P) \tag{72}$$

$$M = (\, 2\, Y / n_t) \tag{73}$$

$$Z = \sqrt{X^2 + M^2} \tag{74}$$

3. Compute $\Phi\,(Y)$, $\Phi\,(M)$ and $\Phi\,(Z)$ as

$$\Phi\,(Y) = Y / [\, 1 - \exp(-Y) \,] \tag{75}$$

$$\Phi\,(M) = M / [\, 1 - \exp(-M) \,] \tag{76}$$

$$\Phi\,(Z) = Z / [\, 1 - \exp(-Z) \,] \tag{77}$$

4. Compute the parameter Θ as

$$(1 / \Theta) = \Phi\,(Y) + \Phi\,(Z) - \Phi\,(M) + 0.5\ [X + M - Z\,] \tag{78}$$

5. Compute $\in_Y$ as

$$\in_Y = (\, Y\, \Theta\,) \tag{79}$$

6. Compute exit temperature (t_2) of tubeside fluid as

$$t_2(cal) = t_1 \pm \in_Y \Delta T(max) \tag{80}$$

The plus sign is to be used if the tubeside fluid is cold fluid and the minus sign if the tubeside fluid is hot fluid.

7. If the above – computed value of t_2 agrees with the value of t_2 specified in the problem within 1°C, then print A_o or A_i. Otherwise, increase A_o or A_i(for example, $A_i = A_i + 0.1\, m^2$)

and repeat the computations starting from Step 2.

Step 6: Computation of number of tubes required

Select exchanger specifications such as OD of tubes (D_o), tube wall thickness (δ) , tube pitch (p_T) and the tubesheet layout (square pitch / rotated square pitch / triangular pitch). Select also the effective length of each tube (L_e). Now, compute the number of tubes required as,

$$N_t\,(cal) = [\,A_i\,/\,(\,\pi\,D_i\,L_e)\,] \quad (81)$$

$$= [\,A_o\,/\,(\,\pi\,D_o\,L_e)\,] \quad (82)$$

The above calculated value of N_t is to be rounded off to the nearest higher standard value with reference to the standard tube count tables (tables 3A to 3F which constitute **database – 3**). The value of A_o(or A_i)) and U_o(or U_i) are to be recomputed based on the above chosen value of N_t . The internal dameter of shell (D_S) is also retrieved from the tube count table (**database– 3**). This has been clearly illustrated in the CAD flowsheet. Select also the baffle spacing (B_S). It is common practice to start the computations by choosing

$$B_S = B_S\,(\,min\,) = (\,D_S\,/\,5\,) \quad (83)$$

This would provide the largest magnitude of shellside heat transfer coefficient (h_o). However, the value B_S would have to be increased subsequently if pressure drop considerations demand so. This is discussed in one of the subsequent steps (Step – 14).

If the baffle spacing at the inlet (B_{Si}) and that at the outlet (B_{So}) are to be chosen different from B_S, then the values of B_{Si} and B_{So} are also to be specified. As stated earlier, larger baffle spacing is often required at the shell inlet as well as at the shell outlet in order to accommodate the shell inlet nozzle and shell outlet nozzle. No doubt, it is always desirable to employ a uniform baffle spacing such that

$$B_{Si} = B_{So} = B_S \quad (84)$$

Once the tubesheet layout has been chosen, it is also necessary to specify the tube pitch parallel to flow (p_p) and that normal to flow (p_n), based on equations (1) to (4).

Step 7: Computation of Tubeside heat transfer coefficient (h_i)

The tubeside heat transfer coefficient (h_i) depends on the tubeside Reynolds number (Re_t) and the Prandtl Number of tubeside fluid (Pr) and these are defined below:

$$Re_t = [\,D_i\,G_t\,/\,\mu_f\,] \quad (85)$$

where

$G_t =$ mass velocity of tubeside fluid

$= (\dot{m} / a_t)$ (86)

$a_t =$ tubeside flow area

$= \pi(D_i^2 / 4) (N_t / n_t)$ (87)

$n_t =$ number of tubeside passes

$Pr = (C_p \mu_f / k_f)$ (88)

In most industrial shell and tube heat exchangers, the tubeside fluid is usually made to execute fully developed turbulent flow (Re_t >10,000) so as to maintain the tubeside heat transfer coefficient at a high magnitude. In such cases, when Re_t is greater than 10000, the value of tubeside heat transfer coefficient could be computed from the Dittus – Boelter equation (modified by Sieder and Tate) and this is reproduced below. This correlation is valid for a Prandtl number range of 0.7 ≤ Pr ≤ 16700 :

$Nu = 0.027 (Re_t)^{0.8}(Pr)^{0.33}\varphi$ (89)

where

$Nu =$ tubeside Nusselt number

$= (h_i D_i / k_f)$ (90)

$\varphi =$ viscosity correction factor

$= (\mu_f / \mu_{fw})^{0.14}$ (91)

$\mu_{fw} =$ viscosity of tubeside fluid at the inside wall temperature (t_{wi}) of tubes

The above equation is applicable for the flow of all Newtonian fluids ***except water***. If the process fluid is water, then the value of tubeside heat transfer coefficient should be estimated from the *dimensional* correlation reported by Perry [1] and subsequently modified by Narayanan and Bhattacharya [2,3]. This correlation is based on the graphical data reported by Eagle and Ferguson [4]:

$$h_i = (1057.0) C_f (1.352 + 0.02 t_m) [(G_t / \rho_f)^{0.8} / D_i^{0.2}] (\varphi) \quad (92)$$

where $C_f = - 0.1864 \ ln(D_i) + 0.22455$ (93)

It must be kept in mind that the above correlation is *dimensional* in nature and all

parameters involved must be expressed in their corresponding SI units. This equation is also valid for only fully developed turbulent flow of water through straight, cylindrical tubes (Re_t >10,000). However, in most commercial heat exchangers, the velocity of cooling water through tubes is maintained at more than 1.8 m/s (to minimize *precipitation fouling*) and consequently, the flow regime shall be in the fully developed turbulent zone.

Precipitation fouling is caused by the dissolved salts present in water such as sulfates, silicates and hydroxides of calcium and magnesium which are called *inverse solubility salts*, since the solubility of these salts decreases with increase in temperature. At high temperatures therefore, these salts precipitate out and deposit on the heat transfer surfaces causing fouling or scaling. The deposited scale being a poor conductor of heat offers additional resistance to heat transfer and thus brings down the performance of the exchanger. At high fluid velocities, the deposited dirt could get re-entrained into the flowing fluid stream and this helps in impeding precipitation fouling. Also, the exit temperature of cooling water should not necessarily be permitted to increase beyond 50C, since scaling occurs predominantly at high temperatures.

It is not yet fully understood why the Dittus – Boelter equation (equation – 89) is not valid for water, though it is applicable to all other Newtonian fluids. A possible reason is that the properties of water (density, thermal conductivity) exhibit unusual (often, anomalous) temperature dependence [1,2,3].

At the outset, the value of viscosity correction factor (φ) may be taken equal to unity and the value of h_i be computed from any of the correlations given above. This value of h_i(i.e, the value h_i at $\varphi = 1.0$) is denoted as h_i' in the CAD flowsheet. The incorporation of φ and the estimation of corrected value of h_i is discussed in one of the subsequent steps. It may also be noted that this correction factor (φ) is not a detrimental parameter. For water and many aqueous solutions, this factor may be taken more or less equal to unity.

Step 8: Computation of Shellside Heat Transfer Coefficient, h_o $(ideal)$

As stated earlier, the flow of shellside fluid is, in fact, tortuous. It flows over the tube bundle in the section between the baffles, thereby executing crossflow. But, as it flows from one crossflow section to another, it executes countercurrent or co-current flow (depending on the flow direction of tubeside fluid). The shellside fluid, thus, executes partly crossflow, partly countercurrent flow and partly co-current or parallel flow. All of the experimental correlations reported in literature are those which consider *true crossflow* or in other words, that consider *ideal crossflow section*. Accordingly, the shellside heat transfer coefficient predicted by these correlations is h_0 (ideal). Correction factors are to be, therefore, incorporated to take care of supplementary effects and thereby to estimate the actual value of shellside heat transfer coefficient (h_0).

For the estimation of h_0 (ideal), one of the reliable correlations is that proposed by Colburn [5]. This correlation is given below:

$$Nu_S = a_o (Re_S)^{0.6} (Pr_S)^{1/3} \varphi_S \quad (94)$$

where Nu_S = shellside Nusselt number

$$= h_0 \text{ (ideal) } D_0 / k_{fs} \quad (95)$$

Re_S = shellside Reynolds number

$$= (D_o G_S / \mu_{fs}) \quad (96)$$

G_S = mass velocity of the shellside fluid based on flow area, a_S

$$= (\dot{m}_S / a_S) \quad (97)$$

a_S = minimum free flow area between baffles at the shell axis

$$= D_S B_S (p_T - D_o) / (n_S p_T) \quad (98)$$

a_o = 0.33, for staggered tubes (for tubes that are in triangular pitch or rotated square pitch arrangement)

= 0.26, for tubes in line (for tubes that are in square pitch arrangement)

Pr_S = Prandtl number of shellside fluid

$$= (C_{PS} \mu_{fS}) / k_{fS} \quad (99)$$

φ_S = viscosity correction factor for shellside fluid

$$= (\mu_{fS} / \mu_{WS})^{0.14} \quad (99a)$$

μ_{WS} = viscosity of shellside fluid at outer wall temperature (t_{wo}) of tubes

The above correlation is valid for $2000 \leq Re_S \leq 32{,}000$. An alternate correlation for the estimation of $h_o(ideal)$ has been proposed by Donohue [6]. This correlation uses a modified shellside Reynolds number that is based on the geometric average of the mass velocity of shellside fluid in the crossflow section (G_S) and that in the baffle window (G_b). Thus

Re'_S = shellside Reynolds number

$$= (D_o G_e) / \mu_{fS} \quad (100)$$

where

$G_e = \sqrt{G_S G_b}$ (101)

G_b = mass velocity of shellside fluid in baffle window

$= (\dot{m}_S / a_b)$ (102)

a_b = free area for flow of shellside fluid in the baffle window (discussed subsequently in Step – 14 under pressure drop computations)

Donohue's correlation often predicts much lower value of h_0 (ideal) as compared to that predicted by Colburn's correlation. Though the approach used by Donohue is more renovated, dubiousness does exist over the accuracy of employing a geometric average of G_S and G_b. These two mass velocities are not always of comparable magnitude.

Alternate correlations have been proposed by McAdams [7] and also by Kern [8]. Kern has defined an equivalent diameter for the shell and has used the same in the correlation. However, the flow area used for defining the equivalent diameter is the free area (free space) between tubes. Since shellside fluid does flow over the tubes (over the tube bundle), the approach of Kern cannot be treated as fully accurate.

After comparing the different experimental correlations available, ***it is recommended that for the usual case of shellside Reynolds number (Re_S) exceeding 3000, Colburn's correlation (equation – 94) be used for computing h_0(ideal).*** No doubt, it is to be multiplied by the appropriately defined correction factors (discussed subsequently) to obtain the actual magnitude of shellside heat transfer coefficient, h_0.

Step 9: Estimation of correction factors and actual shellside heat transfer coefficient (h_o)

As stated above, the value of shellside heat transfer coefficient computed from Colburn's correlation is that for ideal crossflow section, $h_o(ideal)$. In an industrial heat exchanger however, supplementary effects come into play such as baffle configuration effect, baffle leakage effect, bundle bypassing effect and that due to unequal baffle spacing. Correction factors are to be incorporated to account for each of these effects. Thus,

$h_o = h_o(ideal) (J_C J_l J_b J_S)$ (103)

where

J_C = correction factor that accounts for baffle configuration effect,

J_l = correction factor that accounts for shell to baffle leakage and. tube tobaffle leakage,

J_b = correction factor that accounts for bundle by passing effect and J_S = correction factor

that accounts for unequal baffle spacing.

Elaborate graphical data have been reported by Bell [9] for the computation of these correction factors. Bell's graphical data have been fitted into analytical correlations by Narayanan and Bhattacharya [2]. These are discussed below :

The correction factor J_C is to take care of the fact that a portion of shellside fluid that flows through the baffle window executes more or less countercurrent flow or co-current flow, rather than crossflow. Since heat transfer coefficient is highest in crossflow, this tends to bring down the overall magnitude of the shellside heat transfer coefficient. If tubes are avoided in the baffle window (no – tubes – in – baffle window construction), then J_C = 1.0. The correlation developed by Narayanan and Bhattacharya [2] for the estimation of this correction factor is as follows:

$$J_c = c_o + c_1(F_c) + c_2(F_c)^2 + c_3(F_c)^3 \qquad (104)$$

where

F_C = fraction of total tubes in crossflow

$$= 1 + (2 / \pi) \cos\theta_C \sin\theta_C - (2\,\theta_C / \pi) \qquad (105)$$

$$\text{Cos}\,\theta_C = [\,(D_S - 2\,B_C)/\,D_{ot}\,] \qquad (106)$$

B_C is the baffle cut and as stated earlier, for 25% cut segmental baffles that are popularly used, B_C = (D_S / 4). In the above equation (105), θ_C must be expressed ***in radians***.

D_{ot} is called the outer tube limit and it depends on the type of exchanger construction and the shell ID. It is to be kept in mind that in a shell and tube heat exchanger, tubes are laid in the shell within D_{ot} and not within the entire cross – section of the shell. The values of D_{ot} specified by TEMA are listed in Table (4) which constitutes **Database – 4**. It can be seen from table (4) that for pipe shells (lower diameter shells), D_{ot} is around 11 mm less than the shell diameter when a fixed tubesheet construction is used, while it is 29 mm less than the shell diameter for a floating head construction. Similarly, in the case large diameter plate shells, D_{ot} is 13 mm less than the shell diameter in fixed tube sheet exchangers, whereas in floating head exchangers, it is 37 mm less than the shell diameter.

Table 4: Values of Outer Tube Limit (D_{ot}) recommended by TEMA Standards [Database – 4]

	Shell diameter (D_S), mm	D_{ot}, mm	
		Fixed tubesheet	Internal floating head with split backing ring
Plate shells	$>$ 637 mm	D_S – 13 mm	D_S – 37 mm
Pipe shells	$\leq$ 610 mm	D_S – 11 mm	D_S – 29 mm

The values of correlation constants c_o, c_1, c_2, c_3 are listed in Table (5) which constitutes **Database – 5.**

Table 5: Values of Correlation Constants for Computation of Correction Factor J_C (equation –104)

Correlation constant	$F_C \leq 0.6$	$0.6 \leq F_C \leq 0.8$	$0.8 \leq F_C \leq 0.9$	$0.8 \leq F_C \leq 1.0$
c_o	0.531428	0.6406	- 2.1616	557.71946
c_1	0.7737	0.588	7.37824	- 1793.534
c_2	0.0	0.0	- 4.11426	1925.5329
c_3	0.0	0.0	0.0	- 688.7156

J_l is the correction factor to account for the leakage of shellside fluid through the shell-to-baffle clearances and the tube-to-baffle clearances. Its value varies from 0.7 to 0.8. A portion of the shellside fluid flows through the shell to baffle clearances and also through the tube to baffle clearances. These are called the *leakage streams*. Due to these leakage streams, the fraction of shellside fluid executing crossflow gets reduced and this penalizes the shellside heat transfer coefficient. As specified by TEMA, the tube to baffle clearance (δ_{tb}) ranges from 0.4 to 0.8 mm and the shell to baffle clearance (δ_{Sb}) varies from 2.54 mm for small diameter pipe shells to as high as 10.8 mm for large diameter plate shells. The values of δ_{Sb} and δ_{tb} as specified by TEMA are listed in Table (6) which constitutes **Database – 6.** The correlation developed by Narayanan and Bhattacharya [2] for the estimation of this correction factor is given below:

$$J_l = a_o + a_1(S_r) + a_2(S_r)^2 + a_3(S_r)^3 \qquad (107)$$

where

$$S_r = (A_{tb} + A_{Sb}) / A_m \qquad (108)$$

$$S_S = A_{Sb} / (A_{tb} + A_{Sb}) \qquad (109)$$

A_{tb} = tube to baffle leakage area

$$= [\ \pi D_o\ \delta_{tb}\ N_t\ (\ 1+ F_C\ )\ ]\ /\ 2 \qquad (110)$$

A_{Sb} = shell to baffle leakage area

$$= (\pi D_s \delta_{sb} / 2)[1-(\theta / 2\pi)] \qquad (111)$$

δ_{tb} = tube to baffle clearance

δ_{Sb} = shell to baffle clearance

θ = baffle cut angle (in ***radians***)

$$= 2\ Cos^{-1}[\ (D_S - 2\ B_C)/\ D_S\ ] \qquad (112)$$

As stated above, for 25 % cut segmental baffles, $B_C = (\ D_S\ /\ 4\ )$ and therefore, θ = 120^0 or $(2\pi/3)$ radians.

A_m = crossflow area at or near center line

$$= B_S\ [\ D_S\ -\ D_{ot} + \{(\ D_{ot}\ -\ D_o)\ (\ p_T\ -\ D_o\ )\ /\beta p_T\}] \qquad (113)$$

If tubes are arranged on the tubesheet on a triangular pitch layout, then β = 1.0 and if they are laid on a square or rotated square layout, then $\beta = (p_n/p_T)$.

The values of correlation constants a_o, a_1, a_2, a_3 are listed in Table (7) which constitutes **Database – 7.**

Table 6: [Database 6] Recommended Values of Tube to Baffle Clearance (δ_{tb}) and Shell to Baffle Clearance (δ_{sb})

δ_{tb} = 0.8 mm, if maximum unsupported tube length (usually $2B_S$) ≤ 910 mm, δ_{tb} = 0.4 mm, if ($2B_S$) > 910 mm.

	Shell diameter, mm	δ_{Sb} mm
Pipe shells	203.2 – 336.5	2.54
	355.6 – 439.1	3.175
	457.2 – 590.8	3.81
Plate shells	609.6 – 990.6	7.62
	1016.0 – 1371.6	8.89
	Above 1397.0	10.80

Table 7: [Database– 7] Values of Correlation Constants for Computation of Correction Factor J_l (equation – 107)

	S_S	a_0	a_1	a_2	a_3
$S_r \leq_{0.2}$	0.0	0.997	– 2.54167	15.239	– 36.276
	0.25	1.0	– 3.0845	17.2089	– 38.6776
	0.50	0.9957	– 3.804	22.045	– 50.586
	0.75	0.9952	– 4.0808	21.764	– 47.946
	1.0	0.9916	– 5.0	29.0	– 66.532
$_{0.2} < S_r \leq_{0.7}$	0.0	0.8975	– 0.4375	0.0	0.0
	0.25	0.87	– 0.55	0.0	0.0
	0.50	0.8525	– 0.6625	0.0	0.0
	0.75	0.825	– 0.775	0.0	0.0
	1.0	0.7925	– 0.8375	0.0	0.0

The correction factor J_b has been incorporated to take care of the *bundle bypassing effect*. That portion of the shellside fluid which flows through the clearance between the outermost tube and the shell wall has a tendency to flow adjacent to the shell wall and thereby bypass the tube bundle (it does not flow over the tube bundle). In the case of fixed tube sheet exchangers, the clearance between the outermost tube and the shell wall is usually maintained small and hence, this effect is not predominant and the value of J_b shall be quite high (around 0.9). However, in floating head exchangers, J_b values as low as 0.7 have been reported. One of the means of minimizing the bundle bypassing effect is to install sealing strips, which are typically longitudinal strips of metal installed between the outside of the tube bundle and the shell and fastened to the baffles. These strips force back the bypass stream into the main crossflow stream and thereby reduce the bypassing effect and improve the heat transfer coefficient. It must be, however, kept in mind that sealing strips are cumbersome to install and maintain. The correlation developed by Narayanan and Bhattacharya [2] for the estimation of this correction factor is given below:

$$J_b = [\, exp\, (\, -m_1 F_{bP}\,)\,] \qquad (114)$$

where

$$F_{bP} = (\, D_S - D_{ot}\,)\; B_S \;/\; A_m \qquad (115)$$

The value of correlation constant m_1 depends on the values of Re_{Sm} and the ratio ($N_{SS} \;/\; N_C$) and can be retrieved from Table (8) which constitutes **Database – 8**. Here,

Re_{Sm} = modified shellside Reynolds number based on G_m

$$= (\, D_o G_m \;/\; \mu_{fS}\,) \qquad (116)$$

where

G_m = shellside mass velocity based on A_m

$$= (\dot{m}_S \ / A_m) \quad (117)$$

N_{SS} = number of sealing strips installed per cross flow section and N_C = number of tube rows crossed during flow through one crossflow section.

$$= (D_S - 2B_C) / p_P \quad (118)$$

p_P = tube pitch parallel to flow

It is thus clear from Table (8) that when the ratio (N_{SS} / N_C) is equal to 0.5 or more, J_b shall be equal to 1.0 and the bypassing effect shall be absent.

The correction factor J_S is to take care of the effect of unequal baffle spacing on the shellside heat transfer coefficient. It has been explained earlier that due to the presence of nozzles, a larger baffle spacing is often required to be used at the inlet and at the outlet of the exchanger (B_{Si}, B_{So}). If $B_{Si} = B_{So} = B_S$ (which is most preferable), then

$$J_S = 1.0 \quad (119)$$

The value of J_S thus obviously depends on the (B_{Si} / B_S) and (B_{So}/B_S) ratios and the number of baffles used and can be estimated as follows:

$$J_S = (F1 / F2) \quad (120)$$

where

$$F1 = (N_b - 1) + (B_{Si} / B_S)^{0.4} + (B_{So}/B_S)^{0.4} \quad (121)$$

$$F2 = (N_b - 1) + (B_{Si} / B_S) + (B_{So}/B_S) \quad (122)$$

N_b = number of baffles

$$= [(L_e - B_{Si} - B_{So}) /B_S] + 1 \quad (123)$$

Table 8: Values of Correlation Constant for Computation of Correction Factor J_b (Equation – 114)[Database – 8]

N_{SS} / N_C	$Re_{Sm} \geq 100$	$Re_{Sm} < 100$
	m_1	m_1
0.0	1.2344	1.3433
0.05	0.6704	0.72975
0.10	0.5095	0.5811
0.167	0.37895	0.4324
0.30	0.1777	0.2055
0.5 and above	0.0	0.0

Once all the four correction factors have been evaluated, then the value of h_0 can be computed from equation (103). To start with, viscosity correction factor φ_S may be assumed equal to 1.0. Accordingly, the above – computed value of h_0 be designated as h_0'.

Step 10: Viscosity correction

As stated earlier, the viscosity correction factor (φ, φ_S) is not a controlling parameter. For many systems, its value is very close to 1.0. To compute this correction factor, we need to estimate the tube surface temperature (t_{Wi}, t_{Wo}). However, it must be kept in mind that tube surface temperature varies from one end to the other end of the exchanger and it is also a parameter that is difficult to record experimentally. But since, as stated earlier, φ or φ_S is not a highly influencing parameter, we need to determine only an order of magnitude of t_{Wi} and t_{Wo} . In the design computations therefore, approximate estimation of inner surface temperature of tubes (t_{Wi}) and outer surface temperature of tubes (t_{Wo}) is performed from the following ***approximate*** heat balance equations:

$$h_0 A_0 |T_m - t_{Wo}| = h_i A_i |t_m - t_{Wi}| \quad (124)$$

$$= U_{Ci} A_i |T_m - t_m| \quad (125)$$

$$= U_{C0} A_0 |T_m - t_m| \quad (126)$$

where

U_{Ci} , U_{Co} = overall ***clean*** heat transfer coefficient (value of U when fouling coefficients or dirt factors are excluded) based on A_i and based on A_o respectively

It is important to note that the above equation is approximate (since it does not accurately define the temperature difference driving force) and should be used for the approximate estimation of t_{Wi} *and* t_{Wo} *only.* Now, from the above equations,

$$t_{Wi} = t_m \pm [\, U_{Ci}(T_m - t_m) / h_i \,] \quad (127)$$

$$t_{Wo} = T_m \pm [\, U_{Ci} D_i (T_m - t_m) / \; h_o D_o] \quad (128)$$

The plus sign is to be used for the cold fluid and the minus sign for the hot fluid.

The computation of viscosity correction factor φ (or φ_S) based on the above equations involves a trial and error procedure, which is summarized below:

1. Assume the values of t_{Wi} and t_{Wo}. For example, if the tubeside fluid is cold fluid then,

$$t_{Wi} = t_m + 1.0 \quad (129)$$

Similarly, if the shellside fluid is hot fluid, then

$$t_{wo} = T_m - 1.0 \quad (130)$$

2. Put $XI = t_{wi}$ (131)

and $XO = t_{wo}$. (132)

3. Compute μ_{fw} (viscosity of tubeside fluid at t_{wi}) and μ_{ws} (viscosity of shellside fluid at t_{wo}) from the available property value correlations and then, estimate φ and φ_s as,

$$\varphi = (\mu_f/\mu_{fw})^{0.14} \quad (133)$$

$$\varphi_s = (\mu_{fs}/\mu_{ws})^{0.14} \quad (134)$$

4. Compute the corrected values of tubeside heat transfer coefficient (h_i) and that of shellside heat transfer coefficient (h_0) as

$$h_i = h_i'\varphi \quad (135)$$

$$h_o = h_o'\varphi_s \quad (136)$$

5. Compute the ***clean*** overall heat transfer coefficient U_{Ci} (or U_{Co}) as

$$1/U_{Ci} = (1/h_i) + (1/h_o)(D_i/D_o) \quad (137)$$

$$1/U_{Co} = (1/h_o) + (1/h_i)(D_o/D_i) \quad (138)$$

6. Re-compute the tube surface temperatures (t_{wi} and t_{wo}) from equations (127 and 128), using the above computed value of overall ***clean*** heat transfer coefficient, U_{Ci} or U_{Co}.

7. Compute the deviations as

$$DWI = |XI - t_{wi}| \quad (139)$$

$$DWO = |XO - t_{wo}| \quad (140)$$

8. If either DWI or DWO has been found to exceed $0.5°C$, then repeat the computations starting from Step – 2. Otherwise, print the values of h_i and h_o.

Usually, the scheme shall converge within two to three iterations.

Step 11: Computation of overall dirt factor

Compute the overall dirt factor (R_d) as

$$R_d = (1/U_i) - (1/U_{Ci}) \quad (141)$$

$$= (1/U_o) - (1/U_{Co}) \quad (142)$$

If the above-computed value of R_d falls below $R_d\ (min)$, then proceed to Step – 12 for re-computation of the heat transfer surface. Otherwise, proceed to Step – 13 for pressure drop computations.. The recommended values of minimum dirt factor specified by TEMA are listed in Table (8) which constitutes **database – 9.**

Step 12: Re-computation of heat transfer surface

Since the computed value of overall dirt factor has been found to be less than the minimum required value of $R_d\ (min)$, the value of overall heat transfer coefficient U_i (or U_o) is to be decreased and the computations repeated as outlined below :

(i) Put $U_i = U_i - 1.0 \quad (143)$

or

$$U_o = U_o - 1.0 \quad (144)$$

(ii) Re-compute the heat transfer surface as $A_i = Q / [\, U_i F_T (-\Delta T)_{ln}\,] \quad (145)$

or

$$A_i = [NTU\ (max)\, C\ (min)/\ U_i\,] \quad (146)$$

(iii) Repeat the computations starting from **Step – 6.**

The procedure is to be continued until the computed value of overall dirt factor (R_d) exceeds $R_d\ (min)$.

Table – 9: Minimum Recommended Values of Dirt Factor, $R_d(min)$ [Database – 9]

Process fluid	Dirt factor, $R_d(min),\ (m^2.K)\ /\ W$
Fuel oil	0.0009
Machine oil, transformer oil	0.00018
Quenching oil	0.0007
Vegetable oils	0.0006
Organic liquids	0.0002
Refrigerating liquids	0.0002
Brine (cooling)	0.0002
Organic vapours	0.0001
Steam (non-oil bearing)	0.0
Alcohol vapours	0.0
Steam, exhaust (oil bearing)	0.0002
Air	0.0004
Coke oven gas, manufactured gas	0.002

Source: TEMA Standards

Note : In the case of water, with temperature of water ≤ 52 C and water velocity ≥ 1.2 m/s, the recommended value of $R_d\ (min)$ is 0.0001 $(m^2.K)\ /\ W$ for sea water, distilled water and treated boiler feed water, while it is 0.0002 $(m^2.K)\ /\ W$ for brackish water. clean river water and treated make-up water used in cooling towers. At the same water velocity and temperature, $R_d\ (min)$ specified for hard water (over 15 grains / gal) is 0.0006 $(m^2.K)\ /\ W$ and that for muddy or silty river water is 0.0004 $(m^2.K)\ /\ W$.

Step 13: Computation of tubeside pressure drop

Heat exchanger calculations are incomplete, unless the pressure drop in either stream is evaluated and ascertained that neither of them (pressure drop in the tubeside fluid or that in the shellside fluid) exceeds the maximum permissible limit. To note that the operating cost of the exchanger is decided by the magnitude of pressure drop in the two streams. The tubeside pressure drop includes frictional pressure drop (due to *skin friction* between the tube wall and the fluid layer) which is predicted by the modified form of Fanning's equation (corrected for non-isothermal flow) and the additional pressure drop due to flow reversal (by virtue of multipass construction). Thus

$$(-\Delta P_t) = \left[2 f (L_e n_t) G_t^2 / (\rho_f D_i \varphi)\right] + (-\Delta P_r) \qquad (147)$$

where

$(-\Delta P_r)$ = additional pressure drop due to flow reversal = four velocity heads per pass (observed experimentally)

$$= 4 [G_t^2 / (2\rho_f)] n_t = 2 (G_t^2 n_t) / \rho_f \qquad (148)$$

n_t = number of tubeside passes f = tube side friction factor (for non-isothermal flow)

$$= K / Re_t^m \qquad (149)$$

where K and m are empirical constants. The values of these constants are listed in table (10) which constitutes **database – 10**.

Table – 10: Friction factor in Non – isothermal flow Values of Correlation Constants K and m (Equation – 149) [Database – 10]

Re_t	Smooth tubes		Commercial pipes	
	K	m	K	m
≤ 1000	18.0	1.0	18.0	1.0
1000 to 10^5	0.12	0.272	0.105	0.243
10^5 to 10^6	0.087	0.2413	0.0423	0.164

The tubes used in shell and heat exchangers are relatively smooth. Accordingly, in the present case, the values of correlation constants (K and m) are to be retrieved from column – 2 on smooth tubes. Double pipe heat exchangers employ industrial pipes which have a given degree of roughness on their inner surface. In the case of those exchangers therefore, the values of K and m are to be read from column – 3 on commercial pipes. It is also important to keep in mind that the conventional friction factor versus Reynolds number plots (Moody's plots) are not applicable here since those plots are for isothermal flow. The above correlation (149) is based on the graphical data reported by Sieder and Tate and reproduced by Kern [8].

If the above computed value of tubeside pressure drop happens to exceed the maximum permissible value, then computations are to be repeated after selecting a larger tube diameter, starting from **Step – 6**.

Step 14: Computation of shellside pressure drop

The shellside pressure drop is more difficult to estimate accurately. This is because, as discussed earlier, the flow of shellside fluid through the exchanger is too much tortuous, it executes both crossflow and countercurrent flow as well as parallel flow. For flow over a submerged object, the *form drag* comes into play, which is of higher magnitude than skin friction. Since the shellside fluid flows over the tube bundle, the frictional resistance includes form drag and it is more cumbersome to quantify.

For a reasonably reliable estimate of shellside pressure drop therefore, we first estimate the pressure drop for flow through ideal crossflow section, $(-\Delta P_S)\ (ideal)$ and that for flow through ideal baffle window section, $(-\Delta P_W)(ideal)$. The actual value of shellside ptressure drop is then computed by incorporating the correction factors, R_b , R_l and R_S which are similar to the correction factors, J_b , J_l , J_S used for the estimation of shellside heat transfer coefficient. Thus

$$(-\Delta P_S) = R_{Cm}(-\Delta P_S)_(ideal)_+ (R_l N_b)(-\Delta P_W)(ideal) \qquad (150)$$

where

R_{Cm} = combined correction factor

$$= (N_b - 1)(R_b R_l) + (2\ R_b R_S)(1 + N_{CW}/N_C) \qquad (151)$$

$(-\Delta P_S)(ideal)$ = pressure drop in an ideal crossflow section

$$= \left[2\ f_S G_S{}^2 N_C\right] / (\rho_{fS}\ \varphi_S) \qquad (152)$$

f_S = shellside friction factor $(-\Delta P_W)(ideal)$ = pressure drop in an ideal baffle window section

$$= [\, G_b \, G_m \,/\, 2 \, \rho_{fs} \,] \, [\, 2 + 0.6 \;\; N_{cw} \,] \qquad (153)$$

G_b = mass velocity of shellside fluid in baffle window

$$= (\dot{m}_S \,/\, a_b \,) \qquad (154)$$

a_b = free area for flow of shellside fluid in the baffle window

$$= f_b \, (\pi \, D_S^2 \,/\, 4 \,) - N_{tb} \, (\pi \, D_0^2 \,/\, 4 \,) \qquad (155)$$

f_b = fraction of the shell cross-sectional area occupied by the baffle. window

$$= (1 \,/\, \pi \,) \, [\, (\theta \,/\, 2 \,) - \cos(\theta/2 \,) \sin(\theta/2 \,) \,] \qquad (156)$$

θ = baffle cut angle (in ***radians***)

$$= 2 \cos^{-1} [\, (D_S - 2 \, B_C) / \, D_S \,] \qquad (157)$$

N_{tb} = number of tubes in baffle window

$$= (N_t \,/\, 2 \,) \, (\, 1 - F_C \,) \qquad (158)$$

F_C = fraction of total tubes in crossflow (defined earlier in equation – 105)

N_{CW} = number of effective crossflow rows in each baffle window

$$= (\, 0.8 \, B_C \,/\, p_P \,) \qquad (159)$$

R_b, R_l, R_S = correction factor to account for bundle by passing effect, baffle leakages and unequal baffle spacing respectively on shellside pressure drop.

Bell and coworkers [9] have reported extensive graphical data for the estimation of these correction factors as well and Narayanan and Bhattacharya [2] have converted them into analytical correlations through rigorous regression analysis. The correlations developed by them are reproduced below:

$$R_l = \alpha_o + \alpha_1 (S_r) + \alpha_2 (S_r)^2 + \alpha_3 (S_r)^3 \qquad (160)$$

The values of correlation constants $\alpha_0, \alpha_1, \alpha_2, \alpha_3$ are listed in Table (11) which constitutes **Database – 11.**

Table 11: [Database – 11] Values of Correlation Constants for Computation of Correction Factor R_l (equation – 160)

	S_S	α_0	α_1	α_2	α_3
$S_r \leq_{0.2}$	0.0	0.995	– 4.94	26.952	– 58.77
	0.25	0.9947	– 6.651	40.5936	– 95.67
	0.50	0.9985	– 7.3934	37.7854	– 75.146
	0.75	0.993	– 9.3936	56.934	– 132.37
	1.0	0.995	– 11.256	71.358	– 170.295
$_{0.2} < S_r \leq$ 0.7	0.0	0.7267	– 0.5737	0.0	0.0
	0.25	0.66	– 0.71	0.0	0.0
	0.50	0.5933	– 0.8476	0.0	0.0
	0.75	0.5133	– 0.9506	0.0	0.0
	1.0	0.4667	– 1.1476	0.0	0.0

The parameters S_r and S_S have been defined earlier (see equations – 108, 109). The correction factor R_l which takes care of the effect of tube to baffle and shell to baffle leakages on shellside pressure drop is thus analogous to factor J_l defined earlier under computation of shellside heat transfer coefficient. In a similar way, the correction factor R_b is similar to J_b and it takes care of the effect of bundle bypassing effect on shellside pressure drop. It may be computed from

$$R_b = [\, exp\,(\, -m_2 F_{bP}\,)\,] \qquad (161)$$

The value of correlation constant m_2 depends on the modified shellside Reynolds number, Re_{Sm} and the (N_{SS} / N_C) ratio and can be retrieved from Table (12). This table constitutes **Database – 12**. The dimensionless parameter F_{bP} has been defined earlier in equation (115). As evident from table (12), when the number of sealing strips installed is large such that the ratio (N_{SS} / N_C) is equal to or more than 0.5, $R_b = 1.0$.

Table 12: Values of Correlation Constant for Computation of Correction Factor R_b (equation – 161)[Database – 12]

N_{SS} / N_C	$Re_{Sm} \geq_{100}$	$Re_{Sm} <_{100}$
	m_2	m_2
0.0	3.7041	4.3524
0.05	2.0245	2.4183
0.10	1.5270	1.8522
0.167	1.1684	1.30898
0.30	0.5944	0.72975
0.5 and above	0.0	0.0

The correction factor, R_S has been incorporated to account for the effect of unequal baffle spacing on shellside pressure drop. Evidently, its magnitude shall depend on the (B_{Si} / B_S) ratio and the (B_{So}/B_S) ratio, as shown below:

$$R_S = 0.5\,[(B_S/B_{Si})^{1.6} + (B_S/B_{So})^{1.6}] \quad (162)$$

The shellside friction factor f_S is a non-linear function of shellside Reynolds number, Re_S. It is also a function of the tubesheet layout chosen and the tube pitch (p_p,p_n). A reasonably satisfactory estimate of f_S can be obtained from the correlation proposed by Grimson [10]. It is given below:

For staggered tubes,

$$f_S = [\,0.25 + 0.118 / F2\,]\,(Re_S)^{-0.16} \quad (163)$$

where

$$\boldsymbol{F2} = [\,(2\,p_n - D_o) / D_o\,]^{1.08} \quad (164)$$

For tubes in line,

$$f_S = [\,0.044 + 0.08\,(p_p / D_o) / F1\,]\,Re_S^{-0.15} \quad (165)$$

where

$$F1 = [(p_n - D_o)/ D_o\,]^m \quad (166)$$

$$m = 0.43 + 1.13\,(D_o/p_p) \quad (167)$$

Grimson's correlation is valid within the Reynolds number range of $2000 \leq Re_S \leq 40{,}000$.

If the above computed value of shellside pressure drop happens to exceed the maximum permissible value, then a larger value of baffle spacing (B_S) is to be chosen and computations repeated starting from **Step – 8**.

Step 15: Print Results

The entire procedure described above has been illustrated in all details in the CAD flowsheet given in Figures – 7A to 7P.

It is needless to comment that the CAD package presented could very well be re-executed with different pass arrangements and with different choices of son file parameters and the most satisfactory design could be located from the results, keeping the heat transfer

surface requirement, fabrication cost and the pressure drop penalties (both on tubeside as well as on the shellside) in mind. This, in fact, forms the inherent flexibility of all types of CAD (software) packages.

We shall illustrate a numerical example here to demonstrate the applicability of the above-described CAD package. The package is executed with the following Father File parameters:

Shellside fluid : Petroleum Oil (hot fluid), Tubeside fluid : Water (cold fluid)

$\dot{m}_S$ = mass flow rate of shellside fluid = 36300 kg / hr

Inlet temperature of shellside fluid = T_1 = 160^{0}C

Outlet temperature of shellside fluid = T_2 = 45^{0}C

Inlet temperature of tubeside fluid = t_1 = 20°C

Outlet temperature of tubeside fluid = t_2 = 42°C

R_d *(min)* = 0.0005 (m^2. K)/ W

$(-\Delta P_t)(max) = (-\Delta P_S)\,(max) = 60\ kPa$

The results obtained are,

Type of exchanger recommended: 1 – 2 heat exchanger

Mass flow rate of water = $\dot{m}$ = 104198.4 kg / hr

$U_D = U_i$ = 471.5 *W/ (m^2.K)* [finalized by trial, from the prescribed range of 284 – 710 *W/ (m^2.K)*]

Heat transfer surface required = A_i = 111.08 m^2

Heat exchanger specifications : D_o = 19 mm, D_i = 17 mm, L_e = 5.0 m, tubesheet layout = triangular pitch (p_T = 25.4 mm, p_p = 22 mm, p_n = 12.7 mm).

Construction : Fixed tubesheet

Total number of tubes = N_t = 416

Shell ID = D_S = 590.8 mm

Baffle spacing = $B_S = B_{Si} = B_{So}$ = 196.93 mm (finalized by trial)

Baffle cut = B_C = 147.7 mm (25 % cut segmental baffles)

Number of baffles = N_b = 44

Number sealing strips per crossflow section = N_{SS} = 2

Tubeside heat transfer coefficient = h_i = 3228.46 $W / (m^2. K)$

Shellside heat transfer coefficient = h_o = 700.92 $W / (m^2. K)$

R_d *(computed)* = 0.000532 $(m^2. K)/ W$

Tubeside pressure drop = $(-\Delta P_t)$ = 6.0 *kPa*

Shellside pressure drop = $(-\Delta P_S)$ = 9.0 *kPa*

2.2. CAD Package for Rating Problem

As explained earlier, in a rating problem, a heat exchanger of known specifications is available and we have to determine whether this exchanger is suitable for a specific purpose (for performing the specified duty). The overall design procedure is very similar to that involved in the sizing problem, except that we do not have to resort to any trial and error (iterative) computations here. The step by step procedure is summarized below:

Step 1: Specification of father file parameters

As discussed in Step – 1 of the sizing problem, in the father file, five among the six parameters such as the mass flow rate of shellside fluid ($\dot{m}_S$) and that of the tubeside fluid ($\dot{m}$), the four terminal temperatures (t_1, t_2, T_1, T_2) are specified. The sixth unknown parameter is then estimated from the heat balance shown in Step – 3. For example, let the unknown parameter be the mass flow rate of the tube side fluid ($\dot{m}$). This is then evaluated from the overall heat balance as shown in step – 3.

Being a rating problem, the heat exchanger specifications are available and these are also to be listed in the father file, such as number of tubeside passes (n_t), number of shelleside passes (n_S), Inner and outer outer diameter of tubes (D_i , D_o), Tubesheet layout (Triangular / Square / Rotated Square Pitch), Tube pitch (p_T , p_P ., p_n), Effective length of each tube (L_e), Number of tubes (N_t), Shell Diameter (D_S), Baffle spacing (B_S , B_{Si} , B_{So}), Baffle cut (B_C), Number of sealing strips installed per crossflow section (N_{SS}), Also to be specified are the maximum permissible pressure drop on the shellside, $(-\Delta P_S)\,(max)$ and that on the tubeside, $(-\Delta P_t)\,(max)$ and the minimum overall dirt factor prescribed, $R_d(min)$.

Step 2: Estimation of property values of process fluids

Estimate the property values of the tubeside fluid (C_P , ρ_f , μ_f , k_f) and those of the shellside fluid (C_{PS} , ρ_{fs} , μ_{fs} , k_{fs}) at the mean temperature t_m and T_m respectively, as

discussed in Step – 2 of sizing problem.

Step 3: **Overall heat balance**

Determine the unknown parameter (here, $\dot{m}$) from the overall heat balance equation, as shown in Step – 3 of sizing problem. Compute also the overall rate of heat transfer (Q).

Step 4: Computation of tubeside heat transfer coefficient (h_i)

Assuming the viscosity correction factor (φ) to be equal to unity, compute the tubeside heat transfer coefficient from available correlations such as from equation (89) or (92), as described in Step – 7 of sizing problem and denote it as h_i'.

Step 5: Computation of shellside heat transfer coefficient, h_o

Assuming the shellside viscosity correction factor (φ_S) to be equal to unity, compute the shellside heat transfer coefficient as discussed in Steps – 8 and 9 of sizing problem and denote it as h_0' . The value of $h_o(ideal)$ is to be computed first from Colburn's correlation (equation – 94) and thereafter the correction factors ($J_C\, J_l\, J_b\, J_S$) incorporated to obtain the value of h_0' .

Step 6: Viscosity correction

Perform the viscosity correction as described in Step – 10 of sizing problem and estimate the actual value of tubeside heat transfer coefficient (h_i) and that of shellside heat transfer coefficient (h_o).

Step 7: Computation of overall heat transfer coefficient (U_i or U_o)

Compute the overall heat transfer coefficient (U_i or U_o) as

$$(1/U_i) = (1/h_i) + (1/h_o)(D_i/D_o) + R_d\,(\text{min}) \quad (168)$$

$$= (1/U_{Ci}) + R_d\,(\text{min}) \quad (169)$$

$$(1/U_o) = (1/h_o) + (1/h_i)(D_o/D_i) + R_d\,(\text{min}) \quad (170)$$

$$= (1/U_{Co}) + R_d\,(\text{min}) \quad (171)$$

Step 8: Computation of Heat Transfer Surface

Compute the heat transfer surface required (A_i or A_o) using any of the three methods such as the F_T Method, ϵ - NTU Method or Martin's Method as described in Step – 5 of the sizing problem.

Step 9: Computation of required tube length

Compute the effective tube length required, $L_e(req)$ as given below

$$L_e(req) = A_i / (\pi D_i N_t) \quad (172)$$

$$= A_o / (\pi D_o N_t) \quad (173)$$

If the above-computed value of $L_e(req)$ exceeds the value of L_e specified in the father file (Step – 1), then print ***" the exchanger is not suitable for the purpose with respect to heat transfer surface requirement"***. Otherwise, proceed to Step – 10 for the computation of tubeside pressure drop.

Step 10: Computation of tubeside pressure drop

Compute the tubeside pressure drop $(-\Delta P_t)$, as discussed in Step – 13 of the sizing problem. If this value of $(-\Delta P_t)$ exceeds the maximum permissible value, $(-\Delta P_t)(max)$, specified in the father file (Step – 1), then print, ***" the exchanger is not suitable for performing the given duty"***. Otherwise, proceed to Step – 11 for the computation of shellside pressure drop.

Step 11: Computation of shellside pressure drop

Compute the shellside pressure drop $(-\Delta P_S)$, as described in Step – 14 of the sizing problem. If this value of $(-\Delta P_S)$ is found to exceed the maximum permissible value, $(-\Delta P_S)(max)$, specified in the father file, then print, ***" the exchanger is not suitable for performing the given duty"***. Otherwise, proceed to Step – 12.

Step 12: Print: The given exchanger is suitable for performing the specified duty.

The readers are encouraged to prepare the detailed CAD flowsheet for the rating problem by themselves, as an interesting exercise.

3. Improved Design of Shell and Tube Heat Exchangers

Since shell and tube heat exchangers are quite popular in all process industries and power plants, attempts have been made by many authors to propose improved design of these exchangers. However, needless to comment, in many cases, though the heat transfer coefficient (and thereby the heat transfer efficiency of the exchanger) gets enhanced, there is simultaneous increase in the pressure drop penalty (and thereby in the operating cost) and consequently, the net benefit of employing the proposed design becomes marginal. In alternate cases, the modified design demands complex and expensive construction or expensive accessories. Examples are flow interception using corona discharge (expensive accessories), admitting process fluids through multiple jets (too high operating cost), insertion of twisted tapes inside tubes (too

cumbersome when a tube bundle composed of 500 – 1000 tubes are used and fouling fluids are handled, net benefit marginal), installation of fins on tube surfaces (high manufacturing cost, simultaneous increase in pressure drop penalty tends to compensate higher heat transfer coefficient attained unless used for gases) etc.

A novel approach in this connection is the use of variable area construction for shell and tube heat exchangers [11, 12]. A Variable Area Exchanger (VAE) employs a bundle of diverging – converging tubes (periodically constricted tubes) instead of straight, cylindrical tubes, as shown schematically in figures (8) and (8A). Each tube is composed of a number of segments, each segment being made up of two frustums of cones joined base to base. .The tube diameter or cross – sectional area thus varies continuously along the length of the tube. If D_2 is the maximum diameter of each segment, D_1 the minimum diameter and L_S the segment length, then from simple geometry, the angle of divergence / convergence (θ) is predicted by

$$\tan(\theta) = (D_2 - D_1)/L_S \qquad (174)$$

The optimum value of θ reported is 5^0 [11,13] or $\tan(\theta) = (1/12)$. The geometry of each tube thus deviates from straight, cylindrical geometry by only 5^0. If n is the total number of segments per tube, then the total effective length (L_e) of each tube shall be

$$L_e = (n\, L_S) \qquad (175)$$

The specific advantages of using such a construction are,

1.They provide substantially large heat transfer coefficient (350 to 400% higher than, or 3.5 to 4.00 times, that in a conventional heat exchanger of same heat transfer surface per unit length) within a large range of flow rates (both in laminar flow and in turbulent flow), both under constant wall temperature conditions as well as constant wall heat flux conditions.

2. The simultaneous increase in pressure drop penalty has been, however, observed to be relatively negligible (only by 15 to 20 % or 1.15 to 1.2 times).

3. The performance efficiency of these exchangers is thus significantly high, but they do not demand any large scale increase in the operating cost. This has been found to be true while handling Newtonian fluids (water, aqueous solutions, petroleum oils) as well as while handling Non – Newtonian fluids such as suspensions and polymer solutions [14].

4. Since the shellside heat transfer coefficient in a variable area exchanger is substantially large, the shell of the exchanger need not have to be baffled. No doubt, a minimum number of baffles may still be installed, keeping the baffle spacing (B_S) at the maximum permissible value $(B_S = B_S(\max) = D_S)$, to act as support plates for tubes.. In the case of tubesheet layout, it is recommended that the tube hole diameter be kept equal to (or slightly more than) D_2

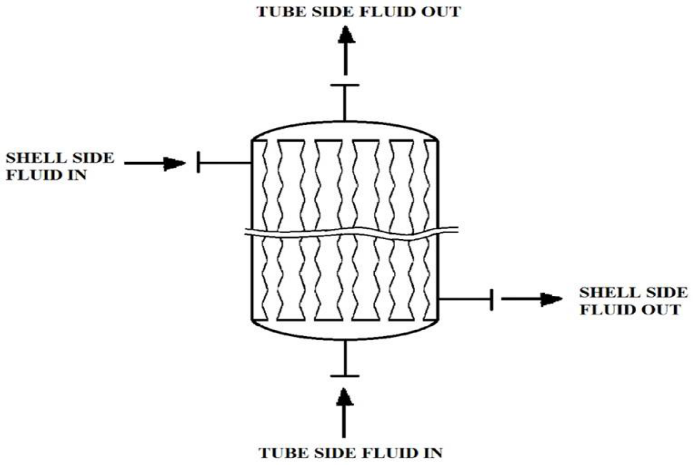

Figure 8: Schematic of Variable Area Shell and Tube Heat Exchanger (showing 1 – 1 construction)

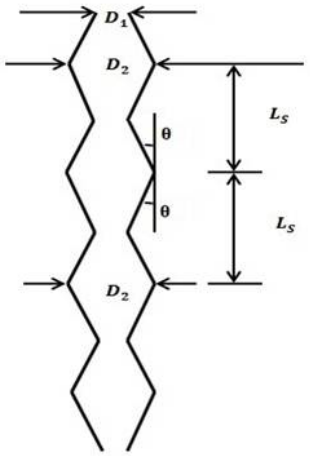

Figure 8A: Schematic of Diverging – Converging Geometry

(the maximum diameter of diverging - converging tube) so as to retain the flexibility of the construction.

5. An additional interesting feature of these exchangers is that they exhibit lower tendency to precipitation fouling. The tortuous wall geometry of the d-c (diverging – converging) tube induces a degree of turbulence into the flow field and this tends to dislodge the deposited dirt from the tube surface and gets it re-entrained into the flowing fluid. If fouling does occur, then cleaning of the tube surface could be accomplished using high pressure liquid jets or by using chemical solvents (chemical cleaning). Mechanical cleaning, no doubt, shall be relatively more troublesome in the present case.

6. Supplementary effects such as bundle bypassing and baffle leakages that tend to diminish the magnitude of shellside heat transfer coefficient shall not be significant in these exchangers. For example, the bundle bypassing effect would not be significant in the proposed design due to the fact that this bypass stream also tends to execute a tortuous flow owing to the diverging – converging nature of the tube wall geometry. The baffle leakage effects (leakage of shellside fluid through shell to baffle and tube to baffle clearances) will also not be predominant since

the shell is to be fitted with minimum number of baffles

The performance characteristics of variable area exchangers have been studied both mathematically as well as experimentally [11 – 14]. Rigorous mathematical models (software packages) have been developed which have been duly verified by comparing with extensive experimental data compiled both on laboratory scale and pilot plant scale.

This construction has been successful not only for the improved design of shell and tube heat exchangers, but also for the design of evaporators / condensers, solar flat plate collectors, solar parabolic trough concentrators (in which the absorber tube is made of variable area design) and also in the case of mass transfer equipment such as gas – liquid absorbers, membrane separation units and column reactors [12].

One of the major reasons for the attractive augmentation characteristics exhibited by these exchangers stems from the fact that the tortuous wall geometry of the d-c (diverging – converging) tube induces additional turbulence into the fluid stream and this increases the intimacy of contacting between the fluid elements. This is substantiated by the fact that the velocity profile in a d-c tube even at low Reynolds numbers ($Re \leq 1500$) has been observed to be flat within the central core of the tube and the velocity is seen to fall sharply to zero at the wall. Such flat velocity profile is obtained in straight cylindrical tubes only in fully developed turbulent flow (at $Re \geq 10000$). It is also to be kept in mind that the onset turbulence in a d-c tube occurs at a much lower Re.

Due to the improved radial mixing of fluid elements, the formation of any stagnant liquid film or thermal layer at the wall of d-c tube is either absent or even if formed, its thickness is quite low. This is evidenced by the nature of velocity and temperature profiles in these systems which exhibit a boundary layer character. The velocity of the fluid falls sharply to zero at the tube wall and the fluid temperature rises sharply in the close vicinity of the heated wall. Such destruction of stagnant layer at the wall reduces the resistance to momentum and heat transport and the transfer coefficient gets enhanced.

Due to the diverging – converging wall geometry of the tube, the flow direction of the fluid varies along the length of the tube (in the converging section, the fluid flows towards the tube axis, while in the diverging section, it flows towards the wall) and the average velocity of the fluid also varies from section to section. This could be causing a type of pressure recovery, like that in a venturi tube. This also helps in providing heat / mass transfer enhancement without the expense of much additional pressure drop.

The thermal penetration distance from the heated wall into the fluid bulk is much larger in the tubes of this geometry as is evident from the enhancement provided. This is in contrast to the assumption usually involved with straight cylindrical tubes (while developing heat transfer

correlations) that the heat penetrates chiefly within a thin annular layer at the wall within which the velocity distribution may even be assumed linear.

The fabrication cost of these exchangers shall be, no doubt, higher. However, this increased initial investment could necessarily be recovered within 1 – 2 years since the exchanger operates with enhanced performance efficiency with relatively little increase in the operating cost.

This design has been successfully adapted to quite a few industries. More large scale industrial utilization of this design must be anticipated keeping in mind the attractive benefits / features of this construction.

4. Nomenclature

a_b = free area for flow of shellside fluid in the baffle window, m^2

a_S = minimum free flow area between baffles at the shell axis, m^2

a_t = tubeside flow area, m^2

A_i = inner heat transfer surface (inside surface area of tubes), m^2

A_m = crossflow area at or near center line, m^2

A_o = outer heat transfer surface (outer surface area of tubes), m^2

A_{Sb} = shell to baffle leakage area, m^2

A_{tb} = tube to baffle leakage area, m^2

B_S = baffle spacing (baffle pitch), *m*

B_{Si} = baffle spacing (baffle pitch) at shell inlet, *m*

B_{So} = baffle spacing (baffle pitch) at shell outlet, *m*

$C\,(\min)$ = smaller of $(\dot{m}C_p)$ and $(\dot{m}_S C_{PS})$, *W/K*

$C\,(\max)$ = larger of $(\dot{m}C_p)$ and $(\dot{m}_S C_{PS})$, *W/K*

C = $C\,(min)\,/\,C\,(max)$, dimensionless

C_p = specific heat of tubeside fluid, *J/(kg.K)*

C_{PS} = specific heat of shellside fluid, *J/(kg.K)*

D_i = inside diameter (ID) of tubes, *m*

D_o = outer diameter (OD) of tubes, *m*

D_{ot} = outer tube limit, *m*

D_S = inside diameter (ID) of shell, *m*

f = tubeside friction factor (for non-isothermal flow), dimensionless

f_S = shellside friction factor (for non-isothermal flow), dimensionless

F_{bP} = bundle bypass coefficient (equation – 115), dimensionless

F_C = fraction of total tubes in crossflow

F_{Cm} = caloric fraction, dimensionless

F_T = correction factor to LMTD for multipass construction, dimensionless

G_b = mass velocity of shellside fluid in baffle window, *kg/(m².s)*

G_e = geometric average mass velocity of shellside fluid (equation – 101), *kg/(m².s)*

G_S = mass velocity of shellside fluid based on flow area a_S, *kg/(m².s)*

G_m = mass velocity of shellside fluid based on flow area A_m, *kg/(m².s)*

G_t = mass velocity of tubeside fluid, *kg/(m².s)*

h_i = tubeside heat transfer coefficient, *W/(m².K)*

h_i' = value h_i when viscosity correction factor ($\varphi) = 1.0$, *W/(m².K)*

h_o = shellside heat transfer coefficient, *W/(m².K)*

h_o' = value h_o when viscosity correction factor ($\varphi_S) = 1.0$, *W/(m².K)*

h_o *(ideal)* = shellside heat transfer coefficient for an ideal crossflow section, *W/(m².K)*

J_C = correction factor that accounts for baffle configuration effect, dimensionless

J_l = correction factor to account for shell to baffle and tube to baffle leakages, dimensionless

J_b = correction factor that accounts for bundle bypassing effect, dimensioless

J_S = correction factor that accounts for unequal baffle spacing, dimensionless

k_f = thermal conductivity of tubeside fluid, *W/(m.K)*

k_{fs} = thermal conductivity of shellside fluid, *W/(m.K)*

K_C = parameter defined in equation (23), dimensionless

K_R = parameter defined in equation (44), dimensionless

K_R' = parameter defined in equation (17), dimensionless

K_S = parameter defined in equation (43), dimensionless

L_e = effective length of each tube, *m*

$\dot{m}$ = mass flow rate of tubeside fluid, *kg/s*

$\dot{m}_S$ = mass flow rate of shellside fluid, *kg/s*

n_s = number of shellside passes

n_t = number of tubeside passes

N_b = number of baffles used

N_C = number of tube rows crossed during flow through one crossflow section

N_{CW} = number of effective crossflow rows in each baffle window

N_{SS} = number of sealing strips installed per crossflow section

N_t = total number of tubes

$NTU\,(max)$ = number of transfer units (maximum)

Nu = tubeside Nusselt number, dimensionless

Nu_S = shellside Nusselt number, dimensionless

p_n = tube pitch normal to flow, *m*

p_P = tube pitch parallel to flow, *m*

p_T = tube pitch (overall), *m*

Pr = Prandtl number of tubeside fluid, dimensionless

Pr_S = Prandtl number of shellside fluid, dimensionless

Q = overall rate of heat transfer, W

R_b = correction factor for bundle bypassing effect on shellside pressure drop, dimensionless

R_l = correction factor for baffle leakages on shellside pressure drop, dimensionless

R_S = correction factor for unequal baffle spacing on shellside pressure drop, dimensionless

R_d = overall dirt factor, *(m².K)/W*

$R_{d(min)}$ = minimum required value of overall dirt factor, *(m².K)/W*

Re_S = shellside Reynolds number, dimensionless

Re'_S = shellside Reynolds number defined by Donohue (equation – 100), dimensionless

Re_{Sm} = modified shellside Reynolds number (equation – 116), dimensionless

Re_t = tubeside Reynolds number, dimensionless

S_r = dimensionless parameter defined in equation (108)

S_s = dimensionless parameter defined in equation (109)

t_1 = inlet temperature of tubeside fluid, K

t_2 = outlet temperature of tubeside fluid, K

T_1 = inlet temperature of shellside fluid, K

T_2 = outlet temperature of shellside fluid, K

t_{am} = arithmetic average temperature of tubeside fluid, K

T_{am} = arithmetic average temperature of shellside fluid, K

t_{cm} = caloric mean temperature of tubeside fluid, K

T_{cm} = caloric mean temperature of shellside fluid, K

t_m = mean temperature of tubeside fluid, K

T_m = mean temperature of shellside fluid, K

t_{Wi} = inner surface temperature of tubes, K

t_{Wo} = outer surface temperature of tubes, K

U_{Ci} = *clean* overall heat transfer coefficient based on A_i, *W/(m².K)*

U_{Co} = *clean* overall heat transfer coefficient based on A_o, *W/(m².K)*

U_D = overall design heat transfer coefficient, *W/(m².K)*

U_i = overall heat transfer coefficient based on A_i, *W/(m².K)*

U_o = overall heat transfer coefficient based on A_o, *W/(m².K)*

Greek Letters

δ_{tb} = tube to baffle clearance, *m*

δ_{Sb} = shell to baffle clearance, *m*

$(-\Delta P_t)$ = tubeside pressure drop, N/m²

$(-\Delta P_r)$ = additional pressure drop due to flow reversal, N/m²

$(-\Delta P_S)$ = shellside pressure drop, N/m²

$(-\Delta P_S)(ideal)$ = pressure drop in ideal crossflow section, N/m²

$(-\Delta P_W)(ideal)$ = pressure drop in ideal baffle window, N/m²

Δt_C = temperature difference of cold fluid, K

Δt_h = temperature difference of hot fluid, K

$\Delta T(max)$ = maximum temperature difference, K

$(-\Delta T)_{ln}$ = logarithmic mean temperature difference, K

($^{\Delta T_C}$) = temperature difference at the cold end of the heat transfer surface / heat exchanger

($^{\Delta T_h}$) = temperature difference at the hot end of the heat transfer surface / heat exchanger

ϵ = heat exchanger effectiveness, dimensionless

θ = baffle cut angle (in ***radians***)

μ_f = viscosity of tubeside fluid at temperature t_m, *kg/(m.s)*

μ_{fs} = viscosity of shellside fluid at temperature T_m, *kg/(m.s)*

μ_{fw} = viscosity of tubeside fluid at the inside wall temperature (t_{Wi}) of tubes, *kg/(m.s)*

μ_{ws} = viscosity of shellside fluid at outer wall temperature (t_{wo}) of tubes, *kg/(m.s)*

ρ_f = density of tubeside fluid, kg / m^3

ρ_{fs} = density of shellside fluid, kg / m^3

φ = viscosity correction factor for tubeside fluid, dimensionless

φ_s = viscosity correction factor for shellside fluid, dimensionless

5. References

1. Perry, RH, Chemical Engineers' Handbook, Sixth edition, McGraw Hill, New York. 1984.

2. Bhattacharya BC, Narayanan, CM, Computer Aided Design of Chemical Process Equipment, New Central Book Agency, Calcutta. 1992.

3. Narayanan CM, Bhattacharya BC, Unit Operations and Unit Processes, Volume 1, CBS Publishers, New Delhi. 2006.

4. Eagle A. Ferguson RM, Proc Roy. Soc, A. 1930; 127: 540.

5. Colburn, AP, Trans Am. Inst. Chem. Eng. 1993; 29: 174.

6. Donohue, D.A., Ind. Eng. Chem.1949; 41: 2499.

7. McAdams, W.H., Heat Transmission, Third Edition, McGraw Hill, New York. 1954.

8. Kern DQ, Process Heat Transfer, McGraw Hill, New York. 1950.

9. Bell KJ, Delaware Method for Shell Design, in Heat Exchangers: Thermal Hydraulic Fundamentals and Design, Kakac et. al (eds.), Hemisphere Publishing Co, New York. 1981.

10. Grimson ED, Trans. Am. Soc. Mech. Eng. 59, 583, 1937; 60, 381, 1938.

11. Narayanan, CM, J Chemical Engineering Japan. 1998; 31: 903 – 909.

12. Narayanan, C.M., Annual Technical Volume (interdisciplinary coordination committee), The Institution of Engineers (I). 2017; 2: 128 – 139.

13. Narayanan CM, Bhattacharya BC, Industrial and Engineering Chemistry Research. 1998; 27: 149 – 155.

14. Narayanan CM. Heat and Mass Transfer (Wärme und Stoffübertragung). 2014; 50: 161 – 168.

Advances in Chemical Engineering

Chapter 5

State of the Art Technologies for Separation of Azeotropic Mixtures

Taha Mahdi[1,2,*]

[1]*Faculty of Chemical Engineering, Universiti Teknologi Malaysia, 81310 Johor Bahru, Malaysia*

[2]*Chemical Engineering, College of Engineering, University of Babylon, Babylon, IRAQ*

[*]***Correspondence to: Taha Mahdi,*** *Chemical Engineering, College of Engineering, University of Babylon, Babylon, IRAQ*

Email: tahamahdi9@gmail.com

Abstract

Azeotropic separation technologies have been classified broadly into two major categories, i.e., distillation and membrane processes. Because normal distillation has limitations for azeotropic mixtures, enhancements have been proposed that either introduce a third component serving as an entrainer in extractive and azeotropic distillation processes or apply a pressure swing distillation system. Among the membrane processes, pervaporation was reported to be most promising for azeotropic separations. More recently, an approach known as process intensification has been proposed for combining multiple processes into single units such as a dividing wall distillation column or exploiting sonication phenomena to break an azeotrope in an ultrasonic distillation system. This paper reviews the state of the art technologies covering all the above mentioned separation techniques. Existing techniques are appraised, and technology gaps are identified. Based on these insights, areas for further development are suggested, aiming at satisfying the process objectives by inherently safer, environmentally benign and economically more attractive techniques.

Keywords: Separation Technologies; Azeotropic Mixtures; Special Distillation Trocesses, Pervaporation; Intensified Processes

List of symbols: A: Light component; B: Heavy component; C: Concentration; D: Diffusivity; F: Feed flow; D: Diffusivity; F: Feed flow: VLE: Vapor liquid equilibria; VLLE: Vapor liquid liquid equilibria; CAMD: Computer aided molecular design; PSD: Pressure swing distillation; THF: Tetra hydrofuran; HP: High pressure; LP: Low pressure; PV: Pervaporation; MTBE: Methyl tertiary-butyl ether; ETBE: Ethyl tertiary-butyl ether; ILs: Ionic liquids; EtOH: Ethanol; DWC: Dividing wall column; FricDiff: Frictional diffusion; AD: Azeotropic distillation; ED: Extractive distillation; R: Gas constant; S: Selectivity; Ncol: Number of columns; Np: Number of pure component; NB: Number of boundaries crossed; Pio: Vapor pressure of component i; T: Temperature; y: Concentration of component in vapor phase; x: Concentration of component in liquid phase; il: Components i in the upper liquid phase; xill: Components i in the lower liquid phase; J: Diffusion flux; Jp: Permeate flux; Jo: Pre-exponential factor; z: Position [length]; θ: Correction factors for high pressure; γ: Activity coefficients; Γ: Activity coefficients in the lower liquid phase; α_ij: Relative volatility of components i and j; α: Overall selectivity of membrane; αs: Sorption selectivity

1. Introduction

The separation of liquid mixtures is an important task in the process industry, and much research has been carried out to meet the requirements of the industry. Of all available liquid separation techniques, distillation stands as the most widely applied technique. Distillation is typically achieved in columns of various sizes with heights ranging from 6 to 60 meters and diameters that range between 0.65 and 6 meters [1]. Despite its widespread use, distillation consumes large amounts of energy that are estimated to be more than 95% of the total energy used for separation processes in chemical process industries [2]. Nevertheless, because distillation offers many processing advantages and is well understood, it remains the preferred process whenever possible.

Distillation is, however, limited in its use when the mixtures to be separated exhibit complex phenomena. An example of these situations is when the mixtures involved form azeotropes, a point at which the vapor phase has the same composition as a liquid phase. There are two types of azeotropic systems: i) a minimum boiling azeotropic system, and ii) a maximum boiling azeotropic system. For such systems, a higher purity product beyond the azeotrope point cannot be achieved using a conventional distillation process. Therefore, alternative methods have been developed to satisfy the separation requirement.

Figure 1 shows some of the currently available technologies for separation of azeotropic mixtures, which can be classified into three main categories: i) enhanced distillation, ii) membrane processes and iii) process intensification. The first category involves enhancement of the distillation process by modifying the process conditions and configurations. These modifications include extractive distillation, azeotropic distillation, and pressure swing distillation. The second category involves utilization of membrane separation technologies such as the pervaporation process. The pervaporation process is advantageous as it offers low energy consumption and better safety and is more environmentally friendly than conventional processes. Nevertheless, the pervaporation process is still limited in terms of applications because it is yet to be proven in large scale applications. Another class of process intensification consists of the development of novel apparatuses and techniques, compared to the present state-

of-art in the chemical process industry. The aim of intensification is to optimize capital, energy, environmental and safety benefits by radical reduction of the physical size of the plant. This technology includes dividing wall column, microwave and ultrasonic techniques. The former introduces changes in column internals whereas the two latter techniques employ microwave and sonication effects to alter the thermodynamic properties of the mixture.

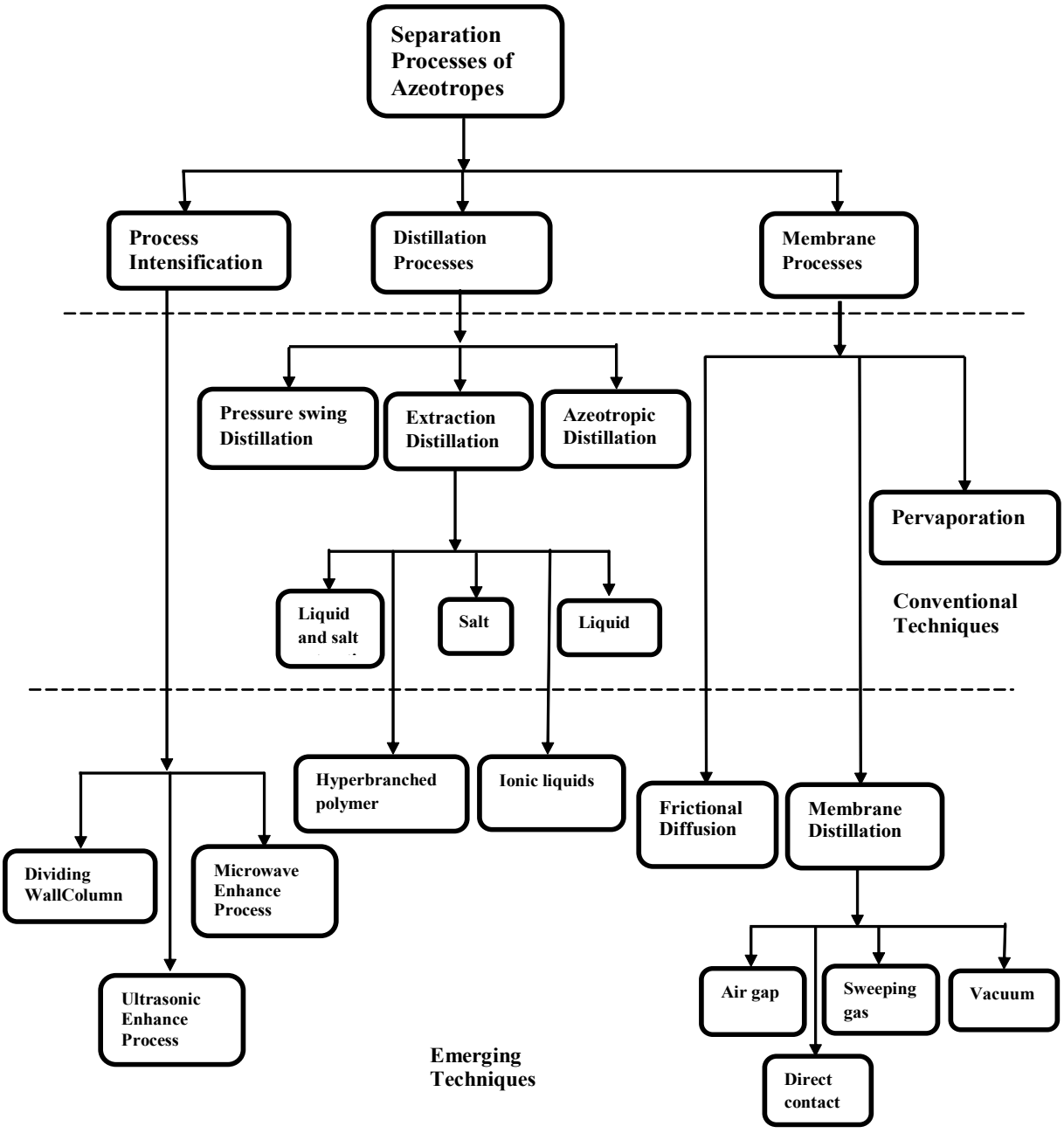

Figure 1: Schematic diagram of various techniques for separation of Azeotropic mixtures.

Due to the importance of the subject, there have been several review articles in various journals and chapters in books dealing with the separation of azeotropic mixtures, elaborating their fundamental theories and applications. For example, the work of Widagdo and Seider [3] concentrated on methods used for analyses, entrainer selection, column design and control of azeotropic distillation. Lei et al. [4] discussed various combinations of extractive distillation and other separation processes. Li et al. [5] addressed the entrainer selection and proposed a mathematical model for the process. Huong et al. [6] published a review on extractive distillation for bio refining of hemicelluloses and added chemicals from fermentation hydrolysates. More

recently, Pereiro et al. [7] reviewed methods utilizing ionic liquids as azeotrope breakers and compared the performance of the new system with conventional extractive distillation.

Similarly, Villaluenga and Mohammadi [8] reviewed the performance of the membrane pervaporation process for separation of benzene and cyclohexane mixtures. The applications of pervaporation and vapor permeation in environmental protection were reviewed by Kujawski [9] The scientific and technological factors governing the separation of organic mixtures by pervaporation were also reviewed by Smitha et al [10]. Despite the significant number of review articles, a comprehensive coverage that addresses the overall technologies is not available and has therefore become the motivation for this paper. In this article, a comprehensive review of the available technologies is provided with elaboration of advantages and disadvantages of each method. Based on these insights, technological gaps are identified and future work is recommended with special emphasis on developing processes that are more energy efficient, environmentally benign and inherently safe.

2. Enhancement of Distillation Process for Separation of Azeotropic Mixtures

Separation of azeotropic mixtures can be achieved by enhancing the separation mechanisms involved in the distillation process to overcome its limitations. The most common strategy is to introduce a third component to alter the thermodynamic equilibrium. By choosing a suitable candidate component, along with the determination of thermodynamic properties such as residue curve maps, optimal values of distillation parameters such as the entrainer amount, reflux ratio and boiler duty and the number of stages can be fixed [11], setting the foundation of the azeotropic and extractive distillation processes. Another approach to enhance the distillation is to manipulate the operating pressure as in the case of pressure swing distillation.

2.1. Distillation processes using an entrainer

Azeotropic and extractive distillation processes have the same common features that basically consist of *two* distillation columns to separate compounds with close boiling points or mixtures that form azeotropes. This separation is normally accomplished by adding a third component known as an entrainer as a separating agent, to increase the relative volatility and alter the vapor liquid equilibrium data of the components that are the most difficult to separate. Added in the liquid phase, the new component alters the activity coefficient of various compounds in different ways, thus affecting the relative volatility of the mixture, thus enabling the new three-part mixture to be separated by normal distillation [12].

2.1.1. Rules of Entrainer selection

The entrainers to be used in the azeotropic and extractive distillation processes are chosen

based on selectivity. Typically, solvents considered are ranked based on their potential to affect the relative volatility of the components, and the solvent that gives the highest relative volatility and the lowest operating costs is selected [13]. The relative volatility of separation of a given mixture of key components *i* and *j* occurs in two phases (vapor-liquid) at equilibrium, as illustrated in Eq. 1:

$$\alpha_{ij} = \frac{y_i/x_i}{y_j/x_j} = \frac{\gamma_i P_i^o}{\gamma_j P_j^o} \qquad (1)$$

Here, x_i and y_i are the molar fractions in the liquid and vapor phase of component (*i*), respectively. The parameter γ_i is the activity coefficient, and P_i^o is the vapor pressure of the pure component. In some cases, for large changes in operating pressure and temperature, the value of α_{ij} is significantly affected, and the azeotrope is eliminated [4]. For small temperature changes, the ratio of P_i^o/P_j^o is almost constant, and the relative volatility can only be affected by introducing a solvent that changes the ratio γ_i/γ_j. This ratio, in the presence of the solvent, is called selectivity, $S_{ij.}$

$$S_{ij} = \left(\frac{\gamma_i}{\gamma_j}\right)_s \qquad (2)$$

There are several other constraints to be considered in choosing the entrainers. These constraints include the requirement that the entrainer should have a boiling point significantly different from the other components to facilitate an easier separation in the second column. Moreover, the entrainer selection should also consider safety, environmental effect, corrosiveness, costs and availability [14].

Ewell et al. [15] studied the relationship between hydrogen bonding and azeotrope formation and classified entrainers into groups according to their molecular interactions. These authors also developed guidelines to identify chemical classes suitable as entrainers for heteroazeotropic and extractive distillations. Based on these guidelines, Berg [16] classifies organic and inorganic mixtures by making use of the molecular structure to identify promising entrainers and suggests that the successful entrainers for extractive distillation should be highly hydrogen-bonded liquids (e.g., water, amino alcohols, amides, phenols alcohols and organic acids). Although it is impossible to choose the best entrainer entirely through experimental work, a large number of computation approaches appear to fit the purpose. These methods include the Pierotti-Deal-Derr method, the Parachor method, the Weimer-Prausnitz method and Computer-Aided Molecular Design (CAMD). Among these methods, CAMD is the most recent and preferred method [17].

2.1.2. Azeotropic distillation process

Azeotropic distillation can be defined as a distillation in which a relatively small amount of the added entrainer forms an azeotrope with one or more of the components in the feed based on differences in polarity [18]. Most of the solvents are highly volatile compared to the components to be separated so that the solvent is taken off from the overhead of the column. Azeotropic distillation processes basically utilize two columns. The first column serves as the main column, and the second column is used for entrainer recovery. In this process, an entrainer leaves the first column from the column overhead with the lighter component, while the heavies are collected as a bottom product. The entrainer and the lighter component are then fed to the second column to produce a high purity product at the bottom while the recovered entrainer is recycled back to the first column.

Azeotropic distillation is usually classified into two classes based on the type of mixtures to be separated: i) homogeneous and ii) heterogeneous azeotropic distillation [12], as illustrated in Figure 2. In the case of homogeneous process, phase split does not appear in the liquid along the whole column, unlike the heterogeneous counterpart, in which the two liquid phases exist in some regions of a composition space. A decanter is used in heterogeneous azeotropic distillation to collect the condensed vapor from the condenser and permits the separation of the two liquid phases. Commonly, these two liquids are the entrainer and the lighter component where the entrainer phase is refluxed back to the column. The other phase is fed to the second column where it is fractionated to remove the dissolved entrainer. The case of heterogeneous mixtures without the use of a decanter at the top of the azeotropic distillation column can be considered as a homogeneous mixture, and at the same time, the liquid composition on a tray or a section of the packing is replaced by the overall liquid composition [19].

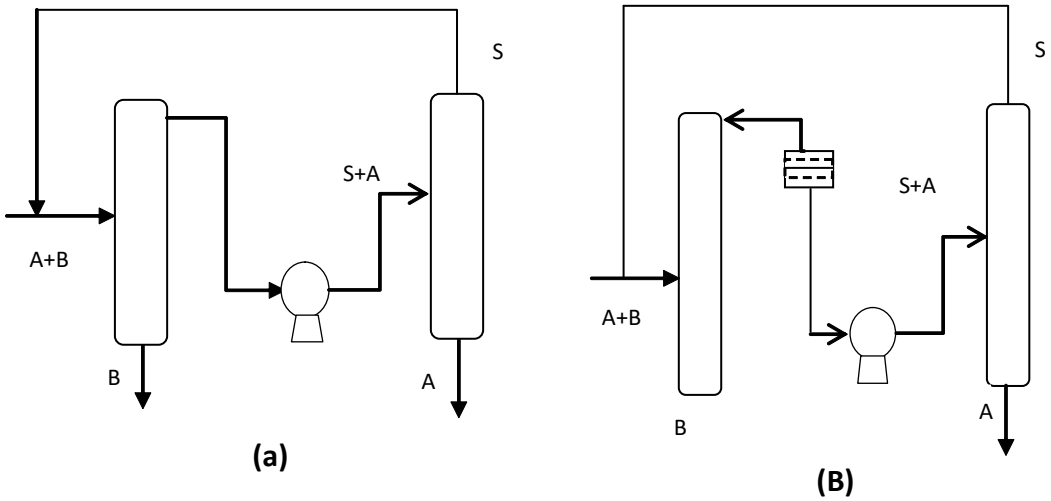

Figure 2: Schematic diagram of an azeotropic distillation, where A and B are light and heavy components of the feed mixture respectively, S is an entrainer component; a) homogeneous process, b) heterogeneous process.

Relative volatility is an important physical quantity as it reflects the influence of the entrainer on the vapor-liquid equilibrium [20]. In the case of heterogeneous azeotropic distillation, the entrainer and the two components *i* and *j* being separated form three phases

on trays of the column, (i.e., vapor-liquid-liquid) and two liquid phases in equilibrium with a vapor phase. For the three-phase equilibrium, the solubility of components *i* and *j* in the upper liquid phase is denoted by x_i^I and x_j^I, respectively. The solubility of components *i* and *j* in the lower liquid phase is denoted by x_i^{II} and x_j^{II}, respectively, and the corresponding activity coefficients are denoted by γ and Γ in the upper and lower liquid phases, respectively. The relative volatility of components *i* and *j* is related to the overall composition x_i by Eq. 3 [3]:

$$\alpha_{ij} = \frac{\gamma_i \Gamma_i p_i^o \theta_i}{\gamma_j \Gamma_j p_j^o \theta_j} \frac{\left(x_i^{II} - X_i\right)\Gamma_j + \left(X_i - x_i^I\right)\gamma_j}{\left(x_j^{II} - X_j\right)\Gamma_i + \left(X_j - x_j^I\right)\gamma_i} \qquad (3)$$

where θ_i and θj are correction factors for high pressure. At low or moderate pressure, the values can be approximated as $\theta j = \theta_i \approx 1$. Eq. 3 represents the relative volatility of components *i* and *j* in a three-phase (vapor-liquid-liquid) at equilibrium.

The key feature of feasible heterogeneous azeotropic distillation is that entrainers and top tray vapor compositions are selected to generate liquid-liquid tie lines, which straddle at least one of the distillation boundaries dividing the two regions containing the two components to be separated. Heterogeneous azeotropic distillation is often preferred industrially over homogeneous azeotropic distillation due to the ease of recovery of the entrainer and the transition across a distillation boundary in the decanter [21]. However, heterogeneous azeotropic distillation suffers from some disadvantages associated with the high degree of nonlinearity, multiple steady states, distillation boundaries, long transients, and heterogeneous liquid-liquid equilibrium, limiting the operating range of the system under different feed disturbances [22]. Moreover, it is difficult to find a model that represents both the vapor-liquid and liquid-liquid equilibrium data accurately for heterogeneous systems. Unstable saddle azeotropes are also difficult to identify experimentally. Furthermore, the examinations based on the rate-based model are necessary, but the studies with the rate-based model for design and analysis of a heterogeneous azeotropic distillation process are quite insufficient [23].

Homogeneous and heterogeneous azeotropic distillation corresponds to the real state of the mixture, consisting of the components to be separated as high purity products. Forming a homogeneous azeotrope neither means that the separation method becomes a homogeneous process nor that it is forming a heterogeneous azeotrope, because the separation method becomes heterogeneous while depending on the physical property of the entrainer used [24]. In addition, for both types of azeotropic distillation, the entrainer must be vaporized through the top of the column, thus consuming much energy. Some of the recent studies on the application of azeotropic distillation as a separation method are listed in **Table 1.**

Table 1: Summary of the latest azeotropic distillation cases with minimum–boiling binary azeotropes

Components to be separated (A+B)	Type azeotropic distillation	Entrainers	Azeotrope B.P. °C	B wt% in Azeotrope	References
Cyclohexane + benzene	Homogeneous	Chlorobenzene	77.8	45.0	[25]
Ethanol + water	Heterogeneous	Cyclohexane	78.2	95.6	[26]
Ethanol + water	Homogeneous	Methanol	78.2	95.6	[27]
Acetic acid + water	Heterogeneous	Butyl acetate	76.6	3.0	[28]
Isopropanol + water	Heterogeneous	Benzene	80.4	87.8	[29]
Isopropanol + water	Heterogeneous	Benzene	80.4	87.8	[30]
Isopropanol + toluene	Homogeneous	Acetone	80.6	58.0	[19]
Acetone + heptanes	Homogeneous	Toluene	---	---	[31]
ethyl acetate + *n*-hexane	Heterogeneous	Acetone	64.8	65.7	[32]
Tetrahydrofuran + water	Heterogeneous	*n*-Pentane	65	95	[33]
Acetontrite + water	Homogeneous	butyl acetate	76.5	83.7	[34]
Acetone + heptane	Homogeneous	Benzene	55.6	93.5	[35]
Acetone + water	Heterogeneous	Toluene	---	---	[36]
1,2Dichlor ethane + water	Heterogeneous	Chlorinated	72.0	80.5	[37]
Phenol + water	Heterogeneous	Toluene	99.76	97.8	[38]
Formic acid + water	Heterogeneous	Propyl Formate	107.1	77.5	[39]
Dichloromethane + acetone	Heterogeneous	Water	---	---	[40]
Ethylene Diamine + water	Heterogeneous	Benzene	119.0	81.6	[40]
1,4-dioxane + water	Heterogeneous	Benzene	87.8	81.6	[41]
Isopropanol + ethanol	Homogeneous	1,3-Dioxolane	---	---	[42]
Ethyl acetate + ethanol	Homogeneous	Ethyl ether	71.8	69.0	[42]

2.1.3. Extractive distillation Process

Extractive distillation involves a relatively nonvolatile entrainer compared to the components to be separated. Therefore, the entrainer is charged continuously near the top of the fractionation column, so that an appreciably high amount of entrainer is maintained on all plates in the tower below its entry. Thus the solvent is removed from the bottom of the tower. An extractive distillation process is more commonly applied in the chemical and petrochemical industries than the azeotropic distillation [43]. Figure 3a shows the principle of this technology, where components A and B are fed to the first column that acts as an extractive column where the solvent (S) is introduced at the top stage. In this process, the lighter component (A) is withdrawn at the top of the first column, while the solvent with other component exits at the bottom. The bottom products of the first column are then fed to the second column, in which the heavier component (B) is withdrawn at the top and the entrainer is separated from the

bottom and recycled back to the first column. The separation in the second column is often easier because of the larger boiling point difference between the high-boiling entrainer and the existing second component, and because the solvent does not form an azeotrope with the second component.

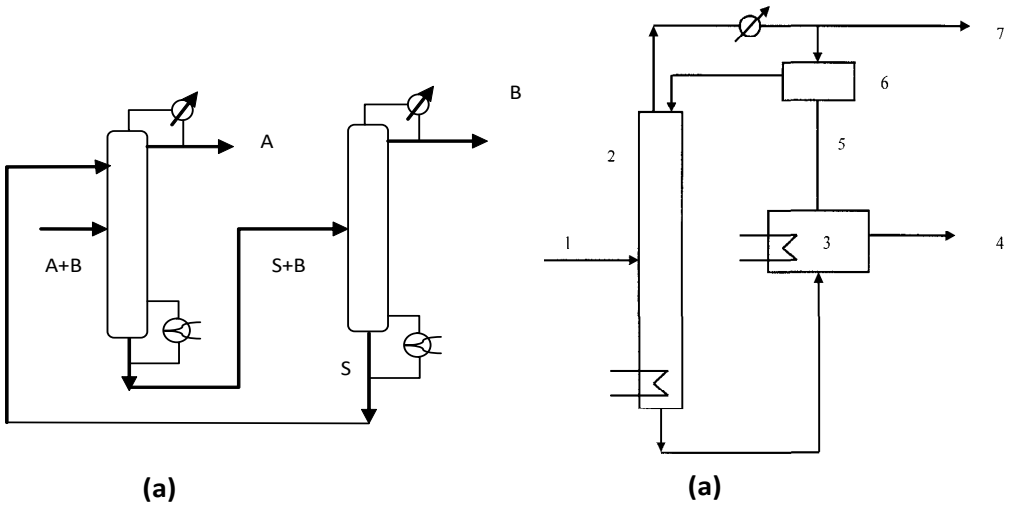

Figure 3: Schematic diagram of an extractive distillation [5]; a) double column process where A and B are light and heavy components of the feed mixture respectively, S is a solvent component. b) single column process with salt: 1- feed stream, 2- column of extractive distillation, 3- equipment for salt recovery, 4- bottom product, 5- the salt recovered, 6- reflux tank and 7- overhead product.

Extractive distillation is more frequently used compared to azeotropic distillation due to better availability of entrainers. Extractive distillation is also better in terms of energy consumption, unlike the azeotropic distillation that is required to vaporize both the solvent and the component into the top of the column [44]. However, extractive distillation cannot produce highly pure product compared to azeotropic distillation because the solvent coming from the bottom of the solvent-recovery column most likely contains impurities that may affect the separation process [45]. Another drawback of the extractive distillation is the number of degrees of freedom when compared with a simple distillation setup. In a simple distillation setup, the degrees of freedom are the reflux ratios and the number of stages of the distillation columns, while in extractive distillation, the entrainer type and its flow rate comprise additional degrees of freedom [46].

Table 2: Comparison between Azeotropic distillation and extractive distillation

Parameters	Azeotropic distillation	Extractive distillation
Common use	Less	More
Energy consumption	More	Less
Solvent coming out	Top	Bottom
Purity of products	Less	More
Flexible selection of solvents	Less	More

Some of the latest examples of the single liquid solvents commonly used in the extractive distillation technique are listed in Table 3. Interested readers can compare the entrainers used in practice with the rules of selecting entrainers. This table shows that there is a difference in the azeotropic percentile of the component and different boiling points in an azeotropic mixture.

Table 3: Summary of the latest studies on extractive distillation for separation of azeotropic mixtures

Mixtures of solvent (A+B)	Entrainer	Type	Azeotrope B.Pt. °C	B wt.% in Azeotrope	reference
Benzene + cyclohexan	*N*,*N*-dimethyl acetamide (DMAC)	Close-boiling and minimum- boiling azeotropes	77.8	45.0	[47]
Tetrahydrofuran + water	Propylene glycol	Minimum-boiling azeotropes	65	95	[48]
Ethyl acetate + chloroform	2-Chloro-butane	Maximum-boiling azeotropes	---	---	[49]
Ethanol + water	DMF	Minimum-boiling azeotropes	78.2	95.6	[50]
Hexane + ethanol	[mmim] [$MeSO_4$]	Minimum-boiling azeotropes	58.7	79.0	[51]
Isopropyl ether + acetone	3-Pentanone	Minimum-boiling azeotropes	53.3	43.5	[52]
Propanone + *di*-isopropyl ether	Putyl ether	Minimum-boiling azeotropes	61	---	[53]
Ethanol + water	Ethylene glycol	Minimum-boiling azeotropes	78.2	95.6	[54]
Ethyl acetate + ethanol	Diethylene triamine	Close-boiling and minimum- boiling azeotropes	71.8	69.0	[55]
Acetone + methanol	Water	Minimum-boiling azeotropes	55.7	88.0	[26]
Methyl acetate + methanol	Dimethylformamide	Minimum-boiling azeotropes	119.0	81.6	[56]
Propylene + propane	Acetonitrile	Close boiling	---	---	[57]
Acetonitrile + water	Ethylene glycol	Minimum boiling azeotrope	76.5	83.7	[34]
C_4 material/ 1,3-butadiene	DMF	Close boiling	126	45	[58]
Acetic acid + water	Tributyl amine	Minimum boiling azeotrope	76.6	3.0	[59]
Di-n-propyl ether + *n*-propyl alcohol	2-Ethoxyethanol	Minimum boiling azeotrope	50	66.5	[60]
Chloroform + methanol	Water	Minimum boiling azeotrope	53.5	13.0	[61]
Ethyl benzene + p-xylene	5-Methyl-2-hexanone	Close boiling	136.1	60	[62]
Isobutyl alcohol + isobutyl acetate	*n*-Butyl propionate	Minimum boiling azeotrope	107.4	55.0	[63]
Methyl acetate + cyclohexane	Carbon tetrachloride	Minimum boiling azeotrope	---	---	[64)

2.1.3.1. Types of entrainers used in extractive distillation

The selection of a separating agent influences the economics of the extractive distillation process. This separating agent can be a liquid solvent, dissolved salt, mixture of liquid solvents, mixture of dissolved salts, ionic liquids and hyperbranched polymers. Based on the type of separating agent, the extractive distillation process can be further divided into five categories that will be discussed in the following sub-sections.

(i) Extractive distillation with a liquid solvent

A schematic diagram of an extractive distillation with liquid solvents is shown in Figure 3a. In this case, a high solvent ratio (i.e., mass ratio of solvent to feed) with values typically in the range of 5 to 8 is used, thus leading to high energy consumption. However, because the solvent can be recovered effectively under normal operating conditions, this scheme remains a preferred choice in industry rather than schemes using any other agents and attracts the interest of many researchers [34,55,58,61,63].

(ii) Extractive distillation with solid salt

In this case, a separating agent in a form of a solid salt is fed at the top of the column, dissolved into the liquid phase, and recovered from the column by evaporation [65]. A schematic diagram of this process is shown in Figure 3b. To suit the process requirements, the solid salt must be soluble in the feed components, nonvolatile and able to flow all the way down the column. The salt extracted from the bottom of the column is then recycled.

The so-called ‘‘salt effect in Vapor-Liquid equilibrium (VLE)’’ refers to the ability of a solid salt that has been dissolved into a liquid phase consisting of two or more volatile components to alter the composition of the equilibrium vapor without itself being present in the vapor. The feed component in which the equilibrium vapor is enhanced is said to have been ‘‘salted out’’ by the salt, while the other feed component is ‘‘salted in.’’ This phenomenon can be described by the following equation which is known as the Setschenow equation and expresses the solubility of a nonelectrolyte in a solid salt solution with a low salt concentration.

$$log\frac{S_o}{S} = K_sC \qquad (4)$$

Here, S_o is the solubility of the salt in pure solvent, S is the solubility of the salt in a salt solution of concentration C (mol/L,), and K_s is the salting coefficient, which has a characteristic value for a given salt-nonelectrolyte pair. A positive value of K_s, corresponds to salting out ($S_o > S$); if K_s, is negative, salting in is observed ($S_o < S$). Species which lower the dielectric constant should be salted out by all electrolytes [4].

Solid salt is a more effective separating agent when compared to the liquid agent, and

requires a much smaller salt ratio, thus leading to a high production capacity and a low energy consumption [66]. Furthermore, because solid salt is not volatile, the product at the top of the column is free from salt impurities and is therefore more environmentally friendly. However, when solid salt is used in industrial operation, dissolution, reuse and transport of the salt that has been introduced causes corrosion of equipment, thus limiting the application of salt in the process industry [5].

(iii) Extractive distillation with the combination of liquid solvent and solid salt

The extractive distillation using a combination of liquid solvent and solid salt has a configuration similar to the system with liquid solvent as shown in Figure 3a. This process is advantageous due to the easier operation offered by the liquid solvent scheme and the high separation ability offered by a solid salt scheme. This process is also suitable for separating both polar and non polar systems. Lei et al. [67] examined the use of N, N-dimethylformamide (DMF) as a solvent to separate a C4 mixture. By adding a small amount of solid salt to DMF, considerable improvement in the relative volatilities of C4 was achieved. These authors also concluded that NaSCN and KSCN are among the best salt additives when criteria such as relative volatilities, price, erosion and availability are considered. However, because solid salts tend to cause corrosion in the equipment and decay easily at high temperatures, a narrow range of suitable solid salts is available for selection.

(iv) Extractive distillation with ionic liquid

The use of Ionic Liquids (ILs) as separating agents in the extractive distillation process is a recent strategy that has been adopted and is often used in processes involving chemical reactions [68]. This process has a configuration similar to the configuration of extractive distillation with solid salt as shown in Figure 3b. The features of this process include salts consisting completely of ions, which are in the liquid state at room temperature. The salts of ionic liquids therefore do not need to be melted by an external heat source [69]. The most outstanding reason for interest in these solvents is the negligible vapor pressure at room temperature [70], leading to a lower risk of worker exposure and minimal loss of solvent to the atmosphere. ILs can be tailored for a specific application by accurate selection of the cations and anions [71]. ILs also have the advantages of liquid solvents in promoting high separation ability. ILs are also suitable for both polar and non polar solvent systems. In addition, extractive distillation with the IL technique has the following advantages [72]:

1) Absence of product impurities at the top of the column, because ionic liquids are not volatile.

2) Suitability for use over a wide temperature range from room temperature to above 300°C, which corresponds to the typical operating conditions of extractive distillation due

to the inherently high volatility of ILs.

3) Suitability of ionic liquids for treatment with a wide variety of materials including organic, inorganic and even polymeric materials.

4) Facile recovery and reuse of ionic liquids.

5) High stability of ionic liquids under the operating conditions of extractive distillation in terms of thermal and chemical conditions.

Taking all of these features into account, the ILs are considered good candidates for application as extracting solvents or entrainers in the separation of azeotropic mixtures, and ILs have demonstrated capabilities to separate many mixtures [73,74]. However, despite the increase in publications addressing azeotropic separations with ILs, these studies are limited to analysis of the liquid-liquid equilibria [75] and vapor-liquid equilibria [76] or simulation of the extractive distillation process with ILs [77].

Extractive distillation with ILs also suffers from some disadvantages such as the long time required to prepare the ionic liquids and the high cost of synthesis of such specialty components [5]. The separation of viscous solutions using this technique is very difficult to manage [7] and the ILs demonstrate moisture sensitivity [72]. Such disadvantages have slowed down the application of this process in industry [5].

(v) Extractive distillation with hyperbranched polymers

A class of highly branched polydisperse macromolecules with a tree like topology with large number of functional groups and three-dimensional polymers such as hyperbranched polymers [78] or dendrimers [79] have recently found a variety of applications in the field of chemical engineering. Most of the applications are related to the absence of chain entanglements and presence of a large number of functional groups within a molecule. Furthermore, the functional groups of hyperbranched polymers allow tuning of their thermal, rheological, and solution properties. This tuning provides the opportunity to design entrainers for a wide variety of applications [80,81]. Unlike the conventional linear polymers, hyperbranched polymers not only show a remarkable selectivity and capacity, but because of a lack of chain entanglements, also show a comparatively low solution and melt viscosity as well as an enormous thermal stability [77].

Recently, Seiler et al [77] suggested the use of hyperbranched polymers as entrainers for extractive distillation for the separation of azeotropic mixtures. In another study, these authors studied the separation of the Tetrahydrofuran (THF)/water and ethanol/water mixtures using different hyperbranched polyesters as entrainers in extractive distillation [82]. Their experimental results illustrated the potential of such entrainers in breaking the azeotropic phase

behavior and concluded that the use of hyperbranched polyesters provides cost savings compared to conventional separation processes. Comparing between dendrimers and hyperbranched polymers, the tedious and complex multistep synthesis of dendrimers results in expensive products with limited use for large-scale industrial applications. For many applications that do not require structural perfection, hyperbranched polymers can circumvent this major drawback of dendrimers. Therefore, a wide variety of applications, which originally seemed conceivable only for dendrimers, were investigated for the statistically branched hyperbranched polymers in the past decade [83].

2.2. Pressure Swing Distillation

Pressure swing distillation (PSD) is a process alternative to the broadly applied azeotropic and extractive distillations. The principle of pressure swing distillation (PSD) is based on the fact that a change in pressure can alter the relative volatility of a liquid mixture, even for liquid mixtures with a close boiling point or those that form an azeotrope. If the operating pressure is increased, the azeotropic point shifts to lower composition values of the light component. The significant positive change in the azeotrope point and enlargement of the relative volatility of azeotropic mixtures allow the separation to take place without any need for a separating agent. Following the early work in 1928 by Lewis [84] and further developments that followed [85-87]. Table 4 shows some of the recent studies on the separation of azeotropic mixtures using PSD.

Table 4: Summary of the latest studies using pressure swing distillation for separation of azeotropes

system	Type	LP(bar)	HP (bar)	Process type	Reference
Acetonitrile + water	Minimum	1.013	2.78	Continuous	[88]
Acetonitrile + water	Minimum	1.013	3.02	Batch	[89]
THF + water	Minimum	1.013	7	Continuous	[87]
THF + water	Minimum	1.013	10	Semicontinuous	[86]
Acetone + methanol	Minimum	1.013	4	Continuous	[90]
Acetone + methanol	Minimum	1.013	10	Batch	[91]
Ethyl acetate + ethanol	Minimum	4	25	Continuous	[92]
Ethyl acetate + ethanol	Minimum	1	10	Batch	[93]
Isobutyl acetate + isobutyl alcohol	Minimum	0.2	1.013	Continuous	[63]
Diamine-ethylene + water	Maximum	1.013	8	Batch	[94]
Ethanol + toluene	Minimum	0.1	1.1	Batch	[29]
di-*n*-propyl ether + *n*-propyl alcohol	Minimum	0.3	1.01	Continuous	[60]
Acetone + *n*-pentane	Minimum	1.013	10	Batch	[94]
Ethanol + water	Minimum	1.013	10	Continuous	(95)

PSD can be operated in three different modes: i) continuous [3, 85], ii) batch [96] and iii) semi-continuous [97[. The dependence of the azeotropic concentration on the system pressure is used for the separation of the mixture. If the feed has a lower light component concentration than the azeotropic point, the feed is introduced into the Low Pressure (LP) column, otherwise the feed has to be fed into the High Pressure (HP) column.

Figure 4 illustrates the separation of a binary mixture with a homogeneous minimum-boiling azeotrope in a continuous PSD. Because the feed stream *F1,* which is a combination of the combination of the fresh feed F with the recovery stream *D2,* has a mole fraction of light component A greater than the azeotropic point, *F1* is fed into the low-pressure column (LP). The objective of this column is to concentrate component B near an azeotropic point of the mixture and to remove pure component A in the column bottom stream. The azeotropic mixture *D1* that leaves the top of the column serves as the feed stream *F2* to the second high-pressure (HP) column to produce pure heavy component B in the bottom stream. The remaining products are recycled from the top to be mixed with fresh feed *F* to the first column. Both columns operate at different pressures that suit the intended separation requirement.

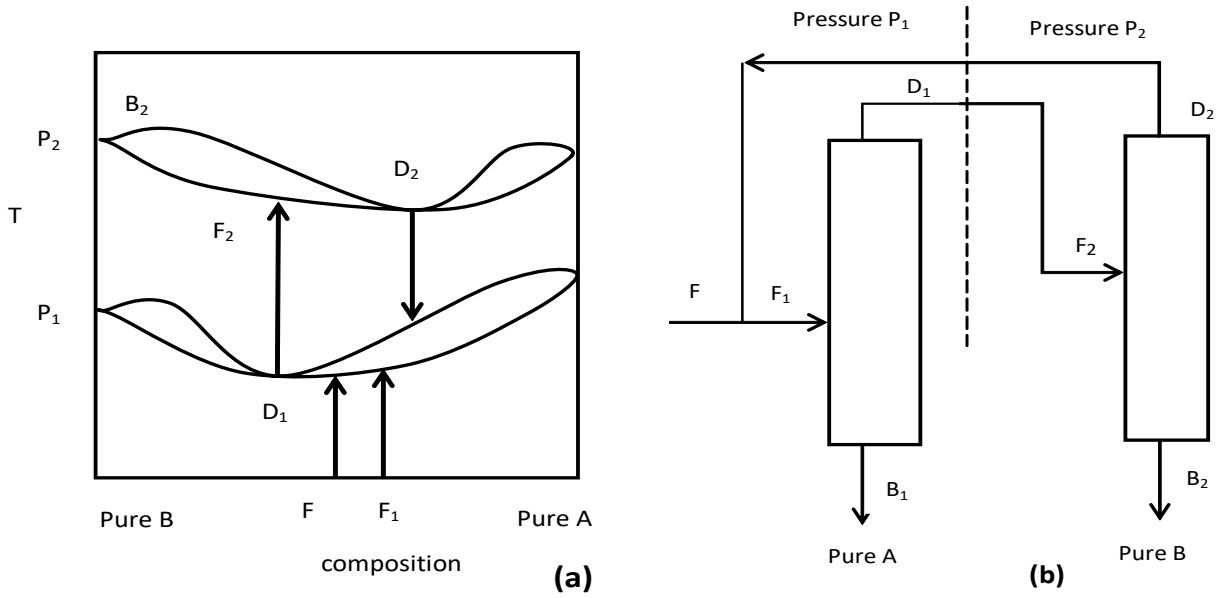

Figure 4: Schematic diagram for continuous pressure-swing distillation: (a) pressure-sensitive minimum-boiling azeotrope and (b) column sequence [90].

In general, vapor-liquid equilibrium calculations can be divided into two types. The starting point for both is the equality of fugacities of a component (*i*) in the vapor and liquid phases, as shown in Eq. [5]. The two types differ in the description of the component fugacities in the vapor (f_i^v) and liquid (f_i^l) phases [87].

$$f_i^v(T,P,y_i) = f_i^l(T,P,x_i) \qquad (5)$$

The correlations of the first types involve a "two-model" approach: one model is used to estimate the vapor phase ($\emptyset_i$) nonidealities while another model is used for the liquid phase (γ_i). The starting equations are:

$f_i^v(T,P,y_i) = \varnothing_i y_i P$ for the vapor phase (6a)

$f_i^l(T,P,x_i) = \gamma_i x_i P_i^{vap}$ for the liquid phase (6b)

where γ_i is the activity coefficient, and $\varnothing_i$ is the fugacity coefficient (for more details, see [85].

In a batch operation, only a single column is used for the separation. Component A is supposed to be the ultimate product in a mixture consisting of components A and B. This process includes two steps: in the first step, the column is initially charged with the feed mixture F into a bottom tank (for a regular batch) and operates at low pressure, as shown in Figure 5. Component B is removed from the bottom of the tower while a mixture close or equal to the azeotropic composition is accumulated at the top. This step runs until the target composition of component B is achieved in the bottom tank. On completion, the process is switched over to the second step, in which the column is recharged with the azeotropic mixture and is operated at high pressure. Thus, component A is obtained from the bottom while the mixture approaches the azeotropic composition at the top. If the initial feed concentration is higher than the azeotropic point, then the first step becomes the high pressure step, and component A is produced at the bottom. To provide high recovery, this cycle may be repeated many times [89].

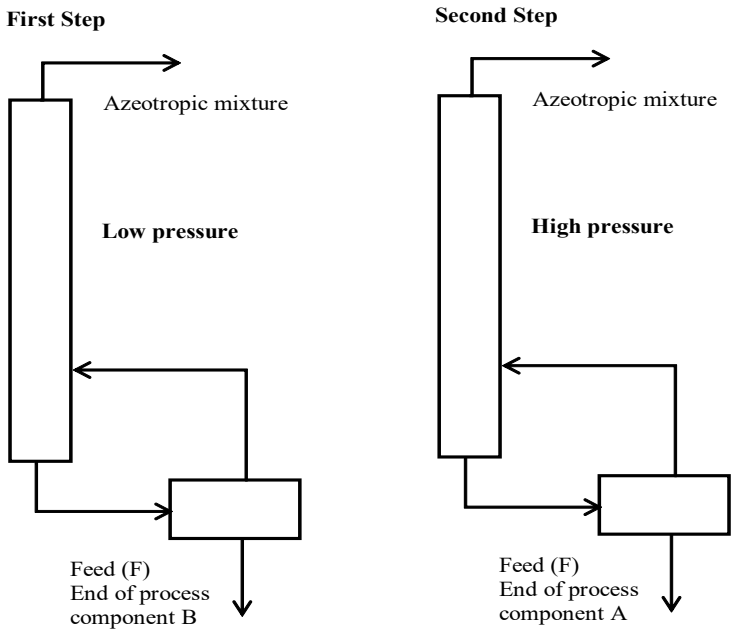

Figure 5: Schematic diagram for regular batch operation of PSD [89].

More recently, a number of novel batch column configurations have been introduced. These novel batch column configurations include an inverted batch process for separation of an acetonitrile/water mixture [89], a middle vessel configuration for separation of the ternary azeotropic mixture of acetone, benzene, and chloroform [98] and multi-vessel design for separating a mixture of methanol–ethanol–propanol–butanol [99].

In semicontinuous operation, only a single distillation column is involved. However, the column operates continuously or periodically. Liquid levels are maintained on the trays or packing, a stream is fed continuously to the reboiler, and cooling water is fed continuously to the condenser. The column operates in two modes, with tanks T1 and T2 alternating as the feed source, and the distillate and bottoms products are also sent to alternate tanks, as shown in **Figure 6**. Operation begins in mode 1, after startup, during which on-specification products (nearly pure A as a bottoms product and distillate near the azeotrope at a low pressure) are achieved. T1 is recharged periodically with fresh feed from S1. The column operates continuously but not at a steady state.

The column alternates between the modes defined as follows: Mode 1: S2 feeds the column. The condensed overhead and off-specification bottoms product is fed to tank T2. S1 has a zero flow rate. The operating mode is low pressure. Mode 2: S3 feeds the column. The overhead and off-specification bottom product is fed to tank T1. S1 feeds tank T1. The operating pressure is high. Product is fed to tank T3 or tank T4 when the bottom composition exceeds high purity in A or B, respectively. The process switches between modes when tank T1 or tank T2 is empty. In each mode, the column has a fixed pressure, reflux and reboil ratio. Modes 1 and 2 operate at low and high pressure, respectively [86].

Compared with continuous processing, semicontinuous PSD has several advantages, including greater plant flexibility and lower investment costs, because the product can be obtained without the need for additional equipment. When semicontinuous operation is compared with batch PSD, the downtime due to liquid holdups is sharply reduced because the compositions near the top of the column approach the azeotropic compositions in the distillate and consequently do not vary greatly as the tower shifts between low- and high-pressure operation [86].

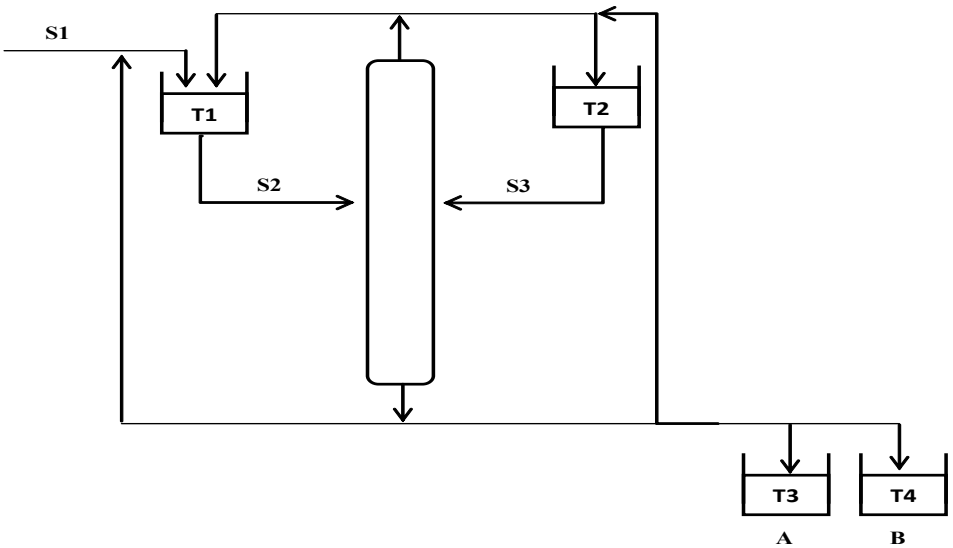

Figure 6: Schematic diagram for semi-continuous operation of PSD [86].

The minimum number of columns required for a given separation can be calculated from Eq.(7), below [86]:

$$N_{col} = N_p + N_B - 1 \quad (7)$$

Here, N_{col} is the minimum number of columns required, N_p is the number of pure component products, N_B is the number of boundaries crossed for PSD (which does not include boundaries that disappear as the pressure changes). For example, for an extractive distillation to separate a ternary mixture, N_B is equal to unity and the number of columns needed is 3 (N_{col} = 3 +1– 1= 3). Consequently, it is unlikely that PSD will be advantageous as the azeotropic point for homogeneous azeotropes may vanish as the pressure decreases to some extent. Thus NB = 0 and the column number is therefore reduced to 2 for PSD.

However, the PSD process has a number of disadvantages, including a higher complexity of operation, resulting in the need for more sophisticated automation and more complex process control. There is also a gap in the experimental data in the literature because industrial applications are seldom published. In spite of the available theoretical knowledge [85], reliable experimental studies are scarce, partly because the operation tends to be limited to atmospheric conditions because operations under nonatmospheric conditions are difficult to establish and generation of such data is expensive [100]. This drawback limits the application of thePSD *process* in industry. Among the limited applications reported is the work of Knapp and Doherty [90] on the separation of tetrahydrofuran and water by continuous PSD

3. Separation of Azeotropic Mixture Using Membrane Technology

A higher energy requirement and a limited choice of entrainers to be used in azeotropic and extractive distillation processes have led to the development of alternative processes such as membrane-based processes [8,101]. Membrane processes may be regarded as “clean technology” due to the lower energy demand and the fact that membrane processes do not require the use of additional chemicals [102]. Within this class of techniques, pervaporation (PV) is most prominent[10,103], and accounts for 3.6% of the total membrane separation applications in chemical and petrochemical operations [104]. Some of the PV applications in industry include removal of water from organic solvents (e.g., dehydration of alcohols, ketones and esters) [105], removal of organic compounds from water [106], and separation of organic-organic azeotropes and isomers [107].

3.1. Pervaporation (PV)

Pervaporation involves permeation of feed components through a membrane, followed by evaporation into the downstream in various rates. A schematic diagram of the PV process is shown in Figure 7. PV separates the liquid feed mixture by partial vaporization through a

dense nonporous membrane. The feed mixture is usually in direct contact with one side of the oliophilic membrane, whereas permeate is removed in a vapor state from the opposite side into a vacuum or sweeping gas and then condensed [108]. The driving force for the separation is the difference in the partial pressures of the components on the two sides of the membrane, and the driving force is not affected by the relative volatility of the mixtures. This driving force for transport is the difference between the liquid feed/retentate and vapors permeated on each side of the membrane. The retentate is the remainder of the feed leaving the membrane feed chamber, which did not permeate through the membrane [109]. However, the use of PV to break azeotropes is restricted because the mass transportation through a thick dense polymer membrane is a slow process [110].

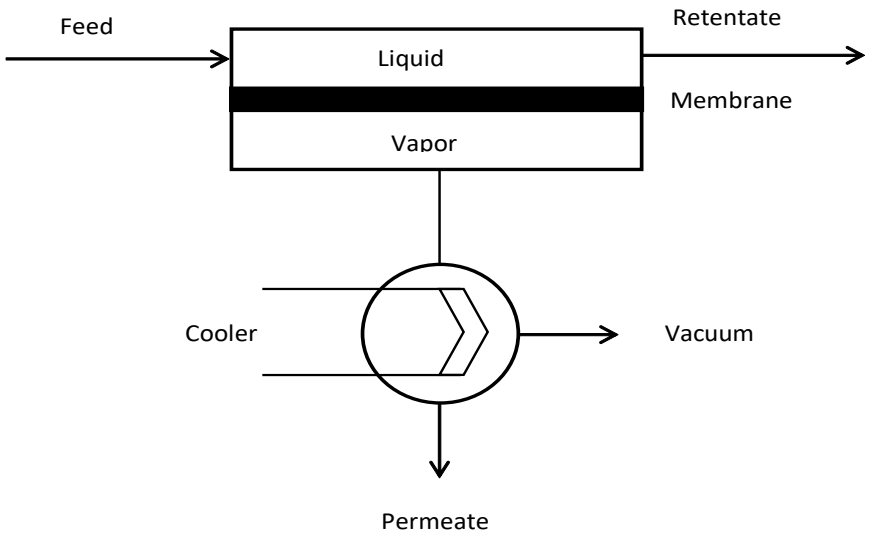

Figure 7: Schematic diagram of pervaporation process.

The main advantages of PV separation technology are that it is not limited by the vapor–liquid equilibrium because it is independent of relative volatilities. This property makes PV a good alternative technique to separate azeotropic and close-boiling point liquid-liquid mixtures [111]. However, because the feed mixtures are in direct contact with the surface of the polymeric membranes, the feed mixtures affect the swelling or shrinking of the membrane materials. Uragami and coworkers [112] proposed an improvement to overcome this disadvantage by vaporizing the feed solution and permeating it through the membrane. In this manner, the swelling or shrinking of the polymeric membrane can be prevented. A polymer with great affinity with one component in the feed is preferred for making PV membranes to obtain higher selectivity. However, the membrane becomes swollen if this affinity exceeds a certain level in a way that makes the membrane lose its integrity, thus necessitating higher selectivity. Aptel et al. [113] and Binning et al [114] proposed that the control of the membrane selectivity prevents the swollen fraction of the skin layer in a PV. Therefore, the choice of the proper membrane material is a crucial factor for a specific separation. In practice, separation by PV is achieved with a small amount of feed mixture as a result of the low permeation rate and therefore a large surface area for the membrane is needed. Increasing the membrane surface area for a larger-scale application is required, and several heat exchangers must be available

to vaporize the permeating component of the feed stream [110]. The PV process is limited by the boiling point of the feed mixture and the temperature sensitivity of the feed components [115].

3.1.1. Factor Influencing PV performance

The separation performance of the PV process is dependent on flux and selectivity. Flux is affected by the operating conditions, while selectivity involves a design decision. The maximum separation potential is provided when a suitable membrane is selected. In a binary system, the selectivity of a membrane is defined as the ratio of the concentrations of components in the permeate to the concentrations of the components in the feed [116]:

$$\alpha = \frac{y_a / y_b}{x_a / x_b} \qquad (8)$$

where α is the selectivity, and x and y are the concentrations of the components in the feed and the permeate, respectively. The *'a'* and *'b'* subscripts refer to the two components to be separated. The selectivity of a membrane is strongly dependent on the membrane affinity for one (or more) component(s) of the feed and the diffusion of the permeating molecules through the membrane matrix. The expected selectivity of a membrane therefore decreases with the increase in the molecular size of the components [117]. The overall selectivity of a membrane can be computed by multiplying the selectivity of sorption, α_s, by the selectivity of diffusion, α_D:

$$\alpha = \alpha_s * \alpha_D \qquad (9)$$

Flux is defined as the rate of permeation of the feed components through a unit area of the membrane at a unit time. Flux is governed by the mass transfer process described by Fick's law of diffusion, as defined by Eq.10, below,

$$J = -D\frac{dC}{dz} \qquad (10)$$

where J is the diffusion flux (mole/m·s), D is the diffusivity (m^2/s), C is the concentration (mole/m^3) and z is the position [length] (m). The negative sign indicates that J is positive when movement is down the gradient, i.e., the negative sign cancels the negative gradient along the direction of positive flux. D is proportional to the squared velocity of the diffusing particles, and the value of D depends on the temperature, the viscosity of the fluid and the size of the particles according to the Stokes-Einstein relationship. The driving force for the one-dimensional diffusion is the quantity $-\partial C / \partial x$ that is the concentration gradient for ideal mixtures. In chemical systems other than ideal solutions or mixtures, the driving force for diffusion of each species is the gradient of the chemical potential of these species [118]. According to Fick's law, the rate of transfer by diffusion is proportional to the concentration gradient in the area of the interface over which the diffusion takes place [119].

The mass transfer in the PV process is also influenced by the operating conditions, including the concentration and composition of the feed, the feed permeate pressure and the temperature. This allows manipulation of the operating variables to suit the process constraints and to find the optimal operating conditions for the maximum mass transfer.

3.1.2. Membrane material selection in PV technology

The work on membrane separations began in 1960 with a wide range of membrane materials including dense metals, zeolites, polymers, ceramics and biological materials. The first manufactured polymeric membranes that found applications for organic solvent dehydration [120], including hydrophilic PV membranes, are still in use in the industry [121]. Recently, ceramic membranes have also been used as selective barriers in PV [122]. Such ceramic membranes are used in a wide range of applications, including separation of mixtures in acid and alkaline environments, which require high thermal and chemical stability [123].

The selection of the membrane polymeric materials for PV applications depends on three important factors, including capacity of sorption, chemical resistance, and mechanical strength. To separate a liquid mixture by the PV process, one of the components of the feed solution must have good interaction with the membrane materials to provide the swelling needed. Table 5 summarizes the performance and design limitations of the various membranes currently available for the separation of azeotropic mixtures.

Table 5: Summary of the latest studies of the pervaporation process for separation of azeotropic mixtures

Binary mixtures (A/B)	Membrane materials	Content of A in feed [wt. %]	Temperature [^{o}C]	Selectivity $\alpha_{A/B}$	Flux [Kg/m^2.h]	References
Water/ethanol	Phosphorylated chitosan	10.23-52.3	70	213	0.58	[124]
Water/1,4-dioxane	Chitosan and Nylon-66	18	40	865	0.09045	[125]
Water/acetic acid	Polymide-6 /PAA	8.7	15	82	0.005	[126]
Isopropanol/water	Chitosan	87.5	70	472	0.39	[127]
Butanol/water	Silicone rubber	0-8	30	45-65	<0.035	[128]
MTBE/water	PDMS	2	50	280	1.2	[129]
Methanol/toluene	Cellulose	5-90	45	1200	15	[130]
Methanol/ ETBE	CAB PEG600DMA	20	40	21	1.4	[131]
Methanol/MTBE	Poly(ether ether ketone)	1-87	30	254-3.2	0.015-0.113	[132]
Methanol/benzene	PFSA on Teflon	31	45	9.6	100.28	[118]
Ethanol/cyclohexane	Polyelectrolyte	12.1	50	106.7	8.7	[133]
Methanol/ cyclohexane	PAN-*g*-MA	5-80	50	<200	<80	[134]
Methanol/MTBE	Chitosan with H_2SO_4	20	25	9.3	1.5	[135]

Ethanol/ETBE	PERVAP 2256	30	50-70	14.2	2.3	[136]
Benzene/ cyclohexane	LDPE	50	25	1.6	10.8	[137]
Toluene/cyclohexane	PS and PAM	75	30	7.9	1400	[138]
Toluene/*n*-hexane	Polyurethane	10-70	25	2.8-5.8	1.1-3.5	[139]
Toluene/*n*-octane	Polyesterimide	50	50	70	10	[140]
Styrene/ ethylbenzene	Polyurethane	20-80	60	1.1-5.7	0.3-1.2	[141]
Ethanol/ethyl acetate	Polydimethylsiloxane PDMS	60	30	3.61	1.397	[142]
Ethanol/cyclohexan	Poly(vinyl pyrolidone)	25-100	54	7.5-47.4	0.05	[143]
Methanol/dimethyl carbonate	Poly(acrylic acid)/poly (vinyl alcohol)	10-90	60	1-6	0.577	[144]
Methanol/methyl acetate	Pervap 2255-30	30	60	-	7.4	[145]
Water /ethanol	Sodium alginate	5.2-38.6	30	2182	0.035	[146]
Toluene/*n*-heptane	MSE-modified	10	85	4.985	4.61	[147]
Dimethyl carbonate/ methanol	Hydrophobic nano-sillca/ polydimethylsiloxane	30	40	3.97	0.702	[148]
Toluene/iso-octane	3,5-Diaminobenzoic	50	100	90	-	[149]
Methanol/MTBE	Poly(lactic acid)	10	30-50	30	15	[150]
Methanol/dimethyl carbonate	Chitosan	10	60	-	0.276	[151]
Methanol/toluene	PVAHII	1.8-18.6	30	0.759-2.88	16-622	[152]
Methanol/TAME	Poly(vinyl alcohol)	97	50	4	175	[153]
Water/ethyl acetate	Polyvinyl alcohol	5.1	60	129	$2.83*10^{-4}$	[154]
Ethanol/ethyl acetate	Na Y	30	130	27-82	2.9	[155]

An efficient and economical membrane separation process can be established by correctly choosing membrane materials with desirable qualities including high selectivity and stability, good permeability, resistance to fouling, and lengthy lifetime [156]. The PV permeability coefficient represents the product of the solution coefficient and the diffusion coefficient. Fouling, which is generally caused by scale formation rather than clogging or blocking of pores, poses a challenge to the economy of the PV together with the membrane life cycle.

3.2. Frictional Diffusion

Frictional Diffusion (also called friction difference, FricDiff) is a separation technology based on differences of diffusivities in a mass separating sweep gas or vapor mixtures. A FricDiff module consists of flows of a target gas mixture (feed side) and a mass separating agent (sweep side) separated by a nonselective porous layer (barrier). FricDiff has been shown

to allow for the breaking of azeotropes in mixtures [157,158]. Development of frictional diffusion (FricDiff) technology for azeotropic mixture separations aims for increasing the energy-efficiency and reducing the use of hazardous solvents in the separation section of a chemical process [159]. As implied by the name, the separation principle that governs FricDiff is the membrane separation method [160].

Figure 8 depicts the mechanism at the molecular level. When considering the diffusion of molecules A and B through a third species C, the smaller molecule A experiences, in terms of diffusion, less hindrance from the so-called sweep gas (counter gas) C than the larger molecule B, resulting in a higher diffusive velocity of A compared to B, which can be exploited to achieve separation of the two gases. The FricDiff apparatus consists of two channels that are separated by a porous layer. The feed mixture A + B enters a side of the device. The sweep gas C enters the other side. In this setup, a counter-current flow pattern is chosen, but the concept works for co-current flow patterns as well. If the pressure gradient needed for convective flow through the channels can be neglected, FricDiff works both isothermally and isobarically on both sides of porous barrier. The separation in FricDiff is based on diffusional processes only [157].

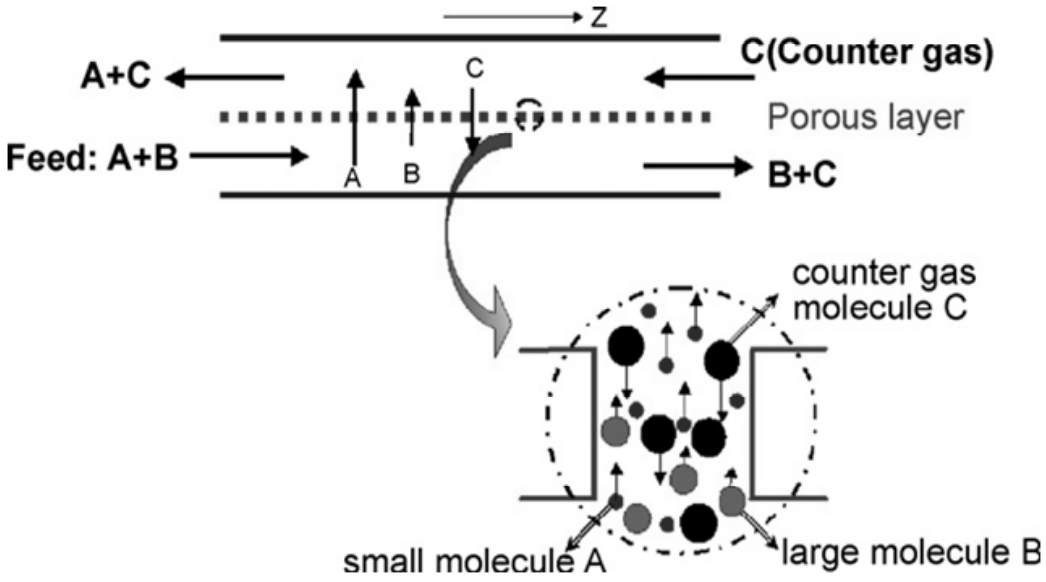

Figure 8: Schematic presentation of the principle of the FricDiff separation technique [157].

Similar to other membrane processes, the driving force for mass transport in FricDiff is the gradient in the chemical potential, which reduces to a gradient in the partial vapor pressure for ideal gases. However, the mechanism for separation between FricDiff and these membrane processes is different. The separation principle in membrane separation processes depends on the type of selective membrane that is used, while in the FricDiff process, separation is based on the difference in transport velocities of the components of the feed mixture in the sweep gas [161].

3.3. Hybrid process distillation/pervaporation

The PV process alone is not sufficient to separate some of the azeotropic mixtures. Thus,

hybrid processes combining distillation and membranes, known as Membrane Distillation (MD), is highly attractive to overcome these limitations [162]. Hybrid MD processes have drawn attention on various occasions [30,163]. However, only a few studies deal with optimization aspects of such a hybrid process with different approaches.

In the MD process, a liquid solution at a high temperature is brought into contact with one side of a porous hydrophobic membrane that acts as a barrier to separate the warm solution (called the feed side) from the permeate in either a liquid or a gaseous phase, which enters a cooling chamber called the permeate side. The hydrophobic nature of the microporous membrane prevents liquids/solutions from entering its pores due to the surface tension forces. As a result, a fixed interface is formed at the pore entrance. If the solution contains at least one volatile component, the temperature difference at the two ends of the pores produces a vapor pressure gradient within the pores. By the driving force, the vapor molecules of the volatile component that is produced by evaporation from the feed solution at the vapor-liquid interface migrate from the feed side to the permeate side of the membrane. At the permeate side, the migrated molecules that depend on the configuration of the membrane used are either condensed or removed in a vapor form from the membrane module. Flowing this way, the solution from the feed side is concentrated [5].

MD is advantageous due to its low cost and low energy consumption but suffers from some drawbacks such as low permeate flux (compared to other separation processes, such as RO), high susceptibility of the permeate flux to the concentration and temperature of the feed conditions due to the concentration and temperature polarization phenomena. The trapped air within the membrane also introduces a further mass transfer resistance, which also limits the MD permeate flux. The amount of heat lost by conduction is quite large [164].

A distillation column and a membrane module can generally be combined in various different configurations. Figure 9 (a-d) shows a schematic diagram for some configurations for a membrane/distillation hybrid process. The membrane module can be placed in the column feed stream as shown in Figure 9a, and this design is called parallel configuration. A series configuration is also available and is considered a special case of the more general solution **(Figure 9b)**, in which the membrane feed stream is taken as a side draw from the column and permeate as well as the retentate streams are fed back into the column. In Figures 9c and 9d, the membrane is located, respectively, on the head and bottom of the column performing the final product stream purification [164].

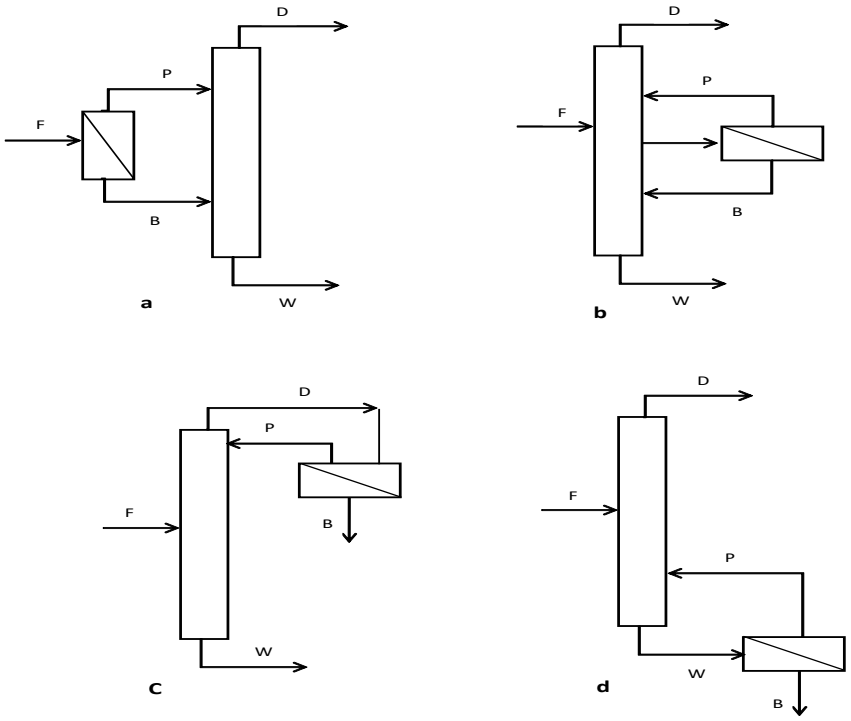

Figure 9: Schematic diagram for various configurations for a membrane/distillation hybrid process [164].

Daviou et al [165] carried out studies on the optimal design of hybrid distillation pervaporation systems for the separation of a methanol/methyl *tert*-butyl ether mixture. Their simulation results using rigorous models show that significant cost reduction can be achieved. Working on isopropanol–water and propylene–propane mixtures, Naidu and Malik [166] illustrate the structural and parametric optimization of a continuous hybrid distillation-pervaporation process with different configurations such as series, parallel, and series-parallel arrangements of pervaporation modules in the network. Their findings proved that the purity of products can be obtained without violating the composition constraints of products and the heat exchange policy that minimizes the required membrane area by increasing the flux through the membrane. Kookos [167] carried out studies on optimal design of hybrid processes for membrane/distillation column using the structural and parametric optimization procedures. The results proved that the economic potential for using hybrid systems is significant.

4. Process Intensification

Process intensification is a process design approach that leads to substantially smaller, cleaner, safer and more energy-efficient process technology [168]. Within the realm of the separation processes discussed in this review, process intensification can be used to increase the functionality of the process as in the case of the dividing wall distillation column, or process intensification can be used to introduce selected process phenomena into the conventional separation [169]. In the following sub-sections, some examples are illustrated.

4.1. Dividing Wall Distillation Column

When more than two products are to be obtained in a distillation process from a multi

component feed, the number of columns required to isolate products at the specified quality is equal to the number of components. Accordingly, plants with multiple products require a large number of possible column sequences, and it is important to determine the optimal number of separation columns in a sequence to reduce operation costs. To overcome such challenges, a distillation column with one longitudinal partition wall welded to the column wall, known as a dividing wall column (DWC), is introduced to reduce the number of columns required. In this case, the middle section of the vessel is split into two sections by inserting a vertical wall at an appropriate position [170].

DWC has found a great appeal in the chemical process industry because it offers significant energy saving along with substantial capital and space reductions. These advantages can be further enhanced by using a recently introduced non-welded wall technology, which allows the use of multiple columns within a shell. Several reviews and research papers have been published on this topic, covering the design [171], simulation [172], control [144, 173], optimization [174] and applications of DWC [175, 176]. However, because this process defines a single operating pressure, the boiling point in the reboiler becomes higher leading to a higher pressure drop and a higher temperature difference [177].

The separation of a ternary mixture of components A, B and C by a DWC is illustrated in Figure 10, with A being the lightest and C the heaviest. In the first half (pre-fractionator) of the DWC, a crude separation is carried out between components A and C. Component A is concentrated at the top of the second half (main column), and C is concentrated at the bottom with component B distributed between the top and the bottom. A liquid from the top section refluxes to the top of both the pre-fractionator and the main fractionator, while the vapor from the bottom section similarly strips the bottom of the pre-fractionator and the main fractionator. Under steady state conditions, the DWC yields the lightest component (A) at the top of the column and the heaviest component (C) at the bottom. The middle component B is withdrawn at a selected stage of the main fractionator where its concentration is at a maximum [175].

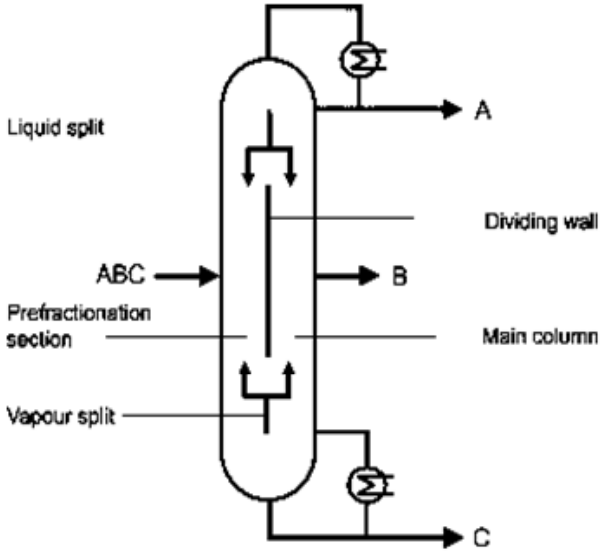

Figure 10: Schematic diagram for a dividing wall column [175].

The DWC technology can also be used in azeotropic separations (A-DWC) [178, 179], extractive distillation [180], and even reactive distillation [181].However, industrial application for the separation of azeotropic mixtures is yet to be realized, and publications are still more focused on theoretical and simulation studies. For example, Briones-Ramírez et al. [182] report an Aspen-Plus simulation of an A-DWC system for isopropanol-water–acetone and isopropanol-water–methanol mixtures and obtain results claiming energy savings of up to 50% compared to a system with a two-column sequence. Sun et al [178] also carry out Aspen-Plus simulation of A-DWC for an ethanol dehydration process with cyclohexane as an entrainer. The results revealed that the proposed A-DWC system managed to save 42.17% of the energy consumption and 35.18% of the overall annual operating costs, along with reduction in greenhouse gas emissions. Kiss and David [183] used a DWC to enhance the bioethanol dehydration in both extractive distillation and azeotropic distillation and obtained energy savings of 10–20% for the novel process intensification alternatives based on DWC, while using fewer equipment units compared to the conventional extractive and azeotropic distillation configurations.

4.2. Microwave Enhanced Process

A microwave heating process is a molecular-level process that has gained substantial attention in academia and industry, including chemical process applications. However, while microwave technology has been introduced for reaction intensification [184], its use in separation processes is currently limited to a few applications such as extraction [185], desorption [186] and drying [187].

In recent years, several studies have focused on understanding of the microwave technology to enhance evaporation and improve the performance of the distillation process, and promising results have been reported [188]. Altman et al. [189] studied the effects of microwave on distillation of a binary system and concluded that the improvements offered by the microwave field occur only when the microwave field interacts directly with the vapor–liquid interface. On azeotropic mixtures, Gao et al. [190] studied the separation of a benzene/ethanol system at 101.33 kPa under various operating conditions and concluded that the azeotropic point is shifted upward from the standard curve when a microwave field is introduced.

The influence of a microwave field on the vapor–liquid equilibrium varies based on the components involved due to the variation in absorption of microwave energy. For example, ethanol is a good microwave absorber, whereas benzene is a poor microwave absorber. Thus, for a benzene/ethanol mixture, the OH groups of ethanol become rotationally excited, and heat is generated, leading to an increase in the overall internal energy of the ethanol molecule. The VLE is shifted because the microwave energy dissipated rapidly into the ethanol, and the heat transfer rate between ethanol and benzene in the vapor–liquid interface is slower than the

interaction of the microwave field with ethanol [190]. As a result, the vapor phase is richer in the high microwave irradiation absorption medium for the binary system, and the liquid phase is exactly the opposite, opening up opportunities for exploiting microwave irradiation in overcoming azeotropic separation.

4.3. Ultrasonic Enhanced Process

The application of ultrasonic waves can be found in various areas of application including biology, medicine, material forming, and the chemical industry [191, 192]. In the process industry, this sonication phenomenon has been exploited in enhancing cleaning, separation and reaction processes [193,194]. Heating, acoustic streaming and ultrasonic cavitation are widely believed to be the main causes for the enhancement [195]. Recently, employment of the potential of the sonication phenomenon for the separation of liquid mixtures has been reported [196,197].

Ultrasonic waves have also been found to be useful in enhancing the distillation process, particularly for the separation of azeotropic mixtures. Ripin et al. [198] and Mudalip et al. [199] studied the effect of ultrasonic waves on the Vapor Liquid Equilibrium (VLE) using typical binary mixtures. These authors also found that ultrasonic waves can positively change the VLE and alter the relative volatility of azeotropic mixtures. The changes in the relative volatility and VLE data for the binary mixtures are caused by the cavitation activity during the transmission of ultrasonic waves in a liquid medium. When the ultrasonic intensity is increased, greater energy enters the liquid medium, producing microbubbles, and this effect is coupled with the creation of vacuum effects inside the liquid. Because sonication is a fast transient process that occurs in microseconds, during this short period, heat and mass transfer processes are very rapid. Although the use of ultrasonic waves does not produce significant net changes in the operating conditions of the distillation process, use of ultrasonic waves does impact the thermodynamics significantly by altering the VLE of the system.

The main advantage of ultrasonic technology is the fact that the azeotrope point can be eliminated by correctly choosing the sonication parameters and other operating conditions. The separation of azeotropic mixtures can be carried out in a single column without the need for a separating agent. The ultrasonic technology is therefore attractive from the perspective of energy requirements and environmental protection. Because ultrasonic technology may also offer a reduction in the equipment size as it reduces the separation requirement by altering the VLE, the technology also offers safety features. Although previous studies [198-200] have illustrated the success on a single stage system, these studies are too sketchy, and the use of a complete ultrasonic-assisted distillation system with the typical industrial separation requirements is yet to be realized. A number of issues must be addressed that include design, safety, operability, control and efficiency.

5. Future Work

Research and development, along with knowledge generation and its adaptation to the chemical process industry, will continue to be driven by individual interests or availability of funding. Due to the importance of the chemical and petrochemical industry to the world economy, studies on even old technologies such as chemical separation continue to be relevant. Considering the separation of azeotropic mixtures, various studies taking different approaches have been reported. However, more studies are needed to improve the economic efficiency and ease of operation while ensuring safety to personnel and the environment.

Because pragmatic practitioners would prefer to stay with conventional processes because they are well-understood and established, azeotropic and extractive distillations would still be the main technologies used for large scale applications in the near future. The search for "perfect" entrainers should therefore be continued by examining existing options or synthesizing new ones aiming at entrainers that are effective in separation, highly selective, energy efficient, and environmentally friendly with minimal safety and health hazards. In this regard, the use of ionic liquids (ILs) and hyperbranched polymers has shown promising potential.

Considering the membrane separation technology routes, because the available surface area and durability play pivotal roles in process operability, research in these areas is likely to continue, as indicated by the increasing number of patents and publications on this subject. The separation community should either develop such processes for small-scale specialty applications or embark on the development of hybrid processes to overcome the surface area limitations.

Process intensification is a fast growing approach in the chemical process industry, offering a wide horizon of options. Because distillation is still considered the preferred process, intensification of the distillation process through a variety of frontier technologies should be explored. For example, by applying sonication to the liquid mixture, the properties of the mixture can be altered, thus opening opportunities for further process development. Some recent studies on ultrasonic distillation have been found to be promising and require additional efforts to formulate workable solutions for industrial applications. Further developments needed in this area include basic thermodynamic studies and the development of process technology involving the formulation of optimal design and operation strategies, the performance of safety and control studies and the development of complete system prototypes.

6. Concluding Remarks

This paper provides a state-of-the-art-review on the conventional and emerging technologies for the separation of azeotropic mixtures. The research areas to be emphasized for

further development are also elucidated. Conventional separation processes such as azeotropic and extractive distillations are observed to be the main technologies used at present and in the near future, with opportunities for improvements by introducing new entrainers with desirable properties. Similarly, while membrane processes offer good efficiency, simplicity of operation and low energy consumption, membrane processes are limited by the surface area requirement and thus may only be suitable for small-scale applications. To extend the applicability, hybrid processes combining membranes with other process technologies might be needed. For the Frictional Diffusion process, although it offers high thermodynamic efficiency and energy reduction and is an inherently irreversible process, it suffers low selectivity and thus requires further improvement. Another potential approach is to exploit the process intensification concept in developing new separation techniques. While some ideas have been implemented (including dividing wall column, microwave and ultrasonic assisted distillation), many issues remain unresolved and therefore require further scrutiny.

In summary, we can conclude that while some workable solutions are readily available, the challenges are numerous, with a wide horizon of opportunities for improvement. The search for better processes should be intensified to expedite countermeasures for environmental and safety threats continually imposed by the process industries on human livelihood. In line with the call for sustainable process development, research in this field should be given sufficient attention by the research community.

7. Reference

1. Kister, H.Z. Distillation design (McGraw-Hill New York). 1992.

2. Ognisty TP. Analyze distillation columns with thermodynamics, Chemical Engineering Progress; (United States). 1995; 91.

3. Widagdo S, Seider, WD. Journal review. Azeotropic distillation, AIChE Journal. 1996: 42; 96-130.

4. Lei Z, Li C. Chen B. Extractive distillation: a review, Separation & Purification Reviews. 2003; 32; 121-213.

5. Lei Z, Chen B. Ding Z. Special distillation processes (Elsevier Science). 2005.

6. Huang H.-J, Ramaswamy S, Tschirner U, Ramarao B. A review of separation technologies in current and future biorefineries, Separation and Purification Technology. 2008l; 62; 1-21.

7. Pereiro, A., Araújo, J., Esperança, J., Marrucho, I. & Rebelo, L. (2012) Ionic liquids in separations of azeotropic systems–A review, The Journal of Chemical Thermodynamics, 46, 2-28.

8. Garcia Villaluenga, J. & Tabe-Mohammadi, A. (2000) A review on the separation of benzene/cyclohexane mixtures by pervaporation processes, Journal of Membrane Science, 169, 159-174.

9. Kujawski, W. (2000) Application of pervaporation and vapor permeation in environmental protection, Polish Journal of Environmental Studies, 9, 13-26.

10. Smitha, B., Suhanya, D., Sridhar, S. & Ramakrishna, M. (2004) Separation of organic–organic mixtures by pervaporation—a review, Journal of Membrane Science, 241, 1-21.

11. Bauer, M. & Stichlmair, J. (1998) Design and economic optimization of azeotropic distillation processes using mixed-integer nonlinear programming, Computers & chemical engineering, 22, 1271-1286.

12. Li, J., Lei, Z., Ding, Z., Li, C. & Chen, B. (2005) Azeotropic distillation: a review of mathematical models, Separation and Purification Reviews, 34, 87-129.

13. Momoh, S. (1991) Assessing the accuracy of selectivity as a basis for solvent screening in extractive distillation processes, Separation science and technology, 26, 729-742.

14. Rodríguez-Donis, I., Gerbaud, V. & Joulia, X. (2001) Entrainer selection rules for the separation of azeotropic and close-boiling-temperature mixtures by homogeneous batch distillation process, Industrial & engineering chemistry research, 40, 2729-2741.

15. Ewell, R., Harrison, J. & Berg, L. (1944) Azeotropic distillation, Industrial & Engineering Chemistry, 36, 871-875.

16. Berg, L. (1969) Azeotropic and extractive distillation: Selecting the agent for distillation, Chem. Eng. Prog, 65, 52-57.

17. Churi, N. & Achenie, L. E. (1996) Novel mathematical programming model for computer aided molecular design, Industrial & engineering chemistry research, 35, 3788-3794.

18. Kumar, S., Singh, N. & Prasad, R. (2010) Anhydrous ethanol: A renewable source of energy, Renewable and Sustainable Energy Reviews, 14, 1830-1844.

19. King, J. M. P., Bañares-Alcántara, R. & Manan, Z. A. (1999) Minimising environmental impact using CBR: an azeotropic distillation case study, Environmental Modelling & Software, 14, 359-366.

20. Mortaheb, H. R. & Kosuge, H. (2004) Simulation and optimization of heterogeneous azeotropic distillation process with a rate-based model, Chemical Engineering and Processing: Process Intensification, 43, 317-326.

21. Meirelles, A., Weiss, S. & Herfurth, H. (1992) Ethanol dehydration by extractive distillation, Journal of Chemical Technology and Biotechnology, 53, 181-188.

22. Gomis, V., Pedraza, R., Francés, O., Font, A. & Asensi, J. C. (2007) Dehydration of ethanol using azeotropic distillation with isooctane, Industrial & engineering chemistry research, 46, 4572-4576.

23. Liu, F.-Z., Mori, H., Hiraoka, S. & Yamada, I. (1993) Phase equilibria and simulation method for heterogeneous azeotropic distillation, Journal of chemical engineering of Japan, 26, 41-47.

24. Chien, I.-L., Wang, C., Wong, D. et al. (2000) Experimental investigation of conventional control strategies for a heterogeneous azeotropic distillation column, Journal of Process Control, 10, 333-340.

25. Silva, L., Mattedi, S., Gonzalez-Olmos, R. & Iglesias, M. (2006) Azeotropic behaviour of (benzene+ cyclohexane+ chlorobenzene) ternary mixture using chlorobenzene as entrainer at 101.3 kPa, The Journal of Chemical Thermodynamics, 38, 1725-1736.

26. Bastidas, P. A., Gil, I. D. & Rodriguez, G. (2010) Comparison of the main ethanol dehydration technologies through process simulation, Paper presented at the Proceedings of 20th European Symposium on Computer Aided Process Engineering—ESCAPE20.

27. Castillo, F. & Towler, G. (1998) Influence of multicomponent mass transfer on homogeneous azeotropic distillation, Chemical engineering science, 53, 963-976.

28. Kurooka, T., Yamashita, Y., Nishitani, H. et al. (2000) Dynamic simulation and nonlinear control system design of a heterogeneous azeotropic distillation column, Computers & Chemical Engineering, 24, 887-892.

29. Modla, G. & Lang, P. (2008) Feasibility of new pressure swing batch distillation methods, Chemical Engineering

Science, 63, 2856-2874.

30. Van Hoof, V., Van den Abeele, L., Buekenhoudt, A., Dotremont, C. & Leysen, R. (2004) Economic comparison between azeotropic distillation and different hybrid systems combining distillation with pervaporation for the dehydration of isopropanol, Separation and purification technology, 37, 33-49.

31. Andersen, H., Laroche, L. & Morari, M. (1995) Effect of design on the operation of homogeneous azeotropic distillation, Computers & chemical engineering, 19, 105-122.

32. Acosta, J., Arce, A., Martínez-Ageitos, J., Rodil, E. & Soto, A. (2002) Vapor-liquid equilibrium of the ternary system ethyl acetate+ hexane+ acetone at 101.32 kPa, Journal of Chemical & Engineering Data, 47, 849-854.

33. Chang, T. & Shih, T. T. (1989) Development of an azeotropic distillation scheme for purification of tetrahydrofuran, Fluid phase equilibria, 52, 161-168.

34. Andrea Ruiz, R., Nelson Borda, B., Alexander, L. R. et al. (2011) Control of an azeotropic distillation process to acetonitrile production, in: E.N. Pistikopoulos, M. C. G. & Kokossis, A. C. (Eds.) Computer Aided Chemical Engineering, pp. 833-838 (Elsevier).

35. Dorn, C., Lee, M. & Morari, M. (1999) Stability and transient behavior of homogeneous azeotropic distillation, Computers & Chemical Engineering, 23, S191-S194.

36. Springer, P., Baur, R. & Krishna, R. (2003) Composition trajectories for heterogeneous azeotropic distillation in a bubble-cap tray column: Influence of mass transfer, Chemical Engineering Research and Design, 81, 413-426.

37. Guedes, B. P., Feitosa, M. F., Vasconcelos, L. S., Araújo, A. B. & Brito, R. P. (2007) Sensitivity and dynamic behavior analysis of an industrial azeotropic distillation column, Separation and purification technology, 56, 270-277.

38. Vasconcelos, C. J. & Wolf-Maciel, M. R. (2004) Heterogeneous azeotropic distillation-operational policies and control, Computer Aided Chemical Engineering, 18, 835-840.

39. Rodriguez-Donis, I., Pardillo-Fontdevila, E., Gerbaud, V. & Joulia, X. (2001) Synthesis, experiments and simulation of heterogeneous batch distillation processes, Computers & Chemical Engineering, 25, 799-806.

40. Lang, P. & Modla, G. (2006) Generalised method for the determination of heterogeneous batch distillation regions, Chemical engineering science, 61, 4262-4270.

41. Skouras, S., Skogestad, S. & Kiva, V. (2005) Analysis and control of heteroazeotropic batch distillation, AIChE journal, 51, 1144-1157.

42. Berg, L. (1999) Separation of ethyl acetate from ethanol by azeotropic distillation (Google Patents).

43. Hilal, N., Yousef, G. & Anabtawi, M. (2002) Operating parameters effect on methanol–acetone separation by extractive distillation, Separation Science and Technology, 37, 3291-3303.

44. Sucksmith, I. (1982) Extractive distillation saves energy, Chem. Eng.(NY);(United States), 89.

45. Gang, L. Z., Qi, Z. R. & You, D. Z. T. W. H. (1999) DEVELOPMENT OF THE PROCESS FOR 2-PROPANOL PRODUCTION BY PRO/II AND COLUMN DESIGN SOFTWARE [J], COMPUTERS AND APPLIED CHEMISTRY, 4, 005.

46. Kossack, S., Kraemer, K., Gani, R. & Marquardt, W. (2008) A systematic synthesis framework for extractive distillation processes, Chemical Engineering Research and Design, 86, 781-792.

47. Vega, A., Díez, F., Esteban, R. & Coca, J. (1997) Solvent selection for cyclohexane-cyclohexene-benzene separation by extractive distillation using non-steady-state gas chromatography, Industrial & engineering chemistry research, 36, 803-807.

48. Xu, S. & Wang, H. (2006) Separation of Tetrahydrofuran–Water Azeotropic Mixture by Batch Extractive Distillation Process, Chemical Engineering Research and Design, 84, 478-482.

49. Stéger, C., Rév, E., Horváth, L. et al. (2006) New extractive configuration separating azeotropic mixture in semi-batch way, Separation and purification technology, 52, 343-356.

50. Shealy, G. S., Hagewiesche, D. & Sandler, S. I. (1987) Vapor-liquid equilibrium of ethanol/water/N, N-dimethylformamide, Journal of Chemical and Engineering Data, 32, 366-369.

51. Pereiro, A. B. & Rodríguez, A. (2009) Effective extraction in packed column of ethanol from the azeotropic mixture ethanol+ hexane with an ionic liquid as solvent, Chemical Engineering Journal, 153, 80-85.

52. Resa, J., González, C. & Ruiz, A. (2000) Experiments of extractive distillation at laboratory scale for the rupture of the azeotropic mixture acetone+ isopropyl ether, Separation and purification technology, 18, 103-110.

53. Resa, J. M., González, C., Betolaza, M. A. & Ruiz, A. (1999) Behaviour of butyl ether as entrainer for the extractive distillation of the azeotropic mixture propanone+ diisopropyl ether. Isobaric VLE data of the azeotropic components with the entrainer, Fluid phase equilibria, 156, 89-99.

54. Ravagnani, M., Reis, M. & Wolf-Maciel, M. (2010) Anhydrous ethanol production by extractive distillation: A solvent case study, Process Safety and Environmental Protection, 88, 67-73.

55. Nieuwoudt, I. & Van Dyk, B. (2002) Separation of ethanol mixtures by extractive distillation (Google Patents).

56. Berg, L. & Yeh, A.-I. (1986) Separation of methyl acetate from methanol by extractive distillation (Google Patents).

57. Liao, B., Lei, Z., Xu, Z., Zhou, R. & Duan, Z. (2001) New process for separating propylene and propane by extractive distillation with aqueous acetonitrile, Chemical Engineering Journal, 84, 581-586.

58. Yang, X., Yin, X. & Ouyang, P. (2009) Simulation of 1, 3-butadiene production process by dimethylfomamide extractive distillation, Chinese Journal of Chemical Engineering, 17, 27-35.

59. Lei, Z., Li, C., Li, Y. & Chen, B. (2004) Separation of acetic acid and water by complex extractive distillation, Separation and purification technology, 36, 131-138.

60. Lladosa, E., Montón, J. B. & Burguet, M. (2011) Separation of di-n-propyl ether and n-propyl alcohol by extractive distillation and pressure-swing distillation: Computer simulation and economic optimization, Chemical Engineering and Processing: Process Intensification, 50, 1266-1274.

61. Van Kaam, R., Rodriguez-Donis, I. & Gerbaud, V. (2008) Heterogeneous extractive batch distillation of chloroform–methanol–water: Feasibility and experiments, Chemical engineering science, 63, 78-94.

62. Lek-utaiwan, P., Suphanit, B., Douglas, P. L. & Mongkolsiri, N. (2011) Design of extractive distillation for the separation of close-boiling mixtures: Solvent selection and column optimization, Computers & Chemical Engineering, 35, 1088-1100.

63. Munoz, R., Monton, J., Burguet, M. &de la Torre, J. (2006) Separation of isobutyl alcohol and isobutyl acetate by extractive distillation and pressure-swing distillation: Simulation and optimization, Separation and purification technology, 50, 175-183.

64. Lelkes, Z., Rev, E., Steger, C. et al. (2003) Batch extractive distillation with intermediate boiling entrainer, Computer Aided Chemical Engineering, 14, 197-202.

65. Barba, D., Brandani, V. &di Giacomo, G. (1985) Hyperazeotropic ethanol salted-out by extractive distillation. Theoretical evaluation and experimental check, Chemical Engineering Science, 40, 2287-2292.

66. Gil, I., Uyazan, A., Aguilar, J., Rodríguez, G. & Caicedo, L. (2008) Separation of ethanol and water by extractive

distillation with salt and solvent as entrainer: process simulation, Brazilian Journal of Chemical Engineering, 25, 207-215.

67. Lei, Z., Zhou, R. & Duan, Z. (2002) Application of scaled particle theory in extractive distillation with salt, Fluid phase equilibria, 200, 187-201.

68. Owens, G. S. & Abu-Omar, M. M. (2002) Comparative kinetic investigations in ionic liquids using the MTO/peroxide system, Journal of Molecular Catalysis A: Chemical, 187, 215-225.

69. Murugesan, S. & Linhardt, R. J. (2005) Ionic liquids in carbohydrate chemistry-current trends and future directions, Current Organic Synthesis, 2, 437-451.

70. Earle, M. J., Esperança, J. M., Gilea, M. A. et al. (2006) The distillation and volatility of ionic liquids, Nature, 439, 831-834.

71. Huddleston, J. G., Visser, A. E., Reichert, W. M. et al. (2001) Characterization and comparison of hydrophilic and hydrophobic room temperature ionic liquids incorporating the imidazolium cation, Green Chemistry, 3, 156-164.

72. Earle, M. J. & Seddon, K. R. (2000) Ionic liquids. Green solvents for the future, Pure and Applied Chemistry, 72, 1391-1398.

73. Dhanalakshmi, J., Sai, P. S. T. & Balakrishnan, A. R. (2013) Study of Ionic Liquids as Entrainers for the Separation of Methyl Acetate–Methanol and Ethyl Acetate–Ethanol Systems Using the COSMO-RS Model, Industrial & Engineering Chemistry Research, 52, 16396-16405.

74. Werner, S., Haumann, M. & Wasserscheid, P. (2010) Ionic liquids in chemical engineering, Annual review of chemical and biomolecular engineering, 1, 203-230.

75. Meindersma, G. W. &de Haan, A. (2008) Conceptual process design for aromatic/aliphatic separation with ionic liquids, Chemical Engineering Research and Design, 86, 745-752.

76. Zhao, J., Dong, C.-C., Li, C.-X., Meng, H. & Wang, Z.-H. (2006) Isobaric vapor–liquid equilibria for ethanol–water system containing different ionic liquids at atmospheric pressure, Fluid Phase Equilibria, 242, 147-153.

77. Seiler, M., Jork, C., Kavarnou, A., Arlt, W. & Hirsch, R. (2004) Separation of azeotropic mixtures using hyperbranched polymers or ionic liquids, AIChE journal, 50, 2439-2454.

78. Seiler, M. (2002) Dendritic polymers–interdisciplinary research and emerging applications from unique structural properties, Chemical engineering & technology, 25, 237-253.

79. Inoue, K. (2000) Functional dendrimers, hyperbranched and star polymers, Progress in Polymer Science, 25, 453-571.

80. Voit, B., Eigner, M., Estel, K., Wenzel, C. & Bartha, J. (2002) Labile hyperbranched polymers used as nanopore-forming agents in polymeric dielectrica, Paper presented at the Macromolecular Symposia.

81. Gao, C. & Yan, D. (2004) Hyperbranched polymers: from synthesis to applications, Progress in Polymer Science, 29, 183-275.

82. Seiler, M., Köhler, D. & Arlt, W. (2003) Hyperbranched polymers: new selective solvents for extractive distillation and solvent extraction, Separation and Purification Technology, 30, 179-197.

83. Sunder, A., Heinemann, J. & Frey, H. (2000) Controlling the growth of polymer trees: concepts and perspectives for hyperbranched polymers, Chemistry-A European Journal, 6, 2499-2506.

84. LEWIS, W. X. (1928) WARREN X (Google Patents).

85. Abu-Eishah, S. I. & Luyben, W. L. (1985) Design and control of a two-column azeotropic distillation system,

Industrial & Engineering Chemistry Process Design and Development, 24, 132-140.

86. Phimister, J. R. & Seider, W. D. (2000) Semicontinuous, pressure-swing distillation, Industrial & engineering chemistry research, 39, 122-130.

87. Lee, J., Cho, J., Kim, D. M. & Park, S. (2011) Separation of tetrahydrofuran and water using pressure swing distillation: Modeling and optimization, Korean Journal of Chemical Engineering, 28, 591-596.

88. Repke, J.-U., Klein, A., Forner, F. & Wozny, G. (2004) Pressure swing distillation for separation of homogeneous azeotropic mixtures in a mass-and heat-integrated column system: operation performance, Paper presented at the Intelligent Control and Automation, 2004. WCICA 2004. Fifth World Congress on.

89. Repke, J.-U., Klein, A., Bogle, D. & Wozny, G. (2007) Pressure swing batch distillation for homogeneous azeotropic separation, Chemical Engineering Research and Design, 85, 492-501.

90. Knapp, J. P. & Doherty, M. F. (1992) A new pressure-swing-distillation process for separating homogeneous azeotropic mixtures, Industrial & engineering chemistry research, 31, 346-357.

91. Modla, G. & Lang, P. (2010) Separation of an Acetone− Methanol Mixture by Pressure-Swing Batch Distillation in a Double-Column System with and without Thermal Integration, Industrial & Engineering Chemistry Research, 49, 3785-3793.

92. Colley, S. W., Fawcett, C. R., Sharif, M. et al. (2009) Process (Google Patents).

93. Modla, G. (2011) Reactive pressure swing batch distillation by a new double column system, Computers & Chemical Engineering, 35, 2401-2410.

94. Modla, G. (2010) Pressure swing batch distillation by double column systems in closed mode, Computers & Chemical Engineering, 34, 1640-1654.

95. Mulia-Soto, J. F. & Flores-Tlacuahuac, A. (2011) Modeling, simulation and control of an internally heat integrated pressure-swing distillation process for bioethanol separation, Computers & Chemical Engineering, 35, 1532-1546.

96. Mujtaba, I. (2004) Batch Distillation. Design and operation, Series on Chemical Engineering, vol (3Imperial College Press, London).

97. Phimister, J. R. & Seider, W. D. (2001) Bridge the gap with semicontinuous distillation, Chemical engineering progress, 97, 72-78.

98. Cheong, W. & Barton, P. I. (1999) Azeotropic distillation in a middle vessel batch column. 1. Model formulation and linear separation boundaries, Industrial & engineering chemistry research, 38, 1504-1530.

99. Wittgens, B. & Skogestad, S. (2000) Closed operation of multivessel batch distillation: Experimental verification, AIChE Journal, 46, 1209-1217.

100. Jafarey, A., Douglas, J. & McAvoy, T. (1979) Short-cut techniques for distillation column design and control. 1. Column design, Industrial & Engineering Chemistry Process Design and Development, 18, 197-202.

101. Baker, R. (2012) Membrane technology and applications (Wiley).

102. Wankat, P. C. (1994) Rate-controlled separations (Springer).

103. Wynn, N. (2001) Pervaporation comes of age, Chem. Eng. Prog, 97, 66-72.

104. Nunes, S. P. & Peinemann, K.-V. (2006) Membrane technology: in the chemical industry (Wiley-VCH).

105. Reddy, D. & Reineke, C. (1988) Dehydration with perfluorosulfonic acid ionomer membranes, Paper presented at

the AIChE Symp. Ser.

106. Bengtsson, E., Trägårdh, G. & Hallström, B. (1993) Concentration polarization during the enrichment of aroma compounds from a water solution by pervaporation, Journal of food engineering, 19, 399-407.

107. Enneking, L., Stephan, W. & Heintz, A. (1993) Sorption and diffusivity measurements of cyclohexane+ benzene and cyclohexene+ toluene mixtures in polyurethane membranes. Model calculations of the pervaporation process, Berichte der Bunsengesellschaft für physikalische Chemie, 97, 912-922.

108. Neel, J. (1991) Introduction to pervaporation, Pervaporation membrane separation processes, Elsevier, Amsterdam, 1-109.

109. Mulder, M. (1996) Basic Principles of Membrane Technology Second Edition (Kluwer Academic Pub).

110. Wang, Y.-C., Teng, M.-Y., Lee, K.-R. & Lai, J.-Y. (2005) Comparison between the pervaporation and vapor permeation performances of polycarbonate membranes, European polymer journal, 41, 1667-1673.

111. Rautenbach, R. & Albrecht, R. (1989) Membrane separation processes.

112. Uragami, T., Saito, M. & Takigawa, K. (1988) Studies on syntheses and permeabilities of special polymer membranes, 69. Comparison of permeation and separation characteristics for aqueous alcoholic solutions by pervaporation and new evapomeation methods through chitosan membranes, Die Makromolekulare Chemie, Rapid Communications, 9, 361-365.

113. Aptel, P., Cuny, J., Jozefowicz, J., Morel, G. & Neel, J. (1972) Liquid transport through membranes prepared by grafting of polar monomers onto poly (tetrafluoroethylene) films. I. Some fractionations of liquid mixtures by pervaporation, Journal of Applied Polymer Science, 16, 1061-1076.

114. Binning, R., Lee, R., Jennings, J. & Martin, E. (1961) Separation of liquid mixtures by permeation, Industrial & Engineering Chemistry, 53, 45-50.

115. Vane, L. (2004) Options for Combining Pervaporation Membrane Systems with Fermentors for Efficient Production of Alcohols from Biomass, Paper presented at the 2004 AIChE Annual Meeting.

116. Drioli, E., Zhang, S. & Basile, A. (1993) On the coupling effect in pervaporation, Journal of membrane science, 81, 43-55.

117. Inui, K., Okumura, H., Miyata, T. & Uragami, T.-i. (1997) Permeation and separation of benzenecyclohexane mixtures through cross-linked poly (alkyl methacrylate) membranes, Journal of membrane science, 132, 193-202.

118. Dutta, B. K. & Sikdar, S. K. (1991) Separation of azeotropic organic liquid mixtures by pervaporation, AIChE journal, 37, 581-588.

119. Richardson, J. F., Harker, J. H. & Backhurst, J. R. (2002) Coulson and Richardson's chemical engineering: Particle technology and separation processes.

120. Sander, U. & Soukup, P. (1988) Design and operation of a pervaporation plant for ethanol dehydration, Journal of membrane science, 36, 463-475.

121. KUJAWSKI, W. (2000) Pervaporative removal of organics from water using hydrophobic membranes. Binary mixtures, Separation Science and Technology, 35, 89-108.

122. Kondo, M., Komori, M., Kita, H. & Okamoto, K.-i. (1997) Tubular-type pervaporation module with zeolite NaA membrane, Journal of Membrane Science, 133, 133-141.

123. Zhou, M., Persin, M. & Sarrazin, J. (1996) Methanol removal from organic mixtures by pervaporation using polypyrrole membranes, Journal of membrane science, 117, 303-309.

124. Sunitha, K., Satyanarayana, S. & Sridhar, S. (2012) Phosphorylated chitosan membranes for the separation of ethanol–water mixtures by pervaporation, Carbohydrate Polymers, 87, 1569-1574.

125. Smitha, B., Dhanuja, G. & Sridhar, S. (2006) Dehydration of 1, 4-dioxane by pervaporation using modified blend membranes of chitosan and nylon 66, Carbohydrate polymers, 66, 463-472.

126. Huang, R., Moreira, A., Notarfonzo, R. & Xu, Y. (1988) Pervaporation separation of acetic acid-water mixtures using modified membranes. I. Blended polyacrylic acid (PAA)-nylon 6 membranes, Journal of applied polymer science, 35, 1191-1200.

127. Anjali Devi, D., Smitha, B., Sridhar, S. & Aminabhavi, T. (2005) Pervaporation separation of isopropanol/water mixtures through crosslinked chitosan membranes, Journal of membrane science, 262, 91-99.

128. Groot, W., van der Lans, R. & Luyben, K. C. A. (1988) Pervaporation of fermentation products: mass transfer of solutes in silicone membranes and the performance of pervaporation in a fermentation, Paper presented at the Proceedings of the Third International Conference on Pervaporation Process in the Chemical Industry, Bakish Materials Corporation, Englewood, NJ.

129. Kujawski, W., Nguyen, Q., Neel, J. & Bakish, R. (1988) Pervaporation of water–alcohols mixtures through Nafion 117 and poly (ethylene-co-styrene sulfonate) interpolymer membranes, Paper presented at the Proc. III Int. Conf. on PV Proc. in the Chem. Ind.(Nancy, France 1988), R. Bakish, Ed., Bakish Materials Co., Englewood.

130. Mandal, S. & Pangarkar, V. G. (2002) Separation of methanol–benzene and methanol–toluene mixtures by pervaporation: effects of thermodynamics and structural phenomenon, Journal of membrane science, 201, 175-190.

131. Billard, P., Nguyen, Q., Leger, C. & Clement, R. (1998) Diffusion of organic compounds through chemically asymmetric membranes made of semi-interpenetrating polymer networks, Separation and purification technology, 14, 221-232.

132. Zereshki, S., Figoli, A., Madaeni, S. et al. (2011) Pervaporation separation of MeOH/MTBE mixtures with modified PEEK membrane: Effect of operating conditions, Journal of Membrane Science, 371, 1-9.

133. Schwarz, H.-H., Apostel, R. & Paul, D. (2001) Membranes based on polyelectrolyte–surfactant complexes for methanol separation, Journal of Membrane Science, 194, 91-102.

134. Ulbricht, M. & Schwarz, H.-H. (1997) Novel high performance photo-graft composite membranes for separation of organic liquids by pervaporation, Journal of membrane science, 136, 25-33.

135. Yong Nam, S. & Moo Lee, Y. (1999) Pervaporation separation of methanol/methyl< i> t</i>-butyl ether through chitosan composite membrane modified with surfactants, Journal of membrane science, 157, 63-71.

136. Ortiz, I., Alonso, P. & Urtiaga, A. (2002) Pervaporation of azeotropic mixtures ETBE/EtOH: influence of membrane conditioning and operation variables on pervaporation flux, Desalination, 144, 67-72.

137. Huang, R. Y. & Lin, V. J. (1968) Separation of liquid mixtures by using polymer membranes. I. Permeation of binary organic liquid mixtures through polyethylene, Journal of Applied Polymer Science, 12, 2615-2631.

138. Park, J. S. & Ruckenstein, E. (1989) Selective permeation through hydrophobic–hydrophilic membranes, Journal of applied polymer science, 38, 453-461.

139. Rautenbach, R. & Albrecht, R. (1980) Separation of organic binary mixtures by pervaporation, Journal of Membrane Science, 7, 203-223.

140. Ho, W. W., Sartori, G., Thaler, W. A. & Dalrymple, D. C. (1990) Polyimide/aliphatic polyester copolymers (Google Patents).

141. Cao, B. & Henson, M. A. (2002) Modeling of spiral wound pervaporation modules with application to the separation

of styrene/ethylbenzene mixtures, Journal of membrane science, 197, 117-146.

142. Sato, K., Sugimoto, K. & Nakane, T. (2008) Separation of ethanol/ethyl acetate mixture by pervaporation at 100–130° C through NaY zeolite membrane for industrial purpose, Microporous and Mesoporous Materials, 115, 170-175.

143. Hasanoğlu, A., Salt, Y., Keleşer, S., Özkan, S. & Dincer, S. (2005) Pervaporation separation of ethyl acetate–ethanol binary mixtures using polydimethylsiloxane membranes, Chemical Engineering and Processing: Process Intensification, 44, 375-381.

144. Wang, S.-J. & Wong, D. S. (2007) Controllability and energy efficiency of a high-purity divided wall column, Chemical Engineering Science, 62, 1010-1025.

145. Gorri, D., Ibáñez, R. & Ortiz, I. (2006) Comparative study of the separation of methanol–methyl acetate mixtures by pervaporation and vapor permeation using a commercial membrane, Journal of membrane science, 280, 582-593.

146. Kalyani, S., Smitha, B., Sridhar, S. & Krishnaiah, A. (2008) Pervaporation separation of ethanol–water mixtures through sodium alginate membranes, Desalination, 229, 68-81.

147. Farshad, F., Iravaninia, M., Kasiri, N., Mohammadi, T. & Ivakpour, J. (2011) Separation of toluene/< i> n</i>-heptane mixtures experimental, modeling and optimization, Chemical Engineering Journal, 173, 11-18.

148. Wang, L., Han, X., Li, J., Zhan, X. & Chen, J. (2011) Hydrophobic nano-silica/polydimethylsiloxane membrane for dimethylcarbonate–methanol separation via pervaporation, Chemical Engineering Journal, 171, 1035-1044.

149. Xu, W., Paul, D. R. & Koros, W. J. (2003) Carboxylic acid containing polyimides for pervaporation separations of toluene/< i> iso</i>-octane mixtures, Journal of Membrane science, 219, 89-102.

150. Zereshki, S., Figoli, A., Madaeni, S. et al. (2010) Poly (lactic acid)/poly (vinyl pyrrolidone) blend membranes: Effect of membrane composition on pervaporation separation of ethanol/cyclohexane mixture, Journal of Membrane Science, 362, 105-112.

151. Chen, J. H., Liu, Q. L., Zhu, A. M., Zhang, Q. G. & Fang, J. (2008) Pervaporation separation of MeOH/DMC mixtures using STA/CS hybrid membranes, Journal of Membrane Science, 315, 74-81.

152. Singha, N., Kuila, S., Das, P. & Ray, S. (2009) Separation of toluene–methanol mixtures by pervaporation using crosslink IPN membranes, Chemical Engineering and Processing: Process Intensification, 48, 1560-1565.

153. Marx, S., Gryp, P. v. d., Neomagus, H., Everson, R. & Keizer, K. (2002) Pervaporation separation of methanol from methanol/< i> tert</i>-amyl methyl ether mixtures with a commercial membrane, Journal of membrane science, 209, 353-362.

154. Xia, S., Dong, X., Zhu, Y. et al. (2011) Dehydration of ethyl acetate–water mixtures using PVA/ceramic composite pervaporation membrane, Separation and Purification Technology, 77, 53-59.

155. Zereshki, S., Figoli, A., Madaeni, S., Simone, S. & Drioli, E. (2010) Pervaporation separation of methanol/methyl tert-butyl ether with poly (lactic acid) membranes, Journal of Applied Polymer Science, 118, 1364-1371.

156. Henley, E. J., Seader, J. D. & Roper, D. K. (2011) Separation process principles (Wiley).

157. Selvi, A., Breure, B., Gross, J., De Graauw, J. & Jansens, P. (2007) Basic parameter study for the separation of a isopropanol–water mixture by using FricDiff technology, Chemical Engineering and Processing: Process Intensification, 46, 810-817.

158. Breure, B., Peters, E. & Kerkhof, P. (2008) Separation of azeotropic mixtures of alcohols and water with FricDiff, Separation and Purification Technology, 62, 349-362.

159. Selvi, A., Schoon, L., Jansens, P. & Bardow, A. (2010) Purity versus recovery in FricDiff separations for feed-side and sweep-side products, Separation and Purification Technology, 76, 95-103.

160. Peters, E., Breure, B., Van den Heuvel, P. & Kerkhof, P. (2008) Transfer units approach to the FricDiff separation process, Industrial & Engineering Chemistry Research, 47, 3937-3942.

161. Breure, B., Schoon, L., Peters, E. A. & Kerkhof, P. J. (2009) Separation of gas mixtures with FricDiff: a comparison between experimental data and simulations, Industrial & Engineering Chemistry Research, 48, 7694-7704.

162. Gonzalez, B. & Ortiz, I. (2002) Modelling and simulation of a hybrid process (pervaporation–distillation) for the separation of azeotropic mixtures of alcohol–ether, Journal of Chemical Technology and Biotechnology, 77, 29-42.

163. Hemwimol, S., Pavasant, P. & Shotipruk, A. (2006) Ultrasound-assisted extraction of anthraquinones from roots of Morinda citrifolia, Ultrasonics Sonochemistry, 13, 543-548.

164. Stephan, W., Noble, R. D. & Koval, C. A. (1995) Design methodology for a membrane/distillation column hybrid process, Journal of membrane science, 99, 259-272.

165. Daviou, M. C., Hoch, P. M. & Eliceche, A. M. (2004) Design of membrane modules used in hybrid distillation/ pervaporation systems, Industrial & engineering chemistry research, 43, 3403-3412.

166. Naidu, Y. & Malik, R. K. (2011) A generalized methodology for optimal configurations of hybrid distillation–pervaporation processes, Chemical Engineering Research and Design, 89, 1348-1361.

167. Kookos, I. K. (2003) Optimal design of membrane/distillation column hybrid processes, Industrial & engineering chemistry research, 42, 1731-1738.

168. Stankiewicz, A. & Moulin, J. (2000) Process Intensification, Chem. Eng. Progress, 22-34.

169. Lutze, P., Román-Martinez, A., Woodley, J. M. & Gani, R. (2012) A systematic synthesis and design methodology to achieve process intensification in (bio) chemical processes, Computers & Chemical Engineering, 36, 189-207.

170. Kolbe, B. & Wenzel, S. (2004) Novel distillation concepts using one-shell columns, Chemical Engineering and Processing: Process Intensification, 43, 339-346.

171. Rangaiah, G., Ooi, E. & Premkumar, R. (2009) A simplified procedure for quick design of dividing-wall columns for industrial applications, Chemical Product and Process Modeling, 4.

172. Segovia-Hernández, J. G., Hernández-Vargas, E. A. & Márquez-Muñoz, J. A. (2007) Control properties of thermally coupled distillation sequences for different operating conditions, Computers & chemical engineering, 31, 867-874.

173. Kiss, A. A. & Rewagad, R. R. (2011) Energy efficient control of a BTX dividing-wall column, Computers & Chemical Engineering, 35, 2896-2904.

174. Rewagad, R. R. & Kiss, A. A. (2012) Dynamic optimization of a dividing-wall column using model predictive control, Chemical Engineering Science, 68, 132-142.

175. Yildirim, Ö., Kiss, A. A. & Kenig, E. Y. (2011) Dividing wall columns in chemical process industry: A review on current activities, Separation and Purification Technology, 80, 403-417.

176. Asprion, N. & Kaibel, G. (2010) Dividing wall columns: Fundamentals and recent advances, Chemical Engineering and Processing: Process Intensification, 49, 139-146.

177. Isopescu, R., Woinaroschy, A. & Draghiciu, L. (2008) Energy reduction in a divided wall distillation column, Revista de Chimie, 59, 812-815.

178. Sun, L.-Y., Chang, X.-W., Qi, C.-X. & Li, Q.-S. (2011) Implementation of ethanol dehydration using dividing-wall heterogeneous azeotropic distillation column, Separation Science and Technology, 46, 1365-1375.

179. Midori, S., Zheng, S. & Yamada, I. (2001) Azeotropic distillation process with vertical divided-wall column,

Kagaku Kogaku Ronbunshu, 27, 756-823.

180. Bravo-Bravo, C., Segovia-Hernández, J. G., Gutiérrez-Antonio, C. et al. (2010) Extractive dividing wall column: Design and optimization, Industrial & Engineering Chemistry Research, 49, 3672-3688.

181. Kiss, A. A., Pragt, J. & Van Strien, C. (2009) Reactive dividing-wall columns—How to get more with less resources?, Chemical Engineering Communications, 196, 1366-1374.

182. Briones-Ramírez, A. & Gutiérrez-Antonio, C. (2009) Dividing wall distillation columns for separation of azeotropic mixtures: Feasibility procedure and rigorous optimization, Computer Aided Chemical Engineering, 26, 555-560.

183. Kiss, A. A. & Suszwalak, D. J. (2012) Enhanced bioethanol dehydration by extractive and azeotropic distillation in dividing-wall columns, Separation and Purification Technology, 86, 70-78.

184. Komorowska, M., Stefanidis, G. D., Van Gerven, T. & Stankiewicz, A. I. (2009) Influence of microwave irradiation on a polyesterification reaction, Chemical Engineering Journal, 155, 859-866.

185. Sridhar, V., Jeon, J.-H. & Oh, I.-K. (2011) Microwave extraction of graphene from carbon fibers, Carbon, 49, 222-226.

186. Meier, M., Turner, M., Vallee, S. et al. (2009) Microwave regeneration of zeolites in a 1 meter column, AIChE journal, 55, 1906-1913.

187. Therdthai, N. & Zhou, W. (2009) Characterization of microwave vacuum drying and hot air drying of mint leaves (< i> Mentha cordifolia</i> Opiz ex Fresen), Journal of Food Engineering, 91, 482-489.

188. Navarrete, A., Mato, R. & Cocero, M. (2012) A predictive approach in modeling and simulation of heat and mass transfer during microwave heating. Application to SFME of essential oil of Lavandin Super, Chemical Engineering Science, 68, 192-201.

189. Altman, E., Stefanidis, G. D., Van Gerven, T. & Stankiewicz, A. I. (2010) Process intensification of reactive distillation for the synthesis of n-propyl propionate: the effects of microwave radiation on molecular separation and esterification reaction, Industrial & Engineering Chemistry Research, 49, 10287-10296.

190. Gao, X., Li, X., Zhang, J., Sun, J. & Li, H. (2013) Influence of a microwave irradiation field on vapor–liquid equilibrium, Chemical Engineering Science, 90, 213-220.

191. Nikitenko, S. I., Venault, L., Pflieger, R. et al. (2010) Potential applications of sonochemistry in spent nuclear fuel reprocessing: A short review, Ultrasonics Sonochemistry, 17, 1033-1040.

192. Zou, Z., Lin, K., Chen, L. & Chang, J. (2012) Ultrafast synthesis and characterization of carbonated hydroxyapatite nanopowders via sonochemistry-assisted microwave process, Ultrasonics Sonochemistry, 19, 1174-1179.

193. Mazvimba, M. T., Yu, Y., Cui, Z.-Q. & Zhang, Y. (2012) Optimization and orthogonal design of an ultrasonic-assisted aqueous extraction process for extracting chlorogenic acid from dry tobacco leaves, Chinese Journal of Natural Medicines, 10, 311-320.

194. Merouani, S., Hamdaoui, O., Saoudi, F. & Chiha, M. (2010) Influence of experimental parameters on sonochemistry dosimetries: KI oxidation, Fricke reaction and H2O2 production, Journal of Hazardous Materials, 178, 1007-1014.

195. Hua, I. & Pfalzer-Thompson, U. (2001) Ultrasonic Irradiation of Carbofuran:: Decomposition Kinetics and Reactor Characterization, Water research, 35, 1445-1452.

196. Bono, A., Sarbatly, R., Krishnaiah, D., San, P. M. & Yan, F. Y. (2008) Effect of ultrasound on liquid phase adsorption of azeotropic and non-azeotropic mixture, Catalysis Today, 131, 472-476.

197. Jung, H. Y., Park, H. J., Calo, J. M. & Diebold, G. J. (2010) Comparison of ultrasonic distillation to sparging of

liquid mixtures, Analytical chemistry, 82, 10090-10094.

198. Ripin, A., Abdul Mudalip, S. K. & Mohd Yunus, R. (2008) Effects of ultrasonic waves on enhancement of relative volatilities in methanol–water mixtures, Jurnal Teknologi, 48, 61–73.

199. Abdul Mudalip, S. K., Ripin, A., Mohd Yunus, R., Sulaiman, S. Z. & Che Man, R. (2011) Effects of Ultrasonic Waves on Vapor-Liquid Equilibrium of Cyclohexane/Benzene, International Journal on Advanced Science, Engineering and Information Technology, 1, 72-76.

200. Ripin, A., Abdul Mudalip, S. K., Sukaimi, Z., Yunus, R. M. & Manan, Z. A. (2009) Effects of Ultrasonic Waves on Vapor-Liquid Equilibrium of an Azeotropic Mixture, Separation Science and Technology, 44, 2707-2719.

Advances in Chemical Engineering

Chapter 6

Application of High Hydrostatic Pressure for Pectin Extraction from Agro-Food Waste and By-Products

Antonela Ninčević Grassino[1*]; Damir Ježek[2]; Sven Karlović[2]; Tomislav Bosiljkov[2]

[1]Department of Chemistry and Biochemistry, Faculty of Food Technology and Biotechnology, University of Zagreb.

[2]Department of Process Engineering, Faculty of Food Technology and Biotechnology, University of Zagreb.

****Correspondence to: Antonela Ninčević Grassino**, Faculty of Food Technology and Biotechnology, University of Zagreb, Pierottijeva 6, 10000 Zagreb, Croatia*

Phone: +385-1-4605-062; Fax: +385-1-4836-083; E-mail: aninc@pbf.hr

Abstract

Food wastes and by-products produced in huge amount from a variety of sources, ranging from agricultural to food processing residues, could be valorized through the extraction and implementation of high-value components as nutritional and pharmacological functional ingredients.

There are many well-recognized extraction techniques, such as pressurized fluid, supercritical fluid, pulsed electric field, and ultrasound-, microwave-, and enzyme-assisted, developed for conversion of agro-food wastes into various edible, food products. These technologies have gained the worldwide acknowledgment for their potential and versatile applications, which depend on type of raw materials and target bio-molecules, the scale of processing (laboratory or industrial), the ratio between production costs and economic values of the compounds to be extracted.

Due to the growing consumers demand for fresh, safe and minimally processed foods has brought the great idea of food scientists

and technologists to develop many non-thermal food processing technologies which cause minimum nutritional and sensory qualities of the processed foods. Today, non-thermal technologies like high pulse electric field, high hydrostatic pressure, irradiation, ultraviolet light, ultrasound, arc discharge, oscillating magnetic fields, light pulses, plasma, chemicals (ozone, carbon dioxide, argon), and combined methods of these technologies are the major areas of researches in the process and food engineering, in order to find their suitability for processing of various food products.

In this attempt, the high hydrostatic pressure, as non-thermally processing method has been also introduced for pectin extractions from a few food waste resources. Therefore, in the present work, an attempt has been made to give an insight about the high pressure processing for valorization of agro-food wastes, its principle and process design in order to explore this novel technology in futures application for extraction of various other food waste rich in diverse bioactive and functional agents, and to develop healthier, novel food products for consumers.

Graphical Abstract

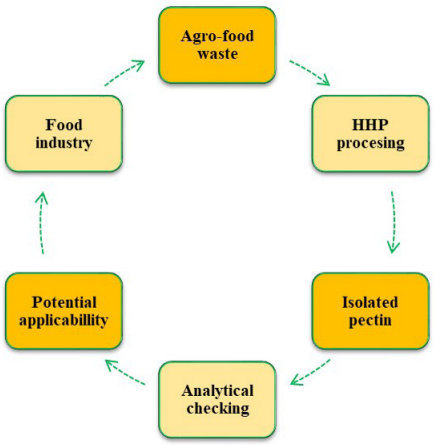

1. Introduction

The fruit and vegetables industrial processing generate a large amount of waste and by-products, such as peels, seeds and leaves. Due to the fact that these bio-organic materials usually presented an environmental problem for the industry, its potential re-utilization for recoveries of different compounds would provide economic advantages for producers. Apart from decreasing the environmental impact, the consumer would take the opportunity that some valuable compounds could be reintroduced into food. Therefore, the main focus of investigations has been placed in the re-utilization of agro-food waste for isolation of certain valuable components, such as pectin. Among various agro-food waste, the red beet [1], cocoa

husks [2], papaya peel [3], sunflower head [4], mango [5,6], banana [7], tomato [8,9] and pomelo [10] peels, hazelnut skins [11], carrots and green beans waste [12], and different other food waste streams [13] have been employed as a non-commercial resources for pectin production.

The current industrial, commercial production of pectin is based on the utilization of citrus peel and apple pomace, a residues gained from juice manufacturing. In that context, the pectin is exclusively extracted in a conventional, chemical way using nitric, hydrochloric and sulfuric acids [14]. Conventional procedure is also used for pectin isolation from a number of other food waste and by-products with mineral or organic acids [14]. In spite of the fact that conventional acid extractions of pectin is simple and efficient, this technique showed some disadvantages, such as long extraction time, degradation of target compounds, and production of contaminants that must be treated.

To overcome these limitations, new and promising extraction methods, such as ultrasound, microwave and enzyme-assisted extractions were recently reported for pectin isolation from plant food waste and by-products [14]. Besides them, another one of novel extraction technique, the high hydrostatic pressure, frequently used for preservation and processing of various foodstuffs, was recently introduced for pectin isolation from orange [15], lime [16] and potato [17] peels, and sugar beet [18].

High pressure processing (HPP), also known as ultra-high pressure (UHP) or high hydrostatic pressure (HHP) as a novel, non-thermal technology, an alternative to traditional thermal treatment, has been developed to assure the production of high quality foods. In comparison to thermal sterilization, which altered the unique sensorial and functional characteristic of foods, the HHP preserves the original properties of processed food, and day-by-day, this technology has a broad range of applications. It is widely used for processing of fruits and vegetables derived products, egg, meat and dairy products, seafood, and alcoholic beverages [19]. Meat and vegetables take the lead with a percentage of 28 and 20 %, respectively, followed by juice and beverages (18 %), and seafood and fish products (14 %). Sauces and dressings (3 %), dairy (1 %), and other food products (16 %) completed the current HHP market, with a near 20 %.

Generally, the HHP processing involves the employment of pressure in the range of 100 to 1200 MPa, with or without application of heat, causing the various physical, chemical and biological changes, due to combined effects of temperature and pressure on processed foods. The applied temperature throughout pressure could range from below 0 °C to above 100 °C, with times extending from a couple of seconds to over 20 min.

This process forces a fluid through a narrow gap valve, resulting in cavitation, turbulence and high shear stress [19]. As a consequence, the microstructure of the matrix is disrupted,

generating particles with a more uniform and smaller size, leading to better texture characteristics and improved physical stability of the isolated compound. For instance, the applied pressure increases plant cell permeability, leading to cell component diffusivity according to the phase behavior theory, i.e. the solubility of the compound is larger while the pressure increases.

Taking into account the growing consumers demand for fresh, safe and minimally processed foods, and considering the fact that there are very limited reports regarding the effect of high hydrostatic pressure on pectin isolation from ago-food waste and by products, this chapter shows the main working principles of HHP technology, which could be applied for further valorization of various ago-food waste and by-products, as a non-commercial resources for pectin production. Some of the most relevant characteristics are written below. In addition, the present chapter shows the chemistry of pectin, its applicability in relation to extraction methodology, and analytical responses, in order to have the whole idea of the pectin processing cycle.

2. Chemistry of Pectin

Pectin is a complex heterogeneous polysaccharide found in the primary cell walls of most plants. It provides mechanical strength and flexibility due to its interaction with other cell wall components. D-galacturonic acid (D-GalA), an isomer of D-glucuronic acid (D-GlcA) was discovered to be a basic constituent of all pectins (**Figure 1**). It is present in three polymeric forms, i.e. homogalacturonan (HG), a linear polymer of α-1-4 linked galacturonic acid, rhamnogalacturonan I (RG-I), a repeating disaccharide of galacturonic acid and rhamnose and rhamnogalacturnon II (RG-II), a homogalacturonic backbone with numerous complex side chains containing rhamnose and other neutral sugars [20-22]. To date, pectins are thought to be composed of at least of 17 kinds of monosaccharides of which D-GalA is the most profuse, followed by D-galactose or L-arabinose [23]. HG the most abundant of the three polymers in which D-GalA units can be partially methyl-esterified at C-6 and acetyl-esterified at O-2 and/or O-3 positions has a large impact on the functional properties of the pectin. When more of 50 % of carboxyl groups of D-GalA units in pectin are esterified with methyl (or methoxyl) groups, this category of pectin is conventionally called high methyl-esterified, with a degree of esterification (DE) > 50 %. Otherwise, the pectin is referred to low methyl-esterified, with DE < 50 %. The DE of the pectin is an important parameter for the definition of its applicability. For instance, high metoxyl pectin forms a gel when it is heated in solution with low pH (2 - 3.5) at a high concentration of sugars (55 - 75 %). On the other hand low metoxyl pectin requites presence of divalent ions, such as calcium, with or without of sugars in a broad pH range (2 - 6).

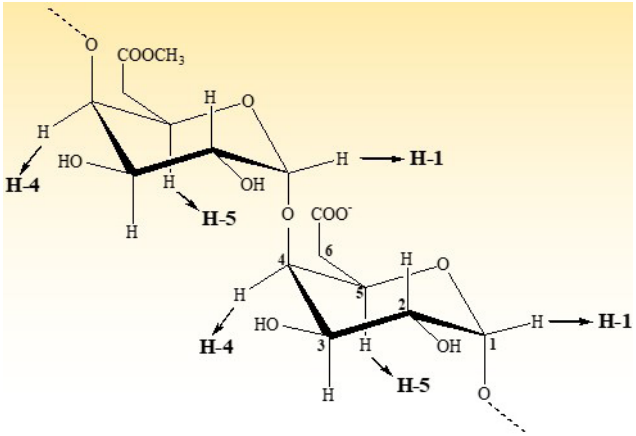

Figure 1: D-galacturonic acid as basis unit of pectin

3. Pectin Resources and Applicability

The traditional sources used for commercial production of pectin are citrus peel [24] and apple pomace [25], the residue left after juice extraction, and sugar beet pulp [26]. Due to the fact that the food processing industry generated different kinds of waste and by-products, a main focus of investigations has been placed in the utilization of their certain components, for instance pectin. In that context, the raw material for pectin production left without proper disposal mechanism could be successfully explored, offering economic advantages in decreasing disposal costs of waste. On the other hand the consumer would take the opportunity that pectin as a soluble dietary fiber could be reintroduced into food.

According to the recent literature reports, the red beet [1], cocoa husks [2], papaya peel [3], sunflower head [4], mango [5,6] banana [7], tomato [8,9] and pomelo [10] peels, hazelnut skins [11], and various other vegetable waste streams [12,13] have been studied as a naturally available resources for non-commercial production of pectin. Their evaluation as an appropriate resource for further pectin utilization is usually performed in three main steps (**Figure 2**): *i*) employment of extraction method and condition, *ii*) isolation of pectin, and *iii*) analytical checking using different tools.

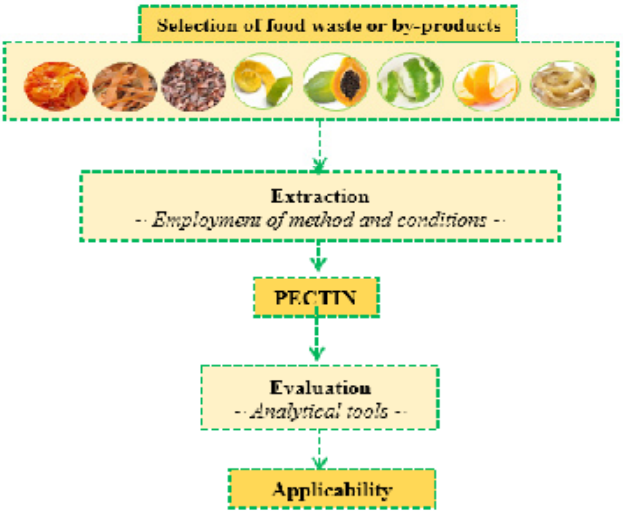

Figure 2: A schematic presentation of pectin production, from selected waste to pectin applicability

Depending on cultivation, maturation stage and storage conditions of raw material, and used extraction techniques and conditions (time, temperature and solvent), the chemical structure, composition and functional properties of pectin vary, and consequently have an influence on pectin further applicability. For instance, pectin as a water soluble carbohydrates is widely used in food processing industry as gelling agents in jams, jellies, confectionery products, as well as a stabilizer in juice and soft drinks made of milk or soy. Pectin could be used as a fat replacer in ice cream and yogurt, and a heat reversible bakery glazing. Pectin is also used in medicine and pharmaceutical industry as anti-inflammatory, anti-coagulant, anti-thrombotic, anti-microbial and anti-tumoral agents [27]. It is also utilized in hepatic regeneration, injury of atherosclerosis, preventions of endotoxemia, and in controls of calorie absorption, obesity and diabetes [27]. Pectin is used as a natural prophylactic, binding agent in tablet formulations, as an emerging prebiotic [28] and as a carrier for targeted controlled delivery of a variety of drugs.

Other applications of pectin are related to its implementation as an eco-friendly tin corrosion inhibitor [8], and carrier in bio-based edible films or coatings preparation [29], as well as an encapsulating material for the production of nano-dispersions [30].

4. Pectin Analysis

In order to responding whereby the processing (extraction) of raw material was carried out, i.e. suitable extraction time, temperature, pH, origin of extracted material, material to solvent ratio and number of extractions, and where the isolated pectin could be utilized, the choice of appropriate analytical method for detection on pectin quality parameters will have an important role. The frequently used ones as a measured of pectin purity are mentioned below.

It is well known that during the processing of bioorganic plant materials via conventional or non-conventional extraction methods can occur that change pectin solubility, polymer size, and degrees of esterification and acetylation. These changes can have important consequences on pectin quality and purity, and thus on its functionality and applicability. The particular cares have to be taken for quantification of galacturonic acid (GalA), degrees of methylation (DM) and acetylation (DA), molecular weight and intrinsic viscosity. According to the EU regulation No. 231/2012 [31], the content of galacturonic acid of food grade pectin should be ≥ 65 %. In contrast to food use, there are no regulations regarding feed use [32].

The volumetric, acid-base titration [33] has been the preferred method for pectin quantification from commercial, as well as novel food waste resources, due to the fact that provides a simultaneous determination of methoxyl (MeO) and anhydrouronic acid (AUA) contents, and degree of esterification [34]. However, this analytical method requires that the pectin be highly purified by acid-alcohol washing in order to remove extracting solvents or salts and convert pectin into free acid form before titration. Moreover, the common problem of

titrimetric method is non-distinction of D-galacturonic acid among other uronic acids, unless the latter are primarily separated by various purification procedures.

Besides titrimetric method, the colorimetric techniques based on variants of chromogenic reagent (carbazole, *meta*-hydroxydiphenyl, 3,5-dimethylphenol or xylenol, sulfamate-*meta*-hydroxydiphenyl, copper-Folin-Ciocalteau and thioglycolic acid) were also utilized for the quantification of uronic acids in pectin isolated from food waste. The coloration obtained is proportional to the amount of uronic acids, after hydrolysis of pectic substances in concentrated sulfuric acid solutions.

Despite its expanded use, the colorimetric methods are not able to discriminate different uronic acid. Therefore, the quantitative measurement is done in terms of total uronic acid content. In addition, with the colorimetric technique another one serious problems are neutral sugars, such as hexoses and pentoses, and their degradation products formed after acid hydrolysis.

Although, colorimetric and titrimetric methods are frequently used up to now, other analytical methods have been developed to avoid the error in galacturonic acid quantification. Due to the fact that neutral sugars made an essential part of pectin, the certain amount of these compounds can be incorporated in pectin extracts gained from various plant materials during isolation, precipitation and purification procedures. In this context, the removal of neutral sugars from crude pectin extracts provides valuable information of its purity, and consequently applicability. Apart from high-pressure anion-exchange chromatography coupled with pulsed amperometric detection (HPAEC-PAD), the composition of the neutral sugars can be examined by GC/FID, GC/MS and HPLC with refractive index and photodiode array detections.

Among chromatographic techniques, high performance size exclusion chromatography (HPSEC) is used for molecular characterization of pectin samples, such as molecular weight, molecular weight distribution, the radius of gyration and intrinsic viscosity.

Furthermore, Fourier transform infrared spectroscopy (FTIR) and nuclear magnetic resonance spectroscopy (NMR) have been proposed as useful spectral techniques for characterization of pectin structure, after its isolation from various plant materials. FTIR provided functional group analysis with characteristic peaks at 3390.6, 2939.0, 1749.0 and 1052.1 cm^{-1}, which are related to -OH, -CH, C=O group of ester and acid, and -COC- stretching of the galacturonic acid. Moreover, the FTIR spectroscopy can be utilized for determination of the degree of esterification. In order to quantify the DE of pectins, a calibration curve based on pectin standard (known DE) was established from the ratio of $A_{1730}/(A_{1730} + A_{1600})$, where 1760 - 1730 cm^{-1} and 1630 - 1600 cm^{-1} bands represent ester carbonyl and free carboxylate groups, respectively.

NMR spectroscopy, i.e. proton -1 (^{1}H NMR) and carbon-13 (^{13}C NMR) can be utilized

for the identification of H and C atoms in extracted pectins, respectively. Therefore, the pectin purity in terms of galacturonic acid can be established on the basis of characteristic peaks (signals) found in ^{1}H and ^{13}C spectrums of pectin extracts.

5. Pectin Extraction

The pectin as a potential marketable component present in various foods wastes and by-products need to be separated from the matrix through selective extraction and modification, ensuring that comply the existing food regulations [31], and meet the consumer standards.

Due to the fact that certain parameters of pectin quality implicate its further applicability, the particular care should be taken to set the extraction conditions, extremely important for pectin dissolution from the sample matrix.

In order to maximize the recovery of pectin into a more suitable form for separation and detection, a simple and efficient, conventional extraction methods have been employed [14]. In the conventional procedure, such as refluxing, the pectin is extracted by treating the raw material using hydrochloric, nitric, sulfuric, and oxalic acids. The hot viscous pectin extract is separated from residues by filtration and centrifugation. Subsequently, the clarified extract is subjected to alcoholic precipitation, purification, drying and milling. The common steps of pectin production are illustrated in **Figure 3**.

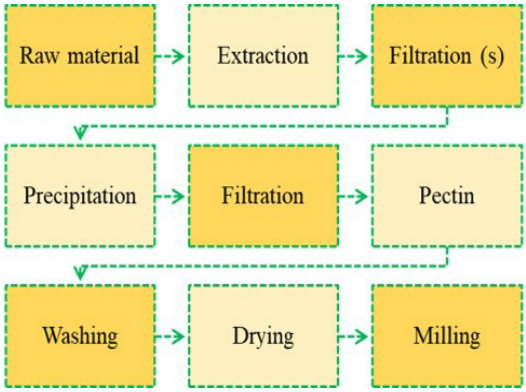

Figure 3: Flow diagram of pectin extraction procedures

Although efficient, the conventional methods showed some disadvantages, such as long extraction time, evaporation of the huge amount of solvent and creation of environmental problems producing hazardous contaminants. To overcome the limitations gained by conventional extraction, the innovative approach based on the application of ultrasound-, microwave- and enzyme- assisted extractions have been recently introduced for pectin isolation from plant food waste and by-products [14].

Besides these greener methods, another one of promising and novel extraction technique, the high hydrostatic pressure (HHP) has been recently introduced for the valorization of few food wastes, such as orange, lime and potato peels [15-17], and sugar beet [18], as non-conventional resources for pectin production. Apart from them, the high pressure homogenization was also

employment for pectin de-polymerization from apple and citrus as industrial, commercial resources, to gain a better understanding on the importance of pectin structure on the impact of high pressure homogenization [35]. The authors have pointed out that high pressure homogenization influence on rheological and textural properties of pectin, and reduce the microbial activity of liquid food system in a continuous process of pectin.

5.1. High hydrostatic pressure: work principles and process parameters

High hydrostatic pressure as a novel, non-thermal method has been developed with the aim to extend the shelf life and freshness of finished food products. As an attractive alternative method to traditional food processing, the HHP was employed for pasteurization and sterilization purposes of various foodstuffs. HHP technology has also numerous other features, listed in **Figure 4**.

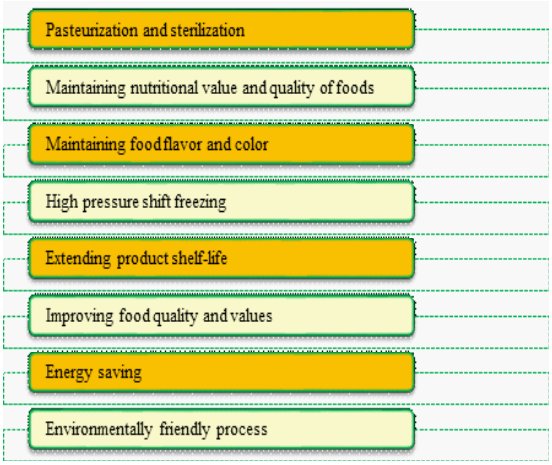

Figure 4: Characteristic of high hydrostatic pressure technology

HHP is available in the modern food industry for the last few decades and usually operate at pressures from 100 - 1200 MPa. It is applied for processing of two categories of foods: *i*) liquid and *ii*) solid and semi-solid, using batch or semi-continuous working mode.

In batch processing, the raw material is sealed in a plastic container, and placed in a pressure chamber for pressurizing, using pure water as the transmitting fluid. The chamber is then decompressed, and the cycle begins again. The cycle time depends on the type of raw material and employed temperature.

In the semi-continuous mode, the raw material is introduced periodically into a high pressure chamber, in which the filling, pressurizing, holding, decompression, and expulsion are occur.

The basic principle of high hydrostatic pressure is governed by "*Le Chatelier*" and isostatic distribution principles as a consequence of changes of three main parameters, i.e. temperature in the high hydrostatic vessel, holding time (maximum set up pressure level) and time of treatment. Therefore, when increasing the pressure at a constant temperature, at the

molecule level, the degree of arrangement of molecules in given substance increases. It results in a restriction of rotational, vibrational and translational motions of molecules [36,37].

Typical configuration of HHP equipment listed in **Figure 5** is pressure vessel (thick-wall stainless cylinder filled with water or propylene glycol), closures (to cover the cylindrical pressure vessel), system for generation and regulation of high pressure (valves, hydraulic and pneumatic pumps and intensifiers), system for process control and regulation of temperature, and handling system for loading and removing of product [36,37].

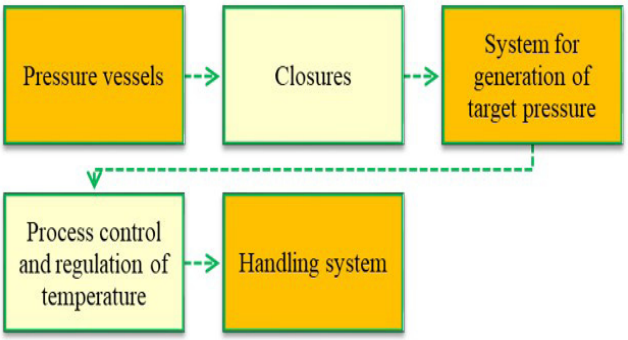

Figure 5: Typical configuration of HHP equipment

To achieve satisfactory results of HHP treatment, the three process parameters, i.e. pressure, time, and temperature must be adequately set. The lowest pressure used in the processing of raw material is around 50 MPa, while the highest pressure reaches the value of 1200 MPa.

As costly repairs and regular services of HHP equipment have shown significant contribution in the final price of processing, pressures for selected operation such as pasteurization or extraction are usually set at a minimum necessary (around 600 MPa) to achieve optimal results.

There are three possible options to choose the pressure for HHP processing of raw materials. The application of constant pressure during the full cycle is the most usual one. In the first part of the cycle, the pressure is build-up from atmospheric to target pressure value. When target pressure is reached, it is maintained during the whole time of processing. In the final part of the cycle, pressure returns to atmospheric, when the processing is finished. Decompression is usually rapid, and it can even be almost instant, depending on the valves and other equipment used.

The second mode of operation uses one or multiple stops at lower pressures (usual range is 150 - 200 MPa) for a preset amount of time. This type of processing can be beneficial for the inactivation of some bacterial spores.

The third option uses pressure pulsing, with one or more fast drops, ranging from maximal to target (lower or atmospheric) pressure values. Although efficient, particularly for

inactivation of microorganisms, this method is the most expensive, in terms of electricity needed for multiple pressurizing cycles and the largest load on the machine [38].

During HHP processes, the wide range of temperatures of pressure transmitting fluid could be employed. They vary between - 50 up to 130 °C. For instance, the temperatures from - 50 to -18 °C could be applied for freezing of various food materials. Extraction and pasteurization treatments usually worked at room temperature, due to economic reason. The higher yield of extract or larger reduction of microorganisms is gained using a slightly elevated temperature. Therefore, it is not unusual that extraction is done at temperature up to 70 °C to maintain the most relevant quality attribute, such as nutritional and antioxidant properties.

The highest temperatures are used in pressure-assisted thermal processing of various foods matrix. This emerging sterilization technique involves the preheating and processing of food materials at temperatures of 75 to 90 °C and 90 to 120 °C, respectively. Due to the fact that pressure-assisted thermal processing utilizes intensive pressure and heat, from the standpoint of engineering, the process applies significant stress of HHP equipment. On the other hand this technique enhanced the stability of valuable food ingredients, such as bioactive compounds.

Although, HHP fall into the category of non-thermal technology, one important factor which must not be disregarded is the rise of temperature during HHP processing of raw materials. The temperature usually increases from 1.5 to 3.0 °C for every 100 MPa, depending on the chemical composition of processed material and pressure fluid [38].

Besides pressure and temperature, the time is the final contributing parameter in the HHP technology. The one full HHP cycle is composed by: *i*) loading time (filling of material in pressure vessel), *ii*) compression time or alternatively pressurizing or pressure come-up time (to achieve preset process pressure), *iii*) pressure hold time (vary from seconds to hours, even days in some operations) and *iv*) unloading time (emptying of material from the pressure vessel). Therefore, the loading and unloading times are fixed, and exclusively dependent on the equipment used. From the practical, economic and commercial aspects of view, the time of 5 min or less is commonly used in HHP processing of raw materials [39].

Although, the high hydrostatic pressure was primarily focused on conservation, and transformation or processing of various products, the great challenges of HHP technology will be the extraction and preservation of bioactive and functional compounds gained from agro-food waste, with its potential application in food and biotechnological industries.

5.2. High hydrostatic pressure extraction of pectin

As it was mentioned previously, the high hydrostatic pressure exclusively used for

preservation and processing of various foodstuffs has been recently explored for pectin extraction from orange, lime and potato peels [15-17], and sugar beet [18]. Some of the most relevant and interesting characteristics of pectin isolation and detection (**Tables 1** and **2**) are described below.

Table 1: Effect of high hydrostatic pressure conditions on pectin yield extracted from few food waste and by-products

Plant material	Treatment conditions			Extraction solvent	Yield	Reference
	Pressure	Time	Temperature		(%)	
	(MPa)	(min)	(°C)			
Orange peel	100-600	5-30	10-55	0.5 M HCl, pH = 1.5	8.0-15.5	[15]
Lime peel	100-200	30	50	0.05 citrate buffer, pH = 4.5, Cellulase/Xylanase	18.6-26.5	[16]
Potato peel	200	5	25	0.25 % oxalic acid/ammonium oxalate, pH = 4.6	/	[17]
Sugar beet	250-550	30	25	0.1 M HCl, pH = 1	/	[18]

Table 2: Analytical approaches used for pectin analysis after HHP extraction from few food waste and by-products (orange, lime and potato peels, and sugar beet)

Pectin quality parameters	Analytical methods/tools	Reference
DE, DA	Acid-base titration	[15], [16], [17], [18]
AUA or GalA	Spectrophotometry	[15], [16]
Monosaccharide	GC/MS	[17]
Intrinsic viscosity	Rheometer, Size Exclusion Chromatography	[16]
Viscosity-average molecular weigh	Rheometer, Size Exclusion Chromatography, Gel permeation chromatography, HPSEC	[16], [17]
Rheological properties	Rheometer	[15], [17], [18]
Activation energy	Rheometer	[15]
Gelling properties	Rheometer	[15]
Structure	FTIR, NMR, AFM, SEM	[17], [18]

Although, HHP processing of various foodstuffs operated in an ample range of pressures (100 - 1200 MPa), temperatures (- 50 - 120 °C) and times (from seconds to hours), the isolation of pectin from orange, lime and potato peels, and sugar beet are performed at pressure of 100 to 600 MPa, with temperature and time up to 550 °C and 30 min, respectively (**Table 1**).

For instance, Guo et al. [15] were applied high pressure of 100 to 600 MPa, holding time of 5 to 30 min and a temperature of 10 to 55 °C. HHP extraction efficiency was evaluated in terms of pectin yield and viscosity. At a constant temperature of 45 °C and pressure-holding time of 15 min, the pectin yield increased (8.0 - 15.5 %) with increases of pressure from 100 to 600 MPa. On the other hand, the pectin viscosity increases up to 500 MPa. Therefore, at the optimal pressure level of 500 MPa, the pectin yield and viscosity increased with the rise of

temperature and time up to 45 °C and 10 min, respectively.

On the based on these results, and with the aim to optimize the extraction, the authors [15] were used two factors, three level design, revealing that pressure of 500 MPa, the temperature of 55 °C and a holding time of 10 min are the optimal HHP conditions for extraction of pectin from orange peel.

In addition, the authors have evaluated the HHP extraction efficiency in comparison with conventional heating (80 - 82 °C, 1 h) and microwave-assisted (80 °C, 21 min) extractions. According to their reports, the HHP provided a higher yield (20.44 %), intrinsic viscosity (0.4276 L/g), and viscosity-average molecular weight (3.063×10^5 Da) than conventional and microwave-assisted extractions.

Furthermore, the Naghshineh et al. [16] were combined enzymatic extraction of the lime peel with HHP treatments employing the pressure of 100 to 200 MPa for 30 min, at 50 °C. Their results showed that the addition of individual enzymes (cellulose or xylanase) or its combination, at pressure of 200 MPa provided higher yields (18.6 - 26.5 %), galacturonic acid content (75.5 - 92.6 %) and degree of esterification (61.8 - 75.7 %) in comparison with conventional acidic (44 % HNO_3, 70 °C) and aqueous (0.05 M citrate buffer, 50 °C) treatments. On the other hand, the pressure and enzyme concentration had no effect on the molecular weight and viscosity of pectin. Thus, without reduction of molecular weight and viscosity of pectin, pressure-treated, enzymatically extracted pectin from lime as an environmentally friendly approach assured lower energy consumption due to a decrease of temperature, time and chemical in comparison to conventional extraction methods.

The high hydrostatic pressure and high pressure homogenization were applied for pectin treatment (200 MPa for 5 min cycling), after its previous isolation from potato peel waste with oxalic acid/ammonium oxalate, at 85 °C for 2 h [17]. According to Xie et al. [17] additional pectin treatments by high pressure led to increases of galacturonic acid content and degree of esterification, as well as the rise of viscosity and emulsifying properties.

In the work obtained by Peng et al. [18] is showed that pressure of 250 to 550 MPa in combinations of three different pH values (3, 7 and 8) of extracting solvent (glycine/HCl and tris/HCl) influenced on molecular weight and degree of esterification, and acetylation of sugar beet pectin. For instance, the molecular weight at pH 3, 7 and 8 significantly decreased with increases of pressure. At pH values of 3 and 7, the degree of esterification is unchanged, and the degree acylation is somewhat smaller than control with increases of pressure. According to results gained by scanning electron microscopy (SEM) and FTIR analyses, the HHP treatments provided successful modification of pectin structure, and its rheological behavior, at three different pH values.

Thus, according to few mentioned reports it is possible to conclude that high hydrostatic pressure as a green processing technique is capable to produce pectin with various physicochemical, rheological and gelling properties, depending on utilized agro-food waste and employed extraction parameters. Considering some of the main high pressure advantages, such as low temperature, short time and less uses of solvents, HHP as non-thermal technology has a great potential for the valorization of agro-food wastes for pectin production. However, further investigations in this area are required, in order to produce pectin on the industrial level, available for consumers.

6. Conclusion

Due to the fact that a number of agro-food wastes increased daily, the employment of novel, eco-friendly and quick HHP technology could have an important impact on pectin recovery. Considering the main HHP processing parameters (pressure, temperature and time), and combine them with other important extracting condition, such as type of solvents, solvent to liquid ratio, and a number of repeated extraction, may lead to modifications of structural, physicochemical and functional properties of pectin.

Therefore, the results of HHP treatment of few mentioned food waste, performed at pressure of up to 600 MPa, mild temperature (up to 55 °C) and time of 5 to 30 min, pointed out that high hydrostatic pressure could be successfully utilized for pectin production from other bioorganic materials, generated by agro-food sectors.

To assure high yields of pectin, and its excellent quality available for consumers, with simultaneous employment of green principles, nowadays, will be the great challenges for scientists.

7. References

1. E.N. Fissore, N.M.A. Ponce, L. Matkovic, C.A. Stortz, A.M. Rojas, L.N. Gerschenson, Isolation of pectin-enriched products from red beet (Beta vulgaris L. var. conditiva) wastes: composition and functional properties. Food Sci. Technol. Int., 2011; 17: 517-527.

2. S.Y. Chan, W.S. Choo, Effect of extraction conditions on the yield and chemical properties of pectin from cocoa husks. Food Chem., 2013; 141: 3752-3758.

3. B.B. Koubala, S. Christiaens, G. Kansci, A.M. Van Loey, M.E. Hendrickx, Isolation and structural characterisation of papaya peel pectin. Food Res. Int., 2014; 55: 215-221.

4. J. Kang, X. Hua, R. Yang, Y. Chen, H. Yang, Characterization of natural low-methoxyl pectin from sunflower head extracted by sodium citrate and purified by ultrafiltration. Food Chem., 2015; 180: 98-105.

5. S. Kauser, A. Saeed, M. Iqbal, Comparative studies on conventional (water-hot acid) and non-conventional (ultrsonication) procedures for extraction and chemical characterization of pectin from peel waste of mango cultivar. Chaunsa. Pak. J. Bot., 2015, 47: 1527-1533.

6. C.H. Geerkens, A. Nagel, K. Meike Just, P. Miller-Rostek, D.R. Kammerer, R.M. Schweiggert, R. Carle, Mango

pectin quality as influenced by cultivar, ripeness, peel particle size, blanching, drying, and irradiation. Food Hydrocoll., 2015; 51: 241-251.

7. D. Gopi, K. Kanimozhi, N. Bhuvaneshwari, J. Indira, L. Kavitha, Novel banana peel pectin mediated green route for the synthesis of hydroxyapatite nanoparticles and their spectral characterization. Spectrochim. Acta A., 2014; 118: 589-597.

8. A. Ninčević Grassino, J. Halambek, S. Djaković, S. Rimac Brnčić, M. Dent, Z. Grabarić, Utilization of tomato peel waste from canning factory as a potential source for pectin production and application as tin corrosion inhibitor, Food Hydrocoll., 2016a; 52: 265-274.

9. A. Ninčević Grassino, M. Brnčić, D. Vikić-Topić, S. Roca, M. Dent, S. Rimac Brnčić, Ultrasound Assisted Extraction and Characterization of Pectin from Tomato Waste, Food Chem., 2016b; 198: 93-100.

10. L.P.T. Quoc, Effect of the assistance of microwave and oxalic acid on the extraction yield of pectin from pomelo (Citrus maxima) peel, Bulg. J. Agric. Sci., 2019; 25: 191-195.

11. Z. Kost'alova, Z. Hromadkova, Structural characterisation of polysaccharides from roasted hazelnut skins, Food Chem., 2019; 286:179-184.

12. S. Christiaens, D. Uwibambe, M. Uyttebroek, B. Van Droogenbroeck, A.M. Van Loey, M.E. Hendrickx, Pectin characterisation in vegetable waste streams: A starting point for waste valorisation in the food industry. LWT - Food Sci. Tech., 2015; 61: 275-282.

13. J. Müller-Maatsch, M. Bencivenni, A. Caligiani, T. Tedesci, G. Bruggeman, M. Bosch, J. Petrusan, et al. Pectin component and composition from different food waste streams, Food Chem., 2016; 201: 37-45.

14. M. Marić, A. Ninčević Grassino, Z. Zhu, F.J. Barba, M. Brnčić, S. Rimac Brnčić, An overview of the traditional and innovative approaches for pectin extraction from plant food wastes and by-products: Ultrasound-, microwaves-, and enzyme-assisted extraction, Trends Food Sci. Technol., 2018; 76: 28-37.

15. X. Guo, H. D. Han, H. Xi, L. Rao, X. Liao, X. Hu, J. Wu, Extraction of pectin from navel orange peel assisted by ultra-high pressure, microwave or traditional heating: A comparison, Carbohyd. Polym., 2012; 88: 441-448.

16. M. Naghshineh, K. Olsen, C.A. Georgiou, Sustainable production of pectin from lime peel by high hydrostatic pressure treatment, Food Chem., 2013; 136: 472-478.

17. F. Xie, W. Zhang, X. Lan, S. Gong, J. Wu, Z. Wang, Effects of high hydrostatic pressure and high pressure homogenization processing on characteristics of potato peel waste pectin, Carbohyd. Polym., 2018; 196: 474-482.

18. X. Peng, T. Mu, M. Zhang, H. Sun, J. Chen, M. Yu, Effects of pH and high hydrostatic pressure on the structural and rheological properties of sugar beet pectin, Food Chem., (2016) 60: 161-169.

19. C.Y. Wang, H.W. Huang, C.P. Hsu, B.B. Yang, Recent Advances in Food Processing Using High Hydrostatic PressureTechnology, Crit. Rev. Food Sci. Nut., (2016) 56: 527-540.

20. D. Mohnen, Pectin structure and biosynthesis, Curr. Opin. Plant Biol., 2008; 11: 266-277.

21. K.H. Caffall, D. Mohnen, The structure, function, and biosynthesis of plant cell wall pectic polysaccharides. Carb. Res., 2009; 344: 1879-1900.

22. B.M. Yapo, Pectic substances: From simple pectic polysaccharides to complex pectins-A new hypothetical model. Carboxyd. Polym., 2010; 86: 373-385.

23. B.M. Yapo, Improvement of compositional quality of monocot pectin extracts contaminated with glucuronic acid-containing components using a step-wise purification procedure, Food Bioprod. Process., 2011; 88: 283-290.

24. P. Putnik, D. Bursać Kovacević, A. Režek Jambrak, F.J. Barba, G. Cravotto, A. Binello, J. M. Lorenzo, et al.,

Innovative “green” and novel strategies for the extraction of bioactive added value compounds from citrus wastes - a review. Molecules, 2017; 22: 1-25.

25. A. Kumar, G.S. Chauhan, Extraction and characterization of pectin from apple pomace and its evaluation as lipase (steapsin) inhibitor, Carbohyd. Polym., 2010; 82: 454-459.

26. H.M. Chen, X. Fu, Z.G. Luo, Properties and extraction of pectin-enriched materials from sugar beet pulp by ultrasonic-assisted treatment combined with subcritical water. Food Chem., 2015; 168: 302-310.

27. F.R. Buss Marenda, F. Mattioda, I. Mottin Demiate, A. de Francisco, C.L. de Oliveira Petkowicz, M.H. Giovanetti Canteri, R. Dias de Mello Castanho Ambroni, Advances in Studies Using Vegetable Wastes to Obtain Pectic Substances: A Review. J. Polym. Environ., 2019; 27: 549-560.

28. B.C.A. Gómez, B. Gullón, R. Yáñez, H. Schols, J.L. Alonso, Prebiotic Potential of Pectins and Pectic Oligosaccharides Derived from Lemon Peel Wastes and Sugar Beet Pulp: A comparative Evaluation. J. Funct. Foods., 2016; 20: 108-121.

29. T. Nisar, X. Yang, A. Alim, M. Iqbal, Z.C. Wang, Y.R. Guo, Physicochemical responses and microbiological changes of bream (Megalobrama ambycephala) to pectin based coatings enriched with clove essential oil during refrigeration. Int. J. Biol. Macromol., 2019; 124: 1156-1166.

30. P.Q.M. Bezerra, M.F.R. de Matos, I.G. Ramos, K.T. Magalhaes-Guedes, J.I. Druzian, J.A.V. Costa, I.L. Nunes, Innovative functional nanodispersion: Combination of carotenoid from Spirulina and yellow passion fruit albedo. Food Chem., 2019; 285: 397-405.

31. Regulation (EU) No.231/2012 laying down specifications for food additives listed in Annexes II and III to Regulation (EC) No 1333/2008 of the European Parliament and of the Council 1, European Commission 9 March 2012.

32. Regulation (EU) No. 68/2013 on the Catalogue of feed materials 1, European Commision 16 January 2013.

33. S. Ranganna, Handbook of analysis and quality control for fruits and vegetable, (2nd ed.), New Delhi: Mc Graw Hill Publishers, (Chapter 2), 1995.

34. A. Ninčević Grassino, F. J. Barba, M. Brnčić, J. M. Lorenzo, L. Lucini, S. Rimac Brnčić, Analytical tools used for the identification and quantification of pectin extracted from plant food matrices, wastes and by-products: A review, Food Chem., 2018; 266: 47-55.

35. A. Shpigelman, C. Kyomugasho, S. Christiaens, A.M. Van Loey, M.E. Hendrickx, The effect of high pressure homogenization on pectin: Importance of pectin source and pH. Food Hydrocoll., 2015; 43: 189-198.

36. S.I. Martínez-Monteagudo, V.M. Balasubramaniam, Fundamentals and Applications of High-Pressure Processing Technology. In: High Pressure Processing of Food: Principles, Technology and Applications (eds. V.M. Balasubramaniam, G.V. Barbosa-Cánovas, H.L.M. Lelieveld), Springer Science+Business Media LLC, New York, 2015, pp. 3-17.

37. S.I. Martinez-Monteagudo, M.D.A. Saldana, Chemical reactions in food system at high hydrostatic pressure. Food Enf. Rev. 2014; 6: 105-127.

38. O.P. Chauhan, Non-thermal Processing of Foods, New York: CRC Press, 2019.

39. T. Koutchma, Adapting High Hydrostatic Pressure (HHP) for Food Processing Operations, Amsterdam: Elsevier, 2014.